Progress in Polymer Science 146 (2023) 101742

Contents lists available at ScienceDirect

Progress in Polymer Science

journal homepage: www.elsevier.com/locate/progpolymsci

Poly(lactic acid) stereocomplexes based molecular architectures: Synthesis and crystallization ☆

Rose Mary Michell[a,b,1], Viko Ladelta[c,1], Edgar Da Silva[d], Alejandro J Müller[d,e,f,*], Nikos Hadjichristidis[c,**]

[a] School of Chemical Sciences & Engineering, Yachay Tech University, Urcuquí 100119, Ecuador
[b] Institut für Physik, Martin-Luther-Universität Halle-Wittenberg, Halle 06099, Germany
[c] Polymer Synthesis Laboratory, Chemistry Program, KAUST Catalysis Center, Physical Sciences and Engineering Division, King Abdullah University of Science and Technology (KAUST), Thuwal 23955, Kingdom of Saudi Arabia
[d] Grupo de Polímeros USB, Departamento de Ciencia de los Materiales, Universidad Simón Bolívar, Apartado 89000, Caracas 1080-A, Venezuela
[e] POLYMAT and Department of Polymers and Advanced Materials: Physics, Chemistry and Technology, Faculty of Chemistry, University of the Basque Country UPV/EHU, Paseo Manuel de Lardizábal 3, Donostia-San Sebastián 20018, Spain
[f] Basque Foundation for Science, IKERBASQUE, Plaza Euskadi 5, Bilbao 48009, Spain

ARTICLE INFO

Article history:
Received 12 May 2023
Revised 1 September 2023
Accepted 16 September 2023
Available online 18 September 2023

Keywords:
Lactides
Polylactides
Stereocomplexes
Synthesis
Macromolecular architecture
Crystallization

ABSTRACT

This review presents the state of the art of complex macromolecular architectures based on polylactide stereocomplexes (PLA-sc) from the viewpoint of synthesis and crystallization. First, we discuss the nomenclature, synthesis, epimerization, and lactide (LA) properties as a bio-derived cyclic dimeric monomer comprising two chiral carbons. Among several polymerization methods, catalytic ring-opening polymerization (ROP) is the most common and versatile technique to access stereoregular (isotactic) PLA, which is the prerequisite to preparing PLA-sc. Combined with other living and controlled/living polymerization techniques, ROP of LA has yielded various PLA-sc-based macromolecular architectures, including copolymers, stars, graft, cyclic, brush, and hybrid materials. New approaches to synthesizing monodisperse discrete oligoLA are also discussed. We show that a small change in the architectures, microstructures, molecular weight, or other chemical and physical modifications affects the behavior of PLA-sc. Moreover, the crystallization of PLA-sc, after more than 30 years of study, still presents many challenges. The crystalline morphology is also a subject of debate. Recent findings suggest a new crystalline unit cell for PLA-sc. Adding a third component or changing chain architecture can significantly modify the prop-

Abbreviations: (RR) DLA, D-lactide; (RS) m-LA, meso-lactide; (SS) LLA, L-lactide; Al(O^iPr)$_3$, aluminum isopropoxide; AlOH, aluminum hydroxide; ATRP, atom transfer radical polymerization; BnOH, benzyl alcohol; CNCs, cellulose nanocrystals; CNFs, cellulose nanofibers; CROP, cationic ring-opening polymerization; D/L-SMP, D/L-supramolecular copolymers; DABCO, 1,4-diazabicyclo [2.2.2]octane; DACA, 3,4-diacetoycinnamic acid; DBU, 1,8-diazabicyclo[5.4.0]undec-7-ene; DBU, diazabicyclo[5.4.0]undec-7-ene; DMAP, 4-(dimethylamino); DPP, diphenylphosphate; DSC, differential scanning calorimetry; EDC·HCl, 1-ethyl-3-(3 dimethylaminopropyl)carbodiimide hydrochloride; EG, epoxy group; EtGly, 3-ethyl-1,4-dioxane-2,5-dione; EVA, poly(ethylene-co-vinyl acetate); G, spherulitic crystallization rate; GOs, Graphene oxides; HAP, hydroxyapatite; HC, homocrystals; HEMA, hydroxyl ethyl methacrylate; IMes, 1,3-dimesitylimidazol-2-ylidene; ISN-PLLA/PDLA, in situ self-nucleating polylactide; LDH, layered double hydroxide; Lu, left-handed upwards; MW, molecular weight; MWCNTs, multi-walled carbon nanotubes; NA, nucleating agents; NHC, N-heterocyclic carbine; OEGMA, oligo(ethylene glycol) methyl ether methacrylate; PBAT, poly(butylene adipate-co-terephthalate); PBS, poly(butylene succinate); PCL, poly(ε-caprolactone); PDLA, poly(D-lactide)/poly(D-lactic acid); PDMAEMA, poly(2-(dimethylamino)ethyl methacrylate); PEG, monomethoxypoly(ethylene glycol); PEG, poly(ethylene glycol); PLA, polylactide/poly(lactic acid); PLA-sc, polylactide stereocomplexes; PLLA, poly(L-lactide)/poly(L-lactic acid); PLOM, polarized light optical microscopy; POSS, polyhedral oligomeric silsesquioxanes; PPRXs, pseudo polyrotaxanes; rac-LA, racemic lactide; RAFT, reversible addition–fragmentation chain-transfer; RCM, ring-closing metathesis; RF, ramie fibers; ROMP, ring-opening metathesis polymerization; ROP, ring-opening polymerization; Ru, right-handed upwards; SC, stereocrystals; SFN, silk fibroin nanodisc; Sn(Oct)$_2$, tin(II) 2-ethylhexanoate/stannous octoate; TBD, triazabicyclodecene; TBDMS, t-butyldimethylsilyl; T_c, crystallization temperature; TfA, triflic acid; T_m, melting temperature; UPy-OH, 2-ureido-4[1H]-pyrimidinone; X_c, crystallinity degree; α-CD, α-cyclodextrin.

☆ This MS is for November 2023, Volume 146.

* Corresponding author at: POLYMAT and Department of Polymers and Advanced Materials: Physics, Chemistry and Technology, Faculty of Chemistry, University of the Basque Country UPV/EHU, Paseo Manuel de Lardizábal 3, Donostia-San Sebastián 20018, Spain.

** Corresponding author at: Polymer Synthesis Laboratory, Chemistry Program, KAUST Catalysis Center, Physical Sciences and Engineering Division, King Abdullah University of Science and Technology (KAUST), Thuwal 23955, Kingdom of Saudi Arabia.

E-mail addresses: alejandrojesus.muller@ehu.es (A.J. Müller), nikolaos.hadjichristidis@kaust.edu.sa (N. Hadjichristidis).

[1] These authors contributed equally to this work.

https://doi.org/10.1016/j.progpolymsci.2023.101742

erties of the formed PLA-sc. The complex relationship between flexibility, nucleation, diffusion, and the interactions needed for the joint crystallization of the enantiomers constitutes a very large source of variables. As a result, PLA-based stereocomplex materials can be tailored by manipulating one or several of these variables.

1. Introduction

Polylactide [i.e. poly(lactic acid) (PLA)] has been the focus of attention for many years due to its bio-based nature and convenient processing quality. However, thermal resistance lack is a feature that must be overcome. Several approaches have been developed: blends, nucleating agents, copolymers, and the most promising one, the stereocomplexes formation [1–9].

PLA stereocomplexes (PLA-sc) are formed by the co-crystallization of the enantiomeric poly(L-lactide) [i.e. poly(L-lactic acid) (PLLA)] and poly(D-lactide) [i.e. poly(D-lactic acid) (PDLA)] chains (See Fig. 1). The presence of hydrogen bonds contributes to the formation of the new co-crystalline structure. Consequently, the stereocrystals (SC) have a higher melting point than the homocrystals (HC); in fact, more than 50 °C higher [1–9]. However, the SC formation process is conditioned by several factors, such as the PLLA and PDLA ratio, the molecular weight, the macromolecular architecture, the presence of solvent, filler, or nucleating agents. An increase in the enantiomers' molecular weight reduces the crystallinity degree of the SC. The influence of molecular weight has been studied but yet not fully understood. Similarly, the formation of the SC, especially on asymmetrical blends, is a subject of debate [1–9].

The goal of obtaining a high thermal resistance material based on PLA has yet to be accomplished; the variation of the above-mentioned parameters could be considered a traditional approach. Recently, the possibilities of generating SC from enantiomers with different macromolecular architectures have been the focus of attention. Moreover, it is possible to control the amount of SC formed according to the distribution of the enantiomers within the molecules or the blend. Generally, the more complex the macromolecular architecture is, the more difficult the SC formation is [9]. However, this decrease in crystallinity could be an advantage, depending on the desired application.

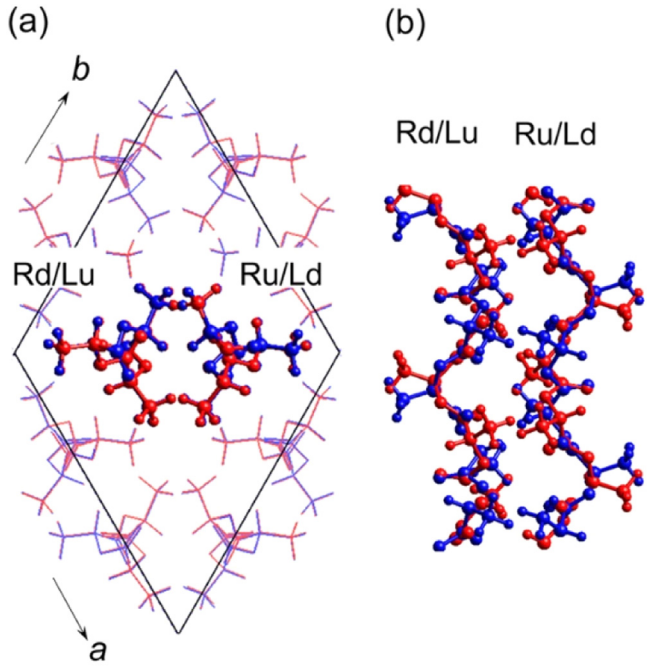

Fig. 1. Crystal structure of PLLA/PDLA stereocomplex. One lattice site is statistically occupied by a pair of right-handed downward (Rd) and left-handed upward (Lu) chains and the neighboring site by a pair of right-handed upward (Ru) and left-handed downward (Ld) chains: (a) along the *c*-axis and (b) along the 110 plane. Adapted with permission from [10].

Additionally, the stereocomplexes have been used as compatibilizers in composites and polymer blends. A small amount of PDLA in a PLLA matrix could form a three-dimensional structure, creating a thermoplastic network. It is possible to use stereocrystals to nucleate homocrystals, improving the thermal resistance of PLLA [2,4,9,11]. A detailed list of the publications made on PLA-sc from 2016 to the present, applications, and relevant information is reported in Table 1 (see the appendix).

Several reviews have been published, in the last decade, on stereocomplexes formation [1–6,9,11,12], crystallization [7,9], and applications [1–5,8,9,11–15]. However, the detailed procedures and challenges in synthesizing such macromolecular architectures (co- and terpolymers, star, comb, graft, brush, hybrid) have never been reviewed. Additionally, the new studies on stereocomplex crystallization since the latest review published [9] show a new and interesting point of view that should be reviewed and analyzed.

In this review, we introduce the fundamental concepts of PLA-sc formation. In addition, a critical discussion on the synthesis of PLAs enantiomers, PLAs based-complex macromolecular architectures, and PLA-sc crystallization is given. Moreover, the combination of various living/controlled polymerization techniques such as atom transfer radical polymerization (ATRP), reversible addition−fragmentation chain-transfer (RAFT) polymerization, anionic polymerization, ring-opening metathesis polymerization (ROMP) with anionic ring-opening polymerization (AROP) of lactides towards unprecedented PLA-sc-based complex macromolecular architectures is presented. In addition, the synthesis and properties of well-defined oligoLA-sc prepared from monodisperse oligoLA (dimer – 64mer) are also discussed.

The influence of the enantiomers blending ratio, molecular weight, molecular architecture, and additives on the SC formation and using SC as compatibilizers, nucleating agents, and physical crosslinkers are critically reviewed. We also provide general conclusions on how SC are formed, the fundamental parameters' influence, and a perspective of what could be the next goals in PLA-sc research. (see Fig. 2)

2. Synthetic aspects of PLA

2.1. Lactic acids, lactides, and polyactides

For decades, polylactide or poly(lactic acid) (PLA) has been known as the most important biopolymer. PLA is a well-known commercial polymer produced from renewable monomers (biobased), biocompatible and biodegradable that has been industrially synthesized on a large scale [16]. The first and the largest producer of various PLA products is Cargill Inc. and Cargill Dow

Table 1
Probabilities of formation of diads, triads, tetrads, pentads, and hexads as functions of the probabilities of additions resulting in the new isotactic (P*i*) and syndiotactic (Ps = 1 – Pi) diads (from Ref. [54,55]).

Dyads					
i	s				
$(P_i + 1)/2$	$(P_i + 1)/2$				
Traids					
ii	is	si			
P_i	$P_s/2$	$P_s/2$			
Tetrads					
iii	isi	iis	sii	sis	
$P_i(P_i + 1)/2$	$P_s/2$	$P_iP_s/2$	$P_iP_s/2$	$P^2{}_s/2$	
Pentads					
iiii	iisi	iiis	siii	isii	isis
$P^2{}_i$	$P_iP_s/2$	$P_iP_s/2$	$P_iP_s/2$	$P_iP_s/2$	$P^2{}_s/2$
Hexads					
iiiii	isii + iisi	iiiis + iisii + siii	iisis + siiis + sisii	isisi	sisis
$P^2{}_i(P_i + 1)/2$	$P_iP_s/2$	$P^2{}_iP_s/2$	$P_iP^2{}_s/2$	$P^2{}_s/2$	$P^3{}_s/2$

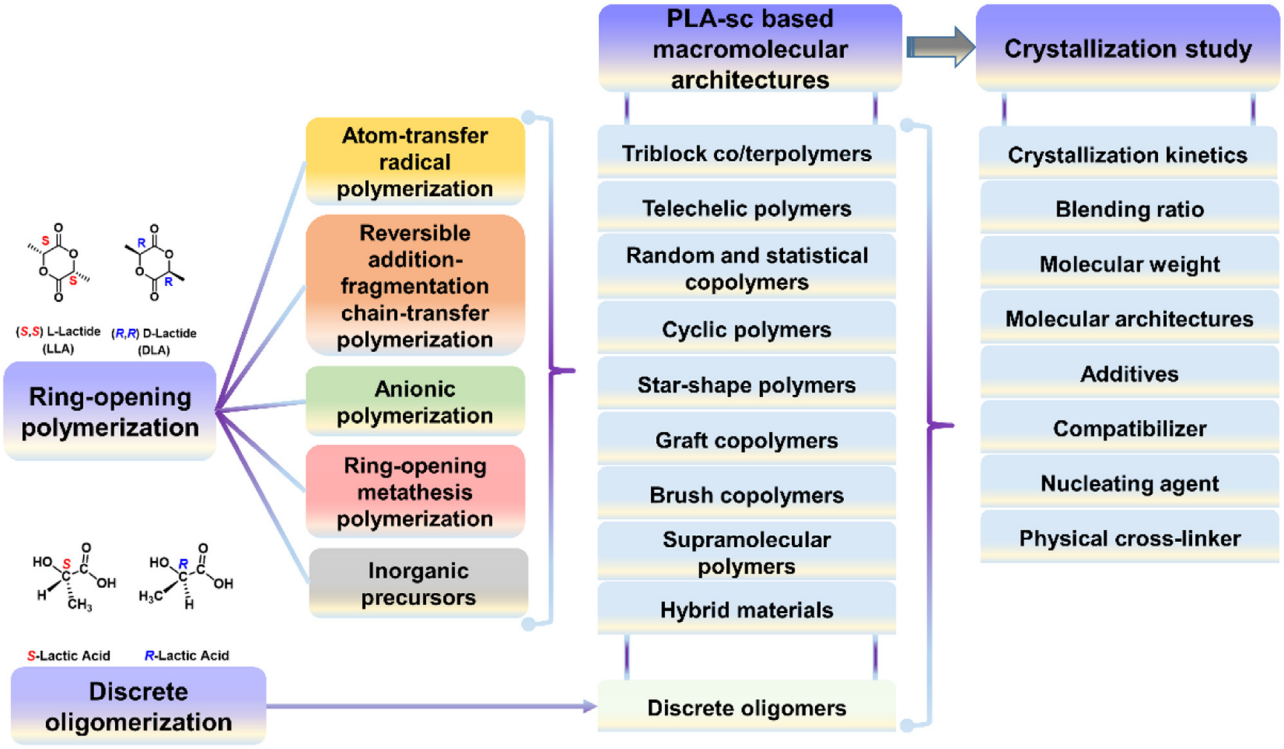

Fig. 2. A general scheme which shows the topics discussed in this review.

LLC (a 50/50 joint venture between Cargill Inc. and Dow Chemical Co.). They have recently developed a solvent-free, low-cost continuous process for the production of PLA from corn-derived dextrose [17]. The resulting PLA is commercialized under the trade name Nature Work. Nowadays, PLA-based products have penetrated the market with various applications such as drug carriers, temporary implants, bone-fixing elements, degradable dishes, and packaging.

The monomer of PLA is lactic acid (IUPAC name: 2-hydroxypropanoic acid), which possesses one chiral atom (C*) adjacent to the carboxylic group (Scheme 1) [16]. Chiral lactic acids are prepared by fermentation of biomass with the help of bacteria. Synthetically, the racemic mixture (LA + DA), is produced via the reaction $CH_3C(=O)H$ + HCN. The intermediate in the synthesis involves lactonitrile which with further hydrolysis to racemic lactic acid [16,18]. Therefore, lactic acid has two enantiomers, which are, according to Fischer's projection, called L (+) lactic acid or D (−) lactic acid (Scheme 1).

In their recent recommendation for nomenclature and terminology of lactic acid-based polymers written by Vert et al., IUPAC encourages to use of the (R)- and (S)- stereodescriptors for the absolute configuration of lactic acid and the corresponding polymers (Chan-Ingold-Prelog rules), although the use of D and L notation (based on Fischer projection) is still acceptable [19]. In their note, Vert et al. wrote:

> "**The stereodescriptors d and l for specifying the absolute configuration, still frequently used in biology, are retained for carbohydrates and amino acids only [20]. Their use for lactic acid enantiomers and derived polymers is hence not recommended, although their frequent use is acknowledged. Their use dates back to the configuration correlation of (R)- and (S)-lactic acid to the d- and l-glyceraldehyde enantiomers, respectively.*
>
> ***(+) or (−) is sometimes inserted to indicate clockwise and counter-clockwise rotation observed in polarimetry. In association with a specific configuration, this complement of information is in-*

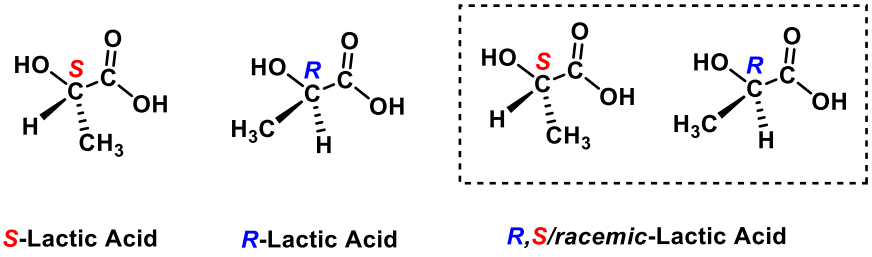

Scheme 1. Structures of L- and D- lactic acids according to the absolute configuration.

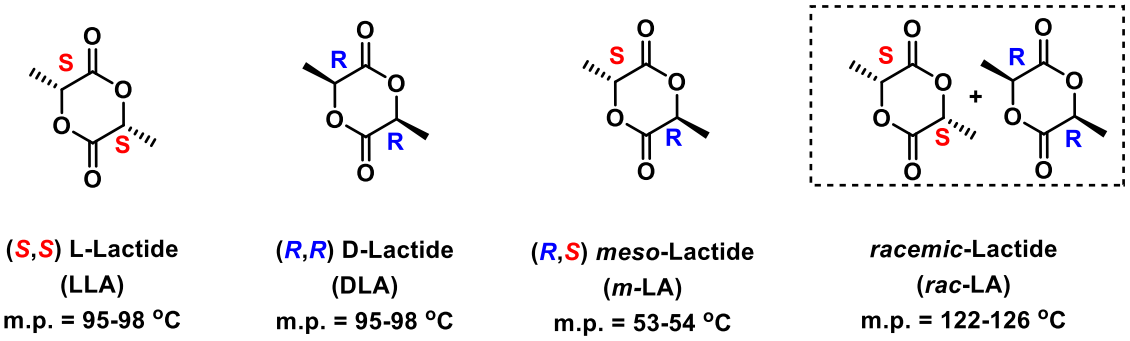

Scheme 2. Structure and melting point of LLA, DLA, *m*-LA, and *rac*-LA.

appropriate and can be misleading because the sign of rotation depends on temperature, wavelength, and solvent. The lower-case d and l are obsolete descriptors formerly used instead of (+) and (−), respectively. They are sometimes mistakenly confused with the descriptors d and l."

In this review, we will follow the IUPAC recommendation using (*R*)- and (*S*)- to describe the absolute configuration of the chiral carbon of lactic acids/lactides and PLA. The corresponding cyclic dimer of lactic acid (derived from two molecules of lactic acids) is called lactide (IUPAC name: 6-dimethyl-1,4-dioxane-2,5-dione). However, since D-lactide (DLA) and L-lactide (LLA) are very common and still acknowledged worldwide, we will use these names to indicate the (*S,S*) and (*R,R*) lactide in this review. Therefore, lactide synthesized from two identical lactic acids generates (*R,R*) D-Lactide and (*S,S*) L-lactide, which is further abbreviated as DLA and LLA. On the other hand, lactide derived from (*R*)-lactic acid or (*S*)-lactic acid), which is called *meso*-lactide (*m*LA) (Scheme 2).

Lactic acid enantiomers are produced by bacteria *via* the fermentation of sugar cane or corn starch. For instance, *S*-lactic acid can be produced by *Lactococcus lactis* LL0018 and *Lactobacillus casei sp.* with lactic acid content up to 99.0 % [21,22]. *R*-lactic acids having enantiomeric purity up to 99.4 can be produced by *Lactobacillus delbrueckii* LD0025 and *Sporolactobacillus inulinus* SI0073 [21,22]. Other bacteria, such as *Lactobacillus helveticus* LH0030, also produce a mixture of *R*-lactic acid and *S*-lactic acid (with a ratio 50.5:49.5), called racemic lactic acid [21].

The purification of lactic acids produced by fermentation is a very challenging process. The procedures can be found in several papers and patents [16,17,23,24]. One of the most common procedures to obtain high-purity LA is by depolymerization of the low molar mass oligo LLA (*o*LLA) under reduced pressure (Scheme 3). The process, which is basically the back-biting reaction of *o*LLA, is regulated by a catalyst, lactic acid concentration, and temperature. In this process, mixtures of LLA, DLA, and *m*-LA are formed with proportions depending on the lactic acid feedstock, temperature, and catalyst applied in the process.

The mass production of LLA relies on the depolymerization of low molecular weight (MW) of L-lactic acid via metal catalysts, such as tin(II) 2-ethylhexanoate/stannous octoate [$Sn(Oct)_2$] [24,25]. Although the results of this process are predominately LLA stereoisomer, it is always contaminated by some amount of *m*-LA as a byproduct or "waste". From the industrial viewpoint, this byproduct is a severe drawback to the production cost [26]. *m*-LA is considered a useless byproduct of LA production because the thermal and mechanical properties of poly(*m*-LA) are less useful for industrial applications. Interestingly, the recent development in catalysis provides elegant methods to convert *m*-lactide into stereoregular PLA [27]. Another source of *m*-LA is obtained from the thermal degradation of PLLA (*rac*-LA/*m*-LA = 2/1) along with cyclic oligomers and their diastereomers as well as CO_2, CO, CH_3CHO, and CH_2=CHCOOH [28,29].

There are several ways to synthesize polylactic acids/polylactides (PLA) from their corresponding monomers. The polymerization methods will be discussed briefly later. Significant attention will be given to anionic ROP because it is the most utilized method to synthesize PLA stereocomplex (PLA-sc) based complex macromolecular architectures.

2.2. Microstructures of PLA

Since lactic acids possess one stereocenter (two stereocenters for the dimers, lactide), the polymerization of lactic acids and lactides in the absence of epimerization (which will be explained later in detail) leads to the formation of stereoregular PLA. Understanding the stereoregularity of PLA is very important for practical applications because stereoregularity strongly affects the thermal and mechanical properties, as well as the crystallization behaviour of PLA [30,31]. *R*-lactic acid and *S*-lactic acid polymerized by polycondensation result in isotactic PLLA and PDLA (Scheme 4). All of the stereocenters in the isotactic PLLA and PDLA are aligned along the same side of the polymer chain ((-*SSSSSS*-) and –*RRRRRR*-) (Scheme 4). Polycondensation of *rac*-lactic acid produces a stereocopolymer, known as atactic PDLLA [22].

On the other hand, lactides are polymerized by ring-opening polymerization (ROP) to produce PLA. The industrial production of PLA mostly relies on this polymerization method [22]. Similar to the case of polycondensation, the ROP of enantiopure LLA

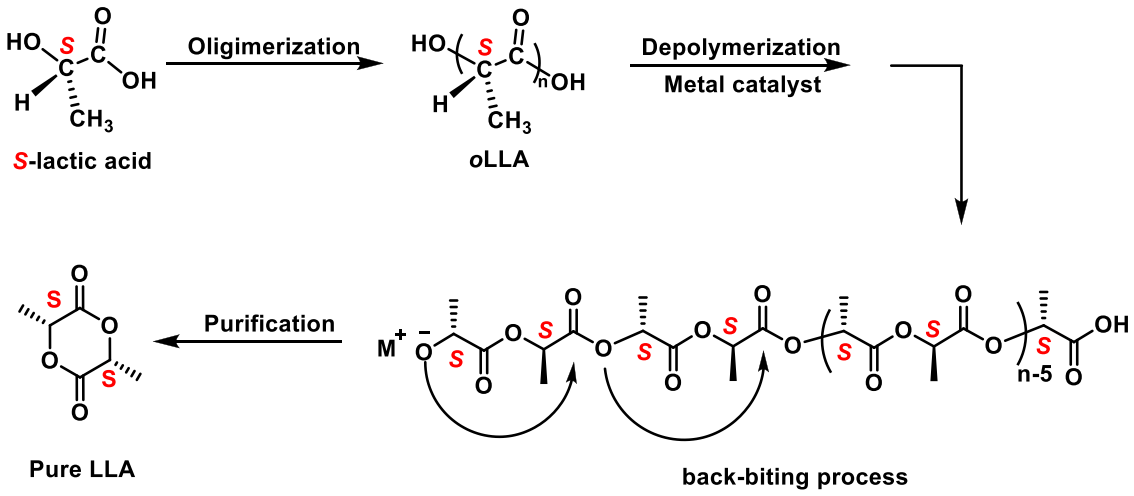

Scheme 3. Synthetic routes toward high-purity LLA.

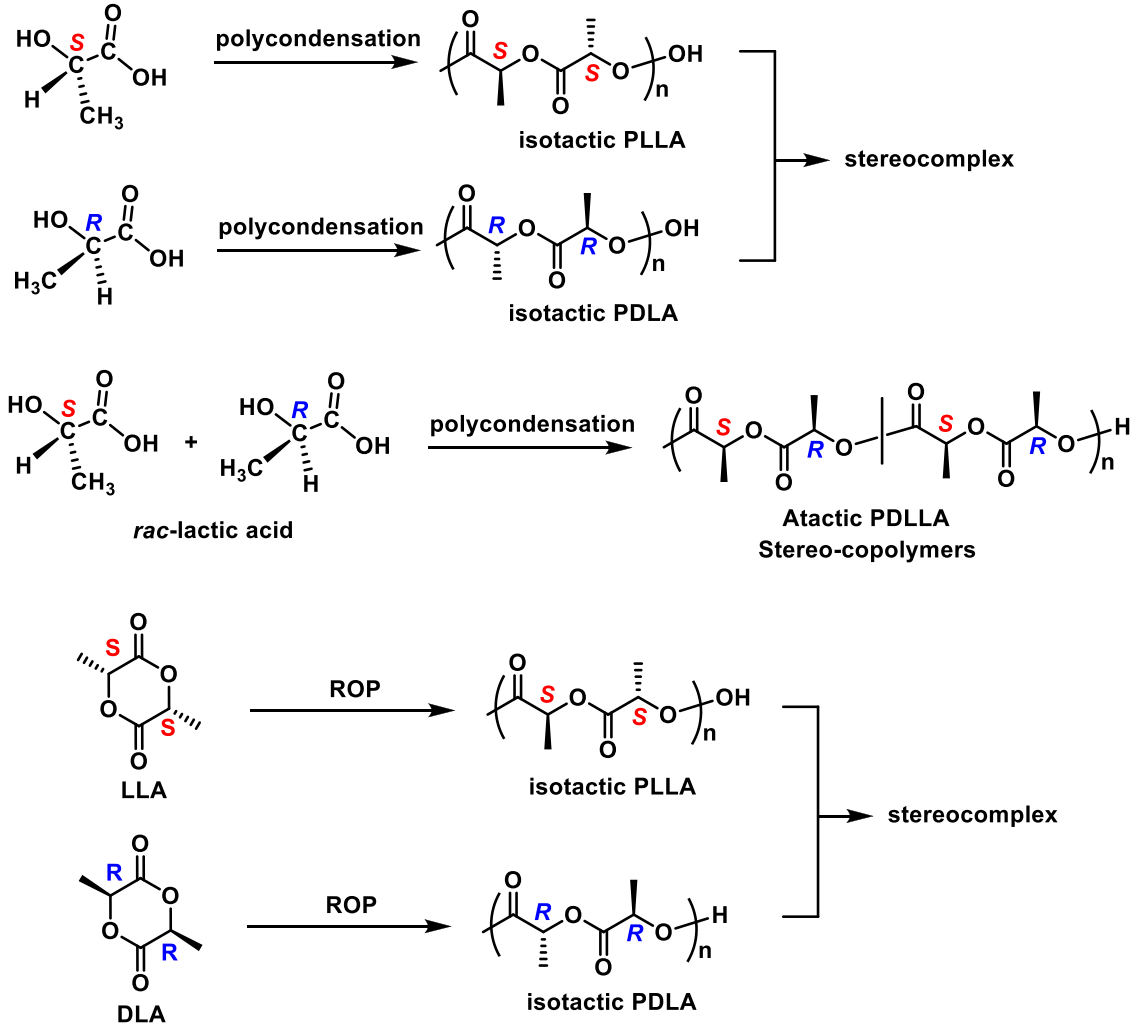

Scheme 4. Possible microstructures of PLA based on the monomer structure used in the polymerization.

and DLA in the absence of epimerization results in an isotactic PLLA and PDLA (Scheme 4). Three different microstructures can be obtained from the ROP of *rac*-LA: (1) syndiotactic PLA, in which the *R* and *S* stereocenters are alternating (-*SRSRSR*-), (2) heterotactic PLA, in which two *R* and *S* stereocentres double alternate (-*SSRRSSRR*-), and (3) atactic PLA, in which the *R* and *S* stereocentres alternate randomly (Scheme 4) [19,32]. Depending on the catalyst, ROP of *m*-LA can lead to either syndiotactic or atactic PLA [19,27,32].

Several factors, such as the degree of selectivity of the catalyst, side reactions, and insertion errors, can affect the polymer microstructure. These factors lead to the formation of more diverse microstructures, such as stereoblock copolymers and tapered stereoblock copolymers. Moreover, a multiblock (stereoblock) copoly-

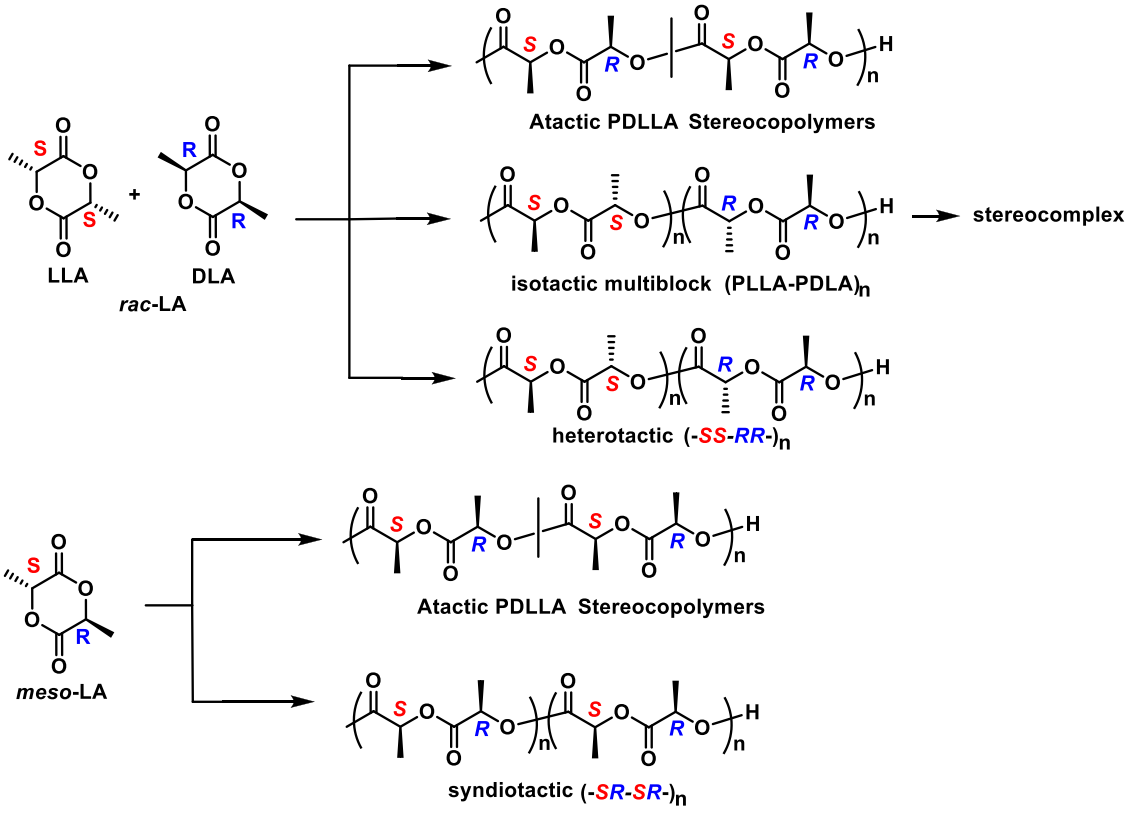

Scheme 4. Continued

mer may form when large numbers of stereo errors or significant chain transfer events occur during the polymerization [32].

The stereoregularity of PLA can be detected in solution using polarimetry and circular dichroism spectroscopy [33–35]. The analysis with a polarimeter follows the assumption that the $\alpha^{22}{}_{D}$ of PLLA with $M_w > 6000$ remains constant at 142° [21,22,33]. On the other hand, circular dichroism spectroscopy can be performed in the range of UV–Vis and IR wavelengths [36–38]. The melting point (T_m) determined by differential scanning calorimetry (DSC) also gives information on the microstructures of PLA [39–43].

The recent development of NMR techniques could give more comprehensive information on the stereoregularity of chiral polymers. For a particular case like PLA, the stereoregularity at the tetrad level can be determined by ^{13}C NMR and homonuclear decoupled ^{1}H NMR analysis [44,45]. Homonuclear decoupled is required because PLA methine protons appear as a quartet signal in the ^{1}H NMR spectrum. It is challenging to perform peak fitting and individual integration on such a spectrum, particularly when the stereoregularity is disturbed [46]. The homonuclear decoupled ^{1}H NMR technique resolves this issue by simplifying the quartet into a singlet peak. This is accomplished by irradiation with an additional radiofrequency to saturate the spin transitions of the neighboring CH_3. As a result, the splitting of methine proton coupling with the CH_3 group will disappear, resulting in a singlet CH peak (δ = 5.15–5.25 ppm) [45].

Additionally, the ^{13}C signals of methine and carbonyl carbon of PLA can also be used to detect the stereoregularity of PLA because these signals are very sensitive to microstructure changes [47–50]. However, the tetrad signal assignments must be done carefully to avoid ambiguity [47,51,52]. The advanced 2D NMR experiments can also be used to support signal assignment [44,53].

Bovey formalism is widely used to define the relationship between the neighboring stereocenter using absolute configuration [32,54]. In a simple case like a diad, the *SS* or *RR* stereo sequences are described as '*iso*' (*i*) diads and the *RS* or *SR* stereo sequences are described as '*syndio*' (*s*) diads. The higher stereocenter sequences like triads, tetrads, and pentads are defined based on the *i* and *s* relation.

In the absence of chain transfer and racemization, the *i*- and *s* diads' probability of formation is defined as P_i and $P_s = 1 - P_i$. P_i and P_s are related to the fraction of the isotactic and syndiotactic diads [49]. Table 1 describes in detail the P_i and P_s formation of diads, triads, tetrads, and pentads of PLA.

2.3. Polycondensation (step-growth polymerization)

2.3.1. Melt polymerization

Direct polycondensation of lactic acids in melt in the absence of a catalyst is considered the first direct polymerization method for the synthesis of PLA [22]. The polymerization contains two equilibria: (1) hydration/dehydration equilibrium of carboxyl and hydroxyl terminals and (2) ring/chain equilibrium between L-lactide and PLLA. Because the direct melt polycondensation results were not promising, the approach was shifted towards melt polycondensation with a bi-component catalyst consisting of Sn(II) compound and *p*-toluenesulfonic acid [56,57]. PLLA is formed by heating the oligomeric L-lactic acid (oligoLLA) at temperatures above T_g but below T_m of PLA. NMR studies reveal that there was no racemization occurred, and dimeric lactic acid formation and other side reactions could be minimized under these conditions (90 % yield) [56]. The highest molecular weight reported was ~320,000 g/mol ($Đ$ = 3.4).

2.3.2. In solution

This process is an expensive, tedious, and less efficient polycondensation of lactic acid. To achieve a successful polycondensation, the final concentration of water in the system should be below one ppm. Catalyst and dry diphenyl ether, a high boiling solvent,

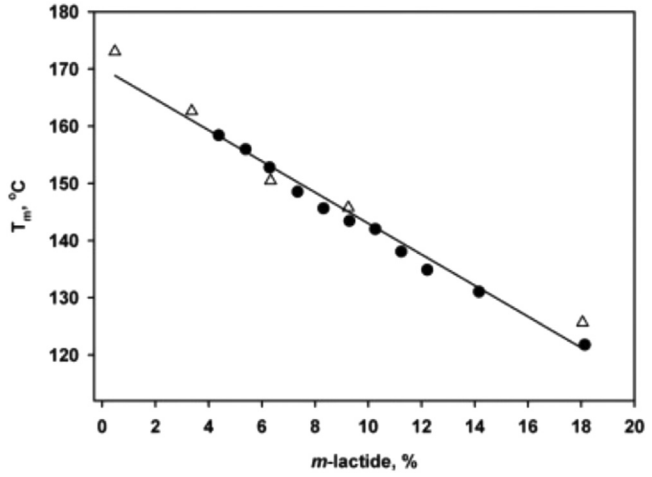

Fig. 3. Dependence of T_m of PLA as a function of % *m*-LA (reproduced from Ref. [62]). (o) Represents values by Witzke [63]; (•) represents values reported by Hartman[59].

are added to the preheated LLA at 130 °C (at this temperature, oligoLLA has already formed) [58,59]. This process could produce PLA with a molar mass of up to 250,000 g/mol.

Although the synthesis of PLA can be realized by polycondensation of lactic acid, the ROP of lactide enables a greater degree of control over the molecular parameters, such as lower polydispersities, higher molecular weight, and high levels of end-group fidelity. The application of ROP techniques also enables control over the order of insertion of monomers into the polymer chain based on their stereochemistry.

2.4. Ring-opening polymerization (chain-growth polymerization)

Several methods can perform the ROP of LA: coordination-insertion ROP with metal catalysts, cationic ROP with protonic acids, anionic ROP initiated by anions or activated by hydrogen transfer/hydrogen bond, formed in the preinitiation stage (mostly by organic catalysts) [32,60,61].

ROP proceeds either in bulk or in solution. If there is no racemization, the ROP of LLA or DLA produces a highly isotactic and crystalline PLA with $T_m \sim 180$ °C. Polymerization of *m*-LA and random copolymerization of *rac*-LA (mixture of LA and DA) results in an amorphous polymer with better solubility and lower rigidity. These PLAs with different melting points, rigidity, crystalline or amorphous, soft, or elastomeric lead to many applications. Obviously, LA's chiral purity and tacticity control during ROP are the most significant factors in producing PLA with targeted/pre-designed thermal (T_g, T_m, X_c) and mechanical properties for specific applications, as shown in Fig. 3.

2.4.1. ROP of LA initiated by anions from organometallic compounds

The initiator for this type of ROP is an anion from organometallic compounds, which attack the carbonyl carbon of lactide and open the lactide ring [64,65]. Among organometallic initiators, lithium alkoxides are the frequently used initiators due to their good solubility. ROP of *rac*-LA with lithium *tert*-butoxides leads to the formation of heterotactic PLA [47]. In general, the stereocontrol of the resulting PLA produces by this type of ROP is very poor. A better stereocontrol can only be achieved by lowering the polymerization temperature [50].

2.4.2. ROP of LA promoted by an organic catalyst

The use of organic catalysts for ROP was first reported in early 1970 via zwitter ionic polymerization of β-propiolactone promoted by phosphine and amine [66–71]. However, major progress on organocatalytic ROP was achieved by Hedrick in early 2000 when he reported the controlled ROP of LA with 4-(dimethylamino) (DMAP) and 4-pyrrolidino-pyridines (PPY) as the catalysts [72,73]. Since this pioneering work, numerous organic catalysts have been used to promote the ROP of LA and other cyclic esters [74–78].

Organocatalytic ROP can proceed in three different mechanisms; initiator activation, monomer activation, and simultaneous activation of the initiator and monomer. The reaction mechanisms are determined by the type of organic catalyst used in the system. The initiator activation mechanism is promoted with organic (super)bases such as DMAP, 1,8-Diazabicyclo[5.4.0]undec-7-ene (DBU), triazabicyclodecene (TBD), and phosphazene superbases [73,79]. The growing chain end is an alkoxy anion with a large organic counter cation. In the case of the monomer activation mechanism, the catalysts are organic acids such as diphenylphosphate (DPP), triflic acid, methanesulfonic acid, and hetero cyclic carbenes [80]. In the absence of an initiator, ROP of LA with *N*-heterocyclic carbine (NHC) leads to the formation of cyclic PLA [78,80]. The pair of (thio)urea/organic bases or other lewis pairs, such as triethyl borane (TEB)/organic bases, promote the ROP of LA through the simultaneous initiator/monomer activation mechanism [81].

To the best of our knowledge, only a few organic catalysts have been applied to the synthesis of PLAs as the precursors for PLA-sc -based macromolecular architectures. The reason is probably because the isotacticity (and therefore the T_m) of PLAs produced by organocatalysts is low. In most cases, the synthesis of highly isotactic PLA using organic catalysts must be performed at low temperatures (<-20 °C) [32,79,82].

2.4.3. Cationic ring-opening polymerization (CROP)

CROP of LA proceeds through an "activated monomer mechanism" (Scheme 5), a polymerization mechanism that was initially used to explain the polymerization of oxiranes [83]. In the activated monomer mechanism, the propagation step occurs via nucleophilic attack of the oxygen atom of a hydroxyl group on an α-carbon atom in the protonated monomer. The compound containing the –OH group acts as an initiator, and the protic acid act as a catalyst [83].

According to Kricheldorf et al., the ROP of LLA can be initiated by triflic acid (TfA) and its methyl ester acid derivative (MeTf). In contrast, weaker protic acids (methane sulfonic acid and trifluoroacetic acid) or Lewis acids such as $BF_3{\cdot}Et_2O$ can not initiate the polymerization [84,85]. They proposed that trifluoromethanesulfonic (triflic) anion plays an important role in CROP. The mechanism for the opening of the methylated LA ring involves an attack by a triflic anion to form a triflic ester end group, which then reacts with subsequent LLA molecules.

2.4.4. Coordination insertion ROP

Coordination insertion ROP/metal-mediated ROP of LA is usually promoted by metal salts and metal complexes with specific ligands [32,86]. The ROP proceeds through the coordination of carbonyl oxygen of LA with the metal center to activate the monomer and stabilize the propagating species. The initiator attacks the activated carbonyl carbon, followed by the ring-opening of the LA, forming a metal alkoxide chain end and continuing the propagation. The selection of ligands has a significant effect on the rate of polymerization as well as the stereocontrol of the resulting PLA [32].

$Sn(Oct)_2$ is the most well-known and most frequently used metal catalyst for ROP of LA [61]. It is cheap and commercially available with a purity of around 95 %, which can be purified further by distillation [87]. The main impurities of the commercial $Sn(Oct)_2$ are octanoic acid and water. ROP of LA using $Sn(Oct)_2$ is so versatile that it can be done in bulk under a non-inert atmo-

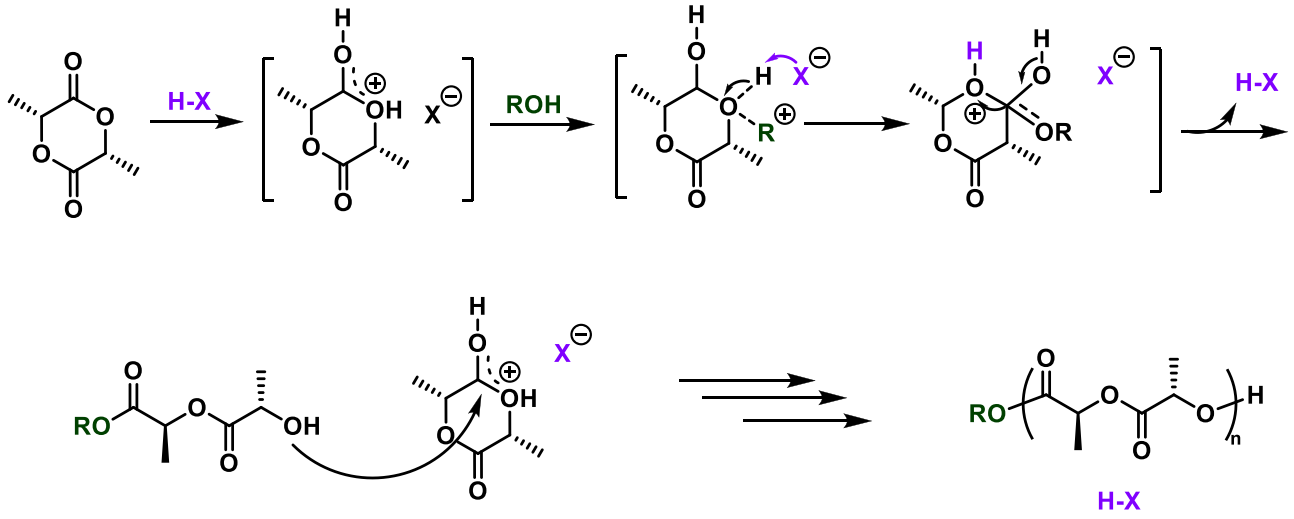

Scheme 5. Cationic ROP based on activated monomer mechanism.

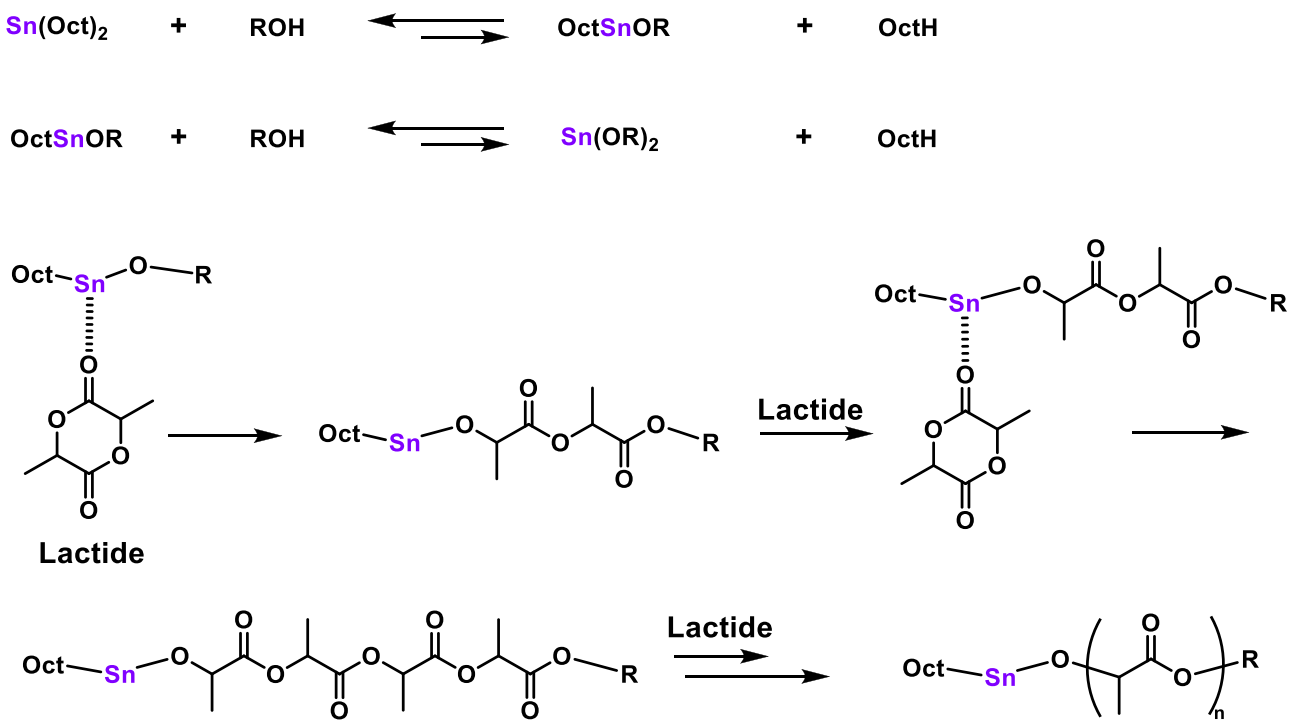

Scheme 6. ROP of lactide with tin octoate by coordination-insertion mechanism.

sphere, even without purification of $Sn(Oct)_2$. The highest M_n of PLA can be achieved by nearly 10^6 g/mol. US food and drug administration approved $Sn(Oct)_2$ as a food additive because, at a concentration of around ten ppm, this compound is considered non-toxic [22,61]. The T_m of PLA synthesized by $Sn(Oct)_2$ is considerably high (145–168 °C), depending on the polymerization conditions. Therefore it is widely used to synthesize PLA as the precursor for PLA-sc [9,35,88].

Penczek and his coworkers have performed many experiments to elucidate the mechanism of ROP of LA catalyzed by $Sn(Oct)_2$. It is now widely accepted that the ROP of LA catalyzed by $Sn(Oct)_2$ proceeds through an "insertion-coordination mechanism" (Scheme 6) instead of a "monomer activation mechanism" [22,80,89,90]. $Sn(Oct)_2$, by itself, is not active at all and requires a transformation into $Sn(OR)_2$ (alkoxides active species). Protic compounds such as R-OH or R-NH_2 are needed as a chain transfer agent to react with $Sn(Oct)_2$ to form covalent tin alkoxides [$Sn(OR)_2$] that act as real initiators [90–94]. The Sn atom of the $Sn(OR)_2$ coordinates with one of the carbonyl oxygen of the LA. Then the LA chain is opened by breaking the acyl-oxygen bond (between the carbonyl group and the endocyclic oxygen) and inserting the opened LA into the tin-oxygen bond (alkoxide) of the catalyst. A similar mechanism is repeated during the chain propagation until all LA molecules are consumed via the insertion into the Sn-oxygen bond (Scheme 6) [90,95,96].

Another common and efficient metal alkoxide catalyst is aluminum alkoxides, such as aluminum isopropoxide ($Al(O^iPr)_3$) [97,98]. Metal atoms such as Al, Mg, Zn, Ca, Fe, Y, Sm, Lu, Ti, and Zr complexed with tri- and tetra-dentate iminophenolato- and aminophenolato-(salen and salan), β-Diketiminato (BDI), and tetradentate amino(bis- and tris-phenolato) are also used as catalysts in the stereoselective ROP of LA [32].

2.5. Epimerization on LA and PLA

Epimerization, or in some cases called racemization, is a process in which the configuration of a chiral center changes. This stereochemistry reaction occurs through the cleavage of acidic C(sp^3)–H bonds, such as the Cα–H of carbonyl compounds (for example, the methine proton of LA/PLA) [99,100]. Epimerization can be a powerful tool for chemists but also give an undesirable side reaction leading to a decrease in optical purity, like in the case of isotactic PLLA [27,100,101]. Because epimerization on PLA forces a stereochemical inversion of the stereocenter (R→S or S→R), its occurrence during polymerization ultimately changes the thermal properties, crystallinity, and biodegradability of the resulting PLA.

Epimerization also affects thermal recycling and thermal degradation of PLLA, generating optical isomers: LA diastereomers (*rac*-LA/*m*-LA = 2/1), cyclic oligomers, and other small molecules [28,58,102,103]. This can cause serious problems in the industrial recycling process of PLA [28,103].

Racemization/epimerization that occurs on LLA during heating (without catalyst) can be monitored by ^{1}H NMR and gas chromatography. The conversion of LLA to *m*-LA (particularly above 200 °C) increases with the increase of heating temperature and time. The rate of this reaction is higher than the rate of conversion into oligo-LLA. This suggests that direct racemization of LLA to *m*-LA occurs exclusively and does not decrease during the oligomerization/oligomer chain reaction. In contrast, if MgO is used as a catalyst, the direct racemization, racemization process *via* oligomerization, and the ester–semiacetal tautomerization on the formed oligomer chain are present in the system [100].

Organic bases are known to trigger the epimerization of PLA. TBD promotes epimerization and chain scission of PLA at 105 °C in toluene [104]. A small amount (1 mol %) of TBD in the system triggers the formation of ca. 30 % D-stereoisomer (from the PLLA system) and 38 % L-stereoisomer (from the PDLA system) [104]. 1,4-diazabicyclo [2.2.2]octane (DABCO),1,8-diazabicyclo[5.4.0]undec-7-ene (DBU), and imidazole can epimerize *m*-LA into LLA and DLA in toluene [26]. Phosphazene superbase *t*-BuP_2 also promotes epimerization at 80 °C in toluene (Scheme 7). This gives two consequences: self-initiation from the deprotonated LLA in the absence of a primary alcohol initiator and deterioration of stereoregularity on the resulting PLLA, which lead to the formation of amorphous PLA [88]. Therefore, for crystallinity studies, the synthesis of PLA using strong organic bases at high temperatures is not preferred.

Epimerization on LA/PLA can also be a useful stereochemistry reaction. For instance, a rapid and quantitative epimerization can be used to convert *m*-LA into *rac*-LA by using DABCO/B(C_6F_5)$_3$ (around 20 ppm) as the catalyst [27]. Subsequently, by applying kinetic resolution *via* a highly enantioselective bifunctional chiral organic catalyst, the *rac*-LA was converted into optically pure isotactic PLLA and DLA [27]. Some other catalysts such as trimeric phosphazene superbase, thiourea, chiral zinc amido-oxazolinate complexes, Al(III) and Fe(III), trinuclear salen complexes, thiolen complexes, ytrium bisphenolate, Zr complexes of tetradentate-diainionic imine-thiobis(phenolate) ligands are also capable on promoting an isoselective ROP of *rac*-LA resulting in isotactic PLA stereoblock [82,105–112].

3. Synthesis of PLA-sc-based complex macromolecular architectures

3.1. PLA homopolymers

The purpose of this section is to discuss the synthesis of PLA-sc-based complex macromolecular architectures (linear block co/terpolymers, cyclic, star, graft, comb, and hybrid materials) that were reported mostly in the last ten years. Those PLA-sc were synthesized via unconventional synthetic methodology and exhibit unique properties/applications.

3.1.1. PLA stereocomplexes-based linear triblock co/terpolymers

PLA-sc based linear triblock copolymers (ABA type) has been reported for many years, and the examples are well documented in the review by Tsuji [9]. These copolymers are made by mixing/blending the equimolar amount of AB diblock copolymers with B, either PLLA or PDLA. This synthetic strategy was used to prepare various non-covalent ABA copolymers for crystallinity, water contact angle, drug delivery, and micelle studies, among others. Some of the most recent examples of polymers (the A block precursors) used to synthesize such copolymers are poly(3-hexylthiophene) (P3HT) [113], poly(2-(dimethylamino)ethyl methacrylate) (PDMAEMA) [114], poly(ethylene glycol) (PEG) [115–117], poly(ε-caprolactone) (PCL) [118–120], polyhydroxybutyrate [121], poly(1,2-propylene succinate) [122], polyurethane [123], and polyvinyl ethers [124]. Polystyrene containing PLA stereoblock, PS-PLLA-PDLA, synthesized by combining ATRP with ROP of LLA, and then DLA have also been reported [125].

Recently, Hadjichristidis and his coworkers have reported for the first time the synthesis and thermal properties of well-defined polystyrene-polylactide sterecomplex-polyisoprene (PS-PLA-sc-PI) and polystyrene-polylactide sterecomplex-poly(2-vinylpyridine) (PS-PLA-sc-P2VP) linear triblock terpolymers by combining anionic polymerization high vacuum technique with ROP (Scheme 8) [35,126]. Their preliminary results open a new horizon for the synthesis of well-defined complex macromolecular architectures based PLA-sc.

Akashi developed a novel method for the in situ simultaneous one-pot polymerization and self-nucleation of PLLA [127]. The new in situ self-nucleating polylactide (ISN)-PLLA/PDLA material has a wide temperature window for thermal processing and acts as a stable nucleating effect even at high temperatures (250 °C) and under repetitive heating. This ISN-PLLA/PDLA allows a broader application of PLA, which is normally limited by its inferior mechanical properties, to various fields related to biodegradable polymers, such as implantable devices, drug delivery, and eco-friendly products.

3.1.2. PLA stereocomplexes-based discrete oligomers

The first discrete oligomer synthesis was reported by Hawker and his coworkers in 2008. The synthesis was carried out by a coupling reaction between an α-protected benzyl dilactic acid with an ω-protected dilactic acid using 1,3-dicyclohexylcarbodiimide or 1-[3-(dimethylamino)propyl]-3-ethylcarbodiimide hydrochloride as the catalyst. This strategy is recognized as the first successful synthesis of monodisperse oligo lactic acid (*o*LA) on a gram scale (Scheme 9) [128].

Hawker an coworkers used *t*-butyldimethylsilyl (TBDMS) ether as the protective group for the hydroxyl group and benzyl (Bn) ester as the protective group for carboxylic acid group. The yields of both deprotection steps and coupling reactions using 1,3-dicyclohexylcarbodiimide or 1-[3-(dimethylamino)propyl]-3-ethylcarbodiimide hydrochloride was high (70–100 %). This robust and efficient synthetic strategy can be developed due to the absence of a requirement to conduct most of the reactions under an inert atmosphere which allowed monodisperse dimer, tetramer, octamer, 16mer, 32mer, and 64mer materials to be prepared in gram quantities and fully characterized using mass spectrometry and size exclusion chromatography.

Studies on crystallization and thermal properties of *o*LA are crucial to understanding the properties of short oligomeric crystalline materials. Discrete-length, isotactic *o*LA has a strong tendency to form a well-organized crystalline phase in which the *o*LA chains form a 10_3 helix with a monomeric rise of 0.3 nm, whereas the

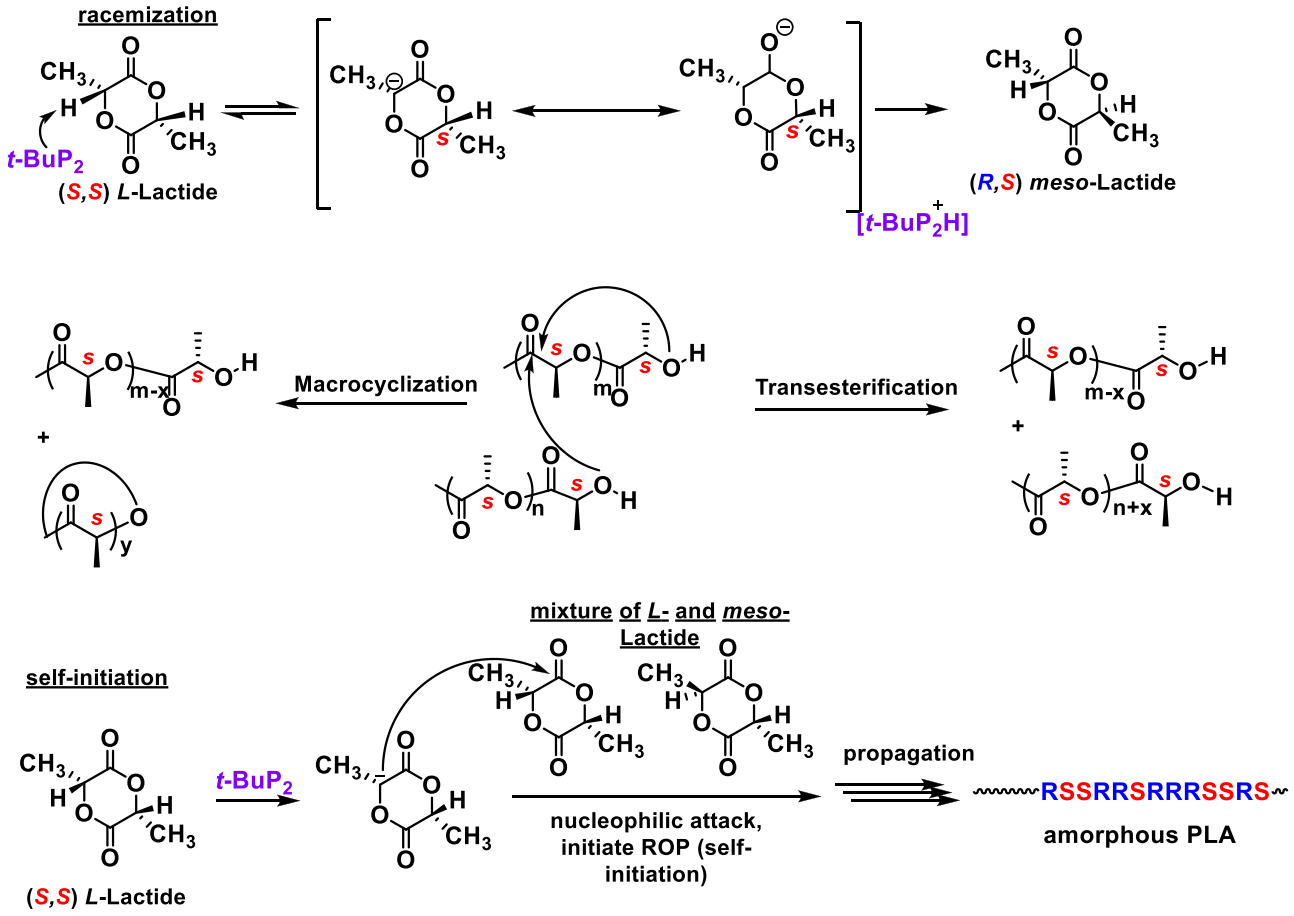

Scheme 7. Plausible side reactions occurred during the ROP of LLA catalyzed by *t*-BuP_2 in toluene at 80 °C.

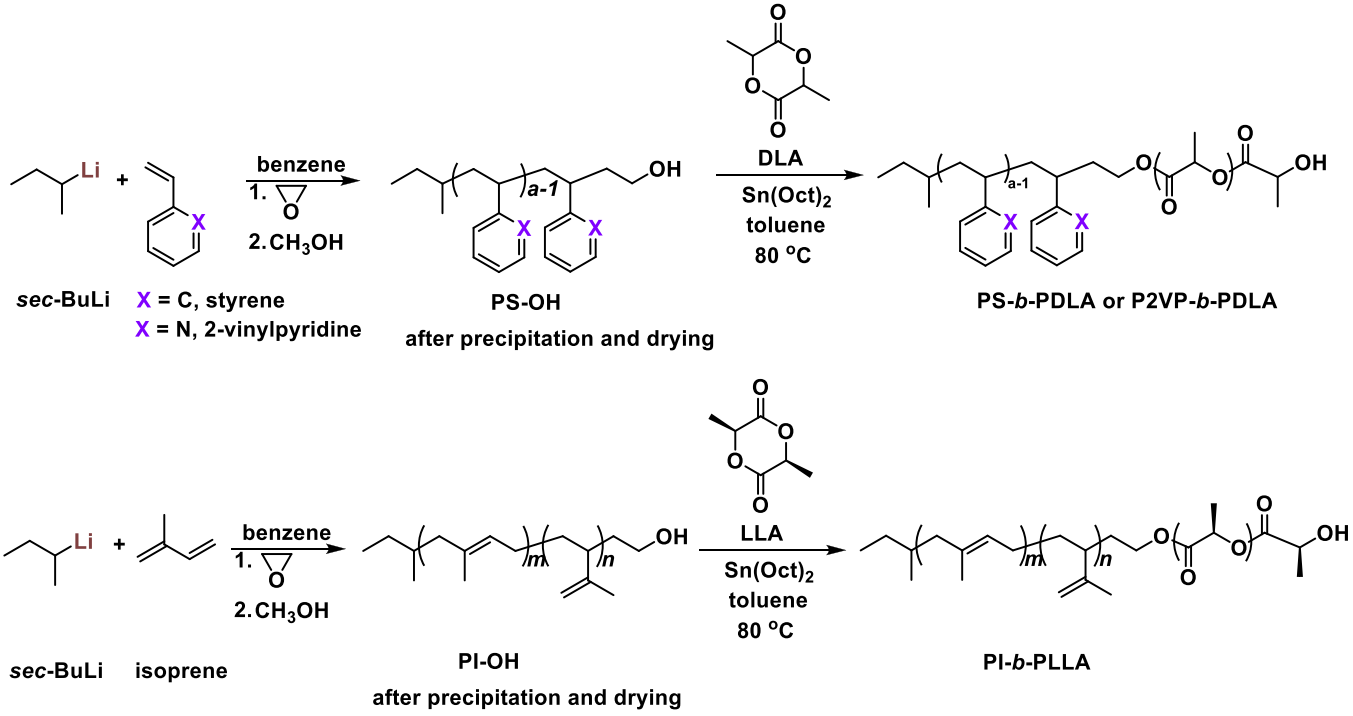

Scheme 8. Synthetic procedures to synthesize PS-PLA-sc-PI and PS-PLA-sc-P2VP triblock terpolymers.

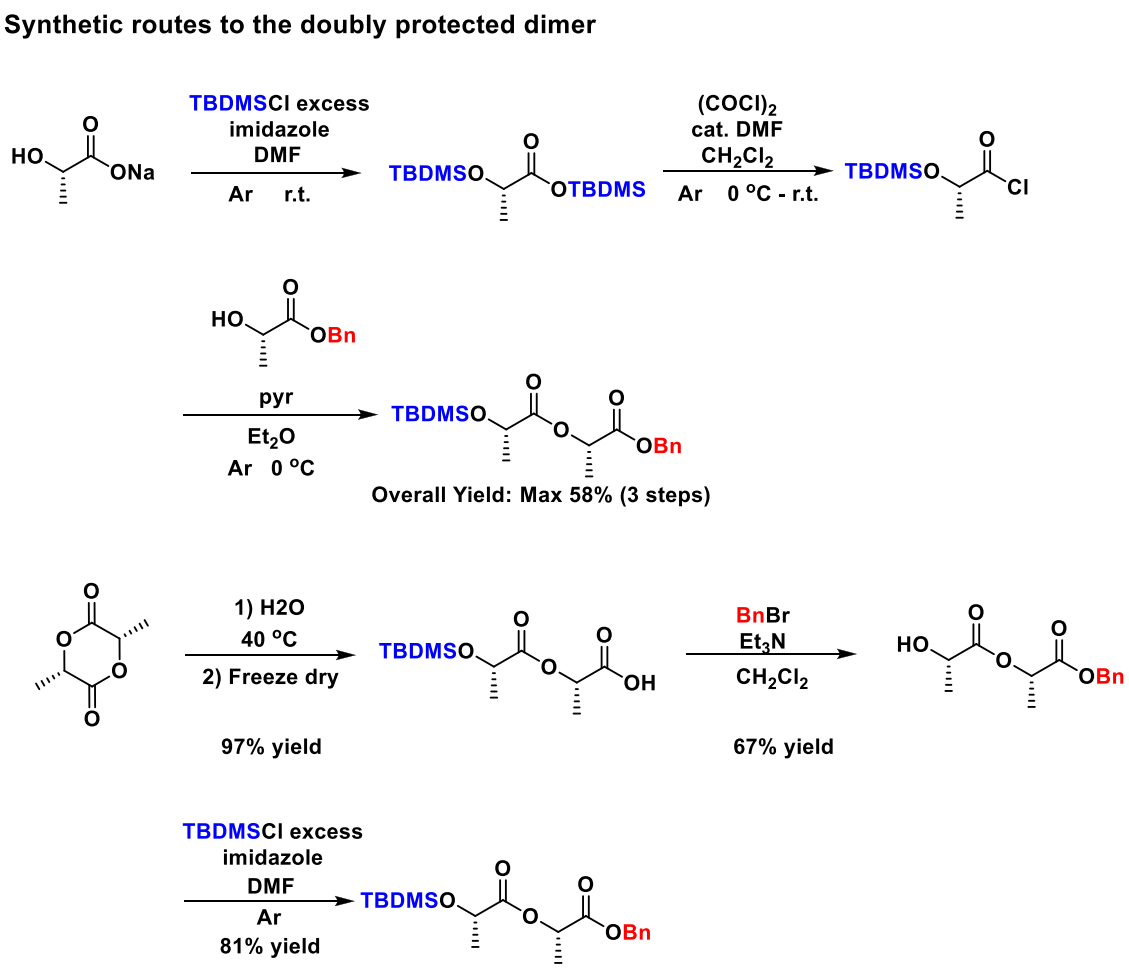

Scheme 9. Synthetic routes for the preparation of discrete oligo lactic acid.

stereocomplex of oligo L-lactic acid (*o*LLA) and oligo D-lactic acid (*o*DLA) adopts a 3_1 helix. The balance between crystallization rate, preorganization in the amorphous state, and the anticipated crystalline structure dimensions is critical for obtaining the crystallization with the least defects [128].

The chemistry developed by Hawker was further expanded by Dong and coworkers with the so-called "exponential iterative method" (Scheme 10) [129]. They showed that absolute control over the width, symmetry, molecular weight distribution, and structural heterogeneity could be achieved through the precise recombination of discrete macromolecules. Depending on crystallization temperature, *o*LLA in dispersed samples adopts distinct molecular arrangements, i.e., solid solution or segregation, due to non-uniform nucleation and growth kinetics. The blending strategy is very robust and can be extended to regulate the chain length heterogeneity of one or multiple blocks of block copolymers or polymers with complicated architectures. In principle, arbitrary distributions could be constructed at will, including those inaccessible through polymerization. Thus, it provides a unique model platform to elucidate the critical contribution of chain length heterogeneity to self-assembly and molecular dynamics, as well as the properties of polymers.

Dong and coworkers also explored the critical contribution of chain length and stoichiometry to the formation of PLA-sc [130]. They prepared PLA-sc from the combination of *o*LLA/*o*DLA mixture having 16, 20, 24, 28, 32, and 48 repeat units. The chain length and

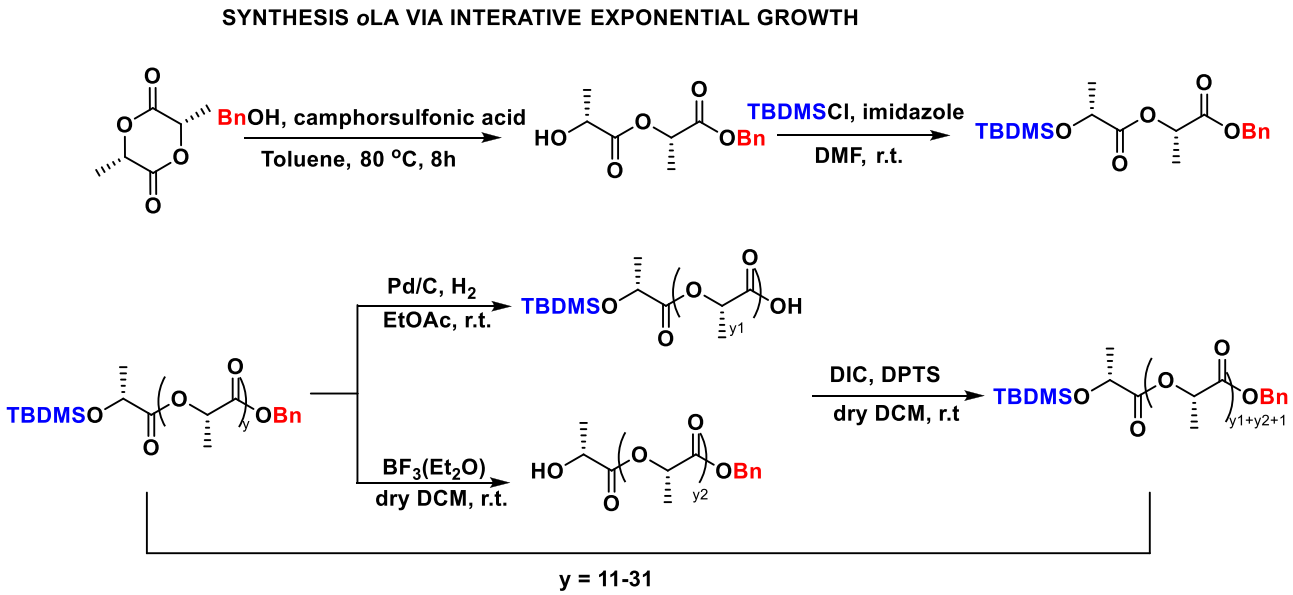

Scheme 10. Synthesis of *o*LA by exponential iterative method.

mole ratio of the enantiomeric oligomer mixtures were precisely regulated, either symmetric or non-symmetric length and composition (Fig. 4).

Four situations were studied (x1 for *o*LLA and x2 for *o*DLA):

1. If x1=x2, long-range ordered PLA-sc form with extended chain conformation.
2. If x1≤x2≤2×1, with the same composition, the mixtures form exclusively uniform PLA-sc lamellae, with only one single melting transition.
3. If x2>2×1, with the same molar composition, there will be enough room for the longer chain to accommodate more than one short enantiomer, and multicomplexation becomes possible, competitive crystallization between SC and homocrystals (HC), both SC and HC coexist.
4. If x2>2×1, but the mol of x2 is two times the mol of x2, HC could be suppressed, and PLA-sc was formed.

Meijer slightly modified Hawker's synthetic protocol in order to synthesize *o*DLA conjugated with oligodimethylsiloxane (*o*DMS). [131] First, one monomeric lactide was opened by using camphorsulfonic acid as a catalyst and benzyl alcohol as the initiator. The ω-OH terminal was protected by TBDMS to afford double-protected lactic acid. The quantity was split into two: half of them was subjected to deprotection of the α-end by removing the benzyl group using a palladium catalyst, while the other half was deprotected at the ω-end using $BF_3{\cdot}Et_2O$. These two compounds were used as the precursors to synthesize discrete oligomers *via* transesterification reaction using 1-ethyl-3-(3 dimethylaminopropyl)carbodiimide hydrochloride (EDC·HCl), and *N,N*-dimethylaminopyridinium *p*-toluene sulfonate (DPTS) as the catalysts. This strategy allows monodisperse dimer, tetramer, octamer, 16mer, 32mer, and 64mer of *o*DLA as well as the conjugation with *o*DMS oligomer to afford diblock co-oligomers, *o*DLA-*o*DMS [131].

Kim et al. reported stereopure *o*LAs, [DLA_n] and [LLA_n] synthesized by convergent synthesis using the dimers of D- or L-lactic acid having TBDMS and benzyl protective groups as the building blocks [132]. The as-synthesized [DLA_{16}] and [LLA_{16}] were orthogonally deprotected and coupled by esterification with EDC·HCl to form stereoblock PLAs, which were coupled with monomethoxy-poly(ethylene glycol) (PEG, M_n = 2000 g/mol, $Đ$ = 1.03) by esterification. [DLA_{24}] and [LLA_{24}] formed stereocomplexes in common organic solvents, which resulted in precipitation. Therefore, [LLA_{24}] was initially coupled with PEG to enhance its solubility during esterification with [DLA_{24}] to afford the desired block copolymer (Fig. 5). They found that in concentrated solutions, intermolecular sterecomplexation takes place on block copolymers of stereoblock PLA and PEG-formed planar nanostructures having unilamellar crystalline cores of stereoblock PLA and precipitated due to crystallization-driven self-assembly (CDSA). In contrast, block copolymer of PEG-*o*LLA-*o*DLA stereoblock in dilute solution undergoes intramolecular stereocomplexation due to the chain folding effect [132].

3.1.3. PLA stereocomplexes-based random and statistical copolymers

Several unprecedented random/statistical co/terpolymers containing glycolide, ethylglycolide, and trimethylene carbonate have recently been reported [133–135] In order to enable access to a series of PLA copolymers having different thermal properties while maintaining the hydrophilic to hydrophobic balance (HHB), a novel lactide isomer 3-ethyl-1,4-dioxane-2,5-dione (EtGly) was used a comonomer in the ROP of LLA (Scheme 11) [134]. The copolymerization was performed using mTBD as a catalyst and benzyl alcohol as an initiator with the initial ratio [M]/[BnOH]/[mTBD] = 100/1/1 for all the polymerizations. The $^1H^1H$– homonuclear decoupling experiment of PLLA and PEtGly reveals that PLLA synthesized under this condition is isotactic, and PEtGly is atactic. Therefore, the addition of EtGly into PLLA forms copolymers with a lower melting point. The desired T_m can be achieved by simply altering the EtGly content, while the HHB of the PLA can be maintained due to the chemical similarity of the polymer backbone.

Jandt and coworkers study the sterecomplexation of equimolar mixtures of P(dLA-*stat*-EtGly) and P(lLA-*stat*-EtGly) having 0, 5, 10, and 20 mol % EtGly contents in THF [136]. The T_m of PLA-sc decreases with increased RtGly content in the copolymers, except for the 5 mol % EtGly (observed on the third heating value). They conclude that small amounts of EtGly might not be able to suppress PLA-sc formation at all but hinder their nucleation in the melt. As a result, if small amounts of EtGly are present, fewer nuclei form from the melt but grow larger in size as they are less hindered by the competitive growth of other crystallites. This indicates that high EtGly contents result in a lower stereocomplexation rate, decreased crystallinity, and lower melting temperatures, thinner crystallites.

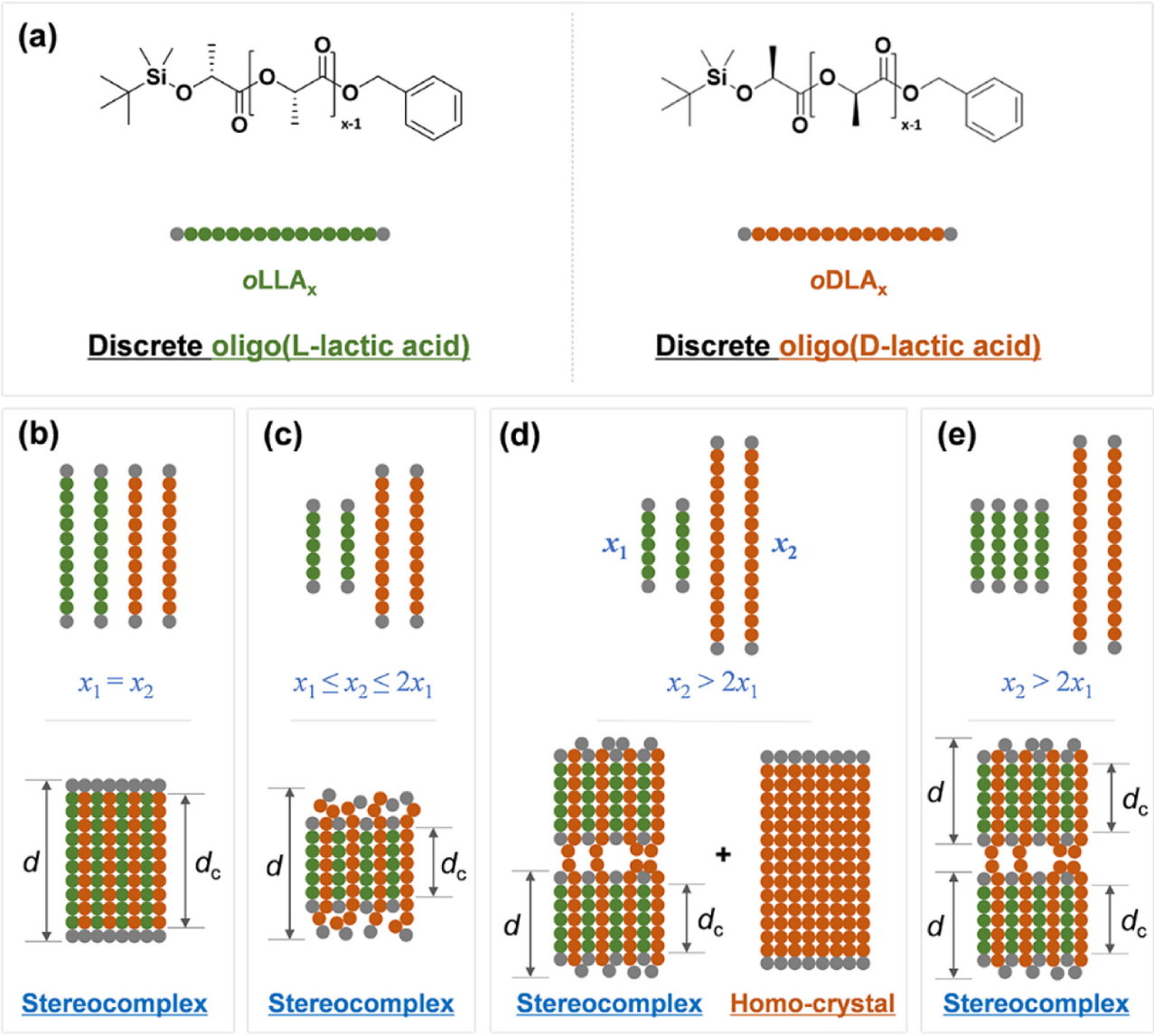

Fig. 4. Chemical structures of *o*LLA/*o*DLA (a) and proposed molecular arrangements of *o*LLA/*o*DLA mixtures with varying chain lengths and compositions (b–e). Adapted with permission from Ref. [130].

3.1.4. PLA stereocomplexes-based telechelic polymers

End-functionalizations (both at the α and ω ends) are a straightforward strategy to improve thermal stability and hydrolytic degradation of PLA and PLA-sc [137–139]. Akashi and coworkers synthesized telechelic PLA with a benzyl group at the α-end and 3,4-diacetoycinnamic acid (DACA) at the ω-end (Fig. 6) [139]. The T_{10} of the telechelic PLAs shows a significant improvement after conjugation with DACA (for example, from 326 to 355 °C), while the T_m only slightly increases compared to their corresponding ω-OH terminated PLAs. Similar increments were also observed on the T_d of PLA-sc, either from the symmetrical/asymmetrical M_n range. In contrast, the T_m of DACA- PLA-sc is lower than the T_m of PLAs, indicating the effect of the chain-end groups at the ω-terminal with DACA [138].

3.2. PLA stereocomplexes-based cyclic polymers

There are two strategies to synthesize cyclic PLA as the precursors for cyclic PLA-sc: (1) cyclization from the end-functional group of PLA and (2) ring-expansion polymerization of LA. For the first strategy, the linear PLA precursors were synthesized using primary alcohol-containing alkene or alkynyl functional groups as the initiator, with $Sn(Oct)_2$ as the catalyst [140]. The ω-end of the PLA homopolymers was modified by an esterification reaction using either 4-azidobenzoic acid, 4-(propargyloxy)benzoic acid, or 4-pentenoic acid. The resulting telechelic PLA contains an ethenyl group at the α-position and either an ethenyl or azido group at the ω-position (Scheme 12). With these precursors, two cyclic stereoblock PLAs possessing head-to-head (HH, azide-alkyne + ring-closing metathesis [RCM]) and head-to-tail (HT, azide-alkene + RCM) linkages between the PLLA and PDLA were synthesized via click chemistry (first) and then RCM (Scheme 12). The authors reported that the different linking agents, linking orientation, and the topology of the PLAs (cyclic vs. linear) affect the melting temperature of the cyclic PLA and PLA-sc [140].

On the other hand, Mehrkhodavandi and Waymouth follow the second strategy [141,142]. For instance, Waymouth and his team synthesized linear and cyclic PLAs using *N*-heterocyclic carbene-mediated ROP of either LLA or DLA [142]. The ROPs were carried out in THF at 25 °C using 1,3-dimesitylimidazol-2-ylidene (IMes, $[I]_0 = 0.006$ M) as the initiator. Benzyl alcohol (BnOH) was used as the initiator for linear PLAs. The homonuclear $^1H^1H$– decoupling

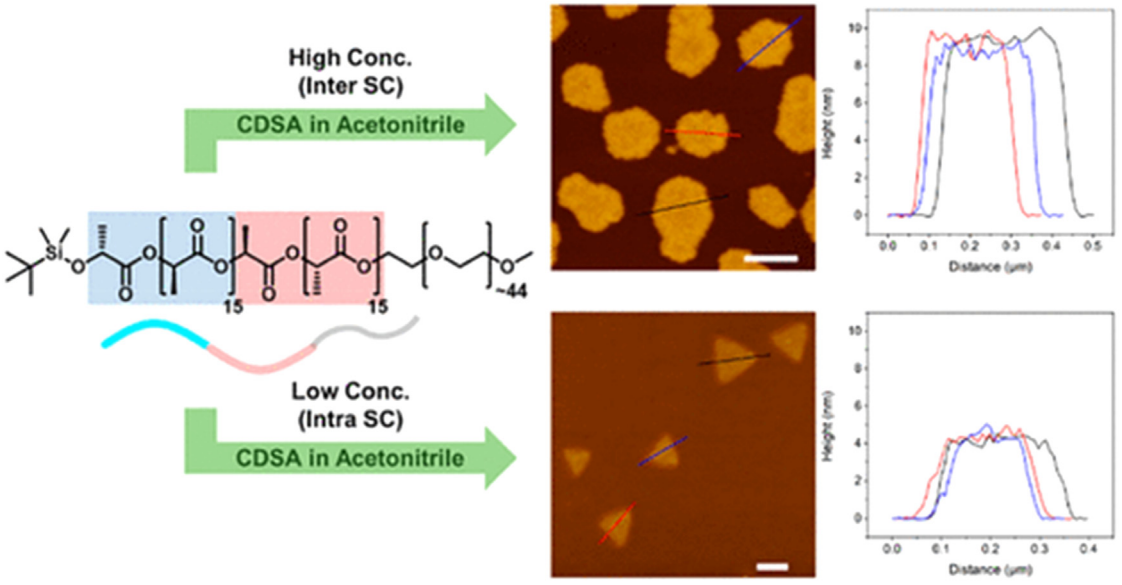

Fig. 5. Schematic representation of the intermolecular and intramolecular stereocomplexation of [DLAn]-[LLAn]-*b*-PEG. Adapted from Ref. [132].

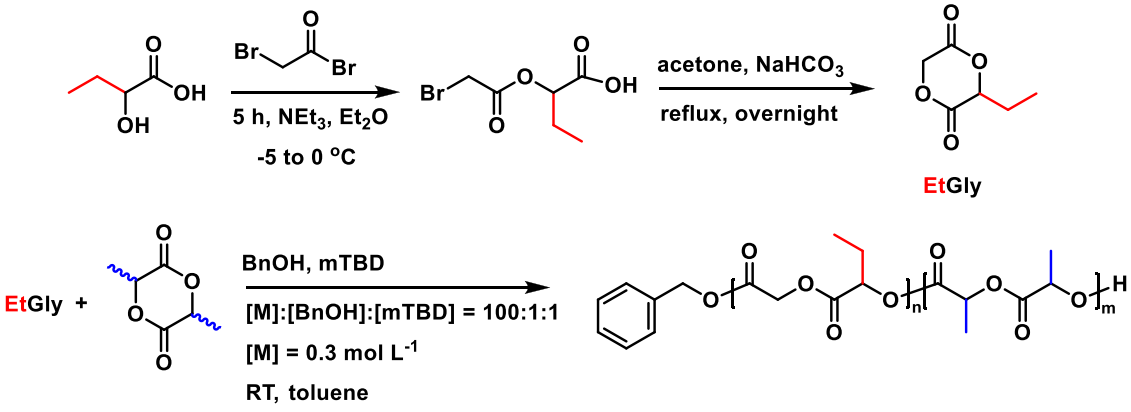

Scheme 11. Schematic representation of the synthetic pathway yielding polyesters with the same hydrophilicity as PLA.

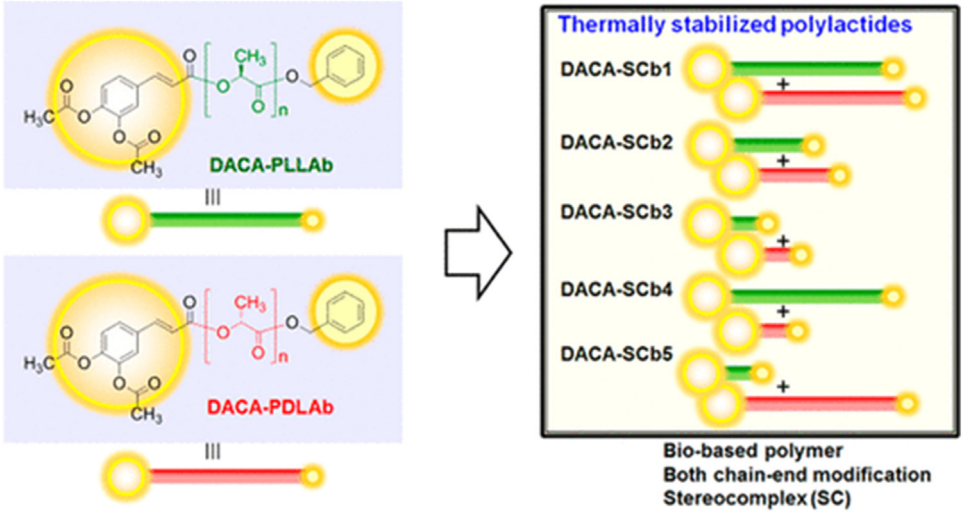

Fig. 6. Chemical structures and schematic illustration of PLA-sc formed from telechelic PLA. Adapted with permission from Ref. [139].

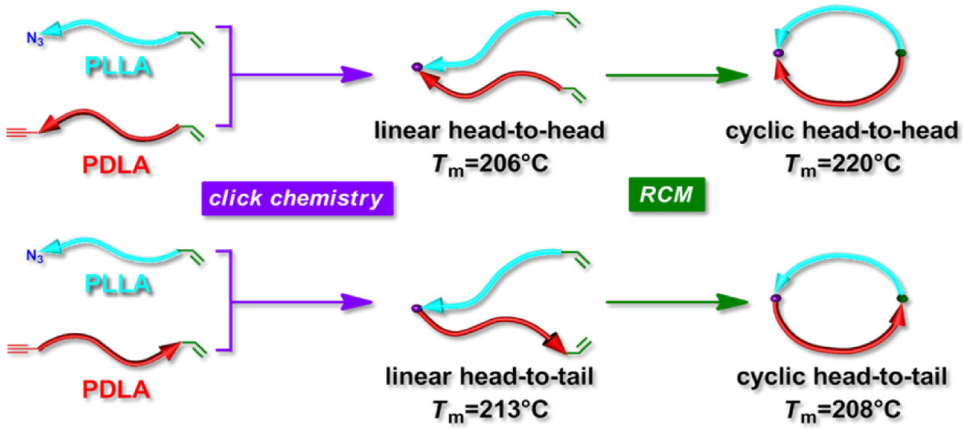

Scheme 12. Synthetic scheme of cyclic stereoblock PLAs with the HH and HT linking orientations of the enantiomeric segments. Adapted with permission from Ref. [140].

experiment reveals that the linear and cyclic PLAs have *iii* tetrad fractions around 86–89 % and 80–82 %, respectively. The corresponding PLA-sc from these precursors were prepared by solvent casting method from DCM solution (10 mg/mL). Cyclic PLAs have T_m lower than the T_m of linear PLAs. The blend of cyclic PLA+linear PLA, as well as cyclic PLLA+linear PDLA, can form PLA-sc, although the T_m value is lower than that of the PLA-sc from linear PLAs [142].

3.3. PLA stereocomplexes-based Star-shape PLA

Most of the star shape PLAs, and their corresponding stereocomplex were synthesized via ROP of multifunctional alcohols or amines (Scheme 13) catalyzed by $Sn(Oct)_2$. Some examples of the multifunctional initiators are from reduced sugar, pentaerythritol, and dipentaerythritol (6-OH groups) [143,144]. More complex initiators such as DAB-Am-32, polypropylenimine dotriacontaamine, generation 4.0 with 32 -NH 2 groups, oligooxetane with ≈13 –OH groups, hyperbranched polyester based on 2,2-bis(hydroxymethyl) propionic acid, and 2-trimethylolpropane (TMP) dendrimer, generation 3.0 terminated with 24 –OH (Scheme 13) were also reported [145].

Stereocomplexes of the linear, high molar mass PLLA and PDLA are known to be not able to reform quantitatively back from the melt in any reasonable time [146]. The ability to restore stereocomplexes during thermal treatment decreases with increasing their molar mass. It has particularly been observed that for macromolecules with M_n above ∼104 g/mol, crystallites of homochiral PLLA and PDLA components coexist with crystallites of the PLA-sc when pure stereocomplexes are melted and then crystallized once again.

Compared to their linear counterparts, the equimolar mixtures of PLA macromolecules with opposite chirality having star-shaped architectures have the advantage of fast crystallization into the stereocomplex crystallites [146,147]. It was also indicated that the mixed stereocomplexes of star-shaped and linear PLAs could be obtained under similar conditions.

It has been observed that both the low molar mass linear PLA as well as multi-arm stars with relatively short arms, when cooled continuously from the melt or heated after rapid cooling from the melt, can more easily form the PLA-sc crystallites than longer linear PLAs and star-shaped PLAs with a lower number of arms (i.e., six arms) [146–148]. This is because, in the cases of higher molar mass linear PLA and star-shaped PLAs with a lower number of arms, a considerable fraction of the homochiral crystallites has been formed. These effects are explained by differences in the mobility of polymer chains in these systems due to cooperative interactions of many helical arms in the PLA stars [146–148]. Biela reported that the equimolar mixtures of star-shaped PLLA and PDLA (composed of 6, ∼13, 24, and 32 arms) crystallize during precipitation into methanol from the DCM solution preferentially in the form of the highly crystalline (up to 70 %) stereocomplexes [149].

Tsuji and coworkers synthesized a 4-arm PLA stereoblock to study the factors that affect the crystallization and sterecomplexation of the molecules (Scheme 14) [150]. They proposed three factors affecting crystallization: 1. M_n of PDLA/PLLA block as well as M_n of 1 arm, 2. Factor A (branching or turnover points), Factor B (intersegmental connection), Factor C (presence of PLLA and PDLA segments in the same molecule), and Factor D (presence of terminal carboxyl group) [150].

Another synthetic strategy to prepare star-shaped PLA-sc is via coupling reaction of PLLA/PDLA precursors (Scheme 15). Linear, 2-arm, and 3-arm PLLA/PDLA were synthesized by organocatalytic ROP catalyzed by DBU initiated by alkyne functionalized alcohols (mono, di- and trifunctional primary alcohol) and azido functionalized alcohol for PLLA and PDLA [151]. In total, nine stereo-miktoarm and homo star-shaped PLAs were synthesized via azide-alkyne click reaction of the precursors. In the case of the click reactions between the azido-functionalized PDLA and the ethynyl-functionalized PLLAs to form stereo-miktoarm PLLAs, a mixture of CH_2Cl_2/1,1,1,3,3,3-hexafluoro-2-propanol (HFIP) has to be used as the solvent because PLA-sc immediately forms and precipitates in the reaction medium. PLA-sc powder of the linear stereoblock and stereo-miktoarm star-shaped PLAs, i.e., PLLA-*b*-PDLA, $(PLLA)_2$-*b*-$(PDLA)_2$, $(PLLA)_3$-*b*-$(PDLA)_3$, $(PLLA)_2$-*b*-PDLA, $(PLLA)_3$-*b*-PDLA, and $(PLLA)_3$-*b*-$(PDLA)_2$ was obtained by slow evaporation the solvent/mixed solvent.

Linear PLLA, linear PDLA, 4sPLLA, and 4sPDLA with the same molecular weight of each arm were synthesized via the ROP of lactides with 3-butyn-1-ol and pentaerythritol as initiators, and $Sn(Oct)_2$ as the catalyst at 115 °C in bulk [152]. The PLA-sc formed from 4sPLLA/PDLA and PLLA/4sPDLA samples showed faster crystallization and a higher degree of crystallinity than that of PLA-sc prepared from 4sPLLA/4sPDLA and PDLA/PLLA. These can be assigned due to a combined effect of higher spherulite density of star-shaped chain and excellent chain mobility of linear chain.

Other examples of star-shaped PLA-sc were prepared by Bai and coworkers. The 2-arm, 3-arm, and 4-arm stereoblock copolymers were formed during melt blending of PDLA/PLLA (50/50) with the initiators (the authors called it reactive modifiers-RMs) at a temperature of 200 °C in the presence of 0.3 % wt triethylamine as a catalyst [153]. The initiators used in this work are the epoxy group (EG) neopentyl glycol diglycidyl ether (2EG), trimethylolpropane triglycidyl ether (3EG), and pentaerythritol glycidyl ether (4EG).

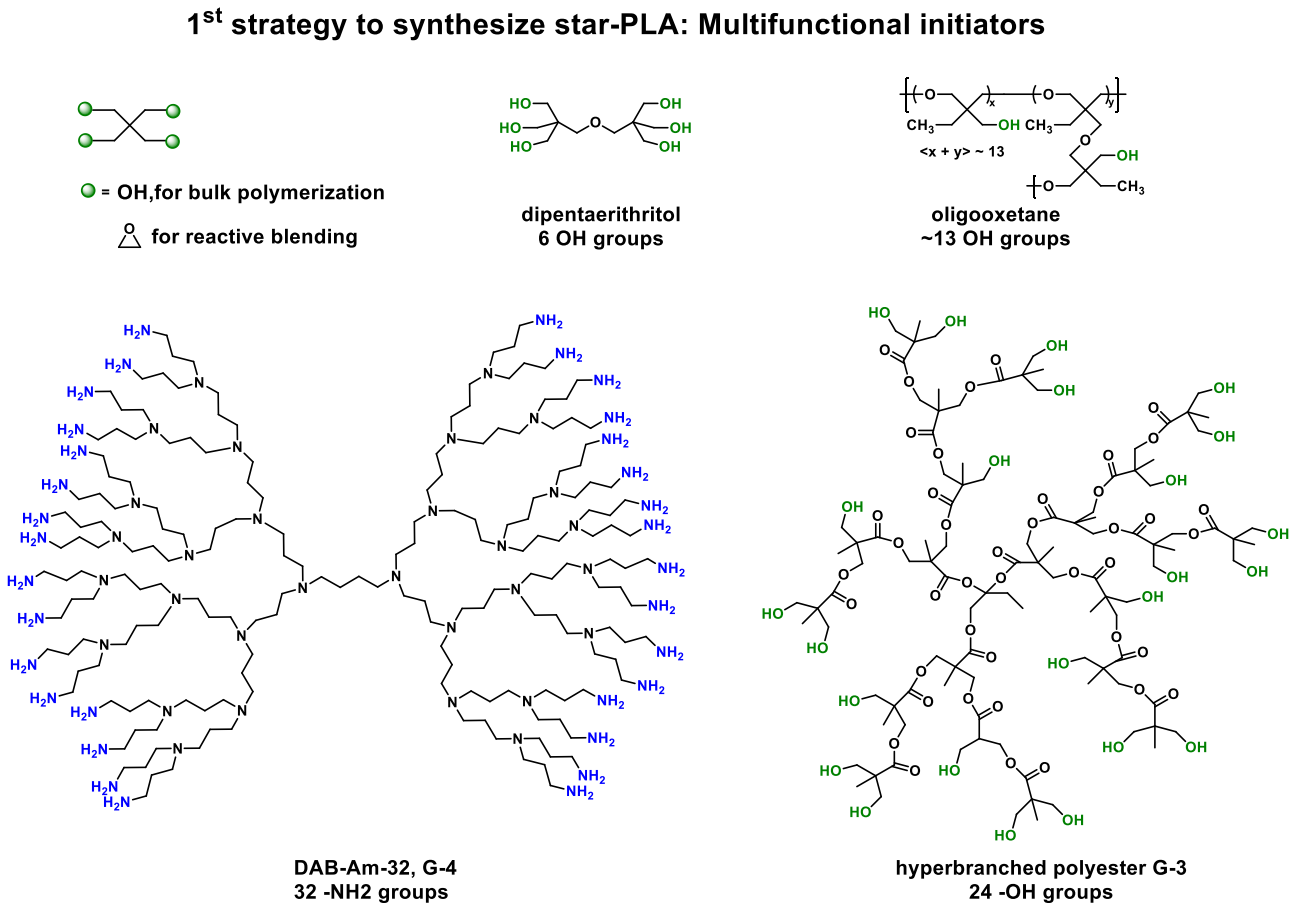

Scheme 13. Multifunctional initiators are used to synthesize multi-arm star PLA.

The occurrence of the coupling reaction between epoxy groups of the RMs and hydroxyl end groups of the PLAs was verified by FT-IR. An exclusive PLA-sc formation can be achieved in the melt-crystallized blends containing only 0.5 wt% modifiers, suggesting a strong stabilizing effect of the copolymers on the alternately arranged PLLA/PDLA chain segments in the molten state as effective compatibilizers. The generation of these copolymers does not significantly increase the melt viscosity of the racemic blends, which makes it possible to rapidly transform the blends into high-performance PLA-sc products via industrial melt processing.

3.4. PLA stereocomplexes-based brush copolymers

In 2014, Grubbs and his team synthesized PLA-containing brush copolymer via a macromonomer approach [154]. Their method involves the synthesis of norbornene macromonomer containing PLLA/PDLA via ROP of LLA/DLA initiated by *N*-(hydroxyethanyl)-*cis*-5-norbornene-*exo*-2,3-di-carboximide catalyzed by 1,3-dimesitylimidazol-2-ylidene at room temperature (Scheme 16). The resulting macromonomers containing PDLA and PLLA were polymerized via ROMP using a 3rd generation Grubbs catalyst. An equal amount of the complimentary brush polymers were mixed in dichloromethane and left dried under the air to afford PLA-sc brush copolymers. Their brief studies revealed that linear PLAs chains could interdigitate into the densely grafted molecular brush copolymers. In contrast, in the case of two brush copolymers with complementary PLAs side chains, the stereocomplexation is restricted to up to 1/3 of the whole PLA repeating unit (from the periphery) [154].

In the same year, Satoh and coworkers synthesized a series of brush random and block copolymers following the same strategy described earlier by Grubbs [155]. They prepared a pair of PLLA/PDLA macromonomers having a norbornene group at the α-end and an OH group at the ω-end (Scheme 16). Another pair was PDLA having a benzyl group at the α-end and norbornene at the ω-end. Random/block copolymerization of these macromonomers via ROMP results in brush copolymers having parallel/antiparallel PLA on the side chains. The high density of brush copolymers and good control over the molecular weight and molecular weight distribution show the versatility of the synthesis of brush copolymers via the norbornene macromonomer approach [155].

Similar to the results reported by Grubbs, Satoh and his team found that the enantiomeric mixture of brush homopolymers does not form stereocomplexes, whereas the brush copolymer immediately forms PLA-sc upon mixing without any indication of homocrystals formation during solvent evaporation. This result is slightly different from Grubbs's work which observed the partial formation of PLA-sc crystals in a mixture with PLA homocrystals. In addition, the orientation of the PLLA/PDLA chain also significantly affects the T_m of PLA-sc. The parallel orientation gave a higher T_m and crystallinity than the anti-parallel mixture.

3.5. PLA stereocomplexes-based based graft copolymers

Epoxy functionalization is the most common way to perform graft copolymerization of PLA to a backbone polymer under bulk (reactive extrusion/blending) conditions (Scheme 17). This strategy is preferred by the industry because it is simple and

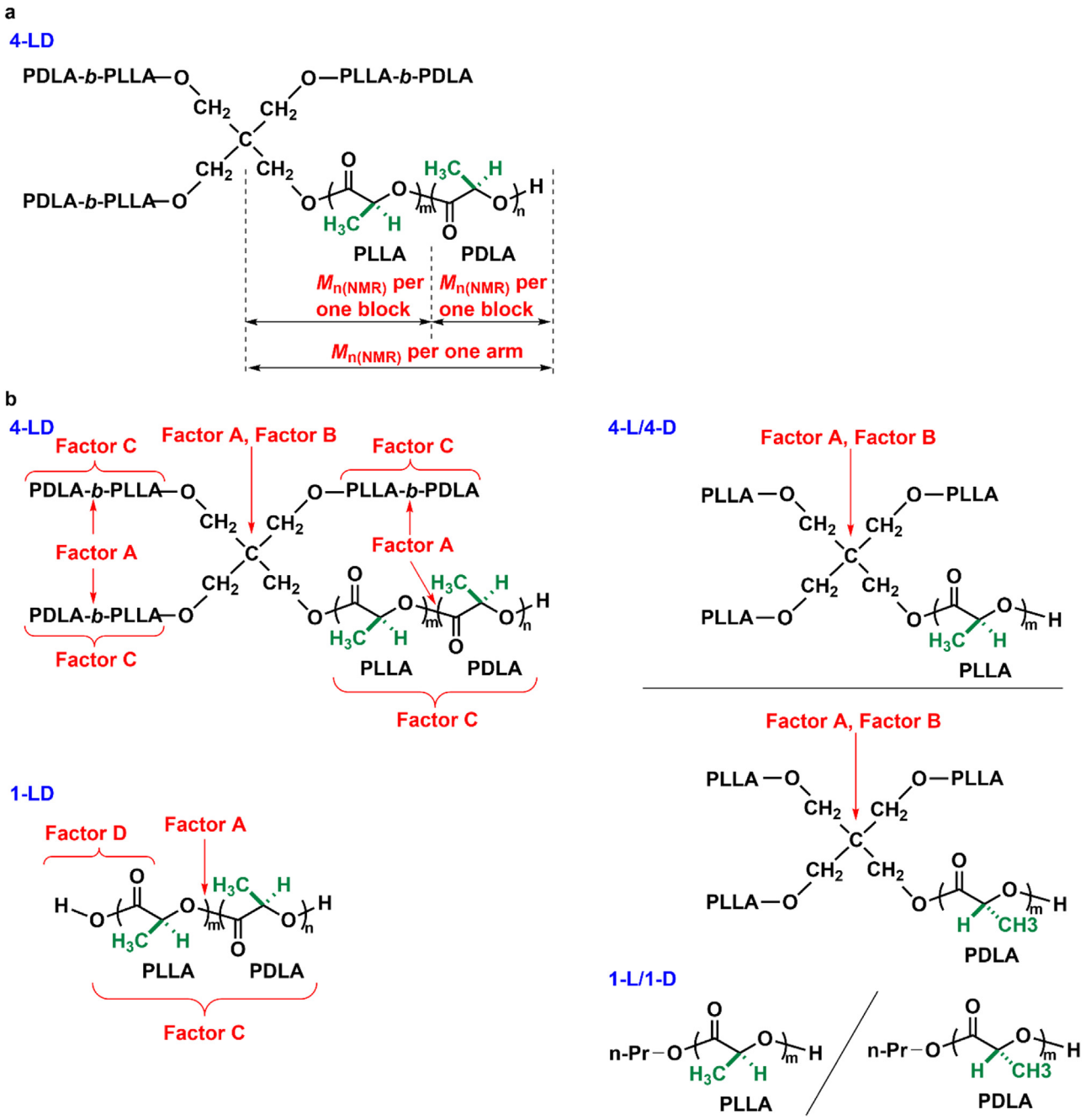

Scheme 14. Molecular structure of 4-LD, $M_{n,(NMR)}$ per one arm and $M_{n,(NMR)}$ per one block (a) and molecular structure of 4-LD, 1-LD, 4-L/4-D, and 1-L/1-D blends. Factor A (branching or turnover points), Factor B (intersegmental connection), Factor C (presence of PLLA and PDLA segments in the same molecule), and Factor D (presence of terminal carboxyl group) (b). Adapted with permission from Ref. [150].

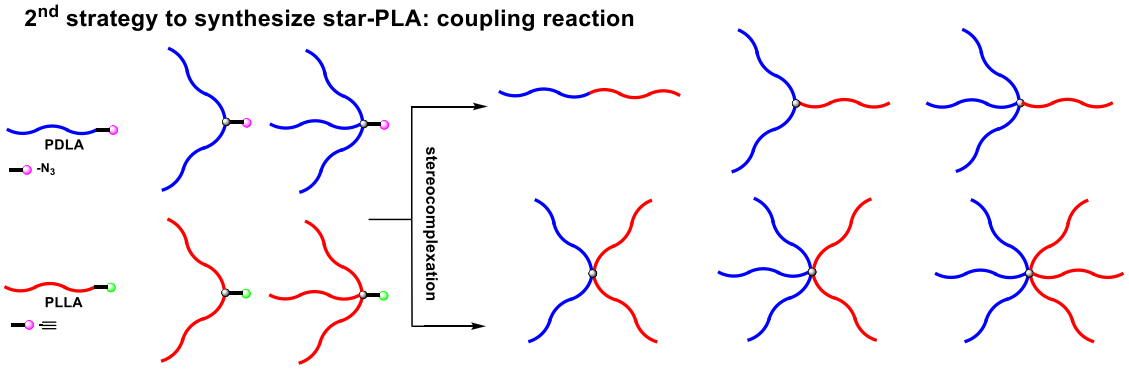

Scheme 15. Synthetic strategy for the stereo-miktoarm star-shaped PLAs as the precursors for star-shaped PLA-sc.

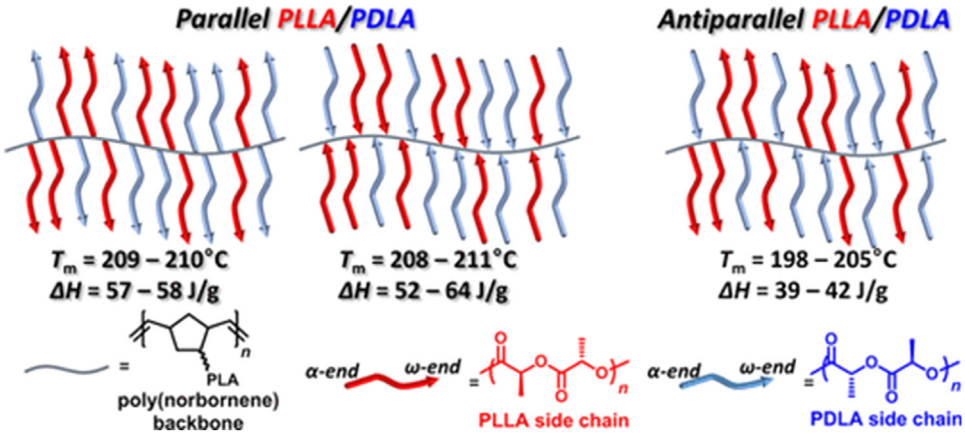

Scheme 16. Schematic representation of parallel/anti-parallel brush random/block copolymers consisting of poly(norbornene) backbone having PLLA and PDLA side chains. Reproduced from Ref. [155].

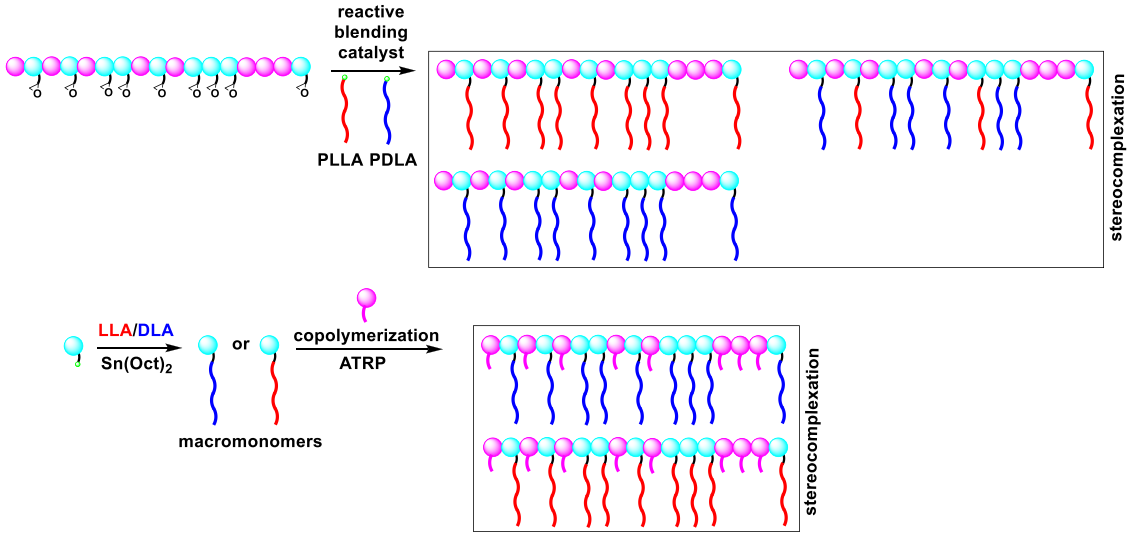

Scheme 17. Two synthetic strategies to prepare graft PLA-sc.

solvent-free. Another method to synthesize graft PLA-sc is via the macromonomer approach (Scheme 17).

Fu and his team performed an in situ grafting of poly(ethylene–methyl acrylate–glycidyl methacrylate) (PE-MA-GMA) with mixed PLLA/PDLA (50/50, w/w) in bulk [156]. The reaction was carried out through reactive melt blending using a mixer operating at 200 °C and 60 rpm for 5 min. *N,N*-dimethylstearylamine was used as the catalyst for the grafting reaction between the terminal hydroxyl groups of PLAs and epoxide groups of PE-MA-GMA. They also used a similar strategy to synthesize PLA-*graft*-epoxy-functionalized oligo(styrene-acrylic) (ESA) via reactive melt blending. The PLLA-*g*-ESA and PDLA-*g*-ESA were mixed with poly(ethylene-*co*-vinyl acetate) (EVA) to form a polymeric material with high impact toughness and heat resistance properties [157].

The reactive blending temperature plays a key role in controlling the process, and the grafting becomes predominant with increasing the blending temperature from 180 to 220 °C. Specifically, the grafting of many PLAs chains onto the PE-MA-GMA main chains can proceed before their PLA-sc crystallization at 200 °C. Thus, sufficient PE-MA-*graft*-PLA copolymers are formed in situ in the blend melts. The PE-MA-*graft*-PLA can substantially improve the melt stability of the PLA-sc matrix as an efficient compatibilizer capable of preventing the complete decoupling of PLLA and PDLA chains from their helical chain pairs by promoting the interchain interactions, which makes it possible to fabricate highly crystalline products with exclusive PLA-sc crystallites through injection molding of the PLLA/PDLA/PE-MA-GMA blends. On the other hand, some PE-MA-*graft*-PLA chains localized at the blend interface can also greatly enhance interfacial adhesion [156].

Super tough PLA was obtained synergistically using the strength of PLA-sc and the flexibility of a crosslinked network of organoalkoxysilane in the PLA matrix [158]. The PLA-sc was plasticized using in situ condensation and grafting of PLA with three different organoalkoxysilanes. The strain was improved significantly without significant loss of tensile strength or modulus. The results confirmed that PLA-grafted-3-(triethoxysilyl)propyl isocyanate (PLA-*g*-ICPTES) rubbery gel showed the highest toughness of the tested silanes. Moreover, the addition of up to 2.5 % of ICPTES showed the most promising results with an elongation at break up to 100 % without any significant loss in tensile strength or modulus, as confirmed by the mechanical tests. The characteristic enhanced thermal stability and mechanical properties of PLA-sc with improved toughness by PLA-g-silane rubbery gel make this approach viable to produce very tough PLA-based materials for many applications [158].

PLA/poly(butylene adipate-*co*-terephthalate) (PBAT) blend has high modulus, strength, flexibility, and processability. It is fully biodegradable and is suitable for environmental applications. However, their immiscibility is a drawback. Li and his team fabricated

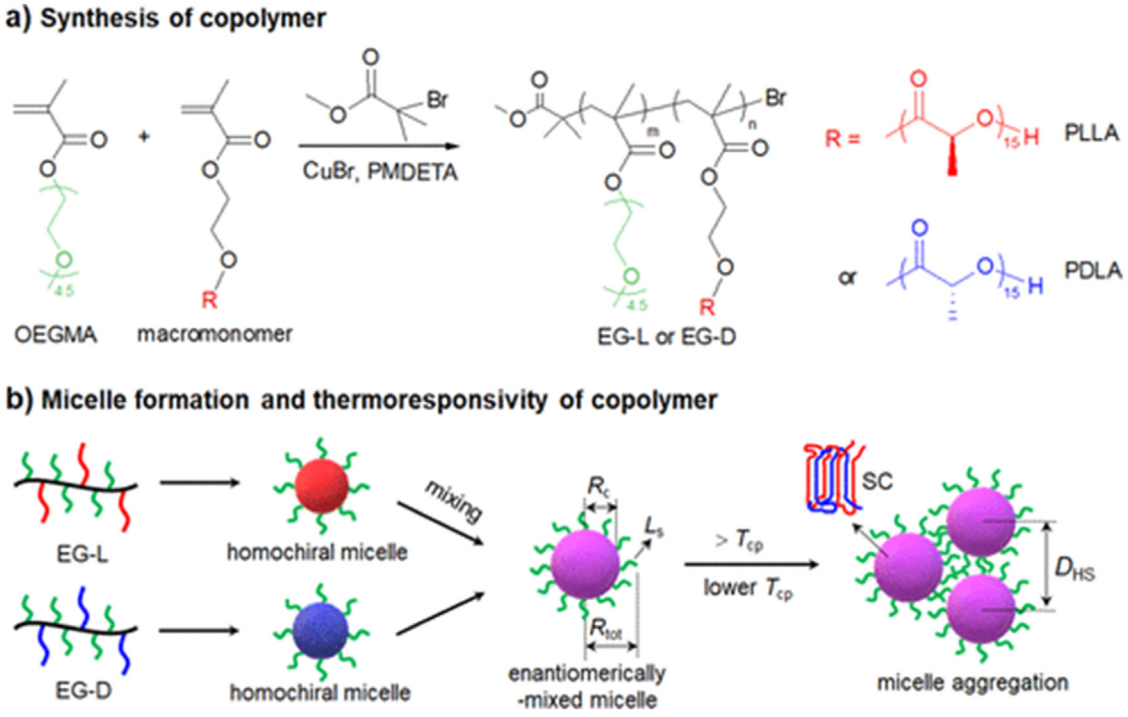

Scheme 18. (a) Synthesis of EG-L and EG-D copolymers. (b) Schematic illustration of a core-shell structure and thermally induced aggregation of EG-L/EG-D enantiomerically mixed micelles. Reproduced from Ref. [160].

a stable co-continuous PLA/PBAT (70/30) blend through reactive blending by taking advantage of the stereocomplexation of PLA [159]. A small amount of [poly(styrene-*co*-glycidyl methacrylate)-*graft*-PDLA] (SG-*g*-PDLA) was used to compatibilized PLLA/PBAT (70/30) blends. The simultaneous stereocomplexation of PLLA and PDLA grafts and the grafting reaction of PBAT leads to both compatibilization and co-continuous morphology. Such stable co-continuous blends with PLA-sc crystals exclusively located at the interface exhibit excellent mechanical properties and increase the crystallization rate of PLLA.

An example of PLA-sc based-graft copolymers via the macromonomers approach was reported by Pan et al. [160]. PLLA and PDLA macromonomers were synthesized by ROP of LLA/DLA using hydroxyl ethyl methacrylate (HEMA) as the initiator and $Sn(Oct)_2$ as the catalyst at 110 °C in toluene (Scheme 18). It was not clear whether, in this condition, the HEMA undergoes self-polymerization. Probably due to the low amount of HEMA, the self-polymerization/crosslink reaction was negligible. The HEMA functionalized PLLA/PDLA macromonomers were copolymerized with oligo(ethylene glycol) methyl ether methacrylate (OEGMA) (M_n = 300 g/mol) by ATRP, resulting in graft copolymers containing PDLA (EG-D) and PLLA (EG-L).

The graft copolymers were self-assembled to form thermoresponsive micelles in an aqueous solution. Due to an enantiomeric mixture of PDLA and PLLA in solution, the individual micelles of EG-L and EG-D merged together, forming larger and denser micelles containing PLA-sc crystals. The mass fraction of EG-D dictates the cloud point temperature of the PLA-sc [160].

3.6. PLA stereocomplexes-based pseudo polyrotaxanes

Pseudo polyrotaxanes (PPRXs) were synthesized via the stereocomplexation of the corresponding axle component (Scheme 19) [161]. The purpose is to locate the position of the bulky α-cyclodextrin (α-CD) moiety along the axle in rotaxane and conceive a new approach that an axle–axle interaction, such as PLA-sc

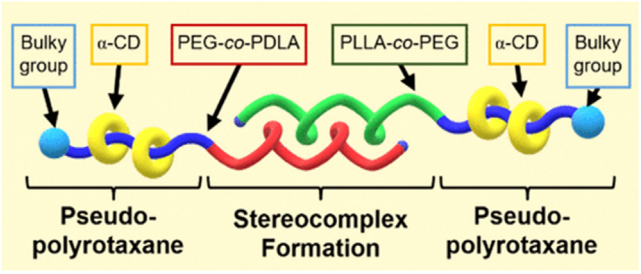

Scheme 19. Schematic illustration of PEG-PDLA and PEG-PLLA block copolymers containing bulky α-CD moiety that was used for the simultaneous formation of PPRX and PLA-sc. Adapted with permission from Ref. [161].

formation, could be utilized for the clarification of the position of the α-CD along the polymers. Three different PPRXs were prepared via the stereocomplexation of α-CD containing co/terpolymers (as the axle). The copolymers/axles in this work are (1) PDLA/PLLA-PEG-PDLA/PLLA (ABA type), (2) 3,5-dimethyl benzyl alcohol initiated PDLA/PLLA-PEG, and (3) Bn-PEG-PDLA/PLLA. Structural analyses by FT-IR and XRD revealed the SC formation of PPRXs, and thermal analyses by DSC and TGA also clarified the simultaneous formation of PPRX and PLA-sc for all the block copolymer samples. These results reveal that the α-CD is exclusively located on the PEG block, while the PDLA/PLLA block can freely form PLA-sc.

3.7. PLA stereocomplexes-based supramolecular copolymers via H-bonding motifs

The thermal stability of PLA-sc could be improved by functionalizing the α and ω end-groups of PLLA/PDLA with hydrogen bonding motifs to form supramolecular (co)polymers (Scheme 20) [162,163]. Biela and coworkers synthesize linear PDLA/PLLA using 2-ureido-4[*1H*]-pyrimidinone (UPy-OH) followed by the reaction with hexamethylene diisocyanate at 150 °C in bulk to form

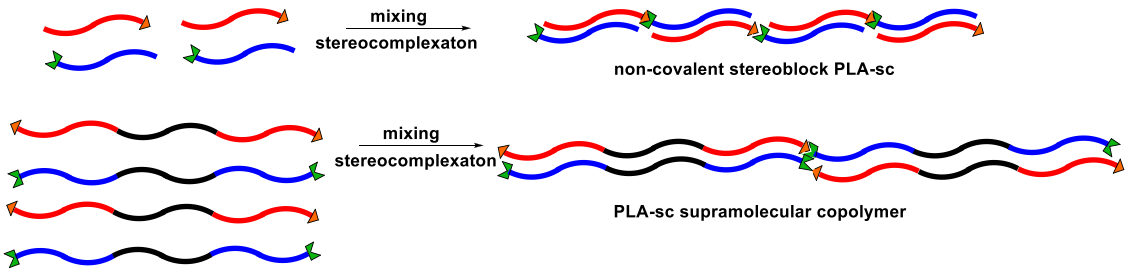

Scheme 20. Synthetic strategy to prepare PLA-sc-based supramolecular (co)polymers.

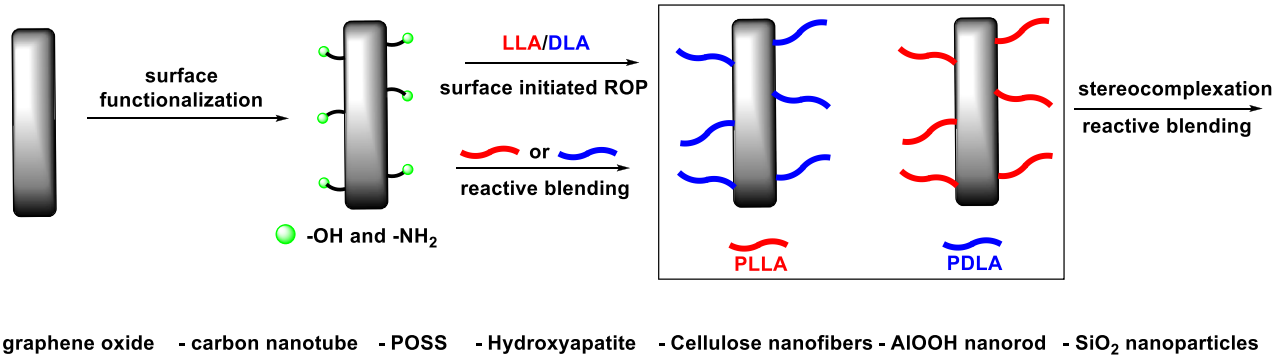

Scheme 21. The synthetic strategies to prepare PLA-sc based hybrid materials.

telechelic UPy-PDLA/PLLA-UPy. Sterecomplexation of the enantiomeric mixture of these telechelic polymers was performed in 1,4-dioxane. DSC results reveal the remarkable increase of the T_m of PLA-sc due to strong quadruple hydrogen bonding of the UPy end groups, which probably favors parallel interactions in the PLA-sc. Moreover, they demonstrated that the morphology of the obtained PLA-sc strongly depends not only on the functionalization of PLA but also on the stereocomplexation medium. PLA-sc from the monofunctionalized PLA usually form microsphere-like particles, whereas PLA-sc from telechelic-functionalized PLA exhibit a fibrous structure [162].

Pan et al. used α,ω-dihydroxy-terminated poly(ethylene-*co*-butylene) (PEB) oligomer containing 38 wt% (55 mol%) ethylene units and 62 wt% (45 mol%) butylene units as the macroinitiator for ROP of DLA/LLA [163]. The resulting PLLA-PEB-PLLA and PDLA-PEB-PDLA triblock copolymers were capped with UPy, which act as self-complementary quadruple hydrogen-bonding units. The resulting telechelic copolymers, denoted as D/L-supramolecular copolymers (D/L-SMP) are amorphous. In contrast, the enantiomeric blends of L-SMPs and D-SMPs are semi-crystalline, probably due to the simultaneous formation of supramolecular stereoblock copolymers and sterecomplexation. The mechanical and shape memory properties of the copolymers are strongly influenced by the degree of sterecomplexation of the PLAs block [163].

3.8. PLA stereocomplexes-based hybrid materials

Similar to the graft- PLA-sc, most of the work on hybrid materials based on PLA-sc follow two major strategies (Scheme 21): (1) surface functionalization of organic/inorganic materials with -OH/-HN_2 groups followed by ROP of LLA/DLA using $Sn(Oct)_2$ as the catalyst, then stereocomplexation, or (2) the grafting of PLLA/PDLA onto the surface of the functionalized organic/inorganic materials via a reactive blending process. The hybrid materials based- PLA-sc are used as filler, compatibilizer, or catalyst support for metal-catalyzed organic reactions.

3.8.1. Polyhedral oligomeric silsesquioxanes (POSS)

Aminopropyl heptaisobutyl POSS (POSS–NH_2) or trans-cyclohexanediolisobutyl POSS (POSS–OH) was added to the PLLA/PDLA solutions, and the solutions were electrospun using a conventional electrospinning system to afford PLA-sc /POSS-NH_2. $PdCl_2$ was incorporated into the resulting PLA-sc /POSS-NH_2 fibers at room temperature, and the catalytic activity of the fibers was tested in a model Heck reaction between iodobenzene and styrene. The researchers found that PLA-sc /POSS-NH_2/Pd fibers were very active in the Heck reaction, easily recovered, and reusable [164].

The addition of POSS-rubber-PDLA core-shell particles greatly toughened PLLA by an over 10-fold increase in elongation at the break while maintaining PLA's high modulus and tensile strength. The rubbery core consists of the quasi-random sequence of PCLLA copolymer synthesized by ROP with POSS as the initiator [165].

Yang used and epoxidized POSS, $POSS_{(epoxy)8}$, as the compatibilizer of PLLA/PDLA and PBAT for an adaptive 3D-printing strategy. The hierarchical crystallization and reaction in three thermal processes, filament preparation, 3D printing, and post-annealing, allowed the controlled formation of stereo-complexed crystallites and covalent coupling between $POSS_{(epoxy)8}$ and POSS- PLA-sc /PBAT resulting in simultaneous improvement in toughness and stiffness [166].

3.8.2. Cellulose/lignin

Oshima added cellulose nanofibers (CNFs) into PLLA/PDLA blends to produce highly crystalline PLA-sc and reduce the content of the homocrystal [167]. CNFs act as effective nucleating agents for PLLA/PDLA blends due to abundant hydroxyl groups on the surface that can interact with PLLA or PDLA chains. The presence of CNF not only enhanced the crystallization rate but also selectively promoted the formation of PLA-sc in PLLA/PDLA blends [167].

Incorporating the surface-grafted cellulose nanocrystals (CNCs) [168,169] and lignin [170–173] with PDLA is also an effective and sustainable way to modify PLLA for various applications. As an example, Ding et al. reported the CNCs with identical content and length of PLLA and PDLA (CNC-*g*-L and CNC-*g*-D) and blended with PLLA. The melt rheological properties and crystallization of

PLLA/CNC-*g*-D are greatly improved due to the formation of PLA-sc [168].

3.8.3. Hydroxyapatite (HAP)

HAP is a common inorganic material for bone tissue engineering [174]. Surface-initiated ROP of DLA was performed using HAP as the initiator and $Sn(Oct)_2$ as the catalyst. Using a selective laser sintering technique, the resulting HAP-g-PDLA was blended with PLLA to form a HAP-g- PLA-sc scaffold. The scaffolds demonstrated both higher tensile strength and modulus as well as better cytocompatibility [174].

3.8.4. Aluminum hydroxide (AlOH)

PLLA/PDLA (L/D) and PBSU (B) were grafted onto the epoxy-modified AlOH nanorods to afford AlOOH-*g*-(D&B) and AlOH-*g*-(L&B) [175]. The grafted AlOH nanorods particles were mixed via melt processing under optimized conditions. Through this work, the simultaneous "interfacial compatibilization" and "interfacial nucleation" of the immiscible blend nanocomposites could be achieved due to the interfacial stabilization of AlOOH nanorods as well as the in-situ formation of PLA-sc crystals (or SC) [175]. A similar strategy was also used for bone repair applications [176].

3.8.5. Carbon nanotubes (CNTs)

Multi-walled carbon nanotubes (MWCNTs) were modified with 4-aminophenethyl alcohol to afford surface-functionalized hydroxyl MWCNT (MWCNT-OH) [177]. It was used as the macroinitiator for the ROP of LLA/DLA in bulk catalyzed by $Sn(Oct)_2$ at 130 °C. The thermal stability of the high MW PLA-sc was strongly influenced by the presence of the PLA-functionalized MWCNTs, even though their concentration in the final material was as low as 0.5 wt%. For example, the T_m of PLA-sc filled with 0.5 wt% MWCNT-*g*-PLLA reaches as high as 242 °C [177].

3.8.6. Graphene oxides (GOs)

GOs are generally prepared by using Hummer's method (with slight modifications) or *via* wet ball milling to afford -OH groups on the surface [178–180]. The mixture of PLLA/PDLA (50/50) was grafted onto the surface of GOs via the solution-coagulation method. The functionalization of GOs with PLA-sc improved thermal and mechanical properties and the resistance of GOs against oxygen permeability [178–180].

3.8.7. Silica nanoparticles (SiO_2)

The silica (SiO_2) surface was coated with low molecular weight PDLA. The resulting hybrid particles were added to PLLA/PBAT blend as fillers to prepare biodegradable nanocomposites. PLA-sc formed during this process uniformly dispersed in the nanocomposites and improved their mechanical strength and toughness [181].

4. Stereocomplexes crystallization

The stereocrystals formed by the PLA stereoisomers have higher thermal stability than the α homocrystals structure. There is a general agreement that the stereocomplexes (PLAsc) are created by the assembly of PDLA and PLLA chains within a single crystalline unit cell, and the chains interact with each other through hydrogen bonding (C-H···O=C). Also, a study by Pan et al. [182] reported another type of interaction, a dipole between the PDLA and PLLA chains; these interactions generate a stronger and denser network, inducing higher stability. Additionally, the experimental evidence agrees with a faster crystallization for the stereocomplexes than the α phase of PLLA.

However, there is some debate about the crystalline structure of PDLA/PLLA stereocomplexes; how are the co-crystals formed?, is there a previous state where the chains interact within the melt? or do the interchain interactions exist only in the crystalline structure? Or must the proportion of D and L isomers be 50:50 within the crystals, or is it possible to obtain a different ratio?

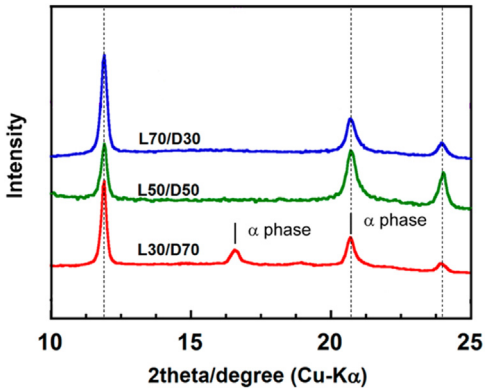

Fig. 7. WAXS diffraction pattern for the stereocomplex crystals at the indicated compositions. The discontinuous line points out the peaks related to the PLA stereocrystals (SC). Figure reproduced from: [36].

To understand the crystallization of stereocrystals (SC), the first logical step is to determine their crystalline unit cell. Fig. 7 shows a typical Wide Angle X-ray diffraction (WAXS) pattern for SC, exhibiting three characteristic peaks at 2Θ = 12, 21, and 24°. However, there are three different models for the unit cell.

Okihara et al. [183] proposed a triclinic unit cell based on X-ray diffraction data. The model suggests that PLLA and PDLA chains have a helical conformation (3/1) within the crystal, and the packing occurs with one chain, PDLA, for example, going upwards, and the other, PLLA in this case, going downwards along the c direction of the crystalline lamellae. In this work, Okihara et al. also proposed an alternative model where the chains with the same handedness at one lattice site are packed upwards and downwards in a statistically disordered manner. (See Fig. 8a and b). The dimensions of the crystalline unit cell are a = b = 0.916 nm, c = 0.870 nm, $\alpha = \beta = 109.2°$ and $\gamma = 109.8°$ and conformed by two polymer chains.

The triclinic unit cell is the most accepted for PLA SC and satisfies the experimental observation in many cases [9]. For example, Watanabe and Kumaki [184] studied the formation of SC in a Langmuir monolayer; they observed the formation of extended-chain crystals with dimensions very close to those expected for the triclinic unit cell [184].

However, Cartier et al. [185] performed an electron diffraction analysis on PLAsc single crystals. They found a hexagonal-type trigonal unit cell, where PLLA and PDLA chains were grouped by three in a molar relation 1:1. They established two modes of packing, R3c, and R$\bar{3}$c. The R3c model establishes that all the chains are packed in the same direction, upwards or downwards. On the other hand, the R$\bar{3}$c model indicates that the chains with the same handedness are statistically arranged, and the neighbor chain has the opposite direction. (See 8c and d). The cell dimensions for this model are a = b = 1.498 nm, c = 0.870 nm, $\alpha = \beta = 90°$, $\gamma = 120°$, and it has six chains per cell [185].

Both models indicated that the crystals could be formed only in a proportion of 50:50; however, recent findings suggest that the crystals could exist in a ratio ranging between 70:30 to 30:70 of D:L chains inside the stereocrystals. Tashiro et al. [10,36] proposed a third model for SC, a P3 model consisting of a disorder arrangement of the L and D isomers within the crystal. In this case, the Left (L) and Right (R) handed chains with upwards or downward directions are statistically placed. For example, in blends with a 40:60 proportion of L and D chains, it is expected that a pair

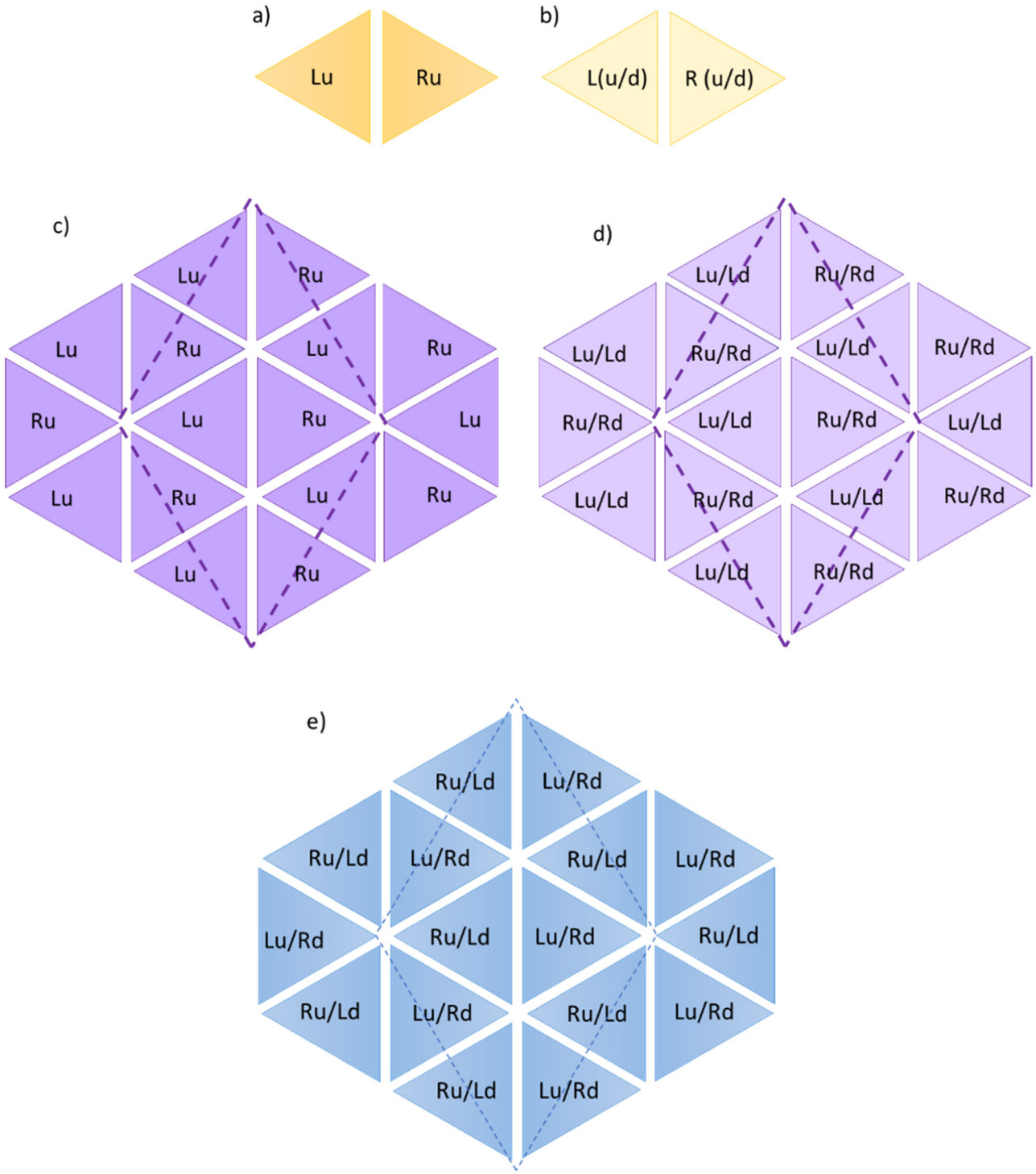

Fig. 8. Schematic representation of the stereocrystals: (a) P1, (b) P1 random, (c) R3c, (d) R3c random, (e) P3 models. Adapted from: [36].

of right-handed upwards (Ru) and left-handed upwards (Lu) is at the adjacent lattice at the same 40/60 ratio. The unit cells contain three sets of these pairs connected by a symmetric relation of the 3-fold rotation axis. (See Fig. 78e).

Tashiro et al. [10,36] supported their X-ray diffraction findings with IR circular dichroism experiments. They found that the composition in the amorphous zone and in the crystal was similar for asymmetric blends. The explanation of this finding indicates that the crystals are not necessarily composed of an equimolecular blend of L and D chains. In the case of SC obtained from the melt, the chains do not have enough mobility and time to form a perfectly equimolecular crystal when the blend is asymmetric. In this case, the melt that crystallizes in SC comprises a random number of L and D chains that crystallize together [10,36].

This model implies that SC formed by a non-equimolecular blend should have a lower melting temperature than those obtained by an equimolecular blend. Since the number of hydrogen bonds should be lower, the energy necessary to melt the crystalline arrangement should be lower too. However, a compilation of the values reported in the literature does not show a clear trend

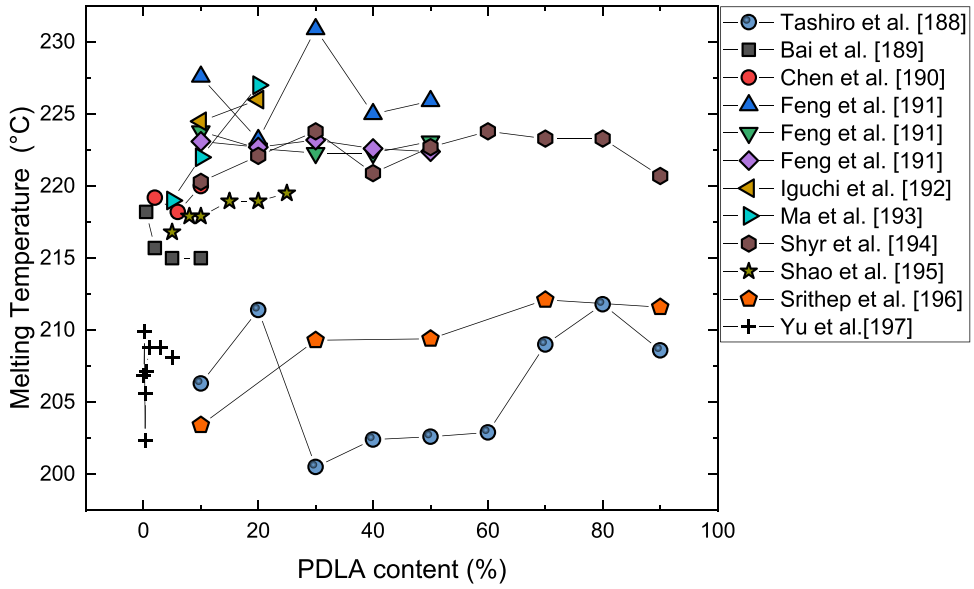

Fig. 9. Stereocrystals melting temperature versus PDLA content for the PDLA. Data extracted from [10,186–194].

of melting point with blend composition (see Table 2 and Fig. 9). The SC melting temperature randomly varies from 200 to 230 °C depending on the molecular weight, the difference between the molecular weight of the D and L components, and the preparation method. According to the thermodynamic stability and the model proposed by Tashiro et al. [10,36], the SC should reach a maximum T_m for equimolecular blends and two minimums at 70:30 and 30:70 ratio. However, as shown in Fig. 9, the experimental evidence collected in this review does not agree with this behavior, even when all the other crucial parameters, like molecular weight and preparation method, remain the same.

Even though there are some experimental evidence supporting the three models; neither of them can satisfy all the findings.

4.1. How are PLLA/PDLA stereocomplexes formed?

As was explained before, there is a general agreement about the intermolecular interactions that make the formation of stereocrystals (SC) possible, i.e., hydrogen bonds between PDLA and PLLA. However, some interactions could be present in the previous molten state before the formation of the nuclei. Henmi et al. [195] studied the formation of SC from the melt using different isothermal crystallization temperatures and monitored the melt changes employing SAXS and WAXS. PLAsc crystals or stereocrystals (SC) were exclusively obtained at temperatures between 210 and 180 °C, since 180 °C is a temperature higher than the melting point of the homocrystals (HC). However, in these conditions, a sub-micron density fluctuation in SAXS could be observed before the formation of SC nuclei. In the case of lower temperatures, where no SC were obtained, this fluctuation was absent. These density fluctuations were correlated by the authors with the formation of PLLA and PDLA intermolecular interactions in the melt. They claimed that this density fluctuation could be originated by localized interactions between PLLA and PDLA chains, possibly denoting the formation of a short-range pre-ordered state by the hydrogen-bonding-like intermolecular interactions.

Zhang et al. [196] studied the formation of hydrogen bonding within SC. The infrared analysis shows a shift in the $\nu as(CH_3)$, and $\nu(C{=}O)$ signals before the formation of SC. Also, Yang et al. [197], found evidence of hydrogen bonding formation before a mesomorphic structure is developed.

Recently, Li et al. [198] provided new evidence for the formation of intermolecular hydrogen bonds in the melt. They used a Flash DSC in a racemic blend with a molecular weight of each component of around 20 Kg/mol. In this case, two different cooling rates were employed, 2.5 and 3000 K/s, to cool the samples to a fixed isothermal crystallization temperature (100, 110, and 120 °C). The samples remained at the fixed temperature and were finally heated to 260 °C. When the samples were cooled at 2.5 K/s, SC were formed first in all the temperatures studied, however the behavior cahnged when the samples were cooled at 3000 K/s, as in this case, the SC emerged first for the higher T_c (110 and 120 °C), but for the lower one, HC were formed first (see Fig. 10a and b). The change in the emerging order was atributted to the different cooling rates.

After an FTIR analysis, see Fig. 10, it was found that hydrogen bonding formed when the sample was cooled at 2.5 K/s, even when DSC scans detected no crystallinity. This evidence indicates that a pre-ordered state in the melt exists if there is enough time for its formation. In the case of the faster scan, the molecules remain apart, and the L/D intermolecular interactions are inhibited during cooling. However, at higher temperatures, the FTIR spectra progressively changed with time, and the 908 cm^{-1} band, associated with the stereocomplexes, was present before any evidence of crystallization in the DSC.

Another finding of Li et al. [198] is that when the sample was cooled at 3000 K/s and isothermally crystallized at 100 °C, the hydrogen bonding was absent in the first 60 s, and HC were formed first. This result could lead to a fundamental conclusion, the formation of SC requires stablishing intermolecular hydrogen bonds previous to the crystallization. On the other hand, the competition between the kinetics of the formation of the hydrogen bonds in the pre-crystalline state and the crystallization of the HC, could explain the difference between the formation of SC or HC. According to these results, the kinetics of hydrogen bonds formation depends on the isothermal temperature and, for the samples studied by Li et al. [198], the hydrogen bonds form faster than the HC at 110 and 120 °C, but at 100 °C the tendency is the opposite.

In a similar work, Zhang et al. studied the isothermal crystallization of SC, and they found that a previous state exists where the chains adopt a helical conformation 10_3, and after the interaction C-H···O=C appears, and the chains change to 3_1 helical con-

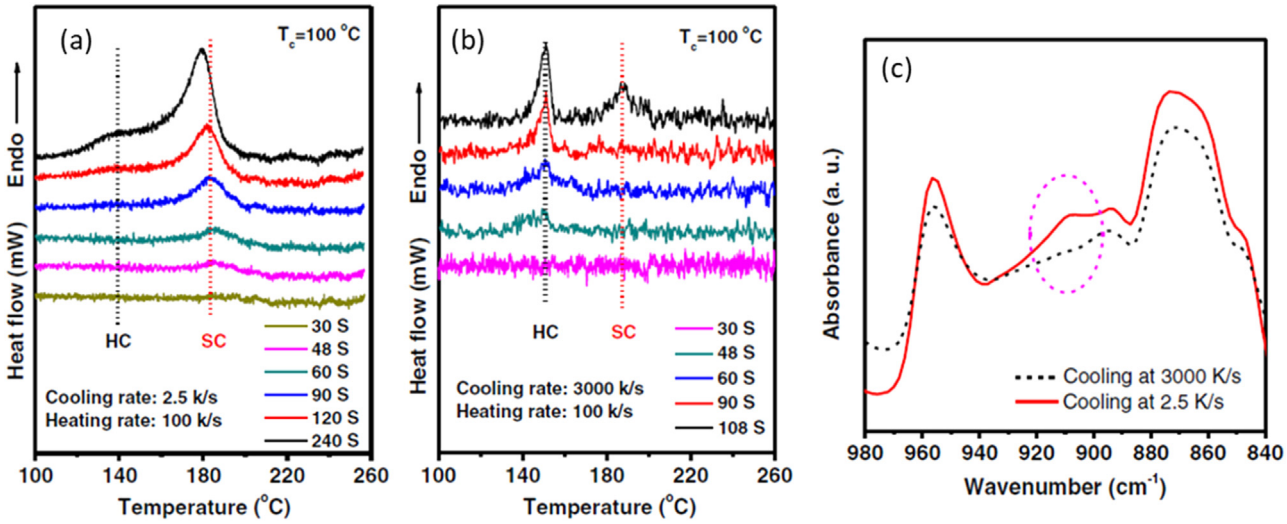

Fig. 10. (a) and (b) heating after the isothermal crystallization at the indicated conditions in a Flash DSC. (c) FTIR spectra after the cooling at 2.5 and 3000 K/s in a Flash DSC. Reproduced from [198].

formations. This confirms the necessity of the hydrogen-bond-like interaction previous to the stereocomplex crystallization [199].

The critical role of the C-H···O=C interaction is confirmed by the work of Li et al. [200,201], who studied the influence of CO_2 during the formation of SC at different temperatures. At higher temperatures, they observed a decrease in SC formation. They explain this behavior as a weakening of the C-H···O=C interaction due to the CO_2 diffusion, especially at higher temperatures.

In summary, any situation that retards the kinetics of hydrogen bond formation could originate a decrease in the amount of SC. On the contrary, if it is possible to enhance or facilitate the formation of hydrogen bonds; consequently, the amount of SC should increase.

The presence of chain interactions within the melt should be reflected in the T_g of the sample in the amorphous state. PDLA has a T_g of 65 to 72 °C and PLLA of 50 to 65 °C. According to the Fox equation, in a blend with 50/50 PDLA/PLLA, the T_g should be 57 to 68 °C; however, the value reported for the blend is 65 to 72 °C [202]. T_g depends on the chemical structure of the homopolymers, the aggregation state, and the interactions between the blend components. Since the chemical structure is unaltered and the sample is amorphous, the increase in T_g should obey to the interactions of the stereoisomers within the blend.

Some authors speculate about the influence of T_g in the formation of SC during isothermal crystallization studies [195,203]. They attribute the lack of SC at low temperatures to the high T_g of PLAs, as the chains that have to establish intermolecular interactions are not mobile enough to start the co-crystallization process. On the other hand, the chains free from those interactions could crystallize and form HC. This suggestion implies that the melt is not homogeneous, and there are domains where the PDLA and PLLA chains are close enough to form these secondary bonds, however, there should be other domains of neat PDLA and PLLA. (See Fig. 11).

Liu et al. [204] studied the effect of a homogeneous melt on the formation of SC in high molecular weight samples. They prepared glassy films employing solvent casting and spin-coating methods. In general, they found that the samples with a high speed of evaporation (spin-coating) led to a homogeneous melt, and the formation of SC was always present even at low crystallization temperatures. On the contrary, low evaporation rates resulted in phase separation, and in the formation of homocrystals. This study could help understanding what happens in the systems with lower molecular weight. It is possible to think that phase separation is incomplete, and three types of domains exist, one for each homopolymer and one where the PLLA and PDLA are together. A detailed study of the glass transition could lead to some clarification on this matter. In summary, the observations related to SC formation indicate that:

- The intermolecular interactions or hydrogen bonding between PDLA and PLLA could be present prior to SC formation. Without these interactions, it is not possible to form SC.
- To originate the interactions, the melt or the glassy state should be homogeneous (i.e., a single phase melt or single phase amorphous state) before SC formation or the material should at least have domains where the stereoisomer forming chains are together in single phase rich regions.
- In asymmetric PDLA/PLLA blends, the probability of finding the domains where the stereoisomers interact is lower than in the symmetric ones, originating a lower crystallization degree in that samples, also favoring the formation of HC.

4.2. Crystallization kinetics

Few studies have been performed on the crystallization kinetics of PLAsc stereocrystals (SC). The reason for this is that the high temperatures needed to melt SC will trigger hydrolytic degradation, modifying the crystallization behavior of the samples. Fig. 12 shows a series of melting peaks for an equimolecular blend of PDLA/PLLA with low molecular weights (9600 and 8600 g/mol, respectively). SC were melted at 225 °C for 3 min, followed by cooling at 20 °C/min to 25 °C and heating to 225 °C. The procedure was repeated five times.

According to Fig. 12, the sample exhibits different melting behavior in each step, which could be explained by degradation. In this case, it is important to use samples with SC only once or at least with the same thermal history to compare the obtained results. We present here original data that comes from previously unpublished studies by the authors of the present work, where the samples were employed only once. Fig. 13a shows the spherulitic growth rate of St_1 stereocomplex in comparison with homo crystals of PLLA formed by $LL^{8.6}$. Since the isothermal crystallization temperature is higher for the SC, it is not possible to do a direct comparison of G values. However, it is possible to observe that the value of G_{max} for SC is much higher than the value achieved by HC. That is to say, the spherulitic growth rate for SC is much

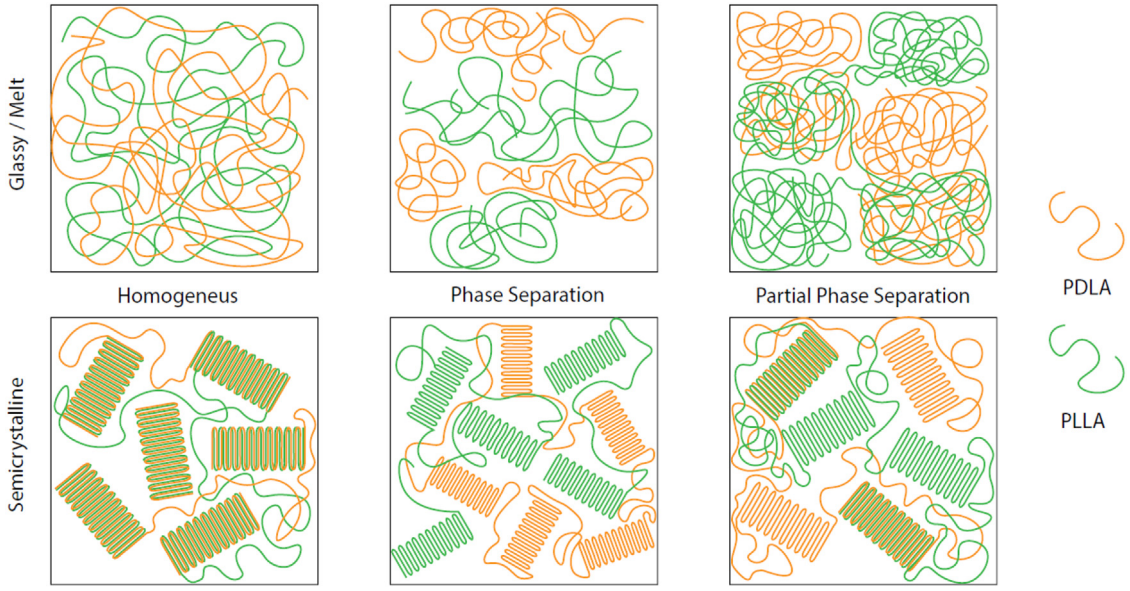

Fig. 11. Schematic representation of (a) homogenous blend, (b) phase separation, (c) partial phase separation during stereocomplex crystallization. Adapted from: [204].

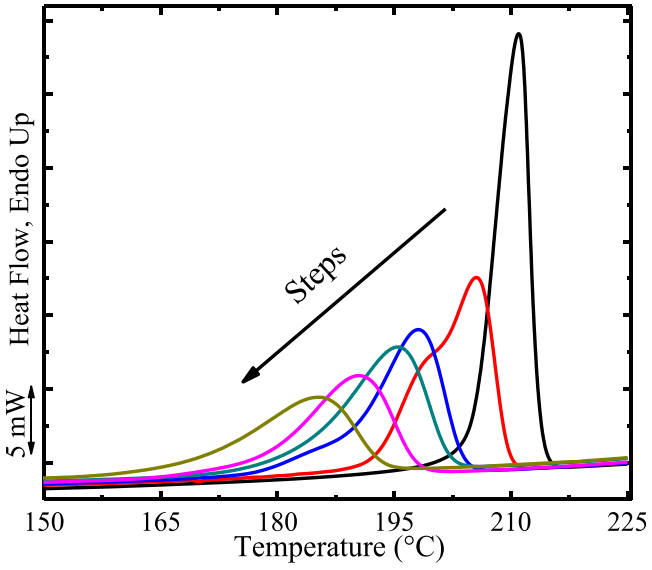

Fig. 12. DSC heating scans for one SC sample after 1 to 5 steps of erasing thermal history followed by cooling.

faster than that for HC. Similar G values have been reported for SC [152,187,191,205–207], also the difference between G values of the HC and SC was reported in the early works of Bouapao and Tsuji [208].

On the other hand, Fig. 13b shows the behavior of the overall crystallization rate as a function of isothermal crystallization temperature. Similarly, the crystallization cannot be compared at identical Tc values due to the difference in the isothermal crystallization temperature range for SC and HC. However, the SC can achieve values of $1/\tau^{1/2}$ (an experimental measure of the overall crystallization rate, which amounts to the inverse of the relative half-crystallization time) higher than those for HC. According to these results, the overall crystallization rate is faster for the SC than for HC. It is important to mention that this behavior depends on the stereocomplex preparation conditions, the molecular weight of the PLLA and PDLA, and the composition. The data presented in Fig. 13 is obtained by direct crystallization from the isotropic melt.

At temperatures higher than the melting point of the homocrystals (HC), the stereocrystals (SC) can crystallize without competition. However, there is competition in the nucleation and growth of the SC and HC at lower temperatures. As was previously mentioned, T_g in the PLLA/PDLA blend is higher than in neat PLLA or PDLA, which could result from the formation of hydrogen bond intermolecular interactions between the enantiomers. This interaction will increase T_g and retard the crystallization of SC at a lower temperature. According to the experimental evidence shown by Lv et al. [203], HC crystallize first at lower temperatures, followed by SC crystallization. In Fig. 14, it is possible to observe a schematic representation of the crystallization rate for HC and SC as a function of the isothermal crystallization temperature. The classic bell shape curve is used to explain the expected behavior. At lower temperatures, near the T_g reported for the blend, the PLLA/PDLA chains have restricted mobility and, consequently, a lower crystallization rate. On the other hand, the PLLA or PDLA neat homopolymers have higher mobility and faster crystallization at those temperatures. Increasing the temperature would increase the mobility of the PLLA/PDLA blend. However, the PLLA or PDLA homopolymer will be near or above their melting temperature, and in consequence, the stability of the crystal embryos would be too low, and the crystallization would be extremely low or even impossible.

Hu et al. [209] studied the spherulite formation in an asymmetrical blend of PLLA/PDLA, with a molecular weight of 1.1×10^5 g/mol. At 100 °C, the SC were formed first; it is possible that for this specific system, the curves schematized in Fig. 14 cross at some point below 100 °C, and the crystallization rate of the SC is higher than that of the HC. In general, the order of crystallization will depend on the relationship between the glass transition temperature and the melting temperature of each system. It is expected that HC will crystallize first at lower temperatures, and at higher temperatures, the SC will exhibit a faster crystallization rate.

The Avrami fit has been applied to SC overall crystallization rate data, and the values obtained for the Avrami index, n, are between 0.81 and 3.98, however, the most common values are around 2 to 2.5 [152,210–218]. In most cases, the reported values do not correspond with the spherulitic morphology commonly observed in SC, indicating that the Avrami theory does not predict the morphology

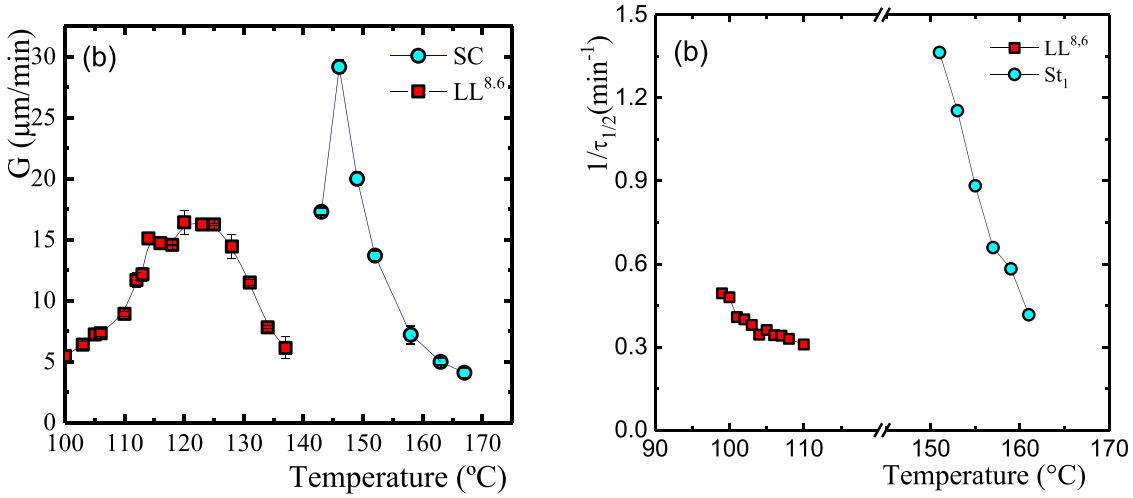

Fig. 13. (a) Spherulitic growing rate and (b) Overall crystallization rate versus isothermal crystallization temperature of the PLAsc St_1 and the $LL_{8.6}$.

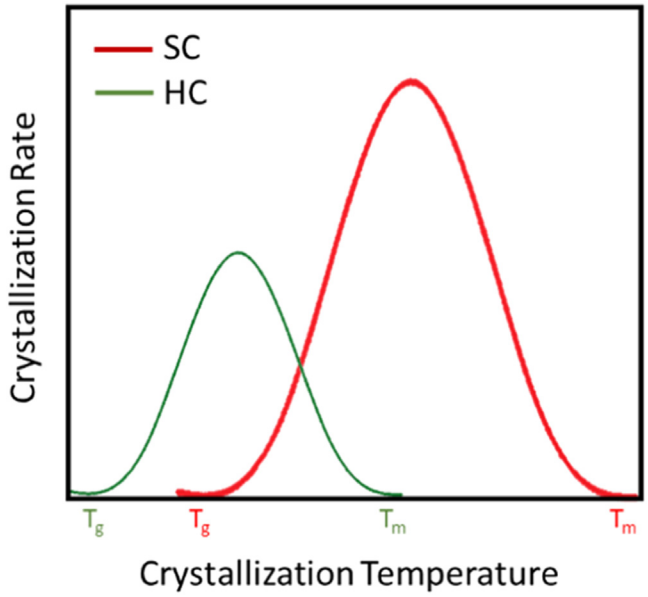

Fig. 14. Schematic representation of the crystallization rate versus isothermal crystallization rate for the SC and HC.

of SC superstructural crystallization. However, the fit of the experimental curves are good. As discussed in the following sections, different parameters influence the crystallization kinetics, like molecular weight, composition, architecture, and additives.

4.3. Molecular weight

The influence of molecular weight on the formation of the SC was reported by Ikada et al. [219] According to their studies, a molecular weight increase affects the amount of SC obtained. For molecular weights higher than 1×10^5 g/mol the SC formation is, in most cases, restricted, and only HC are present in the PDLA/PLLA blends. The melting temperature is independent of the molecular weight, as expected for polymers above a certain Mw. On the other hand, the crystallization degree decreases with the increase in molecular weight. Fig. 15 shows the variation of the crystallinity degree of PLAsc with the molecular weight. The works shown here correspond to symmetrical racemic blends of homopolymers (PDLA/PLLA), where the authors employed different molecular weights without changing any other parameter. The X_c was obtained by DSC non-isothermal tests.

In Fig. 15, it is possible to observe, in almost all the cases, a reduction in X_c with the increase in the Mw; the values are different since other conditions, such as preparation methods, solvents, and concentration, among others, are different for each system. Two main explanations for this behavior are reported in the literature:

1. Phase separation during the evaporation process,
2. A decrease in molecular mobility due to the molecular weight increase which difficults chain diffusion and the crystallization process.

For stereocomplexes prepared from solution, there will be an interaction between the polymer chains and solvent molecules. These dilute solutions undergo an evaporation process to eliminate the solvent and obtain the polymer blend. In the case of the system PDLA/PLLA/solvent, at a high solvent concentration, the predominant interaction should be solvent/PDLA, and solvent/PLLA, in this condition, it is statistically unlikely to have interactions between PLLA and PDLA. However, when the amount of solvent is reduced, the PLLA/PDLA interactions are more probable, then at some point, where the majority of the system is PLLA and PDLA chains, it is possible to get a phase separation of PLLA and PDLA, forming different domains within the system. The main question is why the PLLA/PDLA blends undergo phase separation; the argument is that phase separation is more probable for macromolecules with higher molecular weights [226]. This phase separation could explain why in high molecular weight blends, the formation of a uniform film is not possible under certain conditions, and in consequence, the SC formation is hindered. Based on this argument, it will be possible to establish that if the phase separation is avoided, SC will be obtained independently of the molecular weight [9,204].

Liu et al. [204] studied PLLA/PDLA blends employing different film preparation conditions. The main difference was the rate of solvent evaporation. They found that if the solvent evaporation was fast enough, the PDLA and PLLA remained randomly distributed within the glassy film, and phase separation was avoided entirely. Under those conditions, only SC were obtained, even with a high molecular weight (Mw $\approx 3.4 \times 10^5$ Da). Fig. 16 shows the AFM images of the samples prepared by spin coating at 20 mg/L at 6000 rpm (i.e., fast evaporation method) and by solvent casting with a 10 mg/ml concentration (i.e., slow evaporation method).

Fig. 16 shows a clear phase separation when the preparation method is solvent casting. On the other hand, the quick evap-

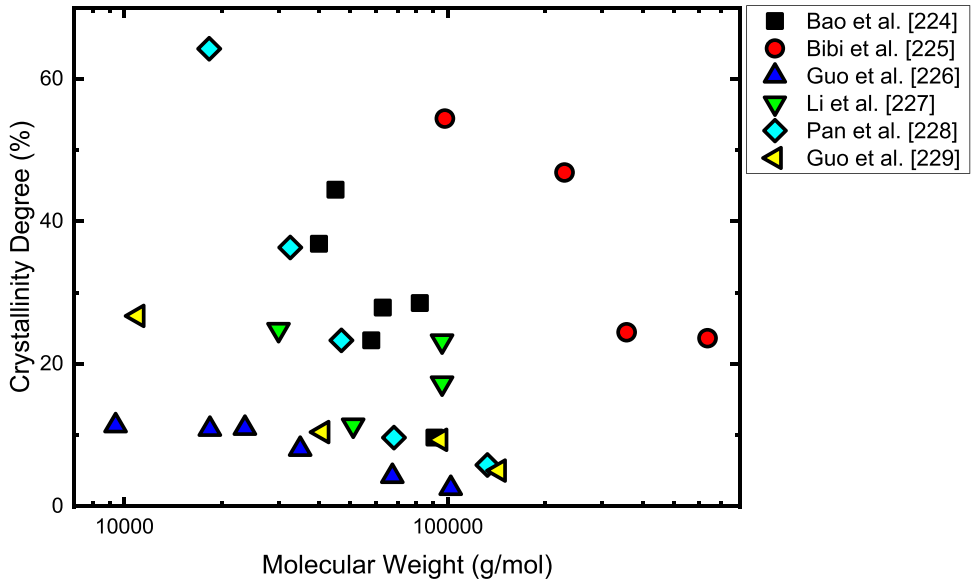

Fig. 15. Variation of the crystallinity degree versus molecular weight for the homopolymer/homopolymer PDLA/PLLA stereocomplexes. Data extracted from [220–225].

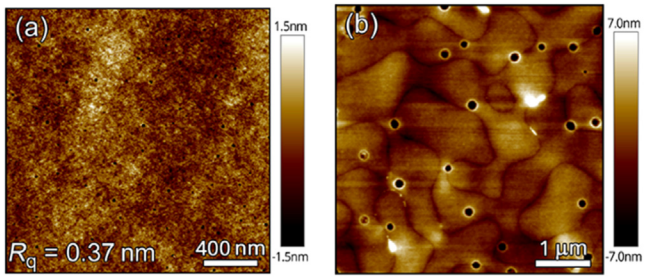

Fig. 16. AFM height images of PDLA/PLLA equimolecular blend prepared by (a) spin-coating at 6000 rpm and 20 mg/ml in CH_2Cl_2. (b) Solvent casting with a concentration of 10 mg/ml in CH_2Cl_2. Reproduced from [204].

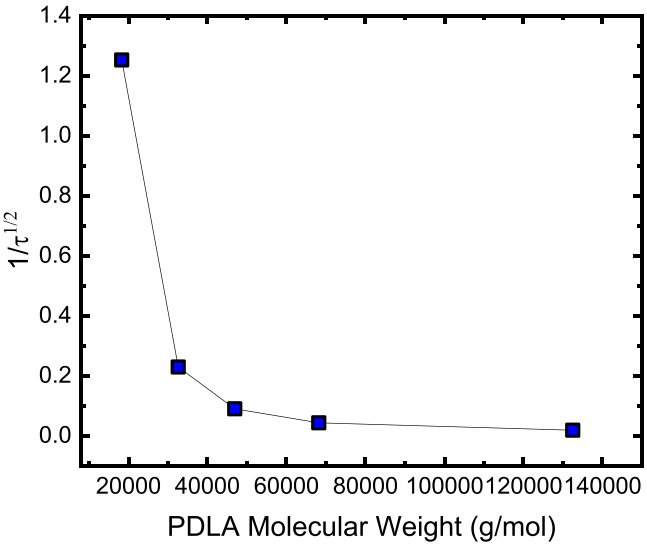

Fig. 17. Variation of $1/\tau^{1/2}$at 160 °C with molecular weight for PLLA/PDLA racemic blends, data obtained from [224].

oration of the solvent provided by spin coating leads to a uniform film. In the case of spin-coating at high velocity, the PDLA and PLLA molecules could form the intermolecular interactions required before the formation of the SC. As a result, the only crystals present in this fast spin-coated sample were the SC at the conditions studied by the authors. However, in the case of solvent casting or low-speed spin coating, phase separation takes place, and HC are predominant. This study evidences that phase separation could be responsible for the lack of SC in a high molecular weight PLA racemic blend.

Forming SC from a homogeneous melt is possible if the cooling process is fast enough to avoid phase separation. The cooling rates of the standard methods of plastic processing are high. Consequently, the conditions obtained during melt blending are expected to remain at the beginning of the cooling process. Some studies report the formation of SC during the injection molding [157,193,227–240] and extrusion [241–248], even with a molecular weight of 1.72 × 10^5 and 1.85 × 10^5 g/mol for PLLA and PDLA, respectively [232]. However, a detailed study of the influence of molecular weight on SC formation during injection molding or extrusion has not been performed yet.

Another important factor in SC formation is molecular mobility. It is widely known that an increase in molecular weight will affect a polymeric crystal's primary nucleation and growth. High molecular weights implies many entanglements, a high viscosity, and a decrease in the crystallization degree [249]. In the case of PDLA/PLLA stereocomplexes, the effect of chain mobility on SC formation is more important than in a homocrystalization process. As two individual polymer chains, one of PLLA and the other of PDLA, must crystallize together, very fast chain diffusion (i.e., high molecular mobility) is necessary. Experimental evidence on the change in the crystallization kinetics of SC formation with different molecular weights confirms this assumption [224].

Pan et al. [224] studied the racemic blend of PLLA/PDLA with molecular weights from 1.8 × 10^4 g/mol to 1.9 × 10^5 g/mol for PLLA, and from 2.2 × 10^4 g/mol to 1.9 × 10^5 g/mol for PDLA. They studied the isothermal melt crystallization and found a clear dependence of $\tau^{1/2}$ with the molecular weight. A lower value of $\tau^{1/2}$ was obtained for the stereocomplex with a PLLA molecular weight of 1.8 × 10^4 g/mol. Fig. 17 shows how the inverse of the half-crystallization time, $1/\tau^{1/2}$, at 160 °C varies with the molecular weight. A clear decrease of the overall crystallization rate (i.e., $1/\tau^{1/2}$) with molecular weight is observed [224].

Another study that supports the idea of the predominance of chain diffusion for SC formation is the one published by Sun

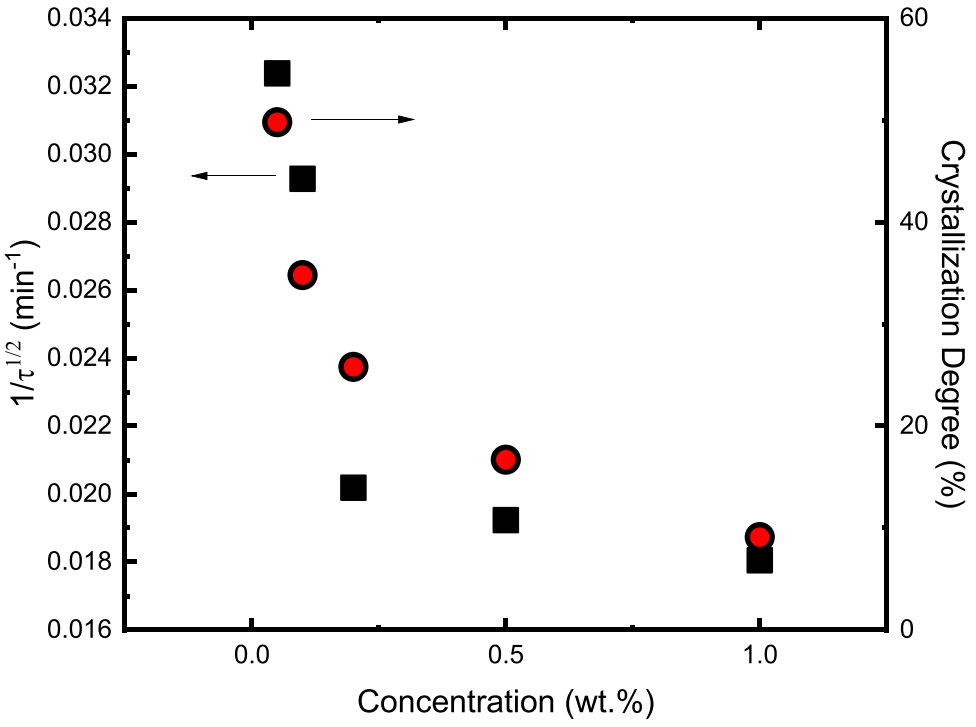

Fig. 18. Variation of the inverse of crystallization half time and crystallization degree versus concentration of the original solution for PLLA/PDLA isothermally crystallized at 180 °C. Data taken from [250].

et al. [250]. They studied the role of chain entanglements on the formation of high molecular weight PLAsc. They employed equimolecular dissolution of commercial PLLA (179 Kg/mol), and PDLA (209 Kg/mol) to prepare blends with different concentrations (from 0.05 to 1 wt%). To avoid the increase in the concentration due to solvent evaporation; they freeze the samples employing liquid nitrogen and then freeze-dry the samples to eliminate the solvent. As a result, a low number of entanglements is present in the samples when the concentration of the solution is low. They found that a lower concentration leads to higher SC content and faster crystallization rate (see Fig. 18). According to the authors, these results prove that chain diffusion is a predominant factor in decreasing SC formation.

In this section, we have summarized the evidence collected in the literature for the reduction of SC formation as molecular weight increases. The two possible explanations, i.e., phase separation or a decrease in molecular diffusion, have solid experimental evidence supporting them. Therefore, it is possible to consider that a combination of these two approaches could be compatible and complementary. As discussed previously, the SC formation requires a pre-state where intermolecular interactions exist. The PDLA and PLLA chains must be close enough to develop these interactions. The formation of these interchain connections requires time, so they are thermodynamically favorable but limited by their kinetics [198]. If phase separation happens, the chains have to diffuse to find the complementary stereoisomer and establish the required interactions; hence, reduced chain mobility would act as an obstacle. On the other hand, if a previous pre-ordered state is formed in the melt, the crystallization will take longer when the molecular weight increases (as diffusion becomes increasingly restricted), and depending on the crystallization conditions, it would possible to avoid the crystallization entirely.

Fig. 19 shows the density of active nuclei for six homopolymers of different molecular weights and the corresponding stereocomplexes (see Section 2.2) as a function of time during isothermal crystallization. PLOM with a 20x magnification was employed for the nuclei observation, and a series of micrographs were recorded every 2 s during 600 s, then the nuclei were contabilized manually. From Fig. 19a, it is possible to observe that nucleation density at a fixed time increases with the homopolymers' molecular weight; however, the behavior is the opposite in the case of SC nucleation (Fig. 19b). As explained before, SC need a pre-formed state for crystallization, and the increase in molecular weight reduces the possibility of forming the intermolecular interactions required. Consequently, the number of active primary nuclei per unit volume decreases due to decreased interactions within the melt. Such a decrease in nucleation density will produce a lower amount of SC.

As already discussed above, the increase in molecular weight decreases the opportunity of establishing the necessary intermolecular interactions between the stereoisomers. A similar result was obtained by He et al. [251] when they studied the crystallization kinetics of five PLLA/PDLA racemic blends with different molecular weights (from 20 to 200 kg/mol), and found a reduction in the nucleation rate of the SC with the increase in the molecular weight.

In a recent study, Liu et al. [252] employed an aryl hydrazide nucleator to enhance SC formation in a high molecular weight PDLA/PLLA racemic blend. They determined that the nucleator facilitates the formation of hydrogen bonding between the components (see Fig. 20) and, consequently, increases the crystallinity degree and the crystallization rate [252].

The work of Liu et al. [252] could help understand the main reason for the lack of crystallinity in racemic blends with high molecular weight: the difficulty in forming hydrogen bonds in the melt state before crystallization. This lack of interaction in the melt could be originated from either phase separation and/or a decrease in chain mobility. Decoupling the effects of phase separation and diffusion would require the design of specific experimental protocols to determine the main factor that originates the lack of SC in a high molecular weight PDLA/PLLA racemic blend.

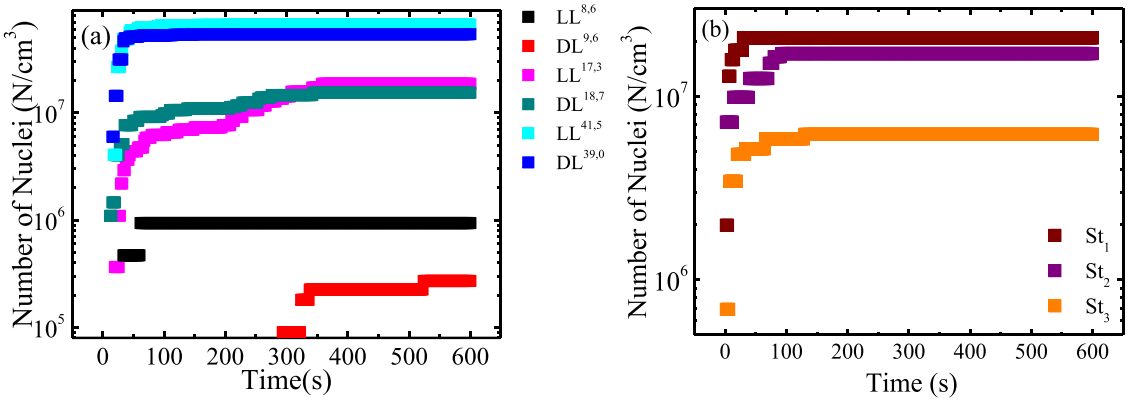

Fig. 19. Number of active nuclei versus crystallization time determined by PLOM with a magnification of 20X for: (a) Homopolymers, T_c = 120 C and (b) The corresponding stereocomplexes, T_c = 120 C.

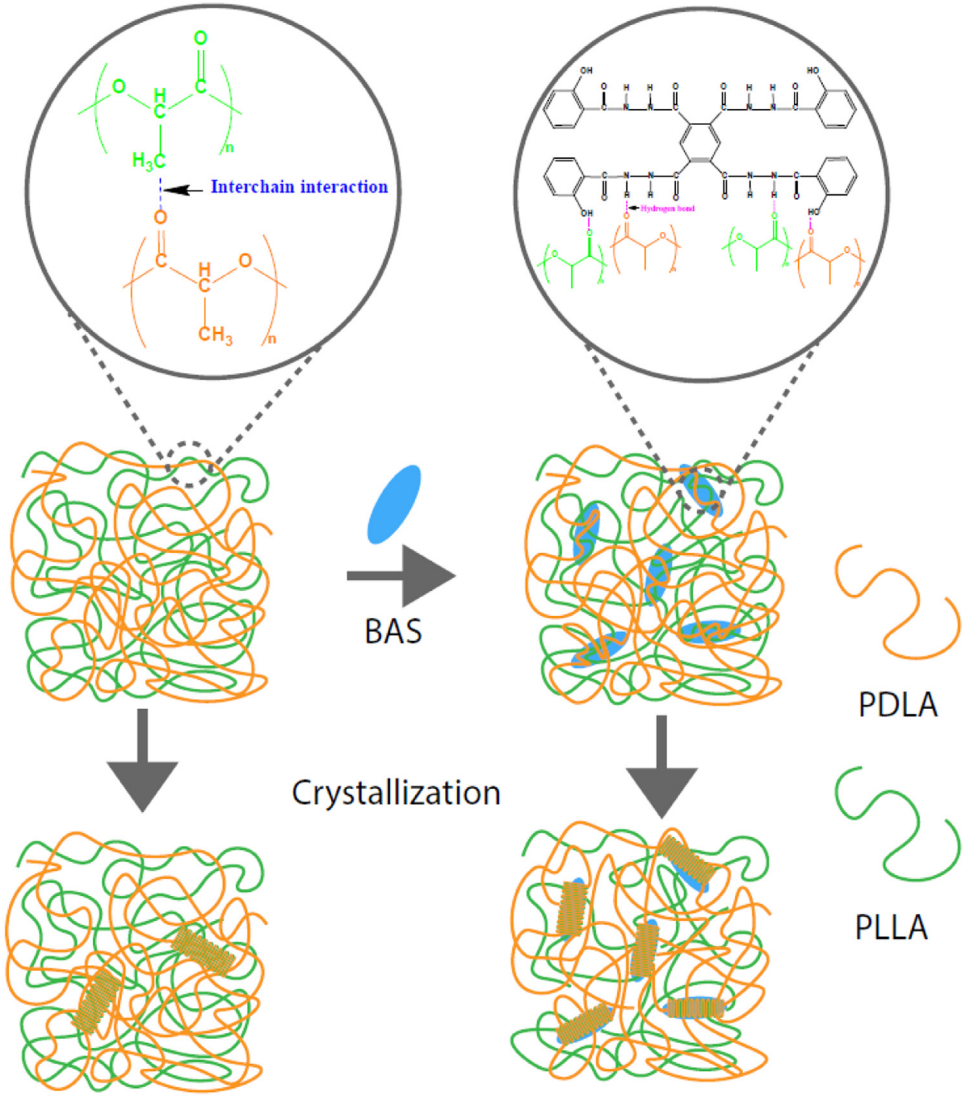

Fig. 20. Schematic representation of the interaction in PLLA/PDLA/BAS. Adapted from Ref. [252].

4.4. Architecture and copolymerization

The polymer architecture can modify the behavior during stereocomplexation. Incorporating a diblock copolymer, branches, or arms affects molecular dynamics and, consequently, the ability to form PLAsc. The change in mechanical and rheological properties made chain architecture or copolymerization attractive, and the combination with the advantages of stereocomplexes increases the attractiveness of these systems (see Table 1).

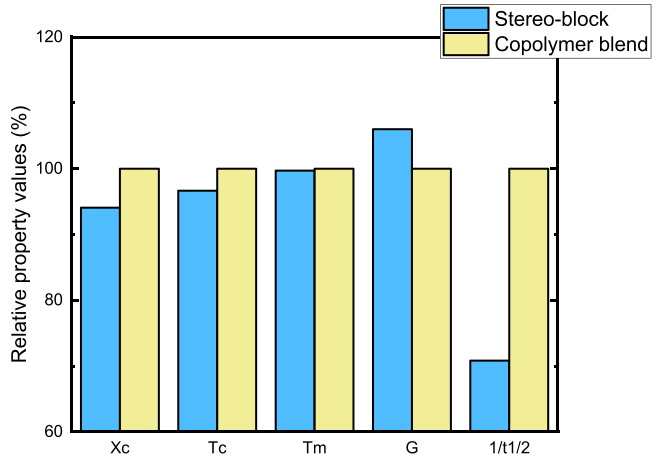

Fig. 21. Percentual value of the stereo block concerning the copolymer blend of the crystallization degree (X_c), crystallization temperature (T_c), melting temperature (T_m), spherulitic radial growth rate at 180 °C, and $1/\tau^{1/2}$. Elaborated with data from [266].

4.4.1. Stereo-copolymers

Incorporating PLA enantiomers in the same polymer chain is another common strategy. It is possible to find different combinations of homopolymers/stereo-copolymers blends or blends of stereo-copolymers. Also, the enantiomers employed are not limited to L, D. The DL stereoisomer is also used as a comonomer. Incorporating L and D stereoisomers within the copolymer modifies the mechanism of PLAsc formation leading to a low global crystallization degree in most cases. On the other hand, depending on the molecular weight, architecture, D:L ratio, and crystallization temperature, the formation of the SC could be preferential over the HC. It is important to mention that the chemical bond between the comonomers prevents possible segregation of the L or D blocks [153,253–259].

The simplest stereo-copolymers are the PDLA-b-PLLA, the influence of the covalent bond is evidenced by the presence of exclusive SC formation in cases not found for PLLA/PDLA blends, for example, high molecular weight components (higher than 20,000 g/mol) and asymmetrical blends [256,260–265]. However, the global crystallization degree is always lower in these systems in comparison with PLLA/PDLA blends.

Tsuji et al. [266] showed SC formation of PLLA-b-PDLA stereo diblock compared to the PLLA-b-PLLA and PDLA-b-PDLA copolymers blends. They found that the crystallinity degree, T_c, and $1/\tau^{1/2}$ are lower for the stereo diblock; however, the values of T_m and G are similar (see Fig. 21). This finding indicates that the covalent bond disturbs the primary nucleation, while growth is not primarily affected.

On the other hand, the incorporation of PDLLA blocks could affect SC formation. For example, Tsuji et al. [267] studied the blends of PLLA-b-PDLLA and PDLA-b-PDLLA. They found that the amount of PDLLA block increases the relative amount of SC within the blend; the SC are exclusively obtained when the amount is near to 50 % of DL. Nevertheless, a further increase will lead to a decrease in SC due to a dilution effect. For the system studied, the crystallization kinetics decreased with DL incorporation; a predominant dilution effect could explain this observation.

Recently, the Tsuji group [268,269] reported two novel architectures for PLA stereocopolymers, random and periodical copolymers. SC are exclusively formed in the following blends: PLLA-ran-PDLA (PLLA rich)/PDLA-ran-PLLA (PDLA rich). The most interesting fact is that homo crystallization is more affected by the crystallizable sequence length than stereocomplex crystallization. Finding SC with shorter sequences than those needed for HC is possible. In Fig. 22, it is possible to observe how the formation of SC in the blends is feasible even with a comonomer content of around 15 %. However, in the unblended copolymer it is not possible to obtain HC when the comonomer content is about 10 %. As expected, the crystallinity degree (X_c) and $T_m{}^0$ decrease with the increase of the comonomer within the copolymers and the blends. That is to say, a higher amount of the non-crystallizable monomer, as well as a shorter sequence of the crystallizable one, leads to a decrease in crystallinity, and the crystals will have a smaller lamellar thickness [268].

On the other hand, the stereocomplexes obtained by the periodical copolymers show a different crystalline structure for the SC. This new finding provides evidence of the possibility of polymorphism for the PLAsc. Fig. 23 shows the WAXD profile for a conventional PLLA, PDLA homopolymers, the periodical copolymer, the blends PLLA/PDLA, and P(LLA-LLA-DLA)/P(DLA-DLA-LLA). In the homopolymer, the typical structure of the α polymorphism of PLA is observed. However, a completely different structure was shown for the periodical stereo copolymers. This modification in the crystalline structure of the copolymers is reflected in the SC; the crystalline structure significantly differs from the traditional pattern presented by the PLAsc. The heating scan after the isothermal crystallization at 100 °C is shown in Fig. 23 for the copolymers and the blend; the SC have a melting temperature ~ 20 °C higher than the copolymers. At 100 °C the WAXD pattern for the blend suggest the formation of crystalline structures like the copolymers and a superimposed structure related to the SC. However, at 120 °C, only SC can form, and it is possible to observe the corresponding pattern. Another interesting fact is that the crystallization rate in this system is higher for SC than for HC, in a similar manner as was discussed for the homopolymer blend [269].

4.4.2. Block copolymers

Incorporating a second comonomer will impact the ability of PLAsc formation (see Table 1). Depending on the comonomer nature, an enhancement of SC formation is reported, or SC have complex trends or hindered [114,116,119,120,122,126,161,211,267,270–307]. The main reason for this dual behavior is the impact on the flexibility and diffusion of the chain. As discussed before, the interactions between the enantiomers within the melt is fundamental for SC formation. If the comonomer is more rigid than PLA, diffusion could be limited, especially if the sterecomplexation happens from the melt. A similar result could occur if the comonomer is miscible with PLA. The interaction with the comonomer could prevent or decrease the interaction with the other enantiomer. To increase the SC is necessary to increase the mobility and favor the diffusion.

DÁmbrosio et al. [295] studied the copolymer blends PLLA-m*b*-PBS/PDLA-m*b*-PBS. As PBS and PLA form a homogeneous melt, the chains of PLLA and PDLA mostly diffuse in the melt to the growing front of the SC. When the amount of PBS increases, the probability of finding an opposite enantiomer is reduced, and in consequence, the SC amount decreases (see Fig. 24). However, PBS is more flexible than PLA, and the block copolymer should be more flexible than the PLA homopolymer. The increase in flexibility helps the formation of SC. The increase in SC crystallization rate is found only when the amount of PBS is relatively low. It is possible that a balance between the flexibility increases and the dilution of the PLA in the melt, results in an acceleration of the crystallization only when the amount of PBS is low, but an increase in the PBS content will originate a reduction in the rate of crystallization (see Fig. 24).

A similar phenomenon was found for copolymers with PEG. PLA and PEG have a limited miscibility that depends on each block's

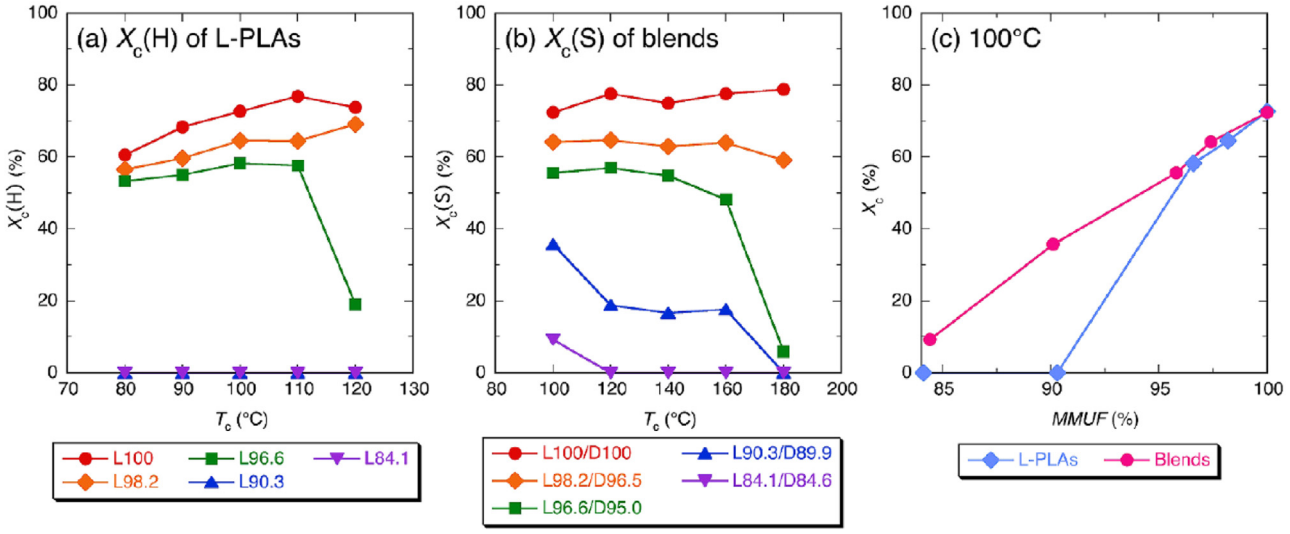

Fig. 22. The X_c (H) values of unblended L-PLAs (a) and X_c (S) of L-PLA/D-PLA blends (b) as a function of T_c, and X_c of unblended L-PLAs and L-PLA/D-PLA blends at T_c = 100 °C as a function of MMUF (c). Reproduced from [268].

molecular weight, composition, and temperature. PEG can influence SC formation in two ways:

1. A dilution effect**,** since PEG chains are miscible or partially miscible with PLA, the interactions between the enantiomers will be more difficult, hence, the presence of PEG chains will decrease the nucleation of SC.
2. The enhancement of the molecular mobility of the chain due to a more flexible comonomer (PEG) would facilitate the reptation of the chains and increase the crystallization rate [161,211,270–276].

Jing et al. [211] studied the blends of PLLA and PDLA-b-PEG-b-PDLA. They studied the influence of the PEG and PDLA block lengths and the ratio L/D. They found a common trend regarding the molecular weight of the PLA component and the L/D ratio. The most interesting result is the analysis regarding the influence of the PEG block on the PLAsc crystallization rate. In Fig. 25, it is possible to observe how the spherulitic growth at 170 °C, which refers only to the secondary nucleation, reaches a maximum when the Mw of the PEG block is 2000 g/mol (regardless of the Mw of the PDLA block), the maximum could be related to a balance between the increase in the mobility of the block copolymer chain and the dilution effect. However, the $1/\tau^{1/2}$ has a more sensitive dependence on the molecular weight of the PEG block. This parameter measures the overall crystallization rate and could reflect the complexity of the influence of the primary nucleation and growth. The maximum is not reached at 2000 g/mol, but at 4000 g/mol, there is a dramatic decrease in the PLAsc crystallization kinetics, which indicates the influence of the PEG in the primary nucleation of the stereocomplexes, especially for the dilution effect.

An interesting new study by Deng et al. [157] shows the effect of reactive blending of PLLA/PDLA with poly(ethylene-co-vinyl acetate) (EVA) and small amounts of epoxy functionalized oligo(styrene-acrylic) (ESA) on the SC formation. This reaction originated a graft copolymer PLA-graft-ESA that acts as a compatibilizer between the PLLA and PDLA, preventing the phase separation in the melt (see Fig. 26). Without the copolymer and after melting, the blends exhibit both HC and SC; however, after incorporating ESA during blending, the blend crystallizes in SC exclusively. This result supports the idea that the melt segregation of PLLA and PDLA phases is responsible for the low amount of SC in some systems.

4.4.3. Star copolymers

Stars are other chain structures of great interest. The type and amount of arms will define the stereocomplexation behavior. In general, branching affects the ability to form SC, reducing the possibility of crystallization. The architecture seems to impose physical constraints on the enantiomers' interaction, especially if both enantiomers are in a star-shaped polymer. The main factors decreasing the interaction in the melt of the enantiomers within a star-shape polymer are [144,150–152,210,214,308–327]:

1. **Terminal groups**. Compared with a linear homopolymer, more terminal groups will increase the free volume, pulling apart the enantiomers and reducing the possibility of the match needed to start the intermolecular interactions needed for SC formation.
2. **Decrease in segmental mobility**. Since a central molecule connects the arms, this automatically restricts mobility, reducing the possibility of finding the opposite enantiomer.
3. **Terminal group interaction**. If the terminal groups can interact, for example, hydrogen bonding between -OH terminal groups, this interaction could further restrict the mobility acting as anchor points.
4. **Combination of D and L enantiomers in the same molecule**. It has been reported that the presence of D and L stereoisomers in the same molecule will decrease the amount of SC formed.

As was discussed before, the glass transition of the PLA stereoisomers is higher than the homopolymers, and that can be interpreted as a signal of an early pre-ordered state preceding SC formation. In the case of the stars, Tsuji et al. [150] reported a lower T_g for the blends of 4 arms PDLA and PLLA polymers than for the linear PLLA/PDLA blend (see Fig. 27). This lower value could result from a higher free volume and decreased interaction between the L and D chains. Despite the lower value of T_g, the T_m was similar, but they reported a lower crystallinity degree.

Tsuji et al. [310] studied a complex system of miktoarm stereocopolymer. The miktoarm star presents a block of PLLA (core), and the outer part of the arms is PDLA. This star can crystallize with SC exclusively, with a melting temperature of 182.3 °C; this value is lower than the reported one for a linear system with a similar molecular weight (around 220–240 °C). The restriction on the mobility could originate the lower temperature and, consequently, a decrease in the lamellar size or a reduction in the stability of the crystal due to a lower amount of interaction. They

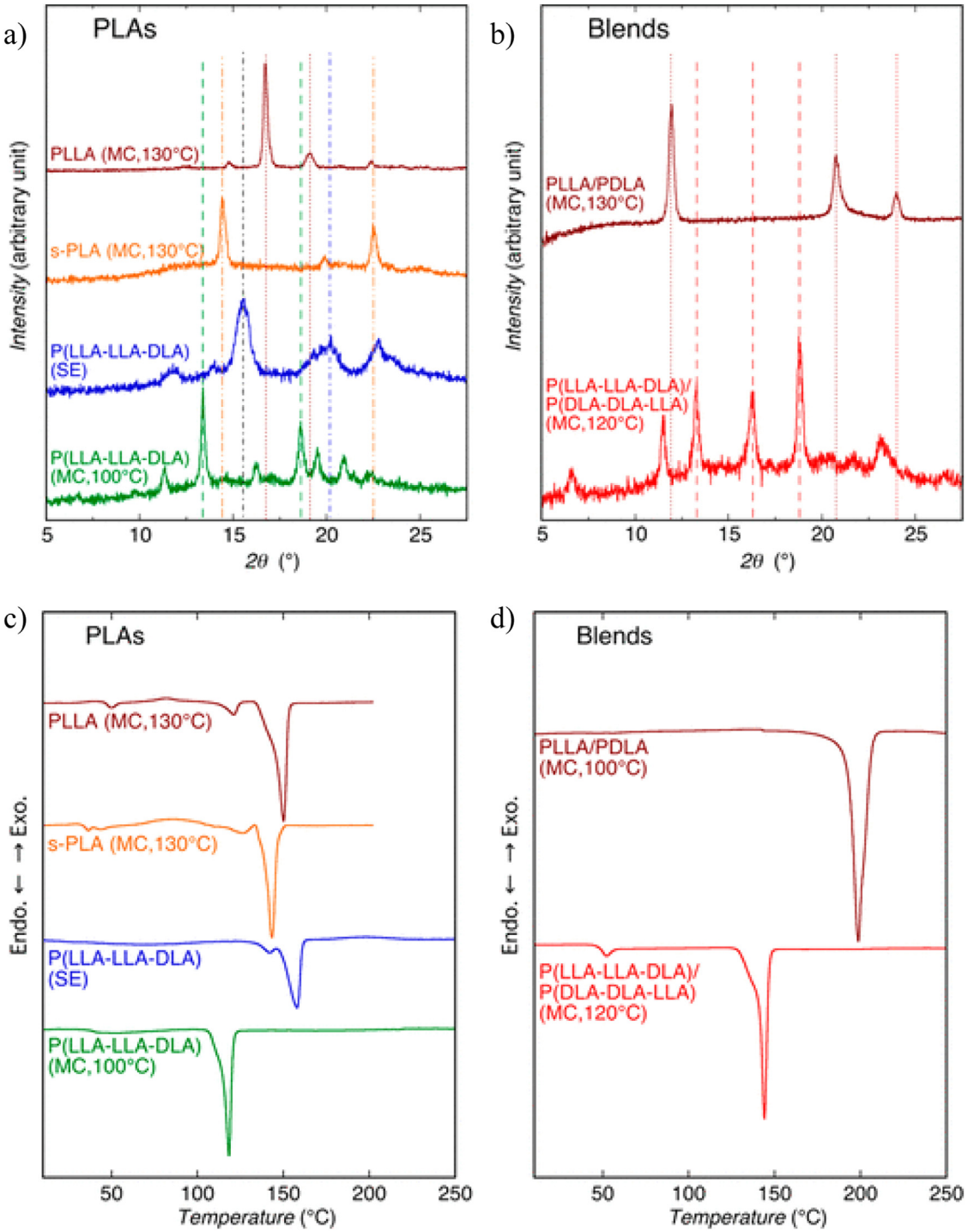

Fig. 23. (a, b) WAXD and (c, d) DSC scans for the indicated conditions and samples. Reproduced from [269].

studied the effect of incorporating a linear polymer with D or L isometry. The incorporation of an equimolecular amount of these homopolymers leads to an increase in the melting temperature and crystallization kinetics, and the linear homopolymer may increase the mobility of the system reaching SC with higher lamellar) thickness (or more interaction within the crystals in a faster way (see Fig. 28).

Tsuji et al. [312] also studied a more complex system, a miktoarm with PDLLA and PDLA or PLA arms. In this case, the miktoarms crystallize in HC only when the D or L is in the star's shell. However, the star/star blends can form SC, even when the D or L enantiomer is in the star's core. As was observed for the linear stereocopolymers with PDLLA blocks, the presence of the DL block reduces the crystallization kinetics and the melting temperature. Interestingly, in all the cases studied in this review, the PLAsc always crystallizes faster than the starting enantiomers, reaching higher crystallization rates. In Fig. 28b, the spherulite radial growth rate for those miktoarm stars is plotted. In this case, It is possible to observe that the crystal growth is faster for the PLAsc spherulites, and the maximum value registered for the SC is higher than the HC spherulites in all the studied isothermal crystallization temperatures.

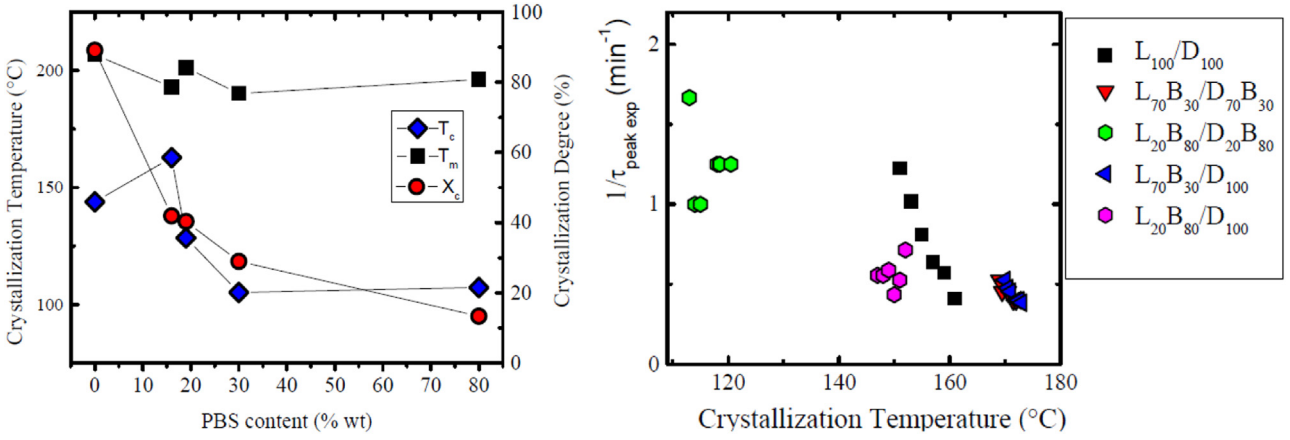

Fig. 24. (a) Crystallization degree, crystallization, and melting temperature versus PBS content for the copolymer/copolymer and copolymer/homopolymer stereocomplexes. (b) Overall crystallization rate versus crystallization temperatures for PLA and PLLA-mb-PBS/PDLA-mb-PBS stereocomplexes. Reproduced from [295].

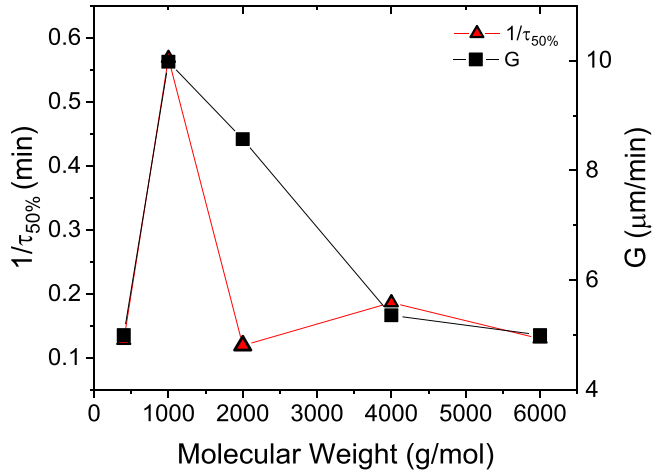

Fig. 25. Variation of the spherulitic growth rate (G) and the inverse of t at 50 % of conversion for the equimolecular blend of PLLA/PDLA-PEG-PDLA with a mole ratio of PEG to PDLA equal to 100, with the PEG block molecular weight. Data extracted from [211].

Praveena et al. [308] published a recent study on the stereocomplexation of PLA stars. They synthesized the star employing a chromophore core, allowing them to easily monitor the distributions of star core in the blends and infer the arm interactions. They studied the distribution of the cores in two different thermal treatments. One equimolecular star/star blend was cooled slowly from the melt, and the other was quenched. Both remain amorphous, but the one obtained from quenching has a mesophase structure that crystallizes in PLAsc when reheated, and the slow cooled remains amorphous. The observation of the cores within the blend shows that the slow cooling induced aggregation of the cores, and the quenching of the amount of aggregation was small. These observations indicate that the arms could interact and crystallize in an antiparallel chain-packing fashion [308]. That is to say, the core aggregation prevents the interaction of the chains that favor the mesophase before the SC crystallization. These results confirm that the SC is only possible when the systems allow the interaction between L and D stereoisomers and that the phase segregation is a plausible reason behind the lack of SC in some systems, like in the high molecular weight PLA.

4.4.4. Long-chain branched PLLA

Other architectures explored are long-chain branched PLAs [328–330]. Zhao et al. [329] reported the formation of stereocomplexes within the LCBPLA/PDLA asymmetrical blends; in this case, only one homopolymer has long branches, and they found an increase in the amount of SC formed by this blend compared to a linear homopolymer. Further studies are needed to understand the role of the branches during the SC formation; even so, the few works prove that it is possible to find SC in asymmetrical blends of LCBPLLA/PDLA [330].

4.5. Composites and nanocomposites

Using fillers or nanofillers is a common strategy to improve the mechanical performance of plastics or confer other uncommon characteristics to plastic materials, like magnetic or electrical characteristics. The stereocomplexes have been mixed with, carbon nanotubes (CNT) [331–340], graphite nanoplatelets [341], nanographite [342], graphene oxide [179,180,217,343–350], graphene nanoplatelets [180,351], nanohydroxyapatite [176,352,353], TiO_2 [354], ramie fiber [355], lignin [170,171,356–359], carbon black [229,360], cellulose [361,362], flax fibers [228,233–235,238,362], hydroxyapatite [174,363–366], cellulose nanocrystals [169,227,367], cellulose nanofibers [167], ZnO [368], silk fibroin nanodisc [369,370], carbon nanofiber [371], nanosilica [372], Au nanoparticles [373], maghemite nanoparticles [374], silver nanowires [375], lycell fibers [362], glass fibers [376], halloysite nanotubes [377], surface–modified magnesium hydroxide (MH) nanoparticles [378], layered double hydroxides (LDH) [379] and organo-modified montmorillonites [380,381]. In general, the studies on blend fillers/SC have two principal reasons: to use SC as a compatibilizer for the samples and enhance PLAsc crystallization. Another approach to SC in a nanocomposite is to use SC as nanofibers [382], or nanoparticles [383–385]; for example, in the study of Moya-Lopez, [383] they employed these particles to enhance the performance of hydrogels meant to be used for drug delivery applications.

The chemical or physical modification of the fibers is used to enhance the compatibility of the composites. An example of physical modification was reported in the work of Liang et al. [355]. They physically decorated ramie fibers (RF) with SC. They use an equimolecular solution of PLLA/PDLA and immerse the RF for 3, 5, and 10 min to obtain an SC coating of the fibers with different thicknesses. Fig. 29 shows the results obtained. The increase of spherulites around the RF proves its function as a nucleating agent, and in consequence, the spherulites of the PLLA matrix surround the RF, and the interactions between the components of the blends are increased.

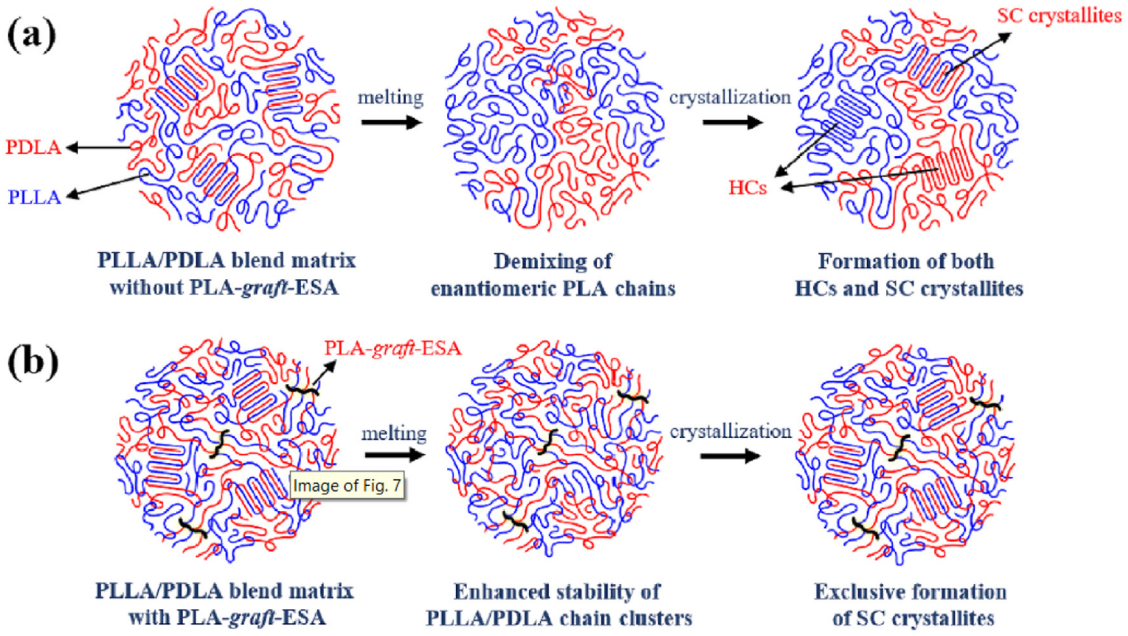

Fig. 26. Schematic representation of the PLA-graft-ESA as a compatibilizer in the blend PLLA/PDLA. Reproduced from [157].

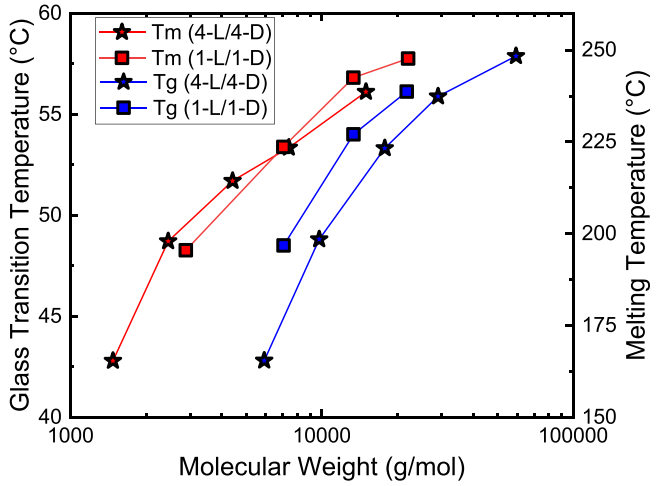

Fig. 27. T_g and T_m versus the molecular weight for the linear PDLA/PLLA and 4 arm star PDLA/4 arm star PLLA blends. Data from [150].

The most common chemical modification of the fillers to reinforce PLLA is the grafting with PDLA, and the idea is that the PDLA from the filler and the PLLA matrix form SC that act as bridges between the blend's phases. An example of this is the work of Jing et al. [354], they synthesized PLLA using TiO_2 as initiator and $Sn(Oct)_2$ as a catalyst. The PLLA and PDLA-g-TiO_2 were blended using solution casting. The result shows that the SC was effectively formed, acting as a nucleator agent for the PLLA matrix. On the other hand, the rheology was modified to create an SC network that works like physical crosslinking points [354].

The composites' mechanical performance was studied, and the improvement of the mechanical properties was reported [349,352], like in the work of Huang et al. [334–336,352,356,360] where they blend PLLA/HA-PDLA with different PDLA molecular weights. They found an increase of up to 14.5 % and 450 % for the tensile strength and elongation at break, respectively, for the composite related to the neat PLLA.

On the other hand, Pandey et al. [369] studied the crystallization of the PLLA/PDLA equimolecular blends in the presence of 1 % of silk fibroin nanodisc (SFN). They show that the SFN has acted as a nucleating agent for the stereocomplexes increasing the crystallization temperature from 107.9 to 131.5 °C (at 5 °C/min cooling scan) and increasing the overall crystallization rate three times and the degree of crystallization twelve times. Similar behavior has been reported for CNT [238,331,337,338], graphene oxide [217,343,346–348], comb-shaped cellulose-g-PLLA [361], nanocrystalline cellulose [386], o-MMT [387], hydroxyapatite-graft-poly(D-lactide) [366], ZnO-g-PLLA [368].

The use of composites could overcome the problems of thermal stability and mechanical properties of PLLA; the use of SC to increase compatibility is a promising strategy. However, in only a few studies, a detailed analysis of the mechanical performance of the blends has been reported, as well as the thermal stability at service conditions. Tests, such as Vicat or softening point evaluation should be performed for those systems to probe their utility under practical applications.

4.6. Nucleating agents and other additives

Using a selective nucleating agent is an alternative for inducing exclusive crystallization of SC or enhancing the crystallization of the stereocomplexes; as discussed before, some fillers can act as nucleating agents. However, this section will discuss using molecules whose main purpose is to perform as nucleating agents (NA). The main goal is that using small quantities of the NA, the crystallization temperature and the crystallization degree increase, with little or no effect on the melting temperature, also to increase the amount of SC and, if it is possible, to make SC the dominant crystalline species within the blend.

Some of the NA employed for the preferential nucleation of SC and to enhance the crystallization of SC in systems where the crystallization is low or even hindered, like in high molecular weigh stereo-blends, are: TMB-5 (aryl amide derivative) [388], zinc phenylphosphonate (PPZn) [389], xylan propionate (XylPr) [390], N,N≈ethylenebis (10-undecenamide) (EBU) [391], tetramethylenedicarboxylic dibenzoylhydrazide (TMC-306) [218,391,392], N,N,N,N′-salicylic tetra(1,2,4,5-benzenetetracarboxylic acid) hydrazide (BAS)

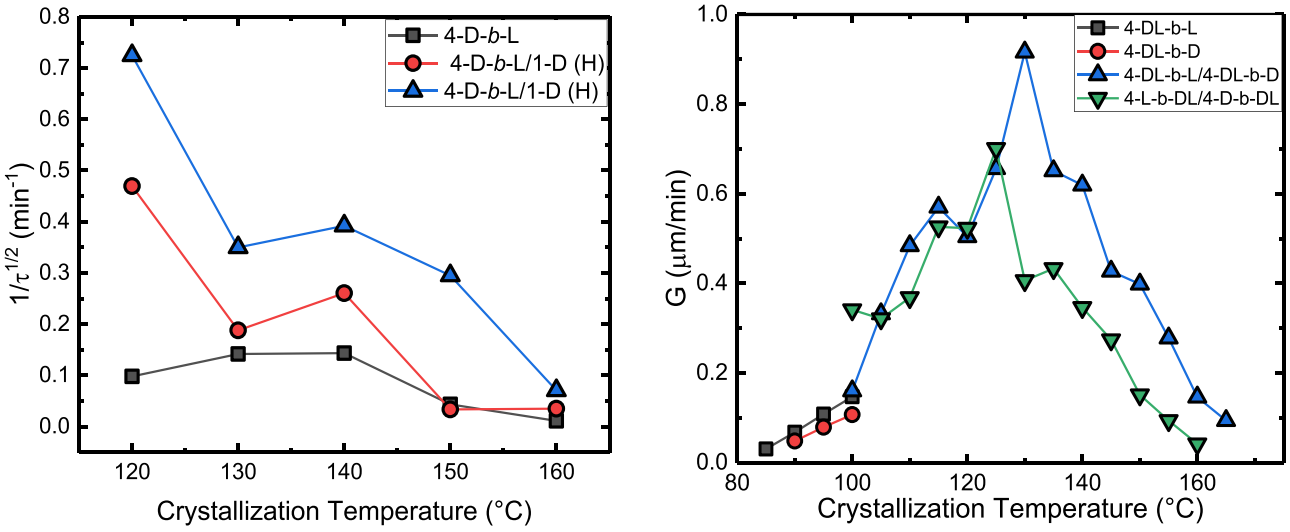

Fig. 28. Variation of (a) $1/\tau^{1/2}$ and (b) spherulitic crystallization rate (G) versus crystallization temperature for the star blends indicated. Data form [310,312].

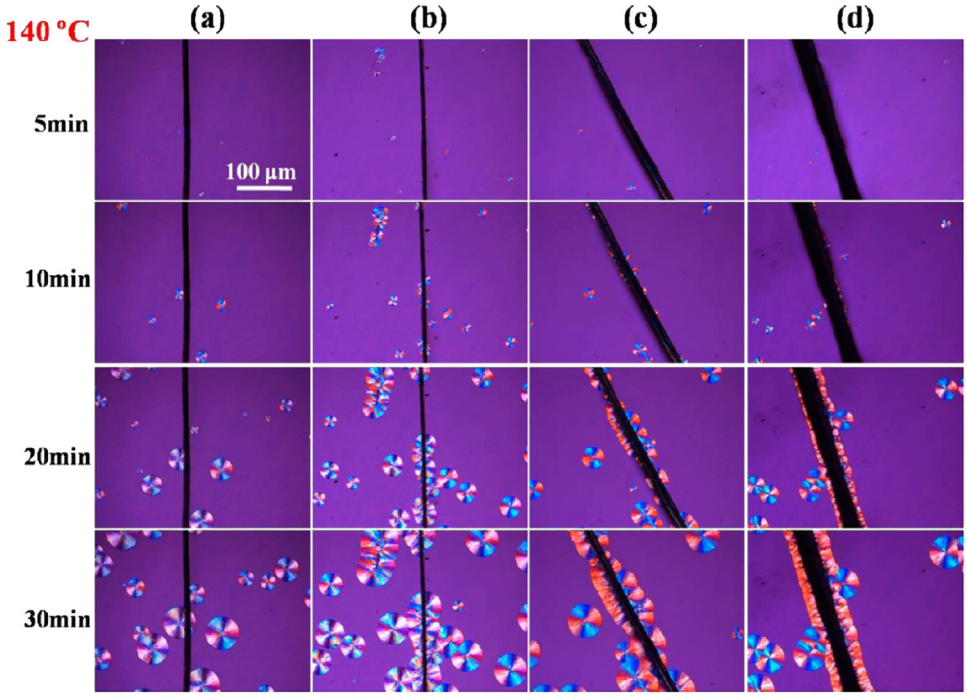

Fig. 29. Isothermal crystallization at 140 °C of (a) PLLA/RF, (b) PLLA/sc-RF3, (c) PLLA/sc-RF5, and (d) PLLA/sc-RF10. Figure from [355].

[252], p-xylene bisalkyl urea (XBU) [215], N,N',N''-tricyclohexyl-1,3,5-benzenetricarboxylamide (BTCA) [216], silsesquioxanes [393] among others [9,394,395].

The use of plasticizers is also reported [218,392,396,397]. The idea is to increase flexibility and favor the preferential formation of SC. As was discussed in the previous sections, one of the possible explanations for the lack of crystallization within the high molecular weight PLLA/PDLA blends is the decrease in molecular mobility. The results shown in those works indicated that the plasticizers and the amount employed effectively enhance SC formation. On the other hand, the use of crosslinking and plasticizers was described by Cui et al. [396]. They obtain a blend with higher thermal stability and a higher SC content thanks to combining both strategies.

In some cases, the inclusion of a third polymer in the blend could either increase the amount of SC or reduce it, as in the case of the copolymers. The results depend on the interaction between the other phase and the PLA [398–410] Li et al. [406] studied the influence of PVAc on SC formation. They used two types of PVAc differing in molecular weight (150 and 480 Kg/mol). Also, they studied three different amounts of the homopolymer in the blend (10, 20, and 30 wt%). Only one T_g was observed for all the samples, so they suggest that the PLA and PVAc homopolymers are miscible in the melt. During PLA crystallization, the PVAc is segregated to the amorphous zone, and they found that when the low molecular weight PVAc is used, the PLAsc crystallization is accelerated, and the amount of crystals increases, becoming the predominant crystal type when they added 30 wt% of PVAc. On the other hand, the high molecular weight will decrease the crystallization kinetics and the amount of SC in the samples. One of the most interesting results is the increase in the thermal-mechanical stability of the samples (especially for the one with 30 wt%. of low molecu-

lar weight PVAc). Even if the Ef́or the ternary blends is lower at low temperatures, its value remains stable at a higher temperature beyond the melting of the homocrystals [406].

4.7. Other effects

As discussed previously, the stereocomplexation process is multivariable. Intrinsic factors like molecular weight and architecture strongly influence SC formation. Similarly, extrinsic factors such as the composition of the blend and the presence of another block, polymer, or filler could alter the process. In some cases, they induce the crystallization of the stereocomplexes and, in other cases, reduce it. Other parameters that may affect SC formation are: shear during the blending process, the use of different types of solvents, temperature, and pressure.

Applying shear to the blends during processing or post-treatment results in higher PLAsc, nucleation density, and improved crystallization kinetics [186,376,411–414]. Similarly, inducing an orientation within the melt could increase the amount of SC in the blend [415–418]. The presence of shear and pressure during conventional processing techniques can influence crystallization; according to a few reports [413,419], the behavior of the PLAsc crystallization within the pressure is complex. The dependence on the processing conditions should be studied further to get a general tendency.

The solvent characteristics determine the amount of SC obtained, especially the solubility parameter (δ) and the vapor pressure (VP) [420]. A higher VP and the similarity between δ of the solvent and the PLA decrease the amount of SC. Other authors have reported similar results; generally, a solvent with relatively low solubility and evaporation rate will facilitate the formation of the SC [338].

4.8. Stereocomplexes as an additive

The stereocomplexes can be used as an additive, especially to increase the crystallization in PLA, as a compatibilizer (as discussed in Section 4.5), to improve the mechanical and thermomechanical behavior, and to create a physical crosslinked path within the PLA and produce changes in its rheological and thermal behavior [123,133,169,236,245,405,421–445].

5. Conclusions and perspective for future research

Lactide (LA) is a bio-derived monomer with unique features due to two chiral carbons in its ring. Under controlled polymerization, LA can form stereoregular (isotactic) polylactide, which is the prerequisite for the formation of polylactide sterecomplexes (PLA-sc). The most versatile method to synthesize stereoregular polylactide is *via* ring-opening polymerization (ROP) of cyclic LA. Despite the rapid advances in catalysis, $Sn(Otc)_2$ is still the most robust, versatile, and easily accessible catalyst to synthesize PLA under a wide range of conditions. Therefore, AROP of LA with Sn(Oct) as the catalyst is widely employed in the synthesis of polymeric percursors for non-covalent complex macromolecular architectures-based PLA-sc. Various macromolecular architectures have been reported, including non-covalent diblock, triblock, multiblock, alternating copolymers, telechelic, cyclic, graft, stars, brush, and hybrid materials. They are synthesized through a combination or ROP with other controlled/living polymerization (anionic, controlled radical, and ring-opening metathesis polymerization). Some of the complex macromolecular architectures were prepared under reactive melt blending/non-solvent conditions, which provide a straightforward strategy to improve the thermal/mechanical properties of polymeric/hybrid materials. On the other hand, new synthetic methodologies to synthesize well-defined monodisperse oligoPLA (from dimer to 64mer) have emerged. All of the aforementioned complex macromolecular architectures have contributed to the advancement of crystallization studies of PLA-sc-based materials.

The formation of SC is governed by several variables that are interconnected between them; the role of each one is a complex task, however, due to a large number of works since 2016 allows us to make some approaches to the role of the most critical characteristics of PLA-sc:

1. *Molecular Weight*. Without any doubt, the increase in molecular weight originates a decrease in the amount of SC. However, the explanation for this effect is still under debate. Two main explanations are accepted, the decrease in the diffusion ability of the larger molecules interrupts the co-crystallization process. The other explanation is based around the phase separation of PLLA and PDLA which increase with Mw. When phase separation occurs, 3 domains can be formed: one PLLA-rich phase, another PDLA-rich phase and a third PDLA/PLLA phase. It is from this last phase, where the PLLA and PDLA chains are molecularly mixed, that SC can be formed.
   In general, the formation of PLA-sc is kinetically less favored in higher-molecular-weight PLLA/PDLA blends. To overcome this obstacle, recently, Rastogi and coworkers synthesized high-molecular-weight PLLA-*b*-PDLA diblock and PDLA-*b*-PLLA-*b*-PDLA triblock copolymers using diphenyl bismuth bromide as a catalyst [446]. They reported the apparent molecular weights of the copolymers detected by SEC to be around 77–530 kg/mol. They found that direct co-crystallization of the PLLA/PDLA enantiomers occurs during the synthesis, leading to the formation of PLA-sc. However, the presence of PLLA and PDLA HCs is still unavoidable.
2. *Architecture*. The more complex the molecular structure, the fewer SC are obtained.
3. *Copolymerization*. In the majority of the copolymers, the presence of a comonomer disturbs the stereocomplexation. However, in some cases, it is possible to increase the amount of SC by increasing the flexibility of the PLA chains.
4. *Composites and Nanocomposites*. The presence of a filler could reduce or increase the amount of SC. It will depend on the ability of the filler to act as a nucleating agent.

The crystallization kinetics is also affected by all the parameters mentioned before. However, the number of studies dealing with this point is not as abundant to allow us to make general conclusions. Although it is well known that the crystallization rate of SC is faster than HC, the presence of a second phase could originate a decrease in the rate (compared to the homopolymers blends) or an increase, depending on the amount and relation between the comonomers.

Future research should be conducted on several aspects of PLA-sc formation. First and foremost is the synthesis of new complex macromolecular architectures containing industrial/bio-related polymeric/inorganic materials such as polyvinylidene fluoride, polyethylene, polyglycolide, magnetic nanoparticles, etc. These new structures/materials will challenge physicists to unravel their mechanical and thermal properties as well as their crystallization behavior. Another aspect to be addressed is to study the high molecular blends, and determine how it is possible to promote the interaction within the melt and prevent the phase segregation, also the inclusion of blocks or homopolymer of different natures or even filler or additives, all of these under the objectives of developing valuable material for the plastic industry. An aspect that should be under rigorous study is the processing techniques to apply the knowledge we have so far on the SC to escalate it on the real-life product.

Funding

All of the sources of funding for the work described in this publication are acknowledged below:

VL and NK thankfully acknowledge the support of King Abdullah University of Science and Technology (KAUST). This work has been supported by KAUST funding. AJM gratefully acknowledges funding from the Basque Government through Grant IT1309-19. This publication is part of the R+D+i project PID2020-113045GB-C21 funded by MCIN/AEI/10.13039/501100011033/.

Declaration of Competing Interest

We wish to confirm that there are no known conflicts of interest associated with this publication and there has been no significant financial support for this work that could have influenced its outcome.

CRediT authorship contribution statement

Rose Mary Michell: Writing – original draft, Methodology, Investigation, Formal analysis, Data curation. **Viko Ladelta:** Writing – original draft, Methodology, Investigation, Formal analysis, Data curation. **Edgar Da Silva:** Formal analysis, Data curation. **Alejandro J Müller:** Writing – review & editing, Supervision, Funding acquisition, Formal analysis, Conceptualization. **Nikos Hadjichristidis:** Funding acquisition, Formal analysis, Conceptualization, Supervision, Writing – review & editing.

Data availability

Data will be made available on request.

Acknowledgments

VL and NH thankfully acknowledge the support of King Abdullah University of Science and Technology (KAUST). This work has been supported by KAUST funding. AJM gratefully acknowledges funding from the Basque Government through Grant IT1309-19. This publication is part of the R+D+i project PID2020-113045GB-C21 funded by MCIN/AEI/10.13039/501100011033/.

Appendix

To summarize the applications and relevant information, we list in Table 1 the publications on PLA-sc from 2010 to the present.

Supporting data from unpublished results

Materials

We employ the following nomenclature for sample identification: L(D)L_{ZZ}, where the superscript zz represents the number average molecular weight in kg/mol. Homopolymers of similar molecular weights (St 1: $LL_{8.6}$/$LD_{9.6}$; St 2: $LL_{17.3}$/$LD_{18.7}$ and St 3: $LL_{41.5}$/LD_{39}) were mixed in equimolar amounts of PLLA and PDLA in a 1 % by weight dichloromethane solution. After complete dissolution, the solvent was evaporated at room temperature until the stereocomplexes were obtained.

DSC

A Perkin-Elmer DSC7 was used for the thermal analysis of the samples, with an inert nitrogen atmosphere and indium and tin as standards. The sample weight was approximately 5 mg and the test speed was 20 °C/min. For the isothermal study, the thermal history of the sample was erased (25 ºC above T_m) and immediately cooled from the melt at 60 °C/min to the defined crystallization temperature. The crystallization exotherm was recorded as a function of time, then the sample was heated at 20 °C/min until complete melting [482,483].

Polarized light optical microscopy (PLOM)

To determine the number of active nuclei as a function of time, we employed a ZEISS-model Mc 80 polarized light optical microscope (with built-in camera), using a 20x objective and a LINKAM TP 91 heating plate. After melting, the sample was cooled to the crystallization temperature T_c, chosen on the basis of the molecular weight and type of blend.

Table 2
PLA-sc published works from 2010 to the present show the melting temperature (T_m) crystallinity degree (X_c), molecular weight, D enantiomer ratio, blending technique, and applications.

Sample	Synthesis Method	T_m (°C)	X_c	Mw (PLLA) (Kg/mol)	Mw (PDLA) (Kg/mol)	D-Ratio (wt%)	Blending technique	Application	REF
PLLA/PDLA	Commercial	222,6 228,1 226,8 230	54.4 46.9 24.4 23.6	94.9 228.1 407.4 620.9	97.9 229.7 357.5 635.4	50	Solution	Use DME to increase the amount of SC	[221]
PLLA/PDLA	Commercial	226	36.0	300	343	50	Solution	Mechanistic understanding of SC formation	[204]
PLLA/PDLA	Commercial	225	44.1	200	215	50	Solution	Mechanistic understanding of SC formation	[447]
PLLA/PDLA	ROP of DLA/LLA, $Sn(Oct)_2$	226	62.0	160	180	50	Solution	The interfacial effect of homocomposite PLA on the PLA-sc crystallization	[448]
PLLA/PDLA	Commercial	215 215 215.7 218.2	NI	160	74	10 5 2 0.5	Solution	Shear time/rate effect on PLA-sc	[186]
PLLA/PDLA	Commercial	212.5 213 213.6 213.7 214 196/214 204/214 216.5	NI	170	120	50	Solution Solution/Sintered (150 °C) Solution/Sintered (160 °C) Solution/Sintered (170 °C) Solution/Sintered (180 °C) Solution/Sintered (190 °C) Solution/Sintered (200 °C) Solution/Sintered (210 °C)	Sintered temperature effect on SC formation	[449]
PLLA/PDLA	Commercial	220.2 222.4 225.6 219.6 221.7 224.7 218.8 220.6 222.7	46.8 50.2 52.9 46.1 49.0 51.7 45.2 46.5 50.6	170	120	50	Melt/sintered (160 °C/700 Mpa) Melt/sintered (180 °C/700 Mpa) Melt/sintered (200 °C/700 Mpa) Melt/sintered (160 °C/500 Mpa) Melt/sintered (180 °C/500 Mpa) Melt/sintered (200 °C/500 Mpa) Melt/sintered (160 °C/300 Mpa) Melt/sintered (180 °C/300 Mpa) Melt/sintered (200 °C/300 Mpa)	Sintered temperature and pressure effect on SC formation	[450]
PLLA/PDLA	ROP of DLA/LLA, $Sn(Oct)_2$/Joncryl® ADR 4368 (0 wt%) ROP of DLA/LLA, $Sn(Oct)_2$/Joncryl® ADR 4368 (0.5 wt%) ROP of DLA/LLA, $Sn(Oct)_2$/Joncryl® ADR 4368 (1.0 wt%) ROP of DLA/LLA, $Sn(Oct)_2$/Joncryl® ADR 4368 (2.0 wt%)	240 239 239 224	60.8 50.6 50.1 38.4	85	88	50	Melt	Effect of Chain extenders on SC formation	[286]

(*continued on next page*)

Table 2 (*continued*)

Sample	Synthesis Method	T_m (°C)	X_c	Mw (PLLA) (Kg/mol)	Mw (PDLA) (Kg/mol)	D-Ratio (wt%)	Blending technique	Application	REF
PLLA/PDLA	ROP of DLA/LLA, initiated by UPy-functionalized alchohol, $Sn(Oct)_2$	219.4 218.2 223.7 227.1 228.2 225.7	44.4 27.9 28.5 36.9 23.3 9.6	44 62 87 41 58 82	45 63 82 40 58 91	50	Solution	Effect of UPy (H-bonding motif) on PLA-sc formation	[220]
PLLA/PDLA	Commercial	219.2 218.2 220	2.5 8.6 15.0	11	124	2 6 10	Solution	Non-equimolar blend of PDLA/PLLA	[187]
PLLA/PDLA	Commercial	224.9	31.9	89	65	50	Melt	Effect of PENTA as additive on PLA-sc formation	[451]
PLLA/PDLA	PLLA: commercial, PDLA: ROP	226.9	53.3	210	100	50	Solution	Effects of temperature and external force on the stereocomplexation	[452]
PLLA/PDLA	Commercial	225.9 225 230.9 223.2 227.6 223.1 222.3 222.3 222.6 223.8 222.4 222.6 223.2 222.7 223.1	11.3 23.3 34.2 41.1 39.1 7.8 9.5 16.4 19.1 14.3 1.2 3.9 7.8 18.5 10.6	7	6	50 40 30 20 10 50 40 30 20 10 50 40 30 20 10	Solution	Effect of different electrospinning method on PLA-sc	[188]
PLLA/PDLA	ROP, $Sn(Oct)_2$	203.8 203.8 205.2 203.1 200.9 199.3	11.3 10.8 11.0 8.0 4.2 2.5	186	9 18 24 35 67 102	10	Solution	Rheology of asmmetric PLLA/PDLA blend	[222]
PLLA/PDLA	ROP of DLA/LLA, $Sn(Oct)_2$	268.5 249.5 220.1	NI	17 21 65	16 21 67	50	Solution	Mechanism of stereocomplexation	[222]
PLLA/PDLA	Commercial	NI	57.9	110	70	50	Solution	Effect of temperature on PLA-sc formation	[212]
PLLA/PDLA	Commercial	NI 224.5 226	6.3 11.4 22.2	160	260	5 10 20	Melt-bleding	Effect of PMMA weight fraction	[189]
PLLA/PDLA	Commercial	218	NI	180	210	50	Solution	Shape memory and hydrolisis behavior	[453]
PLLA/PDLA	Commercial	224.4 212.5 220.3 228.7	24.8 11.4 17.3 23.2	30 51 96 96	37 86	50	Melt-bleding	Thermal and mechanical properties	[223]

(*continued on next page*)

Table 2 (*continued*)

Sample	Synthesis Method	T_m (°C)	X_c	Mw (PLLA) (Kg/mol)	Mw (PDLA) (Kg/mol)	D-Ratio (wt%)	Blending technique	Application	REF
PLLA/PDLA	Commercial	219 222 227	4.0 10.0 24.0	86	135	5 10 20	Solution	Mechanical properties	[454]
PLLA/PDLA	ROP, $Sn(Oct)_2$	215/238.2 227.1/247.4 228.2/247.7 225.7 221.3	64.2 36.3 23.3 9.6 5.8	169 36 47 59 133	183 33 47 68 133	50	Solution	effect of molecular weight	[224]
PLLA/PDLA	ROP, tin(II) 2-ethylhexanoate	213 213 213 213 213 213	58.2 53.0 38.7 46.6 42.2 43.3 28.4	84	49	50	Solution/Acetone crystallization Solution/EA crystallization Solution/THF crystallization Solution/Toluene crystallization Solution/o-xylene crystallization Solution/o-dichlorobenzene crystallization Solution/Benzene crystallization	Effect of solvent on the crystallization	[455]
PLLA/PDLA	Commercial	220.7 223.3 223.3 223.8 222.7 220.9 223.8 222.1 220.3	NI	180	11	90 80 70 60 50 40 30 20 10	Melt-bleding	Crystallization and morphology	[191]
PLLA/PDLA	ROP, $Sn(Oct)_2$	219.5 218.95 218.95 217.9 217.9 216.8	NI	8	8	25 20 15 10 8 5	Solution	morphology and crystal growth	[192]
PLLA/PDLA	ROP, $Sn(Oct)_2$	224.55 222.26	43.3 37.6	95	45	50	Melt-bleding	Injection molding	[192]
PLLA/PDLA	Commercial	211.6 212.1 209.4 209.3 203.4	11.2 27.9 27.6 52.4 21.7	160	95	90 70 50 30 10	Melt-blending	Properties of PLA-sc from injection molding	[193]
PLLA/PDLA	ROP, $Sn(Oct)_2$	206.3 211.4 200.5 202.4 202.6 202.9 209 211.8 208.6	NI	1160	1050	10 20 30 40 50 60 70 80 90	Solution	Crystal packing model for asymmetric SPLA	[10]

(*continued on next page*)

Table 2 (*continued*)

Sample	Synthesis Method	T_m (°C)	X_c	Mw (PLLA) (Kg/mol)	Mw (PDLA) (Kg/mol)	D-Ratio (wt%)	Blending technique	Application	REF
PLLA/PDLA	Commercial	206.82	0.01	100	NI	0.1	Melt-bleding	Physical properties of PLA-sc melt-blown nonwoven	[194]
		209.89	0.01			0.2			
		202.35	0.03			0.3			
		205.6	0.04			0.4			
		207.14	0.06			0.5			
		208.81	0.4			1			
		208.78	0.9			3			
		208.08	2.3			5			
Homopolymer/Homopolymer	Commercial	216	NI	210	70	10	Melt-bleding/Streching	Produce a cost-effective selfreinforced fibers	[415]
		215				5			
		214				3			
		210				1			
PLLA/PDLA	Commercial	211.3	0.0	176	161	50	Melt-bleding/Streching	Produce a industrial-scale SC-PLA fibers	[416]
PLLA/PDLA (2,16 Draw ratio)		211.2	27.8						
PLLA/PDLA (1,3 Draw ratio)		211.2	29.7						
PLLA/PDLA/Transesterification agent		224.3	0.0						
PLLA/PDLA/Transesterification agent (2,08 draw ratio)		224.5	1.4						
PLLA/PDLA/Transesterification agent (1,82 draw ratio)		225.5	19.3						
PLLA/PDLA	Commercial	212	0.02	98	68	5	Melt-bleding	Produce at high resistance PLLA composite	[382]
		214	0.04				Melt spunbond spinning at 190 °C		
		216	0.06				Melt spunbond spinning at 230 °C		
		212	0.03		49		Melt-bleding		
		215	0.08				Melt spunbond spinning at 190 °C		
		218	0.2				Melt spunbond spinning at 230 °C		
		212	0.02		117		Melt-bleding		
		218	0.08				Melt spunbond spinning at 190 °C		
		222	0.2				Melt spunbond spinning at 230 °C		
PLLA/PDLA Unoriented	Commercial	221	3.3	NI	NI	50	Melt-Blending. Bi-oriented	Develop a new Flexible and Hybrid electronics material	[438]
PLLA/PDLA bioriented		218	31.7						
PLLA/PDLA bioriented-Annealed	219	25.9							
PLLA/PDLA bulk	Commercial	219	NI	179	209	50	solution-Freeze drying	Develop a high molecular weigh SC, from low entanglement density samples.	[250]
PLLA/PDLA Freeze solution, Total polymer concentration (1 %)		211							
PLLA/PDLA Freeze solution, Total polymer concentration (0.5 %)		209							
PLLA/PDLA Freeze solution, Total polymer concentration (0.2 %)		211.5							
PLLA/PDLA Freeze solution, Total polymer concentration (0.1 %)		211.5							
PLLA/PDLA Freeze solution, Total polymer concentration (0.05 %)		211							

(*continued on next page*)

Table 2 (*continued*)

Sample	Synthesis Method	T_m (°C)	X_c	Mw (PLLA) (Kg/mol)	Mw (PDLA) (Kg/mol)	D-Ratio (wt%)	Blending technique	Application	REF
PLLA/PDLA	Commercial	178.6/192.8	NI	3	3	50	Solution	Growth of Monolamellar Polymer Crystals	[456]
PLLA/PDLA	Commercial	222.83	2.8	260	20	10	Melt-blending	Use the SC has nucleating agent for PLLA	[441]
		224.5	7.2			20			
		224.5	8.5			30			
		224.83	14.5			40			
		223.33	8.5			50			
PLLA/PDLA (14 h stirring time)	ROP with $Sn(Oct)_2$ (0.5 wt%, as the initiator) and isopropanol as co-initiator	227.7/244.7	35.1	32	31	50	Solution with different stirring time	Evaluate the influence of the solution stirring time on the SC formation	[457]
PLLA/PDLA (50 h stirring time)		227.4./241.4	41.2						
PLLA/PDLA (100 h stirring time)		227.3./240.3	45.0						
PLLA/PDLA (14 h stirring time)		220.4	10.4	58	67				
PLLA/PDLA (50 h stirring time)		219.9	15.3						
PLLA/PDLA (100 h stirring time)		220.1	20.1						
PLLA/PDLA (14 h stirring time)		216.5	8.0	134	102				
PLLA/PDLA (50 h stirring time)		216.4	9.4						
PLLA/PDLA (100 h stirring time)		217.7	16.7						
PLLA/PDLA (no orientation, before foaming)	Commercial	219.5	5.5	210	78	5	Melt-blending. supercritical CO_2 (sc-CO_2) batch foaming process.	Foams with high orientation	[458]
		228.8	9.5			10			
		227.8	17.4			15			
		230.1	25.1			20			
PLLA/PDLA (300 % drawing ratio, before foaming)		219.8	5.9			5			
		225.4	10.9			10			
		229.9	15.5			15			
		229.4	21.7			20			
PLLA/PDLA (500 % drawing ratio, before foaming)		219.5	5.6			5			
		224.3	11.4			10			
		226.9	18.0			15			
		232.5	22.8			20			
PLLA/PDLA (no orientation, After foaming)		219.8	5.5			5			
		224	11.1			10			
		226.2	17.4			15			
		229	25.4			20			
PLLA/PDLA (300 % drawing ratio, After foaming)		224.3	5.9			5			
		226.4	11.4			10			
		229.6	17.2			15			
		229.6	23.0			20			
PLLA/PDLA (500 % drawing ratio, After foaming)		221.4	5.6			5			
		224.6	12.0			10			
		227.2	18.9			15			
		232.3	24.3			20			
PLLA/PDLA	Commercial	217.8	8.6	170	120	10	solution-Freeze drying	Aerogels for oil-water separation	[459]
		218.82	17.4			20			
		217.58	24.4			30			
		216.55	31.8			40			
		218.9	39.8			50			

(*continued on next page*)

Table 2 (*continued*)

Sample	Synthesis Method	T_m (°C)	X_c	Mw (PLLA) (Kg/mol)	Mw (PDLA) (Kg/mol)	D-Ratio (wt%)	Blending technique	Application	REF
PLLA/PDLA (no tension heat-setting)	Commercial	222.5	4.1	173	450	50	Melt-spining + Drawing +tension heat-setting at the indicated temperature	Fibers with high amount of SC	[417]
PLLA/PDLA (tension heat-setting at 160 C)		221.3	33.0						
PLLA/PDLA (tension heat-setting at 170 C)		222.5	36.9						
PLLA/PDLA (tension heat-setting at 180 C)		221.3	50.9						
PLLA/PDLA (tension heat-setting at 190 C)	221.8	57.7							
PLLA/PDLA	Commercial	213.1	2.6	150	NI	2.5	Melt blending-Foaming (CO2)	Foams for oil-water separation	[460]
		213.2	5.4			5			
		215.7	11.3			10			
PLLA/PDLA	Melt/solid polymerization using $Sn(Oct)_2$ as the catalyst.	196.5	26.7	11	11	50	Solution	Study systematically the effect of molecular weight	[225]
		206.1	10.4	41	41				
		211	9.3	95	95				
		215.8	5.0	144	144				
PLLA/PDLA	Commercial	202.7/220.7	8.2	250	120	10	Solution	Study the effect of CO2 pressure on the SC and HC formation	[201]
PLLA/PDLA/CO_2 atmosphere (2 Mpa)		204.8/220.6	9.0			10			
PLLA/PDLA/CO_2 atmosphere (4 Mpa)		206.9/221.4	9.5			10			
PLLA/PDLA/CO_2 atmosphere (6 Mpa)		208.1/221.4	6.5			10			
Mesoporus PLLA/PDLA	commercial	228.8	13.1	91	74	10	Melt-Blending	tridimensional interconnected porous PLA	[461]
		235.2	24.7			20			
		239.8	51.6			30			
		240.5	61.2			40			
Copolymers and its blends									
PLLA-b-PEG-b-PLLA/PDLA	PLLA-PEG-PLLA was synthesized by ROP using $Sn(Oct)_2$ as catalyst and $PEG-(OH)_2$ as initiator. PDLA was synthesized by ROP using dodecanol as the initiator.	209	10.4	37.3	5.7	10	Melt-blending	enhance thermal properties and crystallization of PLA-sc	[278]
		212	23.3			20			
		212	36.0			30			
		213	39.6			40			
PLLA-b-PEG-b-PLLA/PDLA (chain extenders)		210	13.3			10			
		210	25.9			20			
		212	34.0			30			
		213	38.8			40			
PLLA/PEG1K-b-PDLA	PLLA from commercial source. PDLA-PEG-PDLA was synthesized by ROP using $Sn(Oct)_2$ as catalyst and PEG as initiator	215.9	NI	107	24.1	5(b)	Solution	Study the effect of PEG, PDLA block, D/L ratio and crystallization conditions on PLA-sc formation.	[211]
		215.2				4(b)			
		215.5				3(b)			
		213.3				2(b)			
		209.8				1(b)			
PLLA/PEG4K-b-PDLA		215.5			68.3	5(b)			
		215.2				4(b)			
		214.3				3(b)			
		213.6				2(b)			
		209.4				1(b)			
PLLA/PDLA-b-PCVL-b-PDLA	PLLA from commercial source. PDLA-PCVL-PDLA was synthesized by ROP using $Sn(Oct)_2$ as catalyst and DEG as initiator	181.2	0.3	200	0.49	4.02	Solution	To control crystallization, rheology, and thermal properties	[290]
		183	0.5			6.7			
		182.2	0.2		1.04	3.26			
		182.3	1.8			9.78			
		183.3	2.7			16.3			

(*continued on next page*)

Table 2 (*continued*)

Sample	Synthesis Method	T_m (°C)	X_c	Mw (PLLA) (Kg/mol)	Mw (PDLA) (Kg/mol)	D-Ratio (wt%)	Blending technique	Application	REF
PLLA/PDLA-b-PBS-b-PDLA	PLLA from commercial source. PDLA-PBS-PDLA was synthesized by ROP using $Sn(Oct)_2$ as catalyst and PBS as initiator	213.2 213.2 213.2 213.1 215.2 217.5 218.8 220.1 219.8 222.1	NI	65	14.8 25.3 	6 12 18 24 30 7.5 15 22.5 30 37.5	Solution	Toughening of PLLA via PLA-sc formation	[291]
PLLA/4a-PCL(5 kg/mol)-b-PDLA PLLA/4a-PCL(3 kg/mol)-b-PDLA PLLA/4a-PCL(7 kg/mol)-b-PDLA	PLLA from commercial source. $(PCL\text{-}PDLA)_4$ was synthesized by ROP using $Sn(Oct)_2$ as catalyst and pentaerythritol as initiator	195 195 195 196 179	5.0 6.0 8.0 6.0 8.0	253	17.7(c) 16.1[(c)] 18.5(c)	10(c) 15(c) 20(c) 10(c) 10(c)	Melt-blending	Nucleating agent and to enhance physical properties of PLLA via PLA-sc	[462]
PLLA/poly(D-lactide)-b-polyurethane-b-poly(D-lactide)	PLLA and $PBA\text{-}(OH)_2$ from commercial source. PDLA-OH and PLLA-OH, were synthesized by ROP using $Sn(Oct)_2$ as catalyst and dodecanol as initiator. Polyurethane was synthesized using HDI as a linker	212 216 211	NI	176		4 3 2	Melt-blending	Control physical properties of polyurethane	[463]
PLLA/PDLA PLLA/PDLA-b-PEG (1Kg/mol)-b-PDLA PLLA/PDLA-b-PEG (2Kg/mol)-b-PDLA PLLA/PDLA-b-PEG (4Kg/mol)-b-PDLA	PLLA from commercial source. PDLA-PEG-PDLA was synthesized by ROP using $Sn(Oct)_2$ as catalyst and PEG as initiator	188.7 203.7 205.7 197.3	NI	45	2 4 4 4	8 8 8 8	Solution	Effect of PEG block on PLA-sc properties	[271]
PLLA/LB-PCL-b-PDLA PLLA/PCL-b-PDLA	PLLA 4032D from commercial source. LB-PCL-b-DLA was synthesized by ROP DMPA as the initiator, polycondensation of HOOC-PCL-2OH, and then ROP of D-LA with LB-PCL as the macro-initiator	213.5 219.2	3.7 3.0	176	54(c) 68(c)	15 15	Melt-blending	Toughening commercial PLLA	[294]
PLLA/PDLA (1 min) PLLA/PDLA (2 min) PLLA/PDLA (3 min) PLLA/PDLA-co-Glucose (1 min) PLLA/PDLA-co-Glucose (2 min) PLLA/PDLA-co-Glucose (3 min)	PLLA commercial. PDLA and copolymer via melt polymerization $Sn(Oct)_2$	210.8 211.2 211.4 208.4 208.6 208.8	8.2 5.7 2.1 0.4 0.7 1.2	NI	NI	NI	Solution	PLLA films were immersed at the indicated time in PDLA or PDLAG solution	[442]

(*continued on next page*)

Table 2 (*continued*)

Sample	Synthesis Method	T_m (°C)	X_c	Mw (PLLA) (Kg/mol)	Mw (PDLA) (Kg/mol)	D-Ratio (wt%)	Blending technique	Application	REF
PLLA/4-DL-D Star PLLA/PDLA-co-PEG (28,8 % wt) PLLA/PDLA-co-PDMS (24,9 % wt)	PLLA Commercial. 4-DL-D copolymers were synthesized using two-step ring-opening polymerization	213.9 212.4 202.6	20.4 8.5 6.5	124.4	10.2	20	Solution	Influence of comonomers on the SC formation	[276]
linear PLLA/linear PDLA	commercial PLLA, PDLA from ROP, $Sn(Oct)_2$, dodecanol	221.4	14.0	143	191	50	Solution	Effect of comblike topology on PLA-sc crystallization	[464]
linear PLLA/comblike acetate PDLA	ROP, $Sn(Oct)_2$, Cellulose acetate macronitiator	219.1	17.5	143	611				
Cellulose Acetate-g-PLLA/Cellulose Acetate-g-PDLA		222.2	15.0	341	365				
Cellulose Acetate-g-PLLA/Cellulose Acetate-g-PDLA		210.5	15.9	501	365				
Cellulose Acetate-g-PLLA/Cellulose Acetate-g-PDLA		213	21.5	684	467				
Linear PLLA/linear PDLA	ROP	206.8	63.0	5.4	6.1	50	Solution	Crystallization of PLA-mb-PBS	[295]
PLLA-mb-PBS/PDLA-mb-PBS	PLA from ROP, PBS from polycondensation, multiblock from chain coupling	190.2	29.0	14.8	12				
PLLA-mb-PBS/PDLA-mb-PBS		196.2	13.0	7	6.7				
Linear PLLA/PDLA-mb-PBS		192.9	42.0	5.4	12				
PLLA-mb-PBS/Linear PDLA		201.2	40.0	14.8	6.1				
Linear PLLA/PDLA-mb-PBS		193.9	34.0	5.4	6.7				
PLLA-mb-PBS/Linear PDLA		199.2	39.0	7	6.1				
linear PLLA/linear PDLA	ROP, $Sn(Oct)_2$, laryl alcohol as initiator	220.6	4.3	120	102	50	Solution	The efffects of flexible PEG midblocks on the polymorphic crystallization and mechanical properties PLA-sc	[296]
PLLA-PEG(2Kg/mol)-PLLA/PDLA-PEG(2Kg/mol)-PDLA	ROP, $Sn(Oct)_2$, PEG as initiator	220.7	7.5	44	43				
PLLA-PEG(6Kg/mol)-PLLA/PDLA-PEG(6Kg/mol)-PDLA		223.5	9.7	44	42				
PLLA-PEG(20Kg/mol)-PLLA/PDLA-PEG(20Kg/mol)-PDLA		223.5	22.8	45	45				
PLLA-PEG(20Kg/mol)-PLLA/PDLA-PEG(20Kg/mol)-PDLA		224.7	55.7	30	32				
PLLA-PEG(20Kg/mol)-PLLA/PDLA-PEG(20Kg/mol)-PDLA		223.2	68.6	22	20				
Poly(L-lactic acid)-b-Poly(D-lactic acid)	ROP, $Sn(Oct)_2$, coupling of PLLA and PDLA by CuAAC	197.4 218.6 222 224.6 204.2	33.5 39.9 32.3 27.0 18.5	6 31 51 40 22	8 33 59 65 81	50	-	Crystallization kinetics, crystalline structure, and thermomechanical properties of PLA-sc from PLA stereoblock	[297]
PLLA-PHPC-PLLA/PDLA-PHPC-PDLA	ROP, $Sn(Oct)_2$, polycarbonate diols	184 191.3 197.4 203.2 206.7	- - - - -	9.4 21 5.7 11 21	10 20.8 5 10.7 21.1	50	Solution	Effect polycarbonate soft block	[465]

(*continued on next page*)

Table 2 (*continued*)

Sample	Synthesis Method	T_m (°C)	X_c	Mw (PLLA) (Kg/mol)	Mw (PDLA) (Kg/mol)	D-Ratio (wt%)	Blending technique	Application	REF
PLLA-PDLA-PLLA	ROP, $Sn(Oct)_2$, Dodecamethylene glycol,6-Hexamethylenediisocyanate (HMDI)	197.1 206.4 212.2 214.6 207.7	36.8 35.5 35.4 31.8 23.6	2.5 5 7.5 10 40	5 10 15 20 20	50 50 50 50 20	-	Thermomechanical properties of PLA stereomultiblock	[299]
PLLA-b-PEG-b-PLLA/PDLA-b-PEG-b-PDLA	ROP, $(sn(Oct)_2$, PEG diol	216 218 216 217 217	6.5 17.0 23.2 34.2 35.2	90	85.4	10 20 30 40 50	Melt blending	Mechanical properties and heat resistance	[280]
PLLA-b-PCL (9,1 Kg/mol)-b-PDLA	ROP, $(sn(Oct)_2$, PCL diol	207.4 208.6 207.8 207.8 209	4.5 14.9 23.4 27.8 28.0	5.9	5.8	10 20 30 40 50	Solution	Thermoplastic elastomer	[288]
PLLA-b-PCL (8,6 Kg/mol)-b-PDLA		203.7 209.4 209.9 210.2 212.7	5.8 15.0 21.0 30.1 30.4	6.3	5.4	10 20 30 40 50			
PLLA-b-PDLA	ROP, $(sn(Oct)_2$, D-lactid acid as initiator to afford PDLA prepolymer. Then ROP of LLA from PDLA to afford stereodiblock PLAs	185.8 185 202 195.2 210.4 208.9 211.2 208.5 201.8 198.4	0 0.4 0 0 0.1 0 0 1.3 0.4 0	1.57 1.57 3 3 4.96 4.96 4.96 5.1 5.1 5.1	20.43 40.13 0.39 58.8 39.34 89.64 10.34 37.6 72.6 142.9	11.1 7.2 14.4 5.4 28.4 10.6 4.3 38.6 16.6 5.8	-	Effect of short PDLA block	[466]
PDLA-b-PLLA-b-PLLA-b-PDLA	ROP with Tin(II) 2-ethylhexanoate as initiator	184 208.5 210.2	0 2.0 2.1	8.08 17.1 33.2	5.62 11.4 23.2	49.1 49.5 48.2	-	Effect of architecture on SC formation.	[467]
PLLA-alt-GA/PDLA-alt-GA	Discreete oligomerization	187.2	29.2	5.01	4.63	50	Solution	Thermal and mechanical properties	[468]
PLLA-b-PDLLA/PDLA-b-PDLLA	ROP, $(sn(Oct)_2$, 1-hexanol as initiator to afford PDLA prepolymer. Then ROP of LLA from PDLA to afford stereodiblock PLAs	226.9/246 206.8 207.1 187.6	NI	19.3 14.7 10.7 5.03	20.5 14.6 9.57 4.71	50 50 50 50	Solution	The effect of amorphous PDLLA block on the crystallization of PLLA and PDLA	[267]

(*continued on next page*)

Table 2 (*continued*)

Sample	Synthesis Method	T_m (°C)	X_c	Mw (PLLA) (Kg/mol)	Mw (PDLA) (Kg/mol)	D-Ratio (wt%)	Blending technique	Application	REF
Linear PLLA/PDLA/PEG (2Kg/mol)	Commercial	214.5	NI	39	35	60	Solution	The role of PEG crystallization on the SC formation	[469]
		218.7				45			
		215.3				30			
		214.4				40			
Linear PLLA/PDLA/PEG (5 Kg/mol)		220.5				6			
		221.5				4.5			
		220.7				3			
		219				4			
PEG-b-PLLA/PEG-b-PDLA		219.2		31	27	70			
		221.1				60			
		220.1				50			
		220				40			
		218.3				30			
P(L-2HB-co-L-2H3MB)//P(D-2HB-co-D-2H3MB)	Polycondensation, using 5 wt % p-toluenesulfonic acid as the catalyst.	203.7	46.1	9[(c)]	11.9©	50	Solution	Study the SC behavoir of these random copolymers	[303]
poly(D,L-lactide-co-ε-caprolactone)(70 wt% with 0 % CL units)/PLLA/PDLA	poly(D,L-lactide-co-ε-caprolactone), ring-opening polymerization with $Sn(Oct)_2$	221.15	12.3	207	208	15	Solution/Mold compression	Biodegradable shape-memory materials	[407]
poly(D,L-lactide-co-ε-caprolactone)(70 wt% with 7 % CL units)/PLLA/PDLA		220.8	13.65						
poly(D,L-lactide-co-ε-caprolactone)(70 wt% with 14 % CL units)/PLLA/PDLA		223.3	14.44						
poly(D,L-lactide-co-ε-caprolactone)(70 wt% with 23 % CL units)/PLLA/PDLA		220.8	13.81						
PLLA-b-PCL (11 Kg/mol)-PLLA/PDLA-b-PCL (11 Kg/mol)-b-PDLA	Two-step ROP. Macroinitiatior ε-caprolactone with $Sn(Oct)_2$ as catalyst	220.5	8.7	10	10	32.3	Solution	Biomaterial for 3D printing	
PLLA-b-PCL (10 Kg/mol)-PLLA/PDLA-b-PCL (11 Kg/mol)-b-PDLA		219.9	1.9	20	20	39.6			
PLLA-b-PCL (20 Kg/mol)-PLLA/PDLA-b-PCL (23 Kg/mol)-b-PDLA		218.5	6.7	8	9	23.4			
PLLA-b-PCL (22 Kg/mol)-PLLA/PDLA-b-PCL (18 Kg/mol)-b-PDLA		221.8	1.2	16	19	34.5			
PPO-PLLA-sB-PDLA	Ring-opening ROP with $Sn(Oct)_2$ as a catalyst and PPO triol as a macroinitiator	220.6	34.8	8.5[(c)]		51.4	Solution	Develop PLA based materials with high thermal resistance	[259]
		225	36.4	12.1©		52.2			
		225.3	31.5	15.3[(c)]		49.7			
		204.5	11.8	15[(c)]		51.1			

(*continued on next page*)

Table 2 (*continued*)

Sample	Synthesis Method	T_m (°C)	X_c	Mw (PLLA) (Kg/mol)	Mw (PDLA) (Kg/mol)	D-Ratio (wt%)	Blending technique	Application	REF
Star and other complex architectures									
3-arms Star/3-arms Star	ROP + end-group functionalization	200–250	NI	55.00	52.00	50	Solution	Enhance SC formation	[207]
3-arms Star/3-arms Star (end-functionalized by 2-ureido-4[1H]-pyrimidione Homopolymer)				55.00	52.00				
3-arms Star/3-arms Star		200–252		91.00	85.00				
3-arms Star/3-arms Star (end-functionalized by 2-ureido-4[1H]-pyrimidione Homopolymer)		200–253		91.00	85.00				
PLLA/PDLA		200–254		64.00	64.00				
Lineal (end-functionalized by 2-ureido-4[1H]-pyrimidione Homopolymer homopolymer)Lineal (end-functionalized by 2-ureido-4[1H]-pyrimidione Homopolymer homopolymer)		200–255		64.00	64.00				
PLLA/PDLA		200–256		93.00	110.00				
Lineal (end-functionalized by 2-ureido-4[1H]-pyrimidione Homopolymer homopolymer)Lineal (end-functionalized by 2-ureido-4[1H]-pyrimidione Homopolymer homopolymer)		200–257		93.00	110.00				
Lineal PLLA/Densitric star oligomer PDLA	ROP from PAMAM dendrimer	185.9	0.70422535	100.00	2.19–2.55	5	Solution	Removal of Pd catalyst from water	[470]
		182.6	12.6760563			25			
		186.5	26.056338			50			
		161.0	4.22535211		1.07–1.20	50			
1 arm stereoblock PLLA/1 arm stereoblock PDLA	ROP in bulk then in toluene, from multifunctional initiators	223.2	38.5	83.5	83.5	50	-	Topology dependent on SC crystallization	[318]
3 arm stereoblock PLLA/3 arm stereoblock PDLA		219.5	34.8	26.7	26.7	50			
6 arm stereoblock PLLA/6 arm stereoblock PDLA		205.4	32.6	14.0	14.0	50			
1 arm stereoblock PLLA/1 arm stereoblock PDLA		225.9	40.1	202.3	202.3	50			
3 arm stereoblock PLLA/3 arm stereoblock PDLA		218.8	33.3	64.4	64.4	50			
6 arm stereoblock PLLA/6 arm stereoblock PDLA		218.2	29.0	33.4	33.4	50			
hyper-branched Silyl-terminated oligomers of poly(D-lactide)/ linear PLLA	ROP +hydrolitc polycondensation	189	0.7	2.30	3.00	4.9	Solution	Compatibilizer/reinforce particles	[471]
		189	2.1			10.1			
Linear (PLLA)/ Linear PDLA	ROP, $Sn(Oct)_2$ using multifunctional initiators	217	NI	200.00	47.50	5	Solution	Effect of arm number on rheology and thermal properties	[472]
Linear (PLLA)/ stars PDLA		241.3			50.80				
Linear (PLLA)/ stars PDLA		212.6			64.60				
Linear (PLLA)/ stars PDLA		216.1			66.80				

(*continued on next page*)

Table 2 (*continued*)

Sample	Synthesis Method	T_m (°C)	X_c	Mw (PLLA) (Kg/mol)	Mw (PDLA) (Kg/mol)	D-Ratio (wt%)	Blending technique	Application	REF
star-shaped poly(propylene oxide) block poly(D-lactide) block poly(L-lactide) (PPO–PDLA–PLLA) stereoblock copolymers	ROP, $Sn(Oct)_2$, tri-arm oligo PPO	196.6 195.8 192.4	NI	62.00 96.00 140.00		50 33.3 20	Solution	synthesis and thermal properties	[210]
Linear (PLLA)/ Linear PDLA	ROP, $Sn(Oct)_2$ using multifunctional alcohols	222 231/248 226/236/249 235 222 206	NI	70 50.00 32.00 15.00 8.00 4.00	68.00 52.00 31.00 14.00 7.00 5.00	50	solution	growth rate of the spherulite	[205]
3-arms star (PLLA)/3-arms star (PDLA)		220.5/230 226.8/240 232.2 211.8		95.00 60.00 35.00 10.00	105.00 57.00 33.00 9.00				
3-arms star (PLLA)/linear (PDLA)		224.7 228.8/246 220.4/230.7/241.7 225.4 206		130.00 95.00 60.00 35.00 10.00	42.00 31.00 21.00 11.00 5.00				
Linear PLLA/Linear PDLA	ROP, $Sn(Oct)_2$ using multifunctional alcohols	222 222 229	3.5 10.6 35.2	123	5.30	5 10 20	Solution	Heat resistance materials	[421]
Linear PLLA/2-arms PDLA		221 214 208	6.3 15.5 22.5		6.20	5 10 20			
Liner PLLA/3-arms PDLA		196 192 196	4.9 6.3 16.9		6.30	5 10 20			
2-arms etilenglicol-PLLA/2-arms etilenglicol-PDLA	$Sn(Oct)_2$, using ethylene glycol and succinic anhydride as the initiators	188.3	30.3	4.10	4.00	50	Solution	Crystallization of head-head and tail-tail 2 arms PLA	[266]
2-arms etilenglicol-PLLA/2-arms succinic anhydride-PDLA		199.8/203	64.6	4.10	4.30				
2-arms succinic anhydride-PLLA/2-arms etilenglicol-PDLA		198.8/205.2	69.4	4.70	4.00				
2-arms succinic anhydride-PLLA/2-arms succinic anhydride-PDLA		200.6	59.7	4.70	4.30				
4-arms stars steroblocks	$Sn(Oct)_2$, Pentaerytrhitol	213.17 194.38 172.1	NI	54.50 35.20 15.20		50	-	Crystallization of 4-arm star PLA-sc	[150]

(*continued on next page*)

Table 2 (*continued*)

Sample	Synthesis Method	T_m (°C)	X_c	Mw (PLLA) (Kg/mol)	Mw (PDLA) (Kg/mol)	D-Ratio (wt%)	Blending technique	Application	REF
4-arms stars stereoblocks/ Linear PLLA	$Sn(Oct)_2$, propanediol	188	0.1	13.00	15.00	75	Solution	Effects of Chain Directional Change, Coinitiator Moietyand Terminal Group	[473]
4-arms stars stereoblocks/ Linear PLLA		187.1	0.3	2.00	15.00	75			
4-arms stars stereoblocks/ Linear PDLA		186	0.5	15.00	14.00	75			
4-arms stars stereoblocks/ Linear PDLA		188.3	0.3	15.00	1.80	75			
4-arms stereodiblock	$Sn(Oct)_2$, Pentaerytrhitol	155.1	13.9	16.32		30	No blending	The effect of melt quenching on crystallization	[474]
		193.1	31.1	16.20		50			
		146.6	11.8	15.30		70			
4-arm PLLA/4-arm PDLA	$Sn(Oct)_2$, diazidoneopentyl glycol, protection of PLLA end-group before the ROP of DLA	193.17	15.0	10.00	10.00	NI	No blending	Crystallization properties of (PLLA)2-core-(PDLA)2	[214]
4-arm PLLA/linear PDLA		196.47	28.2	10.00	10.00				
Linear PLLA/4-arm PDLA		200.21	30.2	10.00	10.00				
Linear PLLA/Linear PDLA	$Sn(Oct)_2$, Pentaerytrhitol and 3-butyn-1-ol	185.11	21.2	10.70	10.10	50	Solution	Effect of star-shape architecture	[152]
4-arms PLLA/Linear PDLA		193.17	15.0	38.20	10.10	50			
Linear PLLA/4-arm PDLA		196.47	28.2	10.70	39.20	50			
4-arms PLLA/4-arms PDLA		200.21	30.2	38.20	39.20	50			
PLLA Linear /4-arms DL-D1,3	PLLA Commercial. 4-DL-D copolymers were synthesized using two-step ring-opening polymerization	174.60	9.0	67.10	13.70	20	Solution	Study the influence of D blocks length	[144]
PLLA Linear /4-arms DL-D1,8		182.60	15.6		15.60				
PLLA Linear /4-arms DL-D2,6		184.60	16.1		17.90				
SSPLLA/SSPDLA	ring-opening polymerization of l-lactide and d-lactide, using dipyridamole as the macroinitiator and $Sn(Oct)_2$ as the catalyst	225.00	33	60.50	65.00	50	Solution	Study the SC formation in a star-shaped polylactides	[308]
1-L/1-D	ROP, $Sn(Oct)_2$	234.6/ 245.8	62.5	13.50	14.20	50	Solution	Study the influence of PDDLA on the SC formation	[326]
1-L/1-D/1-DL (25 wt%.)		228.9 / 245.7	67.0			37.5			
1-L/1-D/1-DL (50 wt%.)		224.2	80.1			25			
1-L/1-D/1-DL (75 wt%.)		221.6	84.6			12.5			
4-L-D/1-DL		192.8	66.2	13 (a)	13(a)	100*			
4-L-D/1-DL (25 % wt.)		193.3	61.7			*75**			
4-L-D/1-DL (50 % wt.)		191.9	62.4			50*			
4-L-D/1-DL (75 % wt.)		183.6	46.9			25*			
PLLA/PDLA	ROP, $Sn(Oct)_2$	243.1	61.3	8.7	10.5	50	Solution	Study the influence of PLA architecture and the PEG comonomer on the SC formation	[327]
3-arm PLLA/Linear PDLA		230.4	58.8	26.7	10.5				
6-arm PLLA/Linear PDLA		239.9	50.1	51	10.5				
Linear PLLA/ PDLA-b-PEG-b-PDLA		223.9	61.8	8.7	20.4(a)				
3-arm PLLA/ PDLA-b-PEG-b-PDLA		226.7	68.5	26.7	20.4(a)				
6-arm PLLA/ PDLA-b-PEG-b-PDLA		222.5	56.9	51	20.4(a)				

(*continued on next page*)

Table 2 (*continued*)

Sample	Synthesis Method	T_m (°C)	X_c	Mw (PLLA) (Kg/mol)	Mw (PDLA) (Kg/mol)	D-Ratio (wt%)	Blending technique	Application	REF
PLLA/PDLA	Commercial	222.6 219.7 223.2	55.5 56.7 33.8	NI	NI	75 50 25	Melt blending	Develop PLA fibers using SC as reinforcement	[418]
PDLA-4-arm star/Linear PLLA	ROP, $Sn(Oct)_2$, Pentaerythritol	219.1 218.8 218.9	4.7 6.9 10.1	101	89	5 7 10	Melt-blending	Effect of branch structures	[475]
PDLA-comb like/Linear PLLA	ROP, $Sn(Oct)_2$, Triglycerol	220.4 220.1 220.6	4.5 6.6 8.9		85	5 7 10			
PDLA-Hyper branched/Linear PLLA	ROP, $Sn(Oct)_2$, Glycidol	217.5 217.6 217.6	5.9 8.5 11.6		89	5 7 10			
Pentablock poly-D-lactide, poly-L-lactide and poly(1,2-propylene succinate) (58 % wt)	two-step ring-opening polymerization (ROP) of D- and L-lactide using a dihydroxy-terminated PPS as a macro-initiator.	162.3	10.2	4	3.1	21	Solution	Improve the amount of SC using 1,2 Propylene Succinate	[122]
Pentablock poly-D-lactide, poly-L-lactide and poly(1,2-propylene succinate) (32 % wt)		191.8	29.6	13.1	8.5	34			
Pentablock poly-D-lactide, poly-L-lactide and poly(1,2-propylene succinate) (33.8 % wt)		191.9	32.9	13	13.2	36.5			
Pentablock poly-D-lactide, poly-L-lactide and poly(1,2-propylene succinate) (38.1 % wt)		195.3	28.8	13.1	20.1	38.5			
Pentablock poly-D-lactide, poly-L-lactide and poly(1,2-propylene succinate) (39.6 % wt)		199.9	28.5	21.4	10.1	39			
Pentablock poly-D-lactide, poly-L-lactide and poly(1,2-propylene succinate) (40.8 % wt)		200.9	27.7	21.4	12.6	39.5			
Pentablock poly-D-lactide, poly-L-lactide and poly(1,2-propylene succinate) (46.9 % wt)		202.5	29.3	21.4	25.1	42			
Pentablock poly-D-lactide, poly-L-lactide and poly(1,2-propylene succinate) (42.3 % wt)		196.2	22.7	21.4	31.6	43			
Non-Covalent terpolymer PS-b-SC-b-P2VP	"living" anionic polymerization high-vacuum techniques with sec-BuLi as initiator	220.3 223.3 231.1	33.0 38.3 39.3	5.6 7 11	5.5 7.1 10.7	-	Solution	Use the stereocomplexes as physical bonds bettewen PS-PLA/P2VP-PLA copolymers	[126]

(*continued on next page*)

Table 2 (*continued*)

Sample	Synthesis Method	T_m (°C)	X_c	Mw (PLLA) (Kg/mol)	Mw (PDLA) (Kg/mol)	D-Ratio (wt%)	Blending technique	Application	REF
PDLA/PLLA/PLLA-mb-PCL (0 wt%) PDLA/PLLA/PLLA-mb-PCL (5 wt%) PDLA/PLLA/PLLA-mb-PCL (10 wt%) PDLA/PLLA/PLLA-mb-PCL (15 wt%) PDLA/PLLA/PLLA-mb-PCL (20 wt%)	ring-opening polymerization of D-lactide using $Sn(Oct)_2$ as the catalyst	210.4 206.2 197.3 185.2 89.0	19.7 24.2 19.7 17.5 35.5	200 (a)	30.4	50 47.5 45 42.5 40	Solution	Increase the amount for SC	[120]
PDLA/PLLA-PGA-PPDX terpolymers	ring-opening polymerization with $Sn(Oct)_2$ as catalyst.	212.36 213.32 213.78 213.99	32.2 34.1 34.9 34.9	NI	NI	5 10 15 20	Solution	Enhance the crystallization degree of the PLLA	[133]
PLLA/PDLA poly(L-LA-ran-TMC) / poly(D-LA-ran-TMC)	ring-opening polymerization with $Sn(Oct)_2$ as catalyst.	221.6 214.6 206.5	14.1 32.5 42.5	100.9 61.1 71.2	93 54.3 64.5	50 47 44	Solution	UV Shielding film	[135]
PLLA-ALOOH-PBSU/PDLA	Commercial	214.7 215.8 216	6.6 13.9 19.8	68	135	3 6 9	Melt-blending	Develop a biodegradable and thermally stable composite	[175]
LD-4EG-0,5 wt% LD-4EG-0,3 wt% LD-4EG-0,1 wt% PLLA-PDLA	Commercial homopolymer modified with pentaerythritol glycidyl ether (4EG). With triethylamine as a catalyst.	214/218.5 215.9/221.4 217.3 218.3	NI	170 (a)	160 (a)	50	Melt-blending	Increase the amount for SC	[153]
PLLA-Thy/PDLA-Thy	ROP with OH-thymine as initiator	181.9 174.3	59.5 30.1	0.8 0.5	0.8 0.5	50	Solution	Study the influence of stereoregularities on PLA crystallization	[257]
LCB PLLA/PDLA	LCB PLA sample was prepared from linear PLLA by applying gamma irradiation with addition of a 0.4 wt % trifunctional monomer, trimethylolpropane triacrylate (TMPTA). PDLA Commercial	207.3 207.7 208.5 209.2	0.4 2.0 3.9 8.4	87	74	0.5 2 5 10	Solution	Study the formation of SC from LCB PLLA	[330]
LCB PLLA/PDLA	The monomer PETA and DCP were used to modify the liner PLLA and synthesize the LCB PLLA. PDLA commercial	218.0 218.4 218.6 219.5 220.4	1.5 4.1 5.3 9.1 14.2	100	141	1 3 5 8 10	Solution	Study the formation of SC from LCB PLLA	[329]

(*continued on next page*)

Table 2 (*continued*)

Sample	Synthesis Method	T_m (°C)	X_c	Mw (PLLA) (Kg/mol)	Mw (PDLA) (Kg/mol)	D-Ratio (wt%)	Blending technique	Application	REF
Nucleating Agents									
Linear PLLA/PDLA	PLLA: commercial, PDLA: ROP	230.3	21.99	210	100	50	Melt blending	Effect of temperature and external force	[332]
Linear PLLA/PDLA/PEG (10 wt%)		225.6	46.74			45.5			
Linear PLLA/PDLA/TMC-306 (1 wt%)		228.6	48.76			49.5			
Linear PLLA/PDLA/PEG (10 wt%)/TMC-306 (1 wt%)		233.5	55.22			45			
Linear PLLA/PDLA	PLLA: commercial, PDLA: academic source	226.5	43.7	210	100	50	Melt blending	Bioplastic foam with efficient heat resistance and electromagnetic shielding interference	[396]
Linear PLLA/PDLA/TAIC(0.1 wt%)		225.8	43.6			49.9			
Linear PLLA/PDLA/TAIC(0.2 wt%)		225.2	42.8			49.9			
Linear PLLA/PDLA/TAIC(0.3 wt%)		224.4	42.3			49.9			
Linear PLLA/PDLA/TAIC(0.4 wt%)		223.2	41.5			49.8			
Linear PLLA/PDLA/TAIC(0.5 wt%)		223.3	41.6			49.8			
Linear PLLA/PDLA/TAIC(0.4 wt%)/PEG(2.5 wt%)		222.1	46.2			48.6			
Linear PLLA/PDLA/TAIC(0.4 wt%)/PEG(5 wt%)		218.6	47.3			47.2			
Linear PLLA/PDLA/TAIC(0.4 wt%)/PEG(7.5wt%)		217.5	47.3			46.3			
Linear PLLA/PDLA/TAIC(0.4 wt%)/PEG(10 wt%)		219	41.1			45.3			
Linear PLLA/PDLA	PLLA: commercial, PDLA: ROP	221.4	23.6	51	70	50.0	Solution	Effect of nanocrystalline cellulose on PLA-sc crystallization	[386]
Linear PLLA/PDLA/Celulosa Nanocristalina (0.5 %w)		222.9	39.9			49.8			
Linear PLLA/PDLA/Celulosa Nanocristalina (1 % wt)		222.6	41.0			49.5			
Linear PLLA/PDLA/Celulosa Nanocristalina (2 % wt)		222.2	42.3			49.0			
Linear PLLA/PDLA/Celulosa Nanocristalina (5 % wt)		222.5	32.8			47.6			
Linear PLLA/PDLA/zinc phenylphosphonate	ROP, $Sn(Oct)_2$, 1-dodecanol, glycerol, sorbitol	219.5	5.8	143	191	50	Solution	Topology dependent on PLA-sc crystallization	[476]
Linear PLLA/PDLA/zinc phenylphosphonate (0.1 wt%)		217.5	13.0						
Linear PLLA/PDLA/zinc phenylphosphonate (0.5 wt%)		219.9	17.0						
Linear PLLA/PDLA/zinc phenylphosphonate (1 wt%)		215.8	36.4						
Linear PLLA/PDLA/zinc phenylphosphonate (2 wt%)		205.5	34.6						
Linear PLLA/PDLA/zinc phenylphosphonate (3 wt%)		196.6	30.1						
Linear PLLA/PDLA/ Xylan propionate	Commercial	220	NI	270	160	50	Solution	enhance crystallization	[390]

(*continued on next page*)

Table 2 (*continued*)

Sample	Synthesis Method	T_m (°C)	X_c	Mw (PLLA) (Kg/mol)	Mw (PDLA) (Kg/mol)	D-Ratio (wt%)	Blending technique	Application	REF
Linear PLLA/PDLA	Commercial	207	4.4	-	-	7	Melt blending	enhance crystallization and mechanical properties	[391]
Linear PLLA/PDLA/ N,N-ethylenebis (10-undecenamide) (0.5 wt%)		206	4.7			7			
Linear PLLA/PDLA/tetramethylenedicarboxylic dibenzoylhydrazide (0.5 wt%)		207.9	5.3			7			
Linear PLLA/PDLA	Commercial	215.4	21.5	170	120	50	Solution	Enhance the SC formation by using a nucleating agent	[252]
Linear PLLA/PDLA/N, N, N, N′ -salicylic tetra(1, 2, 4, 5-benzenetetracarboxylic acid) hydrazide (0.3 wt%)		218.2	24.6			49.9			
Linear PLLA/PDLA/N, N, N, N′ -salicylic tetra(1, 2, 4, 5-benzenetetracarboxylic acid) hydrazide (0.5 wt%)		218	25.3			49.8			
Linear PLLA/PDLA/N, N, N, N′ -salicylic tetra(1, 2, 4, 5-benzenetetracarboxylic acid) hydrazide (1 wt%)		217.8	26.3			49.5			
Linear PLLA/PDLA/N, N, N, N′ -salicylic tetra(1, 2, 4, 5-benzenetetracarboxylic acid) hydrazide (2 wt%)		217	28.2			49.0			
Linear PLLA/PDLA/N, N, N, N′ -salicylic tetra(1, 2, 4, 5-benzenetetracarboxylic acid) hydrazide (3 wt%)		218.5	31.5			48.5			
Linear PLLA/PDLA/aryl amide (0.5 wt%)	Commercial	217.4	13.7	146	141	49.8	Solution	enhance crystallization	[388]
Linear PLLA/PDLA	PLLA commercial, PDLA was synthesized by ROP	223.5	35.6	210	100	50	Melt blending/Melt spun	Enhance crystallization by PEG and TMC-306	[392]
Linear PLLA/PDLA/PEG (10 wt%)		222.7	42.2			45.5			
Linear PLLA/PDLA/PEG (10 wt%)/TMC-306 (1 wt%)		223.3	16.4			45.0			
Linear PLLA/PDLA	ROP, $Sn(Oct)_2$	215.4	47.2	95	45	50		Improve PLA-sc flexibility	[397]
Linear PLLA/PDLA/**Polysorb ID-37** (2 wt%)		213.1	47.1			49.02	Melt blending		
Linear PLLA/PDLA/**Polysorb ID-37** (4 wt%)		213.1	45.5			48.077			
Linear PLLA/PDLA/**Polysorb ID-37** (8 wt%)		211.2	46.9			46.296			
Linear PLLA/PDLA/**Polysorb ID-37** (16 wt%)		211.1	45.4			43.103			

(*continued on next page*)

Table 2 (*continued*)

Sample	Synthesis Method	T_m (°C)	X_c	Mw (PLLA) (Kg/mol)	Mw (PDLA) (Kg/mol)	D-Ratio (wt%)	Blending technique	Application	REF
Linear PLLA/PDLA	PLLA commercial, PDLA was	219.5	5.8	143	191	50	Solution	Enhance PLA-sc crystallization	[216]
Linear PLLA/PDLA/N,N',N''-tricyclohexyl-1,3,5-benzenetricarboxylamide (0.1 wt%)	synthesized by ROP [$Sn(Oct)_2$]	216.7	8.4			49.95			
Linear PLLA/PDLA/N,N',N''-tricyclohexyl-1,3,5-benzenetricarboxylamide (0.3 wt%)		215.8	12.6			49.85			
Linear PLLA/PDLA/N,N',N''-tricyclohexyl-1,3,5-benzenetricarboxylamide (0.5 wt%)		218.1	22.0			49.751			
Linear PLLA/PDLA/N,N',N''-tricyclohexyl-1,3,5-benzenetricarboxylamide (1 wt%)		220.3	32.0			49.505			
Linear PLLA/PDLA	Commercial	221	9.6	161	215	50	Solution	enhance crystallization and mechanical properties	[477]
Linear PLLA/PDLA/p-xylene bisalkyl urea (4 wt%)		222.4	23.4			48.077			
Linear PLLA/PDLA/p-xylene bisalkyl urea (6 wt%)		223.9	28.5			47.17			
Linear PLLA/PDLA/p-xylene bisalkyl urea (12 wt%)		226.6	25.6			44.643			
Linear PLLA/PDLA/p-xylene bisalkyl urea (18 wt%)		225.2	15.0			42.373			
Linear PLLA/Linear PDLA/3 %-D-Mannitol	Commercial	219	8.0	207	130	48.5	Melt-blendig	Microcellular PLA foam	[394]
Linear PLLA/Linear PDLA/2 %-D-Mannitol		220	10.2			49			
Linear PLLA/Linear PDLA/1 %-D-Mannitol		222	14.8			49.5			
Linear PLLA/Linear PDLA/0,7 %- D-Mannitol		221	15.0			49.65			
Linear PLLA/Linear PDLA/0,3 %- D-Mannitol		220	14.7			49.85			
Linear PLLA/Linear PDLA/0,1 %- D-Mannitol		219	11.2			49.95			
Linear PLLA/Linear PDLA/0 %-D-Mannitol		220	7.2			50			
PLLA/PDLA	Commercial	220.8	9.7	168	87	50	Melt-blendig	increase the amount of SC by adding nucleating agents	[395]
PLLA/PDLA/ PPZn (1 % wt)		220.8	10.8			49.5			
PLLA/PDLA/ Finntalc-M03 (1 % wt)		220.6	10.0			49.5			
PLLA/PDLA/ TMB-5 (5 % wt)		221.1	11.0			49.75			
PLLA/PDLA/ PEG 400 (10 % wt)		219	26.4			45			
PLLA/PDLA/ PEG 1500 (10 % wt)		219.6	16.7			45			
PLLA/PDLA/ NA-21 (1 % wt)		217.5	36.8			49.5			
PLLA/PDLA/ NA-21 (1% wt)/Finn (1 % wt)		216.7	40.3			49			

(*continued on next page*)

Table 2 (*continued*)

Sample	Synthesis Method	T_m (°C)	X_c	Mw (PLLA) (Kg/mol)	Mw (PDLA) (Kg/mol)	D-Ratio (wt%)	Blending technique	Application	REF
Ternary Blends									
PLLA/PDLA	PLLA and PMMA are from commercial source. PDLA were synthesized by ROP	217.1	14.4	210	100	50	Melt-blending	Effect of PMMA wt% on PLA-sc crystallization	[398]
PLLA/PDLA/PMMA(10 wt%)		215.5	20.2			45			
PLLA/PDLA/PMMA(25 wt%)		214.4	26.1			37.5			
PLLA/PDLA/PMMA(50 wt%)		214.8	25.4			25			
PLLA/PDLA	PLLA, PDLA and E-MA-GMA copolymer are from commercial source. Graft copolymer was prepared during reactive melt blending	215.6		170	130	50	Melt-blending	Tough and heat-resistance bioplastic	[156]
PLLA/PDLA/E-MA-GMA (5 wt%)		214.4				47.5			
PLLA/PDLA/E-MA-GMA (10 wt%)		214.2				45			
PLLA/PDLA/E-MA-GMA (15 wt%)		213.6	16.9			42.5			
PLLA/PDLA/E-MA-GMA (20 wt%)		213.1	18.2			40			
PLLA/PDLA/DMSA		215.4				50			
PLLA/PDLA/E-MA-GMA (5 wt%)/DMSA		214.4				47.5			
PLLA/PDLA/E-MA-GMA (10 wt%)/DMSA		212.8				45			
PLLA/PDLA/E-MA-GMA (15 wt%)/DMSA		212.2	35.6			42.5			
PLLA/PDLA/E-MA-GMA (20 wt%)/DMSA		211.8	35.9			40			
PLLA/PDLA	ROP of LA, $Sn(Oct)_2$, Dodecanol as initiator	227	5.2	81.9	91.3	50	Solution	PVPh enhances crystallization of PLA-sc via H-bonding	[400]
PLLA/PDLA/PVPh (10 wt%)		227	13.8			45			
PLLA/PDLA/PVPh (20 wt%)		224	21.0			40			
PLLA/PDLA/PVPh (30 wt%)		223.3	30.0			35			
PLLA/PDLA	ROP of LA, $Sn(Oct)_2$, Dodecanol as initiator	236.6	65.9	95	45	50	Melt-blending	Natural Rubber enhances cystallinity and thermal properties	[401]
PLLA/PDLA/NR (5 wt%)		231	46.7			47.5			
PLLA/PDLA/NR (10 wt%)		230.1	37.2			45			
PLLA/PDLA/NR (20 wt%)		230.1	32.4			40			
PLLA/PDLA/NR (30 wt%)		230.9	25.1			35			
PLLA/PDLA/GPOE (20 wt%)	PLLA and GPOE are from commercial source, PDLA was synthesized by ROP	217.1	1.4	207	110	1	Melt-blending	GPOE enhances crytsallization and rheological properties	[402]
		217.2	3.0			2			
		217.5	4.5			3			
		217.3	5.5			4			
		217.1	6.4			5			
PLLA/PDLA	Commercial source	219.3	8.9	199	216	50	Melt-blending	PVDF enhances polymorphic crystallization of PLA-sc	[403]
PLLA/PDLA/PVDF (10 wt%)		220.1	9.3			45			
PLLA/PDLA/PVDF (30 wt%)		221.2	16.0			35			
PLLA/PDLA/PVDF (50 wt%)		220.6	16.5			25			
PLLA/PDLA/PVDF (70 wt%)		220.4	18.1			15			
PLLA/PDLA/PVDF (90 wt%)		221	30.3			5			
PLLA/PBAT (10 wt%)/PDLA	Commercial source	222.8	7.4	NI		5	Melt-blending	PLA-sc promote PLA/PBAT foaming without cell coalescence	[404]
PLLA/PBAT (10 wt%)/PDLA		233.1	8.3			10			
PLLA/PBAT (20 wt%)/PDLA		229.21	8.9			5			
PLLA/PBAT (20 wt%)/PDLA		230.1	9.8			10			
PLLA/PDLA/PBAT (2 %)	Commercial source	219.1	NI	207	125	49	Melt-blending	PBAT enhances crystallization and mechanical properties of PLA-sc	[405]
PLLA/PDLA/PBAT (5 %)		219.8				47.5			
PLLA/PDLA/PBAT (10 %)		220.3				45			

(*continued on next page*)

Table 2 (*continued*)

Sample	Synthesis Method	T_m (°C)	X_c	Mw (PLLA) (Kg/mol)	Mw (PDLA) (Kg/mol)	D-Ratio (wt%)	Blending technique	Application	REF
PLLA/PDLA	Commercial source	218.3	13.6	207	125	50	Melt-blending	PVAc enhances crystallization and thermal resistance of PLA-sc	[406]
PLLA/PDLA/PVAc (150 kg/mol-10 wt%)		219.4	16.9			45			
PLLA/PDLA/PVAc (150 kg/mol-20 wt%)		218.8	45.0			40			
PLLA/PDLA/PVAc (150 kg/mol-30 wt%)		214.8	51.7			35			
PLLA/PDLA/PVAc (480 kg/mol-10 wt%)		218.5	13.3			45			
PLLA/PDLA/PVAc (480 kg/mol-20 wt%)		217.5	20.1			40			
PLLA/PDLA/PVAc (480 kg/mol-30 wt%)		217.1	26.2			35			
TPU (0 wt%)/PLLA/PDLA	Commercial source	223.9	6.9	160	153	90	Melt-blending. Procesing profile 220–220–190–190	Preparation of one-step nanofibrilated structure	[408]
TPU (50 wt%)/PLLA/PDLA		223.4	2.4			45	Melt-blending. Procesing profile 220–220–190–190		
TPU (50 wt%)/PLLA/PDLA		223.1	2.0				Melt-blending. Procesing profile 200–200–190–190		
TPU (50 wt%)/PLLA/PDLA		222.5	1.5				Melt-blending. Procesing profile 180–180–190–190		
PLLA/PDLA/EVA(20 wt%.)/ESA (0 wt%)	Commercial source	230.5	37.5	170	160	40	Melt-blending, Injection molding	Increase the amount of SC for a melt prepared sample	[157]
PLLA/PDLA/EVA(19.98 wt%.)/ESA (0.1 wt%)		230.5	37.2			39.96			
PLLA/PDLA/EVA(19.94 wt%.)/ESA (0.3 wt%)		230.5	37.5			39.88			
PLLA/PDLA/EVA(19.90 wt%.)/ESA (0.5 wt%)		230.5	37.5			39.8			
PLLA/PDLA	Commercial source	218.4	3.2	NI	NI	6	Melt-Blending Foaming	Develop PLLA based foams with higher thermal resistance.	[410]
PLLA/EGMA (15 wt%.)/PDLA		216	1.8			3			
PLLA/EGMA (15 wt%.)/PDLA		216.3	4.2			6			
PLLA/EGMA (15 wt%.)/PDLA		216.5	4.5			9			
PLLA/PDLA	PLLA and PDLA Commercial source	211	47.0	48	59	50	Solution	Evaluate the effect of plasticizers (POSS-NH2 and POSS-PEG) on the SC formation	[307]
PLLA/PDLA/POSS-NH_2 (10 wt%.)		214	39.6			45			
PLLA/PDLA/POSS-NH_2 (20 wt%.)		210	34.6			40			
PLLA/PDLA/POSS-NH_2 (30 wt%.)		208	28.0			35			
PLLA/PDLA/POSS-PEG (10 wt%.)		221	47.0			45			
PLLA/PDLA/POSS-PEG (20 wt%.)		221	51.8			40			
PLLA/PDLA/POSS-PEG (30 wt%.)		221	28.2			35			

(*continued on next page*)

Table 2 (*continued*)

Sample	Synthesis Method	T_m (°C)	X_c	Mw (PLLA) (Kg/mol)	Mw (PDLA) (Kg/mol)	D-Ratio (wt%)	Blending technique	Application	REF
PLLA/PCL-OH/PDLA-OH	PLLA Commercial source, PDLA-OH ROP with $Sn(Oct)_2$ as catalyst.	180.2 179.3 184.2 181.3	0.0 0.1 0.6 3.4	160	4.2	1 2 5 10	dynamic vulcanization	Increase the thougness of PLLA, using PCL and SC as physical crosslinker	[478]
PLLA/PBS (29.7 % wt.)/St-GMA-g-PDLA-g-PBS PLLA/PBS (29.4 % wt.)/St-GMA-g-PDLA-g-PBS PLLA/PBS (28.5 % wt.)/St-GMA-g-PDLA-g-PBS	PLLA Commercial source. St-GMA-g-PDLA-g-PBS was synthetized by melt blending of PDLA, PBS, and St-GMA with catalyst N, N-Dimehyloctadecy	218.5 221 223	NI	110	59.8	1[(c)] 2© 5(c)	melt blending	Increase the thougness and heat resistance of PLLA, using PBS and SC as compatibilizer	[479]
PDLA/PLLA6.7k, PDLA/MPEG-*b*-PLLA6.7k-*g*-ODG PDLA/MPEG-*b*-PLLA6.7k-*g*-MG PDLA/MPEG-*b*-PLLA6.7k-*g*-glucose	PLLA Commercial source. The PDLA was synthetized by ROP with $Sn(Oct)_2$ as catalyst. The PLLA copolymers by graft coupling using CDI as the bonding agent	199.8 211.7 212.2 212.3 212.8 214.2 214.8 215 216.3 213.1 215.1 217.7 217.1 217.3 200.7 210.9 211.2 211.5	1.0 3.8 9.1 18.9 0.2 0.4 3.5 7.5 12.5 0.4 1.4 5.8 8.3 17.4 0.6 1.1 1.8 5.5	6.7 11.1© 27.5© 46.4©	94.8	99.25 96.25 92.5 85 99.5 99 95 90 80 99.5 99 95 90 80 99 95 90 80	Solution	Study the influence of PEG block on the formation of SC	[480]
PLLA/PDLA PLLA/PDLA/TPU (15 wt%)	Commercial source	232.5 220.5	4.7 0.6 1.0 2.1 2.9 6.9	223	128	5 0.5 1 2 3 5	Melt-blending	Develop Nanofiber with high toghness and thermal resistance	[481]
Composites									
PLLA/PDLA PLLA/PDLA/CNT (5 wt%) PLLA/PDLA/CNT (10 wt%) PLLA/PDLA/CNT (20 wt%) PLLA/PDLA/CNT (30 wt%)	PLLA/PDLA from Commercial source/academic source. CNT/PLA-sc foam from gelation and solvent exchange process	219.2 220.1 219.5 219.4 219.2	47.2 46.3 43.1 45.4 40.2	223	95	50 47.5 45 40 35	Solution	High resistance bioplastic foam	[333]
PLLA/PDLA PLLA/PDLA/CNT-L-D (2 wt%) PLLA/PDLA/CNT-L-D (5 wt%) PLLA/PDLA/CNT-L-D (10 wt%) CNT-L-D	PLA was synthesized by ROP with $Sn(OCt)_2$ as catalyst. PLLA and PDLA was synthesized with lauryl alcohol as the initiator. CNT-L-D was synthesized with CNT-OH as initiator.	221 220 217 217 210	11.4788732 25.5633803 29.7183099 32.1830986 44.5774648	63.5 63.5/7.56 63.5/7.56 63.5/7.56 7.56	62.6 62.6/7.54 62.6/7.54 62.6/7.54 7.54	50(b) 50(b) 50(b) 50(b) 50(b)	Solution	Enhance the crystallization of PLA-sc	[331]

(*continued on next page*)

Table 2 (*continued*)

Sample	Synthesis Method	T_m (°C)	X_c	Mw (PLLA) (Kg/mol)	Mw (PDLA) (Kg/mol)	D-Ratio (wt%)	Blending technique	Application	REF
Py-PLLA/py-PDLA Py-PLLA/py-PDLA/Graphite nanoplatelets	ROP of LA, $Sn(Oct)_2$, pyrenemethanol as the initiator. GnP Pyr-L/Pyr-D SC were prepared by suspension method	207.5 222.8	30.6 NI	7	7	50(b)	Solution	Nanopapers	[341]
PLLA/PDLA PLLA/PDLA/CNT	PLA from commercial source. s-CNT/PLA Composites were prepared by mixing	217 217	34.9 NI	223	85	50(b)	Melt-blending	Enhance the crystallization of PLA-sc	[332]
PLLA/PDLA	PLA and graphene are from commercial source.	205.3 205.3 205.2 205.3 205.3	0.4 1.5 2.1 3.9 11.3	44.1	19.6	1 2 3 5 10	Solution	Enhance SCPL physical properties	[343]
PLLA/PDLA/Graphene (0,1 wt%.)		205.7	0.4			1			
PLLA/PDLA/Graphene (0,5 wt%.)		207.5	0.4						
PLLA/PDLA/Graphene (1 wt%.)		206.5	0.4						
PLLA/PDLA/Graphene (1,5 wt%.)		206.5	0.5						
PLLA/PDLA/Graphene (3 wt%.)		205.7	0.6						
PLLA/TiO2-g-PDLA (5 wt%) PLLA/TiO2-g-PDLA (8 wt%)	PLLA from commercial source. TiO2-g-PDLA was synthesized by ROP, Sn(OCt)2	207 203.6	NI NI	200	NI	5(b) 8(b)	Solution	Rheology	[354]
PLLA/PDLA PLLA/PDLA/CNT (0,001 wt%)	PLA and CNT are from commercial source	223 221.5	60.4 50.4	170	120	50	melt/Sintering	Nucleating agent	[334]
PLLA/PDLA PLLA/PDLA/[bmim][PF6] (2 wt%) PLLA/PDLA/[bmim][PF6] (5 wt%) PLLA/PDLA/[bmim][PF6] (2 wt%)/0.04 wt% Graphene PLLA/PDLA/[bmim][PF6] (2 wt%)/0.1 wt% Graphene	PLA and graphites are from commercial source	223 220 216 220 220	26.4 41.8 39.2 36.6 46.3	100	100	50	Melt-blending	Dispersing agent	[342]
Shark Gelatin/Stereo PLA diblocks nanoparticles	Commercial source	193.93	33.0				Solution	Drug delivery system	[383]
PLLA/PDLA/MWCNT-g-PEG (0 wt%) PLLA/PDLA/MWCNT-g-PEG (0.5 wt%) PLLA/PDLA/MWCNT-g-PEG (1.0 wt%) PLLA/PDLA/MWCNT-g-PEG (1.5 wt%) PLLA/PDLA/MWCNT-g-PEG (2.0 wt%)	Commercial source	200.7 207.8 212.4 211 211.6	22.5 19.2 9.2 6.1 4.1	200	240	50 49.75 49.5 49.25 49	Solution	Effect of MWCNT-g-PEG on PLA-sc	[340]

(*continued on next page*)

Table 2 (*continued*)

Sample	Synthesis Method	T_m (°C)	X_c	Mw (PLLA) (Kg/mol)	Mw (PDLA) (Kg/mol)	D-Ratio (wt%)	Blending technique	Application	REF
PLLA/Ligning-g-PDLA	PLLA-Commercial source.	196.9	0.6	170	9.1	NI	Solution	Develop a biodegradable	[170]
PLLA/Ligning-g-PDLA	Ligning-g-PDLA, Ring-opening	200.7	1.3		9.1	NI		composite	
PLLA/Ligning-g-PDLA	polymerization with ethylene	201.7	1.8		9.1	NI			
PLLA/Ligning-g-PDLA	glycol or pentaerythritol as	206.6	1.7		16	NI			
PLLA/Ligning-g-PDLA	initiator	210.3	3.3		16	NI			
PLLA/Ligning-g-PDLA		213	6.9		16	NI			
PLLA/2 arms PDLA		206.6	1.2		14	NI			
PLLA/2 arms PDLA		210.3	3.2		14	NI			
PLLA/2 arms PDLA		211.9	5.2		14	NI			
PLLA/4 arms PDLA		203.2	1.0		18	NI			
PLLA/4 arms PDLA		205.5	3.3		18	NI			
PLLA/4 arms PDLA		205.4	5.6		18	NI			
PLLA/PDLA/Graphene nanoplatelets (2 wt%)	Commercial source	206/216.9	40.9	253	70	35	Melt-blending	Develop a renewable high thermal conductivity composite	[351]
		204.3/216.3	28.6			30			
		205.3/216.7	29.4			25			
PLLA/PDLA/halloysite nanotubes (3 wt%)	Commercial source	187.8	14.0	238	268	48.5	Solution	Increase the amount of SC	[377]
PLLA/PDLA/ Cellulose nanofibers (0 wt%)	Commercial source	261.8	13.9	170	130	50	Solution	Biocomposite with high content of SC	[167]
PLLA/PDLA/ Cellulose nanofibers (0.5 wt%)		218.9	18.5			49.75			
PLLA/PDLA/ Cellulose nanofibers (1 wt%)		217.7	20.0			49.5			
PLLA/PDLA/ Cellulose nanofibers (2 wt%)		218.8	24.0			49			
PLLA/PDLA/ Cellulose nanofibers (3 wt%)		218.6	30.1			48.5			
PLLA-g-Nanolignin/PDLA	PDLA Commercial source, PLLA-g-Lignigne ROP method with L-lactide as the raw material and −OH of lignin as the initiator using toluene as the solvent	211	1.6			3	Solution	Improve the UV and Heat resistance of PLLA	[171]
		212.4	3.2			6			
		213.8	4.8			9			
		215.2	6.8			12			
		215.9	8.7			15			
PLLA/PDLA-g-Graphene nanoplatelets	PLLA-Commercial source. Graphene-g-PDLA, ring-opening polymerization of D -lactide with the aid of hydroxyl groups of the G-OH surface under the catalytic action of Sn(Oct)2	194.3	0.9	253	NI	1(b)	Melt-blending	Develop a biomaterial with encanced thermal conductivity and resistance.	[180]
		201	6.5			3(b)			
		199.4	24.5			5(b)			

(*continued on next page*)

Table 2 (*continued*)

Sample	Synthesis Method	T_m (°C)	X_c	Mw (PLLA) (Kg/mol)	Mw (PDLA) (Kg/mol)	D-Ratio (wt%)	Blending technique	Application	REF
PLLA/PDLA/ Cellulose fibers (0 %)	Commercial source	222.2	15.1	37	96	40	Melt-blending	Biocomposite with high content of SC	[362]
PLLA/PDLA/ Cellulose fibers (Flax 20 %)		224.4	24.4						
PLLA/PDLA/ Cellulose fibers (Lyocell 20 %)		224.4	28.8						
PLLA/PDLA/Silk fibroin nanodisc (0 wt%)	Commercial source	220	14.5	174	141	49.5	Solution	Biocomposite with high content of SC	[369]
PLLA/PDLA/Silk fibroin nanodisc (1 wt%)		219.6	36.2						
PLLA/PDLA/CNF (4 wt%)	Commercial source	205.7	8.4	253	120	10	Solution	Microelectronic devices	[371]
		209.1	9.5			20			
		210.3	11.2			30			
		208.7	16.7			40			
		209.2	20.7			50			
PLLA/PDLA/nanoHydroxyapatite (0 wt%)	Commercial source	221.7	16.1	NI	NI	5	Melt-blending (Injection Molding, annealing molding temperature 50~C)	Bioresorbable synthetic bone graft substitutes	[371]
PLLA/PDLA/nanoHydroxyapatite (1 wt%)		221.2	14.8						
PLLA/PDLA/nanoHydroxyapatite (5 wt%)		222.1	14.5						
PLLA/PDLA/nanoHydroxyapatite (10 wt%)		222	15.1						
PLLA/PDLA/nanoHydroxyapatite (15 wt%)		221.8	15.8						
PLLA/PDLA/Nanosilica (0 wt%)	Commercial source	220.2	17.0	207	110	50	Solution	Increase the amount of SC	[372]
PLLA/PDLA/Nanosilica (2.5 wt%)		220.9	17.1			48.8			
PLLA/PDLA/Nanosilica (5 wt%)		219.4	22.1			47.6			
PLLA/PDLA/Nanosilica (7.5 wt%)		219.4	22.2			46.5			
PLLA/PDLA/Nanosilica (10 wt%)		219.3	24.3			45.5			

References

[1] Bai H, Deng S, Bai D, Zhang Q, Fu Q. Recent advances in processing of stereocomplex-type polylactide. Macromol Rapid Commun 2017;38:1700454.
[2] Brzeziński M, Biela T. Polylactide nanocomposites with functionalized carbon nanotubes and their stereocomplexes: a focused review. Mater Lett 2014;121:244–50.
[3] Jing Y, Quan C, Liu B, Jiang Q, Zhang C. A mini review on the functional biomaterials based on poly(lactic acid) stereocomplex. Polym Rev 2016;56:262–86.
[4] Li Z, Tan BH, Lin T, He C. Recent advances in stereocomplexation of enantiomeric PLA-based copolymers and applications. Prog Polym Sci 2016;62:22–72.
[5] Luo F, Fortenberry A, Ren J, Qiang Z. Recent progress in enhancing poly(lactic acid) stereocomplex formation for material property improvement. Front Chem 2020;8:688.
[6] Masutani K, Kimura Y. Macromolecular design of specialty polylactides by means of controlled copolymerization and stereocomplexation. Polym Int 2017;66:260–76.
[7] Saeidlou S, Huneault MA, Li H, Park CB. Poly(lactic acid) crystallization. Prog Polym Sci 2012;37:1657–77.
[8] Saravanan M, Domb AJ. A contemporary review on-polymer stereocomplexes and its biomedical application. Eur J Nanomed 2013;5:81–96.
[9] Tsuji H. Poly(lactic acid) stereocomplexes: a decade of progress. Adv Drug Deliver Rev 2016;107:97–135.
[10] Tashiro K, Kouno N, Wang H, Tsuji H. Crystal structure of poly(lactic acid) stereocomplex: random packing model of PDLA and PLLA chains as studied by X-ray diffraction analysis. Macromolecules 2017;50:8048–65.
[11] Nofar M, Sacligil D, Carreau PJ, Kamal MR, Heuzey MC. Poly (lactic acid) blends: processing, properties and applications. Int J Biol Macromol 2019;125:307–60.
[12] Ebrahim Attia AB, Ong ZY, Hedrick JL, Lee PP, Ee PLR, Hammond PT, Yang YY. Mixed micelles self-assembled from block copolymers for drug delivery. Curr Opin Colloid In 2011;16:182–94.
[13] Tutoni G, Becker ML. Underexplored stereocomplex polymeric scaffolds with improved thermal and mechanical properties. Macromolecules 2020;53:10303–14.
[14] Im SH, Im DH, Park SJ, Chung JJ, Jung Y, Kim SH. Stereocomplex polylactide for drug delivery and biomedical applications: a review. Molecules 2021;26:2846.
[15] Paneva D, Spasova M, Stoyanova N, Manolova N, Rashkov I. Electrospun fibers from polylactide-based stereocomplex: why? Int J Polym Mater Polym Biomater 2021;70:270–86.
[16] Castro-Aguirre E, Iñiguez-Franco F, Samsudin H, Fang X, Auras R. Poly(lactic acid)—mass production, processing, industrial applications, and end of life. Adv Drug Deliver Rev 2016;107:333–66.
[17] Vink ETH, Rábago KR, Glassner DA, Gruber PR. Applications of life cycle assessment to natureworks™ polylactide (PLA) production. Polym Degrad Stabil 2003;80:403–19.
[18] Fujishiro S, Kan K, Akashi M, Ajiro H. Stability of adhesive interfaces by stereocomplex formation of polylactides and hybridization with nanoparticles. Polym Degrad Stabil 2017;141:69–76.
[19] Vert M, Chen J, Hellwich KH, Hodge P, Nakano T, Scholz C, Slomkowski S, Vohlidal J. Nomenclature and terminology for linear lactic acid-based polymers (IUPAC recommendations 2019). Pure Appl Chem 2020;92:193–211.
[20] Kahovec J, Kratochvíl P, Jenkins AD, Mita I, Papisov IM, Sperling LH, Stepto RFT. Source-based nomenclature for non-linear macromolecules and macromolecular assemblies (IUPAC recommendations 1997). Pure Appl Chem 1997;69:2511–22.
[21] Hofvendahl K, Hahn–Hägerdal B. Factors affecting the fermentative lactic acid production from renewable resources. Enzyme Microb Technol 2000;26:87–107.
[22] Masutani K, Kimura Y. Chapter 1 PLA synthesis. From the monomer to the polymer. Poly(lactic acid) science and technology: Processing, properties, additives and applications. The Royal Society of Chemistry; 2015. p. 1–36.
[23] Benninga H. A chapter in the history of biotechnology. A history of lactic acid making. Dordrecht: Springer; 1990. p. XXII, 478.
[24] Lunt J. Large-scale production, properties and commercial applications of polylactic acid polymers. Polym Degrad Stab 1998;59:145–52.
[25] Drumright RE, Gruber PR, Henton DE. Polylactic acid technology. Adv Mater 2000;12:1841–6.
[26] Shuklov IA, Jiao H, Schulze J, Tietz W, Kühlein K, Börner A. Studies on the epimerization of diastereomeric lactides. Tetrahedron Lett 2011;52:1027–30.
[27] Zhu JB, Chen EYX. From meso-lactide to isotactic polylactide: epimerization by B/N lewis pairs and kinetic resolution by organic catalysts. J Am Chem Soc 2015;137:12506–9.
[28] Kopinke FD, Remmler M, Mackenzie K, Möder M, Wachsen O. Thermal decomposition of biodegradable polyesters—ii. Poly(lactic acid). Polym Degrad Stab 1996;53:329–42.
[29] McNeill IC, Leiper HA. Degradation studies of some polyesters and polycarbonates—2. Polylactide: degradation under isothermal conditions, thermal degradation mechanism and photolysis of the polymer. Polym Degrad Stab 1985;11:309–26.
[30] MacDonald RT, McCarthy SP, Gross RA. Enzymatic degradability of poly(lactide): effects of chain stereochemistry and material crystallinity. Macromolecules 1996;29:7356–61.
[31] Thakur KAM, Kean RT, Zupfer JM, Buehler NU, Doscotch MA, Munson EJ. Solid state ^{13}C CP-MAS NMR studies of the crystallinity and morphology of poly(L-lactide). Macromolecules 1996;29:8844–51.
[32] Stanford MJ, Dove AP. Stereocontrolled ring-opening polymerisation of lactide. Chem Soc Rev 2010;39:486–94.
[33] Ovitt TM, Coates GW. Stereoselective ring-opening polymerization of meso-lactide: synthesis of syndiotactic poly(lactic acid). J Am Chem Soc 1999;121:4072–3.
[34] Chisholm MH, Eilerts NW, Huffman JC, Iyer SS, Pacold M, Phomphrai K. Molecular design of single-site metal alkoxide catalyst precursors for ring-opening polymerization reactions leading to polyoxygenates. 1. Polylactide formation by achiral and chiral magnesium and zinc alkoxides, (η^3-l)MOR, where L = trispyrazolyl- and trisindazolylborate ligands. J Am Chem Soc 2000;122:11845–54.
[35] Ladelta V, Ntetsikas K, Zapsas G, Hadjichristidis N. Non-covalent PS–SC–PI triblock terpolymers via polylactide stereocomplexation: synthesis and thermal properties. Macromolecules 2022;55:2832–43.
[36] Tashiro K, Wang H, Kouno N, Koshobu J, Watanabe K. Confirmation of the X-ray-analyzed heterogeneous distribution of the PDLA and PLLA chain stems in the crystal lattice of poly(lactic acid) stereocomplex on the basis of the vibrational circular dichroism ir spectral measurement. Macromolecules 2017;50:8066–71.
[37] Praveena NM, Virat G, Krishnan VG, Gowd EB. Stereocomplex formation and hierarchical structural changes during heating of supramolecular gels obtained by polylactide racemic blends. Polymer 2022;241:124530.
[38] Yashima E, Maeda K, Iida H, Furusho Y, Nagai K. Helical polymers: synthesis, structures, and functions. Chem Rev 2009;109:6102–211.
[39] Badrinarayanan P, Dowdy KB, Kessler MR. A comparison of crystallization behavior for melt and cold crystallized poly (L-lactide) using rapid scanning rate calorimetry. Polymer 2010;51:4611–18.
[40] Pratt CF, Hobbs SY. Comparative study of crystallization rates by d.s.c. and depolarization microscopy. Polymer 1976;17:12–16.
[41] Hay JN, Mills PJ. The use of differential scanning calorimetry to study polymer crystallization kinetics. Polymer 1982;23:1380–4.
[42] Kong Y, Hay JN. The measurement of the crystallinity of polymers by DSC. Polymer 2002;43:3873–8.
[43] Stoclet G, Seguela R, Lefebvre JM, Rochas C. New insights on the strain-induced mesophase of poly(D,L-lactide): In situ WAXS and DSC study of the thermo-mechanical stability. Macromolecules 2010;43:7228–37.
[44] Zell MT, Padden BE, Paterick AJ, Thakur KAM, Kean RT, Hillmyer MA, Munson EJ. Unambiguous determination of the ^{13}C and ^{1}H NMR stereosequence assignments of polylactide using high-resolution solution nmr spectroscopy. Macromolecules 2002;35:7700–7.
[45] Thakur KAM, Kean RT, Hall ES, Kolstad JJ, Munson EJ. Stereochemical aspects of lactide stereo-copolymerization investigated by ^{1}H NMR: A case of changing stereospecificity. Macromolecules 1998;31:1487–94.
[46] Robert JL, Aubrecht KB. Ring-opening polymerization of lactide to form a biodegradable polymer. J Chem Educ 2008;85:258.
[47] Kasperczyk JE. Microstructure analysis of poly(lactic acid) obtained by lithium tert-butoxide as initiator. Macromolecules 1995;28:3937–9.
[48] Thakur KAM, Kean RT, Hall ES, Kolstad JJ, Lindgren TA, Doscotch MA, Siepmann JI, Munson EJ. High-resolution ^{13}C and ^{1}H solution NMR study of poly(lactide). Macromolecules 1997;30:2422–8.
[49] Coudane J, Ustariz-Peyret C, Schwach G, Vert M. More about the stereodependence of DD and LL pair linkages during the ring-opening polymerization of racemic lactide. J Polym Sci, Part A: Polym Chem 1997;35:1651–8.
[50] Bero M, Dobrzyński P, Kasperczyk J. Synthesis of disyndiotactic polylactide. J Polym Sci, Part A: Polym Chem 1999;37:4038–42.
[51] Spassky N, Simic V, Montaudo MS, Hubert-Pfalzgraf LG. Inter- and intramolecular ester exchange reactions in the ring-opening polymerization of (D,L)-lactide using lanthanide alkoxide initiators. Macromol Chem Phys 2000;201:2432–40.
[52] Belleney J, Wisniewski M, Le Borgne A. Influence of the nature of the ligand on the microstructure of poly D,L-lactides prepared with organoaluminum initiators. Eur Polym J 2004;40:523–30.
[53] Chisholm MH, Iyer SS, McCollum DG, Pagel M, Werner-Zwanziger U. Microstructure of poly(lactide). Phase-sensitive hetcor spectra of poly(meso-lactide), poly(rac-lactide), and atactic poly(lactide). Macromolecules 1999;32:963–73.
[54] Cheng HN. Stereochemistry of vinyl polymers and NMR characterization. J Appl Polym Sci 1988;36:229–41.
[55] Bovey FA. The stereochemical configuration of vinyl polymers and its observation by nuclear magnetic resonance. Acc Chem Res 1968;1:175–85.
[56] Moon SI, Lee CW, Taniguchi I, Miyamoto M, Kimura Y. Melt/solid polycondensation of L-lactic acid: An alternative route to poly(L-lactic acid) with high molecular weight. Polymer 2001;42:5059–62.
[57] Vouyiouka SN, Karakatsani EK, Papaspyrides CD. Solid state polymerization. Prog Polym Sci 2005;30:10–37.
[58] Masanobu A, Katashi E, Kazuhiko S, Akihiro Y. Basic properties of polylactic acid produced by the direct condensation polymerization of lactic acid. Bull Chem Soc Jpn 1995;68:2125–31.
[59] Hartmann MH. High molecular weight polylactic acid polymers. In: Kaplan DL, editor. Biopolymers from renewable resources. Berlin, Heidelberg: Springer Berlin Heidelberg; 1998. p. 367–411.
[60] Garlotta D. A literature review of poly(lactic acid). J Polym Environ 2001;9:63–84.

[61] Slomkowski S, Penczek S, Duda A. Polylactides—an overview. Polym Adv Technol 2014;25:436–47.
[62] Pretula J, Slomkowski S, Penczek S. Polylactides—methods of synthesis and characterization. Adv Drug Deliver Rev 2016;107:3–16.
[63] Witzke DR. Introduction to properties, engineering, and prospects of polylactide polymers. Michigan State University; 1997.
[64] Ko BT, Lin CC. Synthesis, characterization, and catalysis of mixed-ligand lithium aggregates, excellent initiators for the ring-opening polymerization of L-lactide. J Am Chem Soc 2001;123:7973–7.
[65] Kasperczyk J, Bero M. Stereoselective polymerization of racemic DL-lactide in the presence of butyllithium and butylmagnesium. Structural investigations of the polymers. Polymer 2000;41:391–5.
[66] Jaacks V, Mathes N. Formation of macrozwitterions in the polymerization of β-lactones initiated by tertiary amines. 2nd communication on macrozwitterions 1. Makromol Chem 1970;131:295–303.
[67] Mathes N, Jaacks V. Formation of macrozwitterions in the polymerization of β-propiolactone initiated by betaine. 4th communication on macrozwitterions. Makromol Chem 1971;142:209–25.
[68] Kazanskii KS, Ptitsyna NV. New functional poly(ethylene oxide)s: synthesis and application. Makromol Chem 1989;190:255–65.
[69] Corley LS, Vogl O, Biela T, Michalski J, Penczek S, Słombowski S. Optically active zwitterions. Makromol Chem Rapid Commun 1980;1:715–18.
[70] Corley LS, Vogl O, Biela T, Penczek S, Słomkowski S. Kinetics of zwitterion formation from β-propiolactone and tertiary phosphines. Makromol Chem Rapid Commun 1981;2:47–50.
[71] Biela T, Penczek S, Slomkowski S, Vogl O. Kinetic determination of stereoselectivity in the anionic polymerization of α-ethyl-α-phenyl-β-propiolactone. Makromol Chem 1983;184:811–19.
[72] Nederberg F, Connor EF, Glausser T, Hedrick JL. Organocatalytic chain scission of poly(lactides): a general route to controlled molecular weight, functionality and macromolecular architecture. Chem Commun 2001(20):2066–7.
[73] Nederberg F, Connor EF, Möller M, Glauser T, Hedrick JL. New paradigms for organic catalysts: the first organocatalytic living polymerization. Angew Chem Int Ed 2001;40:2712–15.
[74] Becker JM, Pounder RJ, Dove AP. Synthesis of poly(lactide)s with modified thermal and mechanical properties. Macromol Rapid Comm 2010;31:1923–37.
[75] Dove AP. Organic catalysis for ring-opening polymerization. ACS Macro Lett 2012;1:1409–12.
[76] Naumann S, Dove AP. N-heterocyclic carbenes for metal-free polymerization catalysis: an update. Polym Int 2016;65:16–27.
[77] Mezzasalma L, Dove AP, Coulembier O. Organocatalytic ring-opening polymerization of L-lactide in bulk: a long standing challenge. Eur Polym J 2017;95:628–34.
[78] Kiesewetter MK, Shin EJ, Hedrick JL, Waymouth RM. Organocatalysis: opportunities and challenges for polymer synthesis. Macromolecules 2010;43:2093–107.
[79] Zhang L, Nederberg F, Messman JM, Pratt RC, Hedrick JL, Wade CG. Organocatalytic stereoselective ring-opening polymerization of lactide with dimeric phosphazene bases. J Am Chem Soc 2007;129:12610–11.
[80] Connor EF, Nyce GW, Myers M, Möck A, Hedrick JL. First example of n-heterocyclic carbenes as catalysts for living polymerization: organocatalytic ring-opening polymerization of cyclic esters. J Am Chem Soc 2002;124:914–15.
[81] Xu J, Wang X, Liu J, Feng X, Gnanou Y, Hadjichristidis N. Ionic H-bonding organocatalysts for the ring-opening polymerization of cyclic esters and cyclic carbonates. Prog Polym Sci 2022;125:101484.
[82] Liu S, Li H, Zhao N, Li Z. Stereoselective ring-opening polymerization of rac-lactide using organocatalytic cyclic trimeric phosphazene base. ACS Macro Lett 2018;7:624–8.
[83] Kubisa P, Penczek S. Cationic activated monomer polymerization of heterocyclic monomers. Prog Polym Sci 1999;24:1409–37.
[84] Kricheldorf HR, Dunsing R. Polylactones, 8. Mechanism of the cationic polymerization of l,l-dilactide. Makromol Chem 1986;187:1611–25.
[85] Kricheldorf HR, Kreiser I. Polylactones, 11. Cationic copolymerization of glycolide with L,L-dilactide. Makromol Chem 1987;188:1861–73.
[86] Dechy-Cabaret O, Martin-Vaca B, Bourissou D. Controlled ring-opening polymerization of lactide and glycolide. Chem Rev 2004;104:6147–76.
[87] Kowalski A, Duda A, Penczek S. Kinetics and mechanism of cyclic esters polymerization initiated with tin(ii) octoate, 1. Polymerization of ε-caprolactone. Macromol Rapid Commun 1998;19:567–72.
[88] Ladelta V, Zapsas G, Abou-hamad E, Gnanou Y, Hadjichristidis N. Tetracrystalline tetrablock quarterpolymers: four different crystallites under the same roof. Angew Chem Int Ed 2019;58:16267–74.
[89] Bourissou D, Martin-Vaca B, Dumitrescu A, Graullier M, Lacombe F. Controlled cationic polymerization of lactide. Macromolecules 2005;38:9993–8.
[90] Kowalski A, Duda A, Penczek S. Mechanism of cyclic ester polymerization initiated with tin(II) octoate. 2.† macromolecules fitted with tin(II) alkoxide species observed directly in MALDI−TOF spectra. Macromolecules 2000;33:689–95.
[91] Majerska K, Duda A, Penczek S. Kinetics and mechanism of cyclic esters polymerisation initiated with tin(II) octoate, 4. Influence of proton trapping agents on the kinetics of ε-caprolactone and L,L-dilactide polymerisation. Macromol Rapid Commun 2000;21:1327–32.
[92] Kowalski A, Libiszowski J, Duda A, Penczek S. Polymerization of L,L-dilactide initiated by tin(II) butoxide. Macromolecules 2000;33:1964–71.
[93] Kowalski A, Duda A, Penczek S. Kinetics and mechanism of cyclic esters polymerization initiated with tin(II) octoate. 3. Polymerization of L,L-dilactide. Macromolecules 2000;33:7359–70.
[94] Libiszowski J, Kowalski A, Duda A, Penczek S. Kinetics and mechanism of cyclic esters polymerization initiated with covalent metal carboxylates, 5. End-group studies in the model ε-caprolactone and L,L-dilactide/tin(II) and zinc octoate/butyl alcohol systems. Macromol Chem Phys 2002;203:1694–701.
[95] Ryner M, Stridsberg K, Albertsson AC, von Schenck H, Svensson M. Mechanism of ring-opening polymerization of 1,5-dioxepan-2-one and L-lactide with stannous 2-ethylhexanoate. A theoretical study. Macromolecules 2001;34:3877–81.
[96] Penczek S, Pretula J, Slomkowski S. Ring-opening polymerization. Chem Teach Int 2021;3:33–57.
[97] Kowalski A, Duda A, Penczek S. Polymerization of L,L-lactide initiated by aluminum isopropoxide trimer or tetramer. Macromolecules 1998;31:2114–22.
[98] Ropson N, Dubois P, Jerome R, Teyssie P. Macromolecular engineering of polylactones and polylactides. 20. Effect of monomer, solvent, and initiator on the ring-opening polymerization as initiated with aluminum alkoxides. Macromolecules 1995;28:7589–98.
[99] Wang Y, Hu X, Morales-Rivera CA, Li GX, Huang X, He G, Liu P, Chen G. Epimerization of tertiary carbon centers via reversible radical cleavage of unactivated C(sp_3)–H bonds. J Am Chem Soc 2018;140:9678–84.
[100] Tsukegi T, Motoyama T, Shirai Y, Nishida H, Endo T. Racemization behavior of L,L-lactide during heating. Polym Degrad Stab 2007;92:552–9.
[101] Roy J. 7 - the stability of medicines. In: Roy J, editor. An introduction to pharmaceutical sciences. Woodhead Publishing; 2011. p. 153–81.
[102] Babanalbandi A, Hill DJT, Hunter DS, Kettle L. Thermal stability of poly(lactic acid) before and after γ-radiolysis. Polym Int 1999;48:980–4.
[103] Aoyagi Y, Yamashita K, Doi Y. Thermal degradation of poly[(R)-3-hydroxybutyrate], poly[ε-caprolactone], and poly[(S)-lactide]. Polym Degrad Stab 2002;76:53–9.
[104] Meimoun J, Favrelle-Huret A, Bria M, Merle N, Stoclet G, De Winter J, Mincheva R, Raquez JM, Zinck P. Epimerization and chain scission of polylactides in the presence of an organic base, TBD. Polym Degrad Stab 2020;181:109188.
[105] Abbina S, Du G. Zinc-catalyzed highly isoselective ring opening polymerization of *rac*-lactide. ACS Macro Lett 2014;3:689–92.
[106] Kan C, Hu J, Huang Y, Wang H, Ma H. Highly isoselective and active zinc catalysts for *rac*-lactide polymerization: effect of pendant groups of aminophenolate ligands. Macromolecules 2017;50:7911–19.
[107] Orhan B, Tschan MJL, Wirotius AL, Dove AP, Coulembier O, Taton D. Isoselective ring-opening polymerization of *rac*-lactide from chiral takemoto's organocatalysts: Elucidation of stereocontrol. ACS Macro Lett 2018;7:1413–19.
[108] Pang X, Duan R, Li X, Hu C, Wang X, Chen X. Breaking the paradox between catalytic activity and stereoselectivity: *rac*-lactide polymerization by trinuclear salen–Al complexes. Macromolecules 2018;51:906–13.
[109] Stewart JA, McKeown P, Driscoll OJ, Mahon MF, Ward BD, Jones MD. Tuning the thiolen: Al(III) and Fe(III) thiolen complexes for the isoselective ROP of *rac*-lactide. Macromolecules 2019;52:5977–84.
[110] Stopper A, Okuda J, Kol M. Ring-opening polymerization of lactide with Zr complexes of {ONSO} ligands: from heterotactically inclined to isotactically inclined poly(lactic acid). Macromolecules 2012;45:698–704.
[111] Xu TQ, Yang GW, Liu C, Lu XB. Highly robust yttrium bis(phenolate) ether catalysts for excellent isoselective ring-opening polymerization of racemic lactide. Macromolecules 2017;50:515–22.
[112] Miyake GM, Chen EYX. Cinchona alkaloids as stereoselective organocatalysts for the partial kinetic resolution polymerization of *rac*-lactide. Macromolecules 2011;44:4116–24.
[113] Grancharov G, Coulembier O, Surin M, Lazzaroni R, Dubois P. Stereocomplexed materials based on poly(3-hexylthiophene)-b-poly(lactide) block copolymers: Synthesis by organic catalysis, thermal properties, and microscopic morphology. Macromolecules 2010;43:8957–64.
[114] Boissé S, Kryuchkov MA, Tien ND, Bazuin CG, Prud'homme RE. PLLA crystallization in linear AB and BAB copolymers of L-lactide and 2-dimethylaminoethyl methacrylate. Macromolecules 2016;49:6973–86.
[115] Calucci L, Forte C, Buwalda SJ, Dijkstra PJ. Solid-state NMR study of stereocomplexes formed by enantiomeric star-shaped PEG–PLA copolymers in water. Macromolecules 2011;44:7288–95.
[116] Xie W, Jiang C, Yu X, Shi X, Wang S, Sun Y, Yin M, Wu D. Stereocomplex-induced self-assembly of PLLA-PEG-PLLA and PDLA -PEG-PDLA triblock copolymers in an aqueous system. ACS Appl Polym Mater 2021;3:6078–89.
[117] Kwon Y, Kim KT. Crystallization-driven self-assembly of block copolymers having monodisperse poly(lactic acid)s with defined stereochemical sequences. Macromolecules 2021;54:10487–98.
[118] Purnama P, Jung Y, Kim SH. Stereocomplexation of poly(L-lactide) and random copolymer poly(D-lactide-co-ε-caprolactone) to enhance melt stability. Macromolecules 2012;45:4012–14.
[119] Mulchandani N, Masutani K, Kumar S, Yamane H, Sakurai S, Kimura Y, Katiyar V. Toughened PLA-b-PCL-b-PLA triblock copolymer based biomaterials: effect of self-assembled nanostructure and stereocomplexation on the mechanical properties. Polym Chem 2021;12:3806–24.
[120] Jing Z, Huang X, Liu X, Liao M, Zhang Z, Li Y. Crystallization, thermal and mechanical properties of stereocomplexed poly(lactide) with flexible PLLA/PCL multiblock copolymer. RSC Adv 2022;12:13180–91.

[121] Aluthge DC, Xu C, Othman N, Noroozi N, Hatzikiriakos SG, Mehrkhodavandi P. PLA–PHB–PLAtriblockcopolymers: synthesisbysequential addition and investigationof mechanical and rheological properties. Macromolecules 2013;46:3965–74.
[122] Nishiwaki Y, Masutani K, Kimura Y, Lee CW. Synthesis and mechanochemical properties of biobased abcba-type pentablock copolymers comprising poly-D-lactide (a), poly-L-lactide (b) and poly(1,2-propylene succinate) (c). J Polym Sci 2022;60:2043–54.
[123] Zhou W, Chen X, Yang K, Fang H, Xu Z, Ding Y. Achieving morphological evolution and interfacial enhancement in fully degradable and supertough polylactide/polyurethane elastomer blends by interfacial stereocomplexation. Appl Surf Sci 2022;572:151393.
[124] Seki Y, Kanazawa A, Kanaoka S, Fujiwara T, Aoshima S. Precision synthesis of polylactide-based thermoresponsive block copolymers via successive living cationic polymerization of vinyl ether and ring-opening polymerization of lactide. Macromolecules 2018;51:825–35.
[125] Ge H, Zhang F, Huang H, He T. Interplay between stereocomplexation and microphase separation in PS-b-PLLA-b-PDLA triblock copolymers. Macromolecules 2019;52:1004–12.
[126] Arkanji A, Ladelta V, Ntetsikas K, Hadjichristidis N. Synthesis and thermal analysis of non-covalent PS-b-SC-b-P2VP triblock terpolymers via polylactide stereocomplexation. Polymers 2022;14:2431.
[127] Im SH, Jung Y, Kim SH. In situ homologous polymerization of L-lactide having a stereocomplex crystal. Macromolecules 2018;51:6303–11.
[128] Takizawa K, Nulwala H, Hu J, Yoshinaga K, Hawker CJ. Molecularly defined (L)-lactic acid oligomers and polymers: synthesis and characterization. J Polym Sci, Part A: Polym Chem 2008;46:5977–90.
[129] Tan R, Zhou D, Liu B, Sun Y, Liu X, Ma Z, Kong D, He J, Zhang Z, Dong XH. Precise modulation of molecular weight distribution for structural engineering. Chem Sci 2019;10:10698–705.
[130] Zhou D, Xu M, Li J, Tan R, Ma Z, Dong XH. Effect of chain length on polymer stereocomplexation: a quantitative study. Macromolecules 2021;54:4827–33.
[131] Lamers BAG, van Genabeek B, Hennissen J, de Waal BFM, Palmans ARA, Meijer EW. Stereocomplexes of discrete, isotactic lactic acid oligomers conjugated with oligodimethylsiloxanes. Macromolecules 2019;52:1200–9.
[132] Kwon Y, Ma H, Kim KT. Self-assembly of stereoblock copolymers driven by the chain folding of discrete poly(D-lactic acid-b-L-lactic acid) via intramolecular stereocomplexation. Macromolecules 2022;55:2768–76.
[133] Fan T, Qin J, Dong F, Meng X, Li Y, Wang Y, Liu Q, Wang G. Effects on the crystallization behavior and biocompatibility of poly(LLA-ran-PDO-ran-GA) with poly(D-lactide) as nucleating agents. RSC Adv 2022;12:10711–24.
[134] Bandelli D, Alex J, Helbing C, Ueberschaar N, Görls H, Bellstedt P, Weber C, Jandt KD, Schubert US. Poly(3-ethylglycolide): a well-defined polyester matching the hydrophilic hydrophobic balance of PLA. Polym Chem 2019;10:5440–51.
[135] Tsutsumi C, Nakayama S, Matsubara Y, Nakayama Y, Shiono T. An environmentally adaptable stereocomplex derived from lactide copolymers with improved UV shielding characteristics based on morphological changes. React Funct Polym 2022;173:105148.
[136] Scheuer K, Bandelli D, Helbing C, Weber C, Alex J, Max JB, Hocken A, Stranik O, Seiler L, Gladigau F, Neugebauer U, Schacher FH, Schubert US, Jandt KD. Self-assembly of copolyesters into stereocomplex crystallites tunes the properties of polyester nanoparticles. Macromolecules 2020;53:8340–51.
[137] Asano S, Choi J, Tran TH, Chanthaset N, Ajiro H. The influence of chain-end functionalization and stereocomplexation on the degradation stability under alkaline condition. Polym Adv Technol 2022;33:991–9.
[138] Ajiro H, Hsiao YJ, Thi TH, Fujiwara T, Akashi M. A stereocomplex of poly(lactide)s with chain end modification: simultaneous resistances to melting and thermal decomposition. Chem Commun 2012;48:8478–80.
[139] Ajiro H, Hsiao YJ, Tran HT, Fujiwara T, Akashi M. Thermally stabilized poly(lactide)s stereocomplex with bio-based aromatic groups at both initiating and terminating chain ends. Macromolecules 2013;46:5150–6.
[140] Sugai N, Yamamoto T, Tezuka Y. Synthesis of orientationally isomeric cyclic stereoblock polylactides with head-to-head and head-to-tail linkages of the enantiomeric segments. ACS Macro Lett 2012;1:902–6.
[141] Goonesinghe C, Jung HJ, Roshandel H, Diaz C, Baalbaki HA, Nyamayaro K, Ezhova M, Hosseini K, Mehrkhodavandi P. An air stable cationic indium catalyst for formation of high-molecular-weight cyclic poly(lactic acid). ACS Catal 2022;12:7677–86.
[142] Shin EJ, Jones AE, Waymouth RM. Stereocomplexation in cyclic and linear polylactide blends. Macromolecules 2012;45:595–8.
[143] Nagahama K, Fujiura K, Enami S, Ouchi T, Ohya Y. Irreversible temperature-responsive formation of high-strength hydrogel from an enantiomeric mixture of starburst triblock copolymers consisting of 8-arm PEG and PLLA or PDLA. J Polym Sci A1 2008;46:6317–32.
[144] Dai S, Jiang N, Ning Z, Gan Z. Relationship between crystallization state and degradation behavior of poly(L-lactide)/four-armed poly(D,L-lactide)-block-poly(D-lactide) blends with different poly(D-lactide) block lengths. Polym Int 2021;70:667–78.
[145] Nagahama K, Mori Y, Ohya Y, Ouchi T. Biodegradable nanogel formation of polylactide-grafted dextran copolymer in dilute aqueous solution and enhancement of its stability by stereocomplexation. Biomacromolecules 2007;8:2135–41.
[146] Biela T, Duda A, Penczek S. Enhanced melt stability of star-shaped stereocomplexes as compared with linear stereocomplexes. Macromolecules 2006;39:3710–13.
[147] Tsuji H, Miyase T, Tezuka Y, Saha SK. Physical properties, crystallization, and spherulite growth of linear and 3-arm poly(L-lactide)s. Biomacromolecules 2005;6:244–54.
[148] Hao Q, Li F, Li Q, Li Y, Jia L, Yang J, Fang Q, Cao A. Preparation and crystallization kinetics of new structurally well-defined star-shaped biodegradable poly(L-lactide)s initiated with diverse natural sugar alcohols. Biomacromolecules 2005;6:2236–47.
[149] Biela T. Stereocomplexes of star-shaped poly[(R)-lactide]s and poly[(S)-lactide]s bearing various number of arms. Synthesis and thermal properties. Polymery 2007;52:10.
[150] Tsuji H, Matsumura N, Arakawa Y. Stereocomplex crystallization and homo-crystallization of star-shaped four-armed stereo diblock poly(lactide)s during precipitation and non-isothermal crystallization. Polymer J 2016;48:1087–93.
[151] Isono T, Kondo Y, Otsuka I, Nishiyama Y, Borsali R, Kakuchi T, Satoh T. Synthesis and stereocomplex formation of star-shaped stereoblock polylactides consisting of poly(L-lactide) and poly(D-lactide) arms. Macromolecules 2013;46:8509–18.
[152] Zhou KY, Li JB, Wang HX, Ren J. Effect of star-shaped chain architectures on the polylactide stereocomplex crystallization behaviors. Chin J Polym Sci 2017;35:974–91.
[153] Diao X, Chen X, Deng S, Bai H. Substantially enhanced stereocomplex crystallization of poly(L-lactide)/poly(D-lactide) blends by the formation of multi-arm stereo-block copolymers. Crystals 2022;12:210.
[154] Sveinbjörnsson BR, Miyake GM, El-Batta A, Grubbs RH. Stereocomplex formation of densely grafted brush polymers. ACS Macro Lett 2014;3:26–9.
[155] Isono T, Kondo Y, Ozawa S, Chen Y, Sakai R, Sato S-i, Tajima K, Kakuchi T, Satoh T. Stereoblock-like brush copolymers consisting of poly(L-lactide) and poly(D-lactide) side chains along poly(norbornene) backbone: synthesis, stereocomplex formation, and structure–property relationship. Macromolecules 2014;47:7118–28.
[156] Deng S, Bai H, Liu Z, Zhang Q, Fu Q. Toward supertough and heat-resistant stereocomplex-type polylactide/elastomer blends with impressive melt stability via in situ formation of graft copolymer during one-pot reactive melt blending. Macromolecules 2019;52:1718–30.
[157] Deng S, Yao J, Bai H, Xiu H, Zhang Q, Fu Q. A generalizable strategy toward highly tough and heat-resistant stereocomplex-type polylactide/elastomer blends with substantially enhanced melt processability. Polymer 2021;224:123736.
[158] Jeong J, Ayyoob M, Kim JH, Nam SW, Kim YJ. In situ formation of pla-grafted alkoxysilanes for toughening a biodegradable pla stereocomplex thin film. RSC Adv 2019;9:21748–59.
[159] Chen J, Rong C, Lin T, Chen Y, Wu J, You J, Wang H, Li Y. Stable co-continuous pla/pbat blends compatibilized by interfacial stereocomplex crystallites: toward full biodegradable polymer blends with simultaneously enhanced mechanical properties and crystallization rates. Macromolecules 2021;54:2852–61.
[160] Chang X, Mao H, Shan G, Bao Y, Pan P. Tuning the thermoresponsivity of amphiphilic copolymers via stereocomplex crystallization of hydrophobic blocks. ACS Macro Lett 2019;8:357–62.
[161] Choi J, Takata T, Ajiro H. Pseudo-polyrotaxane stereocomplex with α-cyclodextrin and block copolymers using poly(ethylene glycol) and polylactide. Macromolecules 2021;54:5087–93.
[162] Brzeziński M, Biela T. Supramolecular polylactides by the cooperative interaction of the end groups and stereocomplexation. Macromolecules 2015;48:2994–3004.
[163] Chang R, Shan G, Bao Y, Pan P. Enhancement of crystallizability and control of mechanical and shape-memory properties for amorphous enantiopure supramolecular copolymers via stereocomplexation. Macromolecules 2015;48:7872–81.
[164] Monticelli O, Putti M, Gardella L, Cavallo D, Basso A, Prato M, Nitti S. New stereocomplex pla-based fibers: effect of poss on polymer functionalization and properties. Macromolecules 2014;47:4718–27.
[165] Sun Y, He C. Biodegradable "core–shell" rubber nanoparticles and their toughening of poly(lactides). Macromolecules 2013;46:9625–33.
[166] Yang J, Li W, Mu B, Xu H, Hou X, Yang Y. Simultaneous toughness and stiffness of 3D printed nano-reinforced polylactide matrix with complete stereo–complexation via hierarchical crystallinity and reactivity. Int J Biol Macromol 2022;202:482–93.
[167] Ren Q, Wu M, Weng Z, Zhu X, Li W, Huang P, Wang L, Zheng W, Ohshima M. Promoted formation of stereocomplex in enantiomeric poly(lactic acid)s induced by cellulose nanofibers. Carbohydr Polym 2022;276:118800.
[168] Fang HG, Yang KJ, Xie QZ, Chen X, Wu SL, Ding YS. Influence of interfacial enantiomeric grafting on melt rheology and crystallization of polylactide/cellulose nanocrystals composites. Chin J Polym Sci 2022;40:93–106.
[169] Jiang Y, Zhang Y, Cao M, Li J, Wu M, Zhang H, Zheng S, Liu H, Yang M. Combining 'grafting to' and 'grafting from' to synthesize comb-like NCC-g-PLA as a macromolecular modifying agent of PLA. Nanotechnology 2021;32:385601.
[170] Zhuang Z, Li T, Ning Z, Jiang N, Gan Z. Melt and nucleation reinforcement for stereocomplex crystallites in poly(L-lactide)/lignin-grafted-poly(D-lactide) blend. Eur Polym J 2022;167:111072.
[171] Yang W, Xiao L, Ding H, Xu P, Weng Y, Ma P. Fabrication of UV- and heat-resistant PDLA /PLLA-g-nanolignin composite films by constructing interfacial stereocomplex crystallites. ACS Sustain Chem Eng 2021;47:1587.
[172] Yang W, Qi G, Ding H, Xu P, Dong W, Zhu X, Zheng T, Ma P. Biodegradable poly (lactic acid)-poly (ε-caprolactone)-nanolignin composite films

with excellent flexibility and UV barrier performance. Compos Commun 2020;22:100497.
[173] Kim D, Bahi A, Liu LY, Bement T, Rogak S, Renneckar S, Ko F, Mehrkhodavandi P. Poly(lactide)-modified lignin nanofibers: Investigating the role of polymer tacticity on fiber properties and filtration efficiency. ACS Sustain Chem Eng 2022;10:2772–83.
[174] Shuai C, Yu L, Feng P, Peng S, Pan H, Bai X. Construction of a stereocomplex between poly(d-lactide) grafted hydroxyapatite and poly(L-lactide): toward a bioactive composite scaffold with enhanced interfacial bonding. J Mater Chem B 2022;10:214–23.
[175] Rong C, Chen Y, Chen C, Hu L, Wang H, Li Y. Toward simultaneous compatibilization and nucleation of fully biodegradabe nanocomposites: effect of nanorod-assisted interfacial stereocomplex crystals in immiscible polymer blends. Compos B Eng 2022;234:109708.
[176] Guo N, Zhao M, Li S, Hao J, Wu Z, Zhang C. Stereocomplexation reinforced high strength poly(L-lactide)/nanohydroxyapatite composites for potential bone repair applications. Polymers 2022;14:645.
[177] Brzeziński M, Bogusławska M, Ilčíková M, Mosnáček J, Biela T. Unusual thermal properties of polylactides and polylactide stereocomplexes containing polylactide-functionalized multi-walled carbon nanotubes. Macromolecules 2012;45:8714–21.
[178] Shang H, Ke L, Xu W, Shen M, Fan ZX, Zhang S, Wang Y, Tang D, Huang D, Yang HR, Zhou D, Xu H. Microwave-assisted direct growth of carbon nanotubes at graphene oxide nanosheets to promote the stereocomplexation and performances of polylactides. Ind Eng Chem Res 2022;61:1111–21.
[179] Xu H, Wu D, Yang X, Xie L, Hakkarainen M. Thermostable and impermeable "nano-barrier walls" constructed by poly(lactic acid) stereocomplex crystal decorated graphene oxide nanosheets. Macromolecules 2015;48:2127–37.
[180] Gu T, Sun DX, Qi XD, Yang JH, Zhao CS, Lei YZ, et al. Synchronously enhanced thermal conductivity and heat resistance in poly(L-lactide)/graphene nanoplatelets composites via constructing stereocomplex crystallites at interface. Compos B Eng 2021;224:109163.
[181] Lyu Y, Wen X, Wang G, Zhang Q, Lin L, Schlarb AK, Shi X. 3D printing nanocomposites with controllable "strength-toughness" transition: modification of SiO_2 and construction of stereocomplex crystallites. Compos Sci Technol 2022;218:109167.
[182] Pan P, Yang J, Shan G, Bao Y, Weng Z, Cao A, Yazawa K, Inoue Y. Temperature-variable ftir and solid-state ^{13}C NMR investigations on crystalline structure and molecular dynamics of polymorphic poly(L-lactide) and poly(L-lactide)/poly(D-lactide) stereocomplex. Macromolecules 2012;45:189–97.
[183] Okihara T, Tsuji M, Kawaguchi A, Katayama KI, Tsuji H, Hyon SH, Ikada Y. Crystal structure of stereocomplex of poly(L-lactide) and poly(D-lactide). J Macromol Sci B 1991;30:119–40.
[184] Watanabe K, Kumaki J. Extended-chain crystallization and stereocomplex formation of polylactides in a langmuir monolayer. Polym J 2020;52:601–13.
[185] Cartier L, Okihara T, Lotz B. Triangular polymer single crystals: stereocomplexes, twins, and frustrated structures. Macromolecules 1997;30:6313–22.
[186] Bai J, Wang J, Wang W, Fang H, Xu Z, Chen X, Wang Z. Stereocomplex crystallite-assisted shear-induced crystallization kinetics at a high temperature for asymmetric biodegradable PLLA/PDLA blends. ACS Sustain Chem Eng 2016;4:273–83.
[187] Chen HP, Nagarajan S, Woo EM. Unusual radiating-stripe morphology in nonequimolar mixtures of poly(L-lactic acid) with poly(D-lactic acid). Macromolecules 2020;53:2157–68.
[188] Feng C, Chen Y, Shao J, Hou H. The crystallization behavior of poly(L-lactic acid)/poly(D-lactic acid) electrospun fibers: effect of distance of isomeric polymers. Ind Eng Chem Res 2020;59:8480–91.
[189] Iguchi Y, Akasaka S, Asai S. Formation of pla stereocomplex crystals during melt-blending of asymmetric PLLA/PDLA/PMMA blends of varying miscibility. Polym J 2020;52:225–35.
[190] Ma Y, Li W, Li L, Fan Z, Li S. Stereocomplexed three-arm PPO-PDLA -PLLA copolymers: synthesis via an end-functionalized initiator. Eur Polym J 2014;55:27–34.
[191] Shyr TW, Ko HC, Wu TM. Crystallisation and spherulite morphology of polylactide stereocomplex. Polym Int 2019;68:141–50.
[192] Shao J, Guo Y, Ye S, Xie B, Xu Y, Hou H. The morphology and growth of PLA stereocomplex in PLLA/PDLA blends with low molecular weights. Polym Sci Ser A+ 2017;59:116–23.
[193] Srithep Y, Pholhan D, Turng LS, Akkaprasa T. Stereocomplex formation in injection-molded poly(L-lactic acid)/poly(D-lactic acid) blends. J Polym Eng 2019;39:279–86.
[194] Yu B, Cao Y, Sun H, Han J. The structure and properties of biodegradable PLLA/PDLA for melt-blown nonwovens. J Polym Environ 2017;25:510–17.
[195] Henmi K, Sato H, Matsuba G, Tsuji H, Nishida K, Kanaya T, Toyohara K, Oda A, Endou K. Isothermal crystallization process of poly(L-lactic acid)/poly(D-lactic acid) blends after rapid cooling from the melt. ACS Omega 2016;1:476–82.
[196] Zhang J, Sato H, Tsuji H, Noda I, Ozaki Y. Infrared spectroscopic study of ch3···oc interaction during poly(L-lactide)/poly(D-lactide) stereocomplex formation. Macromolecules 2005;38:1822–8.
[197] Yang CF, Huang YF, Ruan J, Su AC. Extensive development of precursory helical pairs prior to formation of stereocomplex crystals in racemic polylactide melt mixture. Macromolecules 2012;45:872–8.
[198] Li Z, Zhang M, Fan X, Ye X, Zeng Y, Zhou H, Guo W, Ma Y, Shao J, Yan C. Hydrogen bonding assists stereocomplexation in poly(L-lactic acid)/poly(D-lactic acid) racemic blends. J Polym Sci Pol Phys 2019;57:83–8.
[199] Zhang M, Fan X, Guo W, Zhou H, Li Z, Ma Y, Yan C, Dufresne A. Insights into stereocomplexation of poly(lactic acid) materials: Evolution of interaction between enantiomeric chains and its role in conformational transformation in racemic blends. ACS Appl Polym Mater 2022;4:5891–900.
[200] Li S, Liao X, Liu F, Li G. The crystallization morphology and process of stereocomplex crystallites of polylactide under CO_2: the effect of h-bonding and chain diffusion. CrystEngComm 2021;23:8601–11.
[201] Peng Q, Li S, Liu F, Liao X, Li G. Effect of CO_2 on the crystallization of poly(lactic acid) homo-crystallites via influencing the crystal structure of stereocomplex crystallites. CrystEngComm 2023;25:473–83.
[202] Tsuji H. Poly(lactide) stereocomplexes: formation, structure, properties, degradation, and applications. Macromol Biosci 2005;5:569–97.
[203] Lv T, Zhou C, Li J, Huang S, Wen H, Meng Y, Jiang S. New insight into the mechanism of enhanced crystallization of PLA in PLLA/PDLA mixture. J Appl Polym Sci 2018;135:45663.
[204] Liu J, Qi X, Feng Q, Lan Q. Suppression of phase separation for exclusive stereocomplex crystallization of a high-molecular-weight racemic poly(L-lactide)/poly(D-lactide) blend from the glassy state. Macromolecules 2020;53:3493–503.
[205] Shao J, Guo Y, Xiang S, Zhou D, Bian X, Sun J, Li G, Hou H. The morphology and spherulite growth of pla stereocomplex in linear and branched PLLA/PDLA blends: effects of molecular weight and structure. CrystEngComm 2016;18:274–82.
[206] Cao ZQ, Sun XR, Bao RY, Yang W, Xie BH, Yang MB. Carbon nanotube grafted poly(L-lactide)-block-poly(D-lactide) and its stereocomplexation with poly(lactide)s: the nucleation effect of carbon nanotubes. ACS Sustain Chem Eng 2016;4:2660–9.
[207] Bao J, Chang R, Shan G, Bao Y, Pan P. Promoted stereocomplex crystallization in supramolecular stereoblock copolymers of enantiomeric poly(lactic acid)s. Cryst Growth Des 2016;16:1502–11.
[208] Bouapao L, Tsuji H. Stereocomplex crystallization and spherulite growth of low molecular weight poly(L-lactide) and poly(D-lactide) from the melt. Macromol Chem Phys 2009;210:993–1002.
[209] Hu J, Wang J, Wang M, Ozaki Y, Sato H, Zhang J. Investigation of crystallization behavior of asymmetric PLLA/PDLA blend using raman imaging measurement. Polymer 2019;172:1–6.
[210] Li W, Ma Y, Fan Z. Effect of poly(L-lactide)/poly(D-lactide) block length ratio on crystallization behavior of star-shaped asymmetric poly(L(D)-lactide) stereoblock copolymers. Polym Eng Sci 2015;55:2534–41.
[211] Jing Z, Shi X, Zhang G. Competitive stereocomplexation and homocrystallization behaviors in the poly(lactide) blends of PLLA and PDLA-PEG-PDLA with controlled block length. Polymers 2017;9:107.
[212] Hortós M, Viñas M, Espino S, Bou JJ. Influence of temperature on high molecular weight poly(lactic acid) stereocomplex formation. Express Polym Lett 2019;13:123–34.
[213] Jing Z, Shi X, Zhang G. Rheology and crystallization behavior of asymmetric PLLA/PDLA blends based on linear PLLA and PDLA with different structures. Polym Adv Technol 2016;27:1108–20.
[214] Xie P, Wang J, Li J, Cheng Q, Zhou K, Ren J. Miktoarm star-shaped poly(lactic acid) copolymer: synthesis and stereocomplex crystallization behavior. J Polym Sci, Part A: Polym Chem 2019;57:814–26.
[215] Xie Q, Han L, Shan G, Bao Y, Pan P. Promoted stereocomplex formation and two-step crystallization kinetics of poly(L-lactic acid)/poly(D-lactic acid) blends induced by nucleator. Polym Cryst 2019;2:e10057.
[216] Xie Q, Han L, Shan G, Bao Y, Pan P. Polymorphic crystalline structure and crystal morphology of enantiomeric poly(lactic acid) blends tailored by a self-assemblable aryl amide nucleator. Acs Sustain Chem Eng 2016;4:2680–8.
[217] Souza DHS, Santoro PV, Diasa ML. Isothermal crystallization kinetics of poly(lactic acid) stereocomplex/graphene nanocomposites. Mater Res 2018;21:e20170352.
[218] Cui L, Wang Y, Guo Y, Liu Y, Zhao J, Zhang C, Zhu P. Cooperative effects of nucleation agent and plasticizer on crystallization properties of stereocomplex-type poly(lactide acid). Polym Adv Technol 2016;27:1301–7.
[219] Ikada Y, Jamshidi K, Tsuji H, Hyon . Stereocomplex formation between enantiomeric poly(lactides). Macromolecules 1987;20:904–6.
[220] Bao J, Chang X, Shan G, Bao Y, Pan P. Synthesis of end-functionalized hydrogen-bonding poly(lactic acid)s and preferential stereocomplex crystallization of their enantiomeric blends. Polym Chem 2016;7:4891–900.
[221] Bibi GJY, Lim JC, Kim SH. A faster approach to stereocomplex formation of high molecular weight polylactide using supercritical dimethyl ether. Polym Korea 2015;39:453–60.
[222] Guo Y, Shao J, Hou H. The toughening behavior of PLLA and its asymmetric PLLA/PDLA blends with lower optical purity. J Appl Polym Sci 2017; 134.
[223] Li Y, Li Q, Yang G, Ming R, Yu M, Zhang H, Shao H. Evaluation of thermal resistance and mechanical properties of injected molded stereocomplex of poly(L-lactic acid) and poly(D-lactic acid) with various molecular weights. Adv Polym Tech 2018;37:1674–81.
[224] Pan P, Han L, Bao J, Xie Q, Shan G, Bao Y. Competitive stereocomplexation, homocrystallization, and polymorphic crystalline transition in poly(L-lactic acid)/poly(D-lactic acid) racemic blends: molecular weight effects. J Phys Chem B 2015;119:6462–70.
[225] Guo M, Wu W, Wu W, Gao Q. Competitive mechanism of stereocomplexes and homocrystals in high-performance symmetric and asymmetric poly(lactic acid) enantiomers: qualitative methods. ACS Omega 2022;7:41412–25.
[226] Lodge TP, Hiemenz PC. Polym chem. 2nd ed. CRC Press; 2007.

[227] Boruvka M, Behalek L, Lenfeld P, Brdlik P, Habr J, Wongmanee S, Bobek J, Pechociakova M. Solid and microcellular polylactide nucleated with PLA stereocomplex and cellulose nanocrystals. J Therm Anal Calorim 2020;142:695–713.
[228] Zhang H, Li Y, Yang G, Yu M, Shao H. Effect of interfacial modification on the thermo-mechanical properties of flax reinforced polylactide stereocomplex composites. J Polym Eng 2020;40:403–8.
[229] Liu Z, Ling F, Diao X, Fu M, Bai H, Zhang Q, Fu Q. Stereocomplex–type polylactide with remarkably enhanced melt-processability and electrical performance via incorporating multifunctional carbon black. Polymer 2020;188:122136.
[230] Liu Z, Fu M, Ling F, Sui G, Bai H, Zhang Q, Fu Q. Stereocomplex–type polylactide with bimodal melting temperature distribution: toward desirable melt-processability and thermomechanical performance. Polymer 2019;169:21–8.
[231] Srithep Y, Pholharn D, Turng LS. Veang-In O. Injection molding and characterization of polylactide stereocomplex. Polym Degrad Stab 2015;120:290–9.
[232] Fu M, Liu Z, Bai D, Ling F, Bai H, Zhang Q, Fu Q. Low-temperature sintering of stereocomplex-type polylactide nascent powder: from compression molding to injection molding. Macromol Mater Eng 2018;303:1800178.
[233] Ming R, Yang G, Li Y, Wang R, Zhang H, Shao H. Flax fiber-reinforced polylactide stereocomplex composites with enhanced heat resistance and mechanical properties. Polym Compos 2017;38:472–8.
[234] Ming R, Yang G, Li Y, Zhang H, Shao H. Preparation and characterization of flax fiber reinforced polylactide stereoco MPLEX composites. Gaofenzi Cailiao Kexue Yu Gongcheng/Polym Mater Sci Eng 2015;31:169–72 and 77.
[235] Li Y, Yang G, Ming R, Li Q, Yu M, Zhang H, Shao H. Preparation and interfacial modification of flax fiber reinforced polylactide stereocomplex composite. Gaofenzi Cailiao Kexue Yu Gongcheng/Polym Mater Sci Eng 2016;32:109–14.
[236] Liu Z, Luo Y, Bai H, Zhang Q, Fu Q. Remarkably enhanced impact toughness and heat resistance of poly(L -lactide)/thermoplastic polyurethane blends by constructing stereocomplex crystallites in the matrix. ACS Sustain Chem Eng 2016;4:111–20.
[237] Dai J, Bai H, Liu Z, Chen L, Zhang Q, Fu Q. Stereocomplex crystallites induce simultaneous enhancement in impact toughness and heat resistance of injection-molded polylactide/polyurethane blends. RSC Adv 2016;6:17008–15.
[238] Zhang H, Ming R, Yang G, Li Y, Li Q, Shao H. Influence of alkali treatment on flax fiber for use as reinforcements in polylactide stereocomplex composites. Polym Eng Sci 2015;55:2553–8.
[239] Samuel C, Cayuela J, Barakat I, Müller AJ, Raquez JM, Dubois P. Stereocomplexation of polylactide enhanced by poly(methyl methacrylate): improved processability and thermomechanical properties of stereocomplexable polylactide-based materials. ACS Appl Mater Interfaces 2013;5:11797–807.
[240] Xu H, Tang S, Chen J, Yin P, Pu W, Lu Y. Thermal and phase-separation behavior of injection-molded poly(L-lactic acid)/poly(D-lactic acid) blends with moderate optical purity. Polym Bull 2012;68:1135–51.
[241] Shyr TW, Ko HC, Chen HL. Homocrystallization and stereocomplex crystallization behaviors of as-spun and hot-drawn poly(L-lactide)/poly(D-lactide) blended fibers during heating. Polymers 2019;11:1502.
[242] Gao XR, Niu B, Hua WQ, Li Y, Xu L, Wang Y, Ji X, Zhong GJ, Li ZM. Rapid preparation and continuous processing of polylactide stereocomplex crystallite below its melting point. Polym Bull 2019;76:3371–85.
[243] Rapp G, Samuel C, Odent J, Raquez JM, Dubois P, Bussiere PO, Gardette JL, Therias S. Peculiar effect of stereocomplexes on the photochemical ageing of pla/pmma blends. Polym Degrad Stab 2018;150:92–104.
[244] Gupta A, Katiyar V. Cellulose functionalized high molecular weight stereocomplex polylactic acid biocomposite films with improved gas barrier, thermomechanical properties. ACS Sustain Chem Eng 2017;5:6835–44.
[245] Wang L, Lee RE, Wang G, Chu RKM, Zhao J, Park CB. Use of stereocomplex crysallites for fully-biobased microcellular low-density poly(lactic acid) foams for green packaging. Chem Eng J 2017;327:1151–62.
[246] Gallos A, Fontaine G, Bourbigot S. Reactive extrusion of stereocomplexed poly-L, D-lactides: Processing, characterization, and properties. Macromol Mater Eng 2013;298:1016–23.
[247] Gallos A, Fontaine G, Bourbigot S. Reactive extrusion of intumescent stereocomplexed poly-l,d-lactide: characterization and reaction to fire. Polym Adv Technol 2013;24:130–3.
[248] Ramy-Ratiarison R, Lison V, Raquez JM, Duquesne E, Dubois P. Synthesis of melt-processable pla-based stereocomplexes through a sustainable melt-approach. Green Chem 2014;16:1759–63.
[249] Mandelkern L. Crystallization of polymers: Volume 2: Kinetics and mechanisms. 2 ed. Cambridge: Cambridge University Press; 2004.
[250] Sun C, Zheng Y, Xu S, Ni L, Li X, Shan G, Bao Y, Pan P. Role of chain entanglements in the stereocomplex crystallization between poly(lactic acid) enantiomers. ACS Macro Lett 2021;10:1023–8.
[251] He Y, Liu D, Wang J, Pan P, Hu W. Tammann analysis of the molecular weight selection of polymorphic crystal nucleation in symmetric racemic poly(lactic acid) blends. Macromolecules 2022;55:3661–70.
[252] Liu H, Zhou W, Chen P, Bai D, Cai Y, Chen J. A novel aryl hydrazide nucleator to effectively promote stereocomplex crystallization in high-molecular-weight poly(L-lactide)/poly(D-lactide) blends. Polymer 2020;210:122873.
[253] Fukushima K, Kimura Y. A novel synthetic approach to stereo-block poly(lactic acid). Macromol Symp 2005;224:133–44.
[254] Fukushima K, Hirata M, Kimura Y. Synthesis and characterization of stereoblock poly(lactic acid)s with nonequivalent D/L sequence ratios. Macromolecules 2007;40:3049–55.
[255] Fukushima K, Chang YH, Kimura Y. Enhanced stereocomplex formation of poly(L-lactic acid) and poly(D-lactic acid) in the presence of stereoblock poly(lactic acid). Macromol Biosci 2007;7:829–35.
[256] Fukushima K, Kimura Y. An efficient solid-state polycondensation method for synthesizing stereocomplexed poly(lactic acid)s with high molecular weight. J Polym Sci, Part A: Polym Chem 2008;46:3714–22.
[257] Xu S, Li X, Sun C, Ni L, Xu W, Yuan W, et al. Controllable crystallization and lamellar organization in nucleobase-functionalized supramolecular poly(lactic acid)s: Role of poly(lactic acid) stereostructure. Polymer 2021;232:124148.
[258] Zhu Q, Zhou ZP, Hao TF, Nie YJ. Significantly improved stereocomplexation ability in cyclic block copolymers. Chin J Polym Sci 2023;41:432–41.
[259] Wuyou Y, Qi X, Dongyang L, Shida G, Zhongyong F, Qing L. Crystallization behavior of stereoblock polylactide with high sequence regularity structure. Polym Adv Technol 2022;33:4381–90.
[260] Hirata M, Kimura Y. Thermomechanical properties of stereoblock poly(lactic acid)s with different PLLA/PDLA block compositions. Polymer 2008;49:2656–61.
[261] Hirata M, Kobayashi K, Kimura Y. Synthesis and properties of high-molecular-weight stereo di-block polulactides with nonequivalent D/L ratios. J Polym Sci, Part A: Polym Chem 2010;48:794–801.
[262] Hirata M, Kobayashi K, Kimura Y. Enhanced stereocomplexation by enantiomer adjustment for stereo diblock polylactides with non-equivalent D/L ratios. Macromol Chem Phys 2010;211:1426–32.
[263] Masutani K, Lee CW, Kimura Y. Synthesis and thermomechanical properties of stereo triblock polylactides with nonequivalent block compositions. Macromol Chem Phys 2012;213:695–704.
[264] Masutani K, Lee CW, Kimura Y. Synthesis of stereo multiblock polylactides by dual terminal couplings of poly-L-lactide and poly-D-lactide prepolymers: a new route to high-performance polylactides. Polymer 2012;53:6053–62.
[265] Hirata M, Masutani K, Kimura Y. Synthesis of ABCBA penta stereoblock polylactide copolymers by two-step ring-opening polymerization of L -and D -lactides with poly(3-methyl-1,5- pentylene succinate) as macroinitiator (c): development of flexible stereocomplexed polylactide materials. Biomacromolecules 2013;14:2154–61.
[266] Tsuji H, Tamai K, Kimura T, Kubota A, Tahahashi A, Kuzuya A, Ohya Y. Stereocomplex- and homo-crystallization of blends from 2-armed poly(L-lactide) and poly(D-lactide) with identical and opposite chain directional architectures and of 2-armed stereo diblock poly(lactide). Polymer 2016;96:167–81.
[267] Tsuji H, Iguchi K, Arakawa Y. Stereocomplex- and homo-crystallization behavior, structure, morphology, and thermal properties of crystalline and amorphous stereo diblock copolymers, enantiomeric poly(L-lactide)-b-poly(DL-lactide) and poly(D-lactide)-b-poly(DL-lactide). Polymer 2021;213:123226.
[268] Tsuji H, Ohsada K, Arakawa Y. Stereocomplex- and homo-crystallization behavior, polymorphism, and thermal properties of enantiomeric random copolymers of L- and D-lactic acids from the melt. Polymer 2021;228:123954.
[269] Tsuji H, Yamasaki M, Arakawa Y. Synthesis and stereocomplexation of new enantiomeric stereo periodical copolymers poly(L-lactic acid-L-lactic acid-D-lactic acid) and poly(D-lactic acid-D-lactic acid-L-lactic acid). Macromolecules 2021;54:6226–37.
[270] Xie Q, Han L, Zhou J, Shan G, Bao Y, Pan P. Homocrystalline mesophase formation and multistage structural transitions in stereocomplexable racemic blends of block copolymers. Polymer 2020;189:122180.
[271] Song Y, Wang D, Jiang N, Gan Z. Role of PEG segment in stereocomplex crystallization for PLLA-b-PEG b -PDLA blends. ACS Sustain Chem Eng 2015;3:1492–500.
[272] Li R, Wu Y, Bai Z, Guo J, Chen X. Effect of molecular weight of polyethylene glycol on crystallization behaviors, thermal properties and tensile performance of polylactic acid stereocomplexes. RSC Adv 2020;10:42120–7.
[273] Nakajima M, Nakajima H, Fujiwara T, Kimura Y, Sasaki S. Nano-ordered surface morphologies by stereocomplexation of the enantiomeric polylactide chains: specific interactions of surface-immobilized poly(D-lactide) and poly(ethylene glycol)-poly(L-lactide) block copolymers. Langmuir 2014;30:14030–8.
[274] Abebe DG, Fujiwara T. Controlled thermoresponsive hydrogels by stereocomplexed PLA-PEG-PLA prepared via hybrid micelles of pre-mixed copolymers with different PEG lengths. Biomacromolecules 2012;13:1828–36.
[275] Bao J, Mao H, Li X, Zhou J, Dong X, Chen S, et al. Salt-induced changes in sol-to-gel transition and structure of stereocomplexable poly(lactic acid)/poly(ethylene glycol) copolymers. Macromol Chem Phys 2021;222:2000354.
[276] Li W, Wang M, Luo H, Niu Y, Huang Y, Li G. Influence of miscible and immiscible sequences of poly(D-lactide) copolymers on the competition of stereocomplex- and homo-crystallization in poly(L-lactide) blends. Polymer 2021;218:123519.
[277] Srisuwan Y, Baimark Y. Improvement of water resistance of thermoplastic starch foams by dip-coating with biodegradable polylactide-b-polyethylene glycol-b-polylactide copolymer and its blend with poly(D-lactide). Prog Org Coat 2021;151:106074.
[278] Baimark Y, Pasee S, Rungseesantivanon W, Prakymoramas N. Flexible and high heat-resistant stereocomplex PLLA-PEG-PLLA/PDLA blends prepared by melt process: Effect of chain extension. J Polym Res 2019;26:218.
[279] Baimark Y, Rungseesantivanon W, Pasee S, Prakymoramas N. Preparation of chain-extended stereocomplex PLLA-PEG-PLLA/PDLA-PEG-PDLA blends for

potential use as flexible and high heat-resistant bioplastics. Int J Eng Res Technol 2019;12:513–18.
[280] Pasee S, Baimark Y. Improvement in mechanical properties and heat resistance of PLLA-b-PEG-b-PLLA by melt blending with PDLA-b-PEG-b-PDLA for potential use as high-performance bioplastics. Adv Polym Tech 2019;44:1–4.
[281] Baimark Y, Kittipoom S. Influence of chain-extension reaction on stereocomplexation, mechanical properties and heat resistance of compressed stereocomplex-polylactide bioplastic films. Polymers 2018;10:1218.
[282] Baimark Y, Srisuwan Y. Effects of block structure and poly(propylene glycol) block length on stereocomplexation and mechanical properties of poly(propylene glycol)-b-polylactide blend films. Polymers (Korea) 2018;42:385–93.
[283] Pholharn D, Cheerarot O, Baimark Y. Stereocomplexation and mechanical properties of polylactide-b-poly(propylene glycol)-b-polylactide blend films: Effects of polylactide block length and blend ratio. Chin J Polym Sci 2017;35:1391–401.
[284] Pakkethati K, Baimark Y. Plasticization of biodegradable stereocomplex polylactides with poly(propylene glycol). Polym Sci - A 2017;59:124–32.
[285] Srisuwan Y, Baimark Y. Improvement in stereocomplexation of poly(L-lactide)/poly(D-lactide) blended bioplastics by melt blending with epoxidized natural rubber. Int J Appl Eng Res 2017;12:15086–90.
[286] Baimark Y, Srihanam P. Influence of chain extender on thermal properties and melt flow index of stereocomplex PLA. Polym Test 2015;45:52–7.
[287] Caixia Z, Yuan J, Jingfeng H, Zou G, Li J. Non-isothermal and isothermal crystallization behavior of polylactic/poly(D-lactic) blends with various molecular weights of poly(D-lactic) acid. Polym Sci - A 2019;61:875–89.
[288] Shi X, Jing Z, Zhang G, Xu Y, Yao Y. Fully bio-based poly(ε-capolactone)/poly(lactide) alternating multiblock supramolecular polymers: synthesis, crystallization behavior, and properties. J Appl Polym Sci 2017;134:45575.
[289] Jing Z, Shi X, Zhang G, Lei R. Investigation of poly(lactide) stereocomplexation between linear poly(L-lactide) and PDLA-PEG-PDLA tri-block copolymer. Polym Int 2015;64:1399–407.
[290] Jing Z, Li J, Xiao W, Xu H, Hong P, Li Y. Crystallization, rheology and mechanical properties of the blends of poly(L-lactide) with supramolecular polymers based on poly(D-lactide)–poly(ε-caprolactone-co-δ-valerolactone)–poly(D-lactide) triblock copolymers. RSC Adv 2019;9:26067–79.
[291] Liu Y, Shao J, Sun J, Bian X, Chen Z, Li G, Chen X. Toughening effect of poly(D-lactide)-b-poly(butylene succinate)-b-poly(D-lactide) copolymers on poly(L-lactic acid) by solution casting method. Mater Lett 2015;155:94–6.
[292] Si WJ, Zhang H, Li YD, Huang C, Weng YX, Zeng JB. Highly toughened and heat resistant poly(L-lactide)/poly(ε-caprolactone) blends via engineering balance between kinetics and thermodynamics of phasic morphology with stereocomplex crystallite. Compos B Eng 2020;197:108155.
[293] Tien ND, Prud'homme RE. Crystallization and morphology of ultrathin films of poly(D-lactide) with BAB block copolymers in which the a block is made of poly(L-lactide). Polymer 2017;117:25–9.
[294] Yang DD, Liu W, Zhu HM, Wu G, Chen SC, Wang XL, Wang YZ. Toward super–tough poly(L-lactide) via constructing pseudo-cross-link network in toughening phase anchored by stereocomplex crystallites at the interface. ACS Appl Mater Interfaces 2018;10:26594–603.
[295] D'Ambrosio RM, Michell RM, Mincheva R, Hernández R, Mijangos C, Dubois P, Müller AJ. Crystallization and stereocomplexation of PLA-mb-PBS multi-block copolymers. Polymers 2017;10:8.
[296] Han L, Yu C, Zhou J, Shan G, Bao Y, Yun X, Dong T, Pan P. Enantiomeric blends of high-molecular-weight poly(lactic acid)/poly(ethylene glycol) triblock copolymers: Enhanced stereocomplexation and thermomechanical properties. Polymer 2016;103:376–86.
[297] Han L, Xie Q, Bao J, Shan G, Bao Y, Pan P. Click chemistry synthesis, stereocomplex formation, and enhanced thermal properties of well-defined poly(L-lactic acid)-b-poly(D-lactic acid) stereo diblock copolymers. Polym Chem 2017;8:1006–16.
[298] Kobayashi K, Kanmuri S, Kimura Y, Masutani K. Synthesis and properties of stereo mixtures of enantiomeric block copolymers of polylactide and aliphatic polycarbonate. Polym Int 2015;64:641–6.
[299] Masutani K, Kobayashi K, Kimura Y, Lee CW. Properties of stereo multi-block polylactides obtained by chain-extension of stereo tri-block polylactides consisting of poly(L-lactide) and poly(D-lactide). J Polym Res 2018;25:74.
[300] Tsuji H, Tajima T. Non-isothermal crystallization behavior of stereo diblock polylactides with relatively short poly(D-lactide) segments from the melt. Polym Int 2015;64:54–65.
[301] Gardella L, Cavallo D, Colonna S, Fina A, Monticelli O. Novel poly(L-lactide)/poly(D-lactide)/poly(tetrahydrofuran) multiblock copolymers with a controlled architecture: Synthesis and characterization. J Polym Sci, Part A: Polym Chem 2014;52:3269–82.
[302] Gardella L, Mincheva R, De Winter J, Tachibana Y, Raquez JM, Dubois P, Monticelli O. Synthesis, characterization and stereocomplexation of polyamide 11/polylactide diblock copolymers. Eur Polym J 2018;98:83–93.
[303] Tsuji H, Osanai K, Arakawa Y. Stereocomplex and individual crystallization behavior of symmetric or enantiomeric substituted poly(lactic acid)s random copolymers with high crystallizabilities. Polymer 2021;237:124352.
[304] Baimark Y, Rungseesantivanon W, Prakymoramas N. The effect of mold conditions on heat resistance of injection-molded stereocomplex polylactide-b-polyethylene glycol-b-polylactide bioplastic. Mater Plast 2021;58:11–22.
[305] Jing Z, Huang X, Liu X, Liao M, Li Y. Poly(lactide)-based supramolecular polymers driven by self-complementary quadruple hydrogen bonds: construction, crystallization and mechanical properties. Polym Int 2023;72:39–53.
[306] Choi J, Ajiro H. Preparation of stereocomplex and pseudo-polyrotaxane with various cyclodextrins as wheel components using triblock copolymer of poly(ethylene glycol) and polylactide. Soft Matter 2022;18:8885–93.
[307] Luo C, Li S, Yang M, Xiao W. Effect of poss-NH_2-grafted different plasticizers on the crystallization properties of sc-poly (L-lactic acid). J Polym Res 2022;29:516.
[308] Praveena NM, Nagarajan S, Gowd EB. Stereocomplexation of enantiomeric star-shaped poly(lactide)s with a chromophore core. CrystEngComm 2021;23:2122–32.
[309] Sugane K, Takahashi H, Shimasaki T, Teramoto N, Shibata M. Stereocomplexation, thermal and mechanical properties of conetworks composed of star-shaped L-lactide, D-lactide and ε-caprolactone oligomers utilizing sugar alcohols as core molecules. Polymers 2017;9:582.
[310] Tsuji H, Ozawa R, Arakawa Y. Stereocomplex crystallization of star-shaped four-armed stereo diblock poly(lactide) from the melt: Effects of incorporated linear one-armed poly(L-lactide) or poly(D-lactide). J Phys Chem B 2017;121:9936–46.
[311] Tsuji H, Sakamoto Y, Arakawa Y. Stereocomplex- and homo-crystallization and phase-transition behavior of relatively high-molecular-weight linear one- and two-armed and star-shaped four-armed poly(L-lactide)/poly(D-lactide) blends. Macromol Chem Phys 2017;218:1700286.
[312] Tsuji H, Ogawa M, Arakawa Y. Homo- and stereocomplex crystallization of star-shaped four-armed stereo diblock copolymers of crystalline and amorphous poly(lactide)s: Effects of incorporation and position of amorphous blocks. J Phys Chem B 2016;120:11052–63.
[313] Tsuji H, Matsumura N. Stereocomplex crystallization of star-shaped 4-armed equimolar stereo diblock poly(lactide)s with different molecular weights: Isothermal crystallization from the melt. Macromol Chem Phys 2016;217:1547–57.
[314] Tsuji H, Matsumura N, Arakawa Y. Stereocomplex crystallization and homocrystallization of star-shaped four-armed stereo diblock poly(lactide)s with different L-lactyl unit contents: isothermal crystallization from the melt. J Phys Chem B 2016;120:1183–93.
[315] Li W, Chen X, Ma Y, Fan Z. The accelerating effect of the star-shaped poly(D-lactide)-block-poly(L-lactide) stereoblock copolymer on PLLA melt crystallization. CrystEngComm 2016;18:1242–50.
[316] Tsuji H, Ozawa R, Matsumura N. Effect of incorporated star-shaped four-armed stereo diblock poly(lactide) on the crystallization behavior of linear one-armed poly(L-lactide) or poly(D-lactide). Polym J 2016;48:209–13.
[317] Tsuji H, Matsumura N, Arakawa Y. Correction to "stereocomplex crystallization and homocrystallization of star-shaped four-armed stereo diblock poly(lactide)s with different L-lactyl unit contents: Isothermal crystallization from the melt" (J Phys Chem B (2016) 120:6 (1183-1193) 10.1021/acs.Jpcb.5b11813). J Phys Chem B 2016;120:3257.
[318] Han L, Shan G, Bao Y, Pan P. Exclusive stereocomplex crystallization of linear and multiarm star-shaped high-molecular-weight stereo diblock poly(lactic acid)s. J Phys Chem B 2015;119:14270–9.
[319] Shibata M, Katoh M, Takase H, Shibita A. Stereocomplex formation in stereoblock copolymer networks composed of 4-armed star-shaped lactide oligomers and a 2-armed ε-caprolactone oligomer. Polym Chem 2015;6:4123–32.
[320] Jing Z, Shi X, Zhang G, Qin J. Synthesis, stereocomplex crystallization and properties of poly(L-lactide)/four-armed star poly(D-lactide) functionalized carbon nanotubes nanocomposites. Polym Adv Technol 2015;26:223–33.
[321] Pasee SCO, Baimark Y. Preparation of stereocomplex polylactide bioplastics from star-shaped/linear polylactide blending. Orient J Chem 2015;31:1551–8.
[322] Cheerarot O, Baimark Y. Thermal and mechanical properties of biodegradable star-shaped/linear polylactide stereocomplexes. J Chem 2015;2015:206123.
[323] Tsuji H, Yamashita Y. Highly accelerated stereocomplex crystallization by blending star-shaped 4-armed stereo diblock poly(lactide)s with poly(D-lactide) and poly(L-lactide) cores. Polymer 2014;55:6444–50.
[324] Tsuji H, Suzuki M. Hetero-stereocomplex crystallization between star-shaped 4-arm poly(L-2-hydroxybutanoic acid) and poly(D-lactic acid) from the melt. Macromol Chem Phys 2014;215:1879–88.
[325] Geschwind J, Rathi S, Tonhauser C, Schömer M, Hsu SL, Coughlin EB, Frey H. Stereocomplex formation in polylactide multiarm stars and comb copolymers with linear and hyperbranched multifunctional PEG. Macromol Chem Phys 2013;214:1434–44.
[326] Tsuji H, Nogata S, Tsukamoto N, Arakawa Y. Comparative study on the effects of incorporating poly(D,L-lactide) and solvent on stereocomplex crystallization and homocrystallization in unconstrained and constrained poly(L-lactide)/poly(D-lactide) systems. Polym J 2023;55:75–84.
[327] Wang J, Griffin A, Qiang Z, Ren J. Synergistic effect of star-shaped architecture and poly(ethylene glycol) moieties on poly(lactic acid) stereocomplex crystallization behaviors. Polym Int 2023;72:366–75.
[328] Li J, Ye W, Fan Z, Lu Z. Stereocomplex poly(lactic acid) vascular stents by 3D-printing with long chain branching structures: Toward desirable crystallization properties and mechanical performance. Polym Adv Technol 2021;32:97–110.
[329] Zhao Z, Tang D, Jia S, Ai T. Favorable formation of stereocomplex crystals in long-chain branched poly(L-lactic acid)/poly(D-lactic acid) blends: impacts of melt effect and molecular chain structure. J Mater Sci 2021;56:6514–30.

[330] Xu C, Zhang J, Bai J, Ding S, Wang X, Wang Z. Two-stage crystallization kinetics and morphological evolution with stereocomplex crystallite-induced enhancement for long-chain branched polylactide/poly(D-lactic acid) blends. Ind Eng Chem Res 2021;60:5319–29.
[331] Cao ZQ, Sun XR, Bao RY, Yang W, Xie BH, Yang MB. Role of carbon nanotube grafted poly(L-lactide)-block-poly(D-lactide) in the crystallization of poly(L-lactic acid)/poly(D-lactic acid) blends: Suppressed homocrystallization and enhanced stereocomplex crystallization. Eur Polym J 2016;83:42–52.
[332] Cui CH, Yan DX, Pang H, Xu X, Jia LC, Li ZM. Formation of a segregated electrically conductive network structure in a low-melt-viscosity polymer for highly efficient electromagnetic interference shielding. ACS Sustain Chem Eng 2016;4:4137–45.
[333] Cui CH, Yan DX, Pang H, Jia LC, Xu X, Yang S, Xu JZ, Li ZM. A high heat-resistance bioplastic foam with efficient electromagnetic interference shielding. Chem Eng J 2017;323:29–36.
[334] He S, Bai H, Bai D, Ju Y, Zhang Q, Fu Q. A promising strategy for fabricating high-performance stereocomplex-type polylactide products via carbon nanotubes-assisted low-temperature sintering. Polymer 2019;162:50–7.
[335] Liu H, Bai H, Bai D, Liu Z, Zhang Q, Fu Q. Design of high-performance poly(L-lactide)/elastomer blends through anchoring carbon nanotubes at the interface with the aid of stereocomplex crystallization. Polymer 2017;108:38–49.
[336] Liu H, Bai D, Bai H, Zhang Q, Fu Q. Constructing stereocomplex structures at the interface for remarkably accelerating matrix crystallization and enhancing the mechanical properties of poly(L-lactide)/multi-walled carbon nanotube nanocomposites. J Mater Chem 2015;3:13835–47.
[337] Yang S, Zhong GJ, Xu JZ, Li ZM. Preferential formation of stereocomplex in high-molecular-weight polylactic acid racemic blend induced by carbon nanotubes. Polymer 2016;105:167–71.
[338] Yang S, Xu JZ, Li Y, Lei J, Zhong GJ, Wang R, Li ZM. Effects of solvents on stereocomplex crystallization of high-molecular-weight polylactic acid racemic blends in the presence of carbon nanotubes. Macromol Chem Phys 2017;218:1700292.
[339] Quan H, Zhang SJ, Qiao JL, Zhang LY. The electrical properties and crystallization of stereocomplex poly(lactic acid) filled with carbon nanotubes. Polymer 2012;53:4547–52.
[340] Li S, Luo C, Tang F, Xiao W, Fang M, Sun J, Chen W. Effect of polyethylene glycol modified MWCNTS-OH on the crystallization of PLLA and its stereocomplex. J Polym Res 2022;29:162.
[341] Eleuteri M, Bernal M, Milanesio M, Monticelli O, Fina A. Stereocomplexation of poly(lactic acid)s on graphite nanoplatelets: From functionalized nanoparticles to self-assembled nanostructures. Front Chem 2019;7:176.
[342] Gardella L, Furfaro D, Galimberti M, Monticelli O. On the development of a facile approach based on the use of ionic liquids: Preparation of PLLA (SC–PLA)/high surface area nano-graphite systems. Green Chem 2015;17:4082–8.
[343] Girdthep S, Sankong W, Pongmalee A, Saelee T, Punyodom W, Meepowpan P, Worajittiphon P. Enhanced crystallization, thermal properties, and hydrolysis resistance of poly(L-lactic acid) and its stereocomplex by incorporation of graphene nanoplatelets. Polym Test 2017;61:229–39.
[344] Sun Y, He C. Synthesis and stereocomplex crystallization of poly(lactide)-graphene oxide nanocomposites. ACS Macro Lett 2012;1:709–13.
[345] Wang LN, Wang PYG, Wei JG. Graphene oxide–graft-poly(L-lactide)/poly(L-lactide) nanocomposites: mechanical and thermal properties. Polymers 2017;9:429.
[346] Wu X, Chen X, Fan Z. Influence of graphene nanosheets on stereocomplex crystallization behaviors of star-shaped poly (D(L)-lactide) stereoblock copolymer. Polym Adv Technol 2018;29:632–40.
[347] Xu H, Feng ZX, Xie L, Hakkarainen M. Graphene oxide-driven design of strong and flexible biopolymer barrier films: from smart crystallization control to affordable engineering. ACS Sustain Chem Eng 2016;4:334–49.
[348] Xu LQ, Zhao YQ. Preparation, foaming and characterization of poly(L-lactic acid))/poly(D-lactic acid)-grafted graphite oxide blends. Int Polym Proc 2018;33:127–34.
[349] Zhang D, Lin Y, Wu G. Polylactide-based nanocomposites with stereocomplex networks enhanced by GO-g-PDLA. Compos Sci Technol 2017;138:57–67.
[350] Liu H, Bai D, Du S, Li X, Bai H, Fu Q. Stereocomplex crystallization induced significant improvement in transparency and stiffness–toughness performance of core-shell rubber nanoparticles toughened poly(L-lactide) blends. Macromol Mater Eng 2021;306:2100021.
[351] Gu T, Sun DX, Xie X, Qi XD, Yang JH, Lei YZ, Wang Y. Constructing segregated structure with multiscale stereocomplex crystallites toward synchronously enhancing the thermal conductivity and thermo-mechanical properties of the poly(L-lactic acid) composites. Compos Sci Technol 2022;219:109257.
[352] Huang G, Du Z, Yuan Z, Gu L, Cai Q, Yang X. Poly(L-lactide) nanocomposites containing poly(D-lactide) grafted nanohydroxyapatite with improved interfacial adhesion via stereocomplexation. J Mech Behav Biomed Mater 2018;78:10–19.
[353] Boruvka M, Cermak C, Behalek L, Brdlik P. Effect of in-mold annealing on the properties of asymmetric poly(L-lactide)/poly(D-lactide) blends incorporated with nanohydroxyapatite. Polymers 2021;13:2835.
[354] Jing Z, Shi X, Zhang G, Li J. Rheology and crystallization behavior of PLLA/TiO_2-g-PDLA composites. Polym Adv Technol 2015;26:528–37.
[355] Liang YY, Xu JZ, Li Y, Zhong GJ, Wang R, Li ZM. Promoting interfacial transcrystallization in polylactide/ramie fiber composites by utilizing stereocomplex crystals. ACS Sustain Chem Eng 2017;5:7128–36.
[356] Liu R, Dai L, Hu LQ, Zhou WQ, Si CL. Fabrication of high-performance poly(L-lactic acid)/lignin-graft-poly(D-lactic acid) stereocomplex films. Mater Sci Eng, C 2017;80:397–403.
[357] Liu R, Dai L, Zou Z, Si C. Drug-loaded poly(L-lactide)/lignin stereocomplex film for enhancing stability and sustained release of trans-resveratrol. Int J Biol Macromol 2018;119:1129–36.
[358] Purnama P, Kim SH. Biodegradable blends of stereocomplex polylactide and lignin by supercritical carbon dioxide-solvent system. Macromol Res 2014;22:74–8.
[359] Zhuang Z, Li T, Jin T, Zhou Z, Ning Z, Jiang N, Gan Z. Crystallization behavior of lignin-grafted-poly(D-lactide) and its promotion effect on poly(L-lactide) crystallization. Beijing Huagong Daxue Xuebao (Ziran Kexueban). /. J Beijing Univ Chem Technol (Nat Sci Edit) 2021;48:34–40.
[360] Liu H, Bai D, Bai H, Zhang Q, Fu Q. Manipulating the filler network structure and properties of polylactide/carbon black nanocomposites with the aid of stereocomplex crystallites. J Phys Chem C 2018;122:4232–40.
[361] Ma P, Jiang L, Xu P, Dong W, Chen M, Lemstra PJ. Rapid stereocomplexation between enantiomeric comb-shaped cellulose-g-poly(L-lactide) nanohybrids and poly(D-lactide) from the melt. Biomacromolecules 2015;16:3723–9.
[362] Zhang H, Li Q, Edgar KJ, Yang G, Shao H. Structure and properties of flax vs. Lyocell fiber-reinforced polylactide stereocomplex composites. Cellulose 2021;28:9297–308.
[363] Chuan D, Fan R, Wang Y, Ren Y, Wang C, Du Y, Zhou L, Yu J, Gu Y, Chen H, Guo G. Stereocomplex poly(lactic acid)-based composite nanofiber membranes with highly dispersed hydroxyapatite for potential bone tissue engineering. Compos Sci Technol 2020;192:108107.
[364] Gupta A, Prasad A, Mulchandani N, Shah M, Ravi Sankar M, Kumar S, Katiyar V. Multifunctional nanohydroxyapatite-promoted toughened high-molecular-weight stereocomplex poly(lactic acid)-based bionanocomposite for both 3D-printed orthopedic implants and high-temperature engineering applications. ACS Omega 2017;2:4039–52.
[365] Hong Z, Zhang P, He C, Qiu X, Liu A, Chen L, Chen X, Jing X. Nano-composite of poly(L-lactide) and surface grafted hydroxyapatite: Mechanical properties and biocompatibility. Biomaterials 2005;26:6296–304.
[366] Wang M, You LC, Guo YQ, Jiang N, Gan ZH, Ning ZB. Enhanced crystallization rate of poly(L-lactide)/hydroxyapatite-graft-poly(D-lactide) composite with different processing temperatures. Chin J Polym Sci 2020;38:599–610.
[367] Xie Q, Wang S, Chen X, Zhou Y, Fang H, Li X, Cheng S, Ding Y. Thermal stability and crystallization behavior of cellulose nanocrystals and their poly(L-lactide) nanocomposites: Effects of surface ionic group and poly(D-lactide) grafting. Cellulose 2018;25:6847–62.
[368] Xu P, Lv P, Wu B, Ma P, Dong W, Chen M, Du M, Ming W. Smart design of rapid crystallizing and nonleaching antibacterial poly(lactide) nanocomposites by sustainable aminolysis grafting and in situ interfacial stereocomplexation. ACS Sustain Chem Eng 2018;6:13367–77.
[369] Pandey AK, Takagi H, Igarashi N, Shimizu N, Sakurai S. Enhanced formation of stereocomplex crystallites in poly(L-lactic acid)/poly(D-lactic acid) blends by silk fibroin nanodisc. Polymer 2021;229.
[370] Kumar PA. Studies on enhancement in crystallization behavior of poly (lactic acid) by silk fibroin nanodisc. J Fiber Sci Technol 2021;77:155–61.
[371] Gu T, Sun DX, Qi XD, Yang JH, Lei YZ, Wang Y. Heat resistant and thermally conductive polylactide composites achieved by stereocomplex crystallite tailored carbon nanofiber network. Chem Eng J 2021;418:129287.
[372] Li Y, Zhao L, Han C, Xiao L. Thermal and mechanical properties of stereocomplex polylactide enhanced by nanosilica. Colloid Polym Sci 2021;299:1161–72.
[373] Fan X, Luo Z, Ye E, You M, Liu M, Yun Y, Loh XJ, Wu YL, Li Z. AuNPs decorated PLA stereocomplex micelles for synergetic photothermal and chemotherapy. Macromol Biosci 2021;21:2100062.
[374] Deng YF, Zhang D, Zhang N, Huang T, Lei YZ, Wang Y. Electrospun stereocomplex polylactide porous fibers toward highly efficient oil/water separation. J Hazard Mater 2021;407:124787.
[375] Zhou J, Yu J, Bai D, Lu J, Liu H, Li Y, Li L. AgNW/stereocomplex-type polylactide biodegradable conducting film and its application in flexible electronics. J Mater Sci: Mater Electr 2021;32:6080–93.
[376] Xu JZ, Li Y, Li YK, Chen YW, Wang R, Liu G, Liu SM, Ni HW, Li ZM. Shear-induced stereocomplex cylindrites in polylactic acid racemic blends: Morphology control and interfacial performance. Polymer 2018;140:179–87.
[377] Wei Y, Tian Y, Tian X, Fu Z, Zhao L. Induction of stereocomplex crystallization in poly(L-lactide)/poly(D-lactide) blends with high molecular weight by halloysite nanotubes. Macromol Chem Phys 2022;223:2100356.
[378] Baek SW, Kim JH, Song DH, Kim DS, Park CG, Han DK. Enhanced mechanical properties and anti–inflammation of poly(L–Lactic Acid) by stereocomplexes of PLLA/PDLA and surface–modified magnesium hydroxide nanoparticles. Polymers 2022;14:3790.
[379] Chen Q, Auras R, Corredig M, Kirkensgaard JJK, Mamakhel A. Uysal-Unalan I. New opportunities for sustainable bioplastic development: tailorable polymorphic and three-phase crystallization of stereocomplex polylactide by layered double hydroxide. Int J Biol Macromol 2022;222:1101–9.
[380] Furuhashi Y, Morioka K, Tamegai H, Yoshie N. Preparation and some properties of stereocomplex-type poly(lactic acid)/layered silicate nanocomposites. J Appl Polym Sci 2013;127:1615–22.
[381] Purnama P, Jung Y, Kim SH. An advanced class of bio-hybrid materials: bionanocomposites of inorganic clays and organic stereocomplex polylactides. Macromol Mater Eng 2013;298:263–9.

[382] Jalali A, Romero-Diez S, Nofar M, Park CB. Entirely environment-friendly polylactide composites with outstanding heat resistance and superior mechanical performance fabricated by spunbond technology: Exploring the role of nanofibrillated stereocomplex polylactide crystals. Int J Biol Macromol 2021;193:2210–20.
[383] Moya-Lopez C, Juan A, Donizeti M, Valcarcel J, Vazquez JA, Solano E, Chapron D, Bourson P, Bravo I, Alonso-Moreno C, Clemente-Casares P, Gracia-Fernández C, Longo A, Salloum-Abou-Jaoude G, Ocaña A, Piñeiro MM, Hermida-Merino C, Hermida-Merino D. Multifunctional PLA/gelatin bionanocomposites for tailored drug delivery systems. Pharmaceutics 2022;14:1138.
[384] Putri OD, Petchsuk A, Bayram S, Opaprakasit P. Ultrasonicate-assisted preparation of eumelanin-loaded nano/microparticles based on polylactide stereocomplex. Mater Today: Proc 2022;66:3025–30.
[385] Yan Z, Wang Y, Li T, Xu P, Huang J, Jiang J, Zhang X, Xia B, Wang S, Dong W. Dual-functional NIR/UV-shielding poly(lactic acid) nanocomposite films through CWO@PDA core–shell nanoparticles. New J Chem 2022;46:15064–70.
[386] Feng Y, Lv P, Jiang L, Ma P, Chen M, Dong W, Chen Y. Enhanced crystallization kinetics of symmetric poly(L-lactide)/poly(D-lactide) stereocomplex in the presence of nanocrystalline cellulose. Polym Degrad Stab 2017;146:113–20.
[387] Srithep Y, Pholharn D, Turng LS. Characterization of stereocomplex polylactide/nanoclay nanocomposites. Int Polym Proc 2017;32:121–8.
[388] Xiong Z, Zhang X, Wang R, De Vos S, Joziasse CAP, Wang D. Favorable formation of stereocomplex crystals in poly(L-lactide)/poly(D-lactide) blends by selective nucleation. Polymer 2015;76:98–104.
[389] Han L, Pan P. Enhanced stereocomplex crystallization of high-molecular-weight poly (lactic acid). In: Proceedings of the materials engineering and sciences division 2015 - core programming area at the 2015 AIChE annual meeting; 2015. p. 652–61.
[390] Ishii D, Kimishima M, Otake K, Iwata T. Enhanced crystallization of poly(lactide) stereocomplex by xylan propionate. Polym Int 2016;65:339–45.
[391] Khwanpipat T, Seadan M, Suttiruengwong S. Effect of PDLA and amide compounds as mixed nucleating agents on crystallization behaviors of poly (L-lactic acid). Materials 2018;11:1139.
[392] Tu C, Cao X, Zhang RD, Wang DW, Cui L. Effects of posttreatment on the properties of modified PLLA/PDLA fibers. Polym Adv Technol 2018;30:254–63.
[393] Herc AS, Lewiński P, Kaźmierski S, Bojda J, Kowalewska A. Hybrid sc-polylactide/poly(silsesquioxane) blends of improved thermal stability. Thermochim Acta 2020;687:178592.
[394] Li W, Ren Q, Zhu X, Wu M, Weng Z, Wang L, Zheng W. Enhanced heat resistance and compression strength of microcellular poly (lactic acid) foam by promoted stereocomplex crystallization with added D-mannitol. J CO_2 Util 2022;63:102118.
[395] Körber S, Moser K, Diemert J. Development of high temperature resistant stereocomplex PLA for injection moulding. Polymers 2022;14:384.
[396] Cui L, Wang Y, Zhang R, Liu Y. Design high heat-resistant stereocomplex poly(lactide acid) by cross-linking and plasticizing. Adv Polym Tech 2018;37:2429–35.
[397] Srithep Y, Pholharn D. Plasticizer effect on melt blending of polylactide stereocomplex. e-Polymers 2017;17:409–16.
[398] Bao RY, Yang W, Liu ZY, Xie BH, Yang MB. Polymorphism of a high-molecular-weight racemic poly(L-lactide)/poly(D-lactide) blend: Effect of melt blending with poly(methyl methacrylate). RSC Adv 2015;5:19058–66.
[399] Bai H, Bai D, Xiu H, Liu H, Zhang Q, Wang K, Deng H, Chen F, Fu Q, Chiu FC. Towards high-performance poly(L-lactide)/elastomer blends with tunable interfacial adhesion and matrix crystallization via constructing stereocomplex crystallites at the interface. RSC Adv 2014;4:49374–85.
[400] Pan P, Bao J, Han L, Xie Q, Shan G, Bao Y. Stereocomplexation of high-molecular-weight enantiomeric poly(lactic acid)s enhanced by miscible polymer blending with hydrogen bond interactions. Polymer 2016;98:80–7.
[401] Pholharn D, Srithep Y, Morris J. Melt compounding and characterization of poly(lactide) stereocomplex/natural rubber composites. Polym Eng Sci 2018;58:713–18.
[402] Yan X, Zhao Y, Hao Y, Pan H, Zhang H, Wang Z, Dong L. Crystallization behavior, rheology, mechanical properties, and enzymatic degradation of poly(L-lactide)/poly(D-lactide)/glycidyl methacrylate grafted poly(ethylene octane) blends. Fibers Polym 2017;18:2049–59.
[403] Yu C, Han L, Bao J, Shan G, Bao Y, Pan P. Polymorphic crystallization and crystalline reorganization of poly(L-lactic acid)/poly(D-lactic acid) racemic mixture influenced by blending with poly(vinylidene fluoride). J Phys Chem B 2016;120:8046–54.
[404] Shi X, Qin J, Wang L, Ren L, Rong F, Li D, Wang R, Zhang G. Introduction of stereocomplex crystallites of PLA for the solid and microcellular poly(lactide)/poly(butylene adipate-co-terephthalate) blends. RSC Adv 2018;8:11850–61.
[405] Zhang Y, Shi H, Cheng H, Han C, Wang L. Enhancement of the properties of poly(L-lactide)/poly(butylene adipate-co-terephthalate) blends by introduction of stereocomplex polylactide crystallites. Thermochim Acta 2022;715:179272.
[406] Li Y, Zhao L, Han C, Xiao L, Yu Y, Zhou G, Xu M. Effect of the molecular weight of poly(vinyl acetate) on the polymorphism and thermomechanical properties of poly(L-lactic acid)/poly(D-lactic acid) blends. J Therm Anal Calorim 2022;147:3171–84.
[407] Hashimoto K, Kurokawa N, Hotta A. Controlling the switching temperature of biodegradable shape memory polymers composed of stereocomplex polylactide/poly(D,L-lactide-co-ε-caprolactone) blends. Polymer 2021;233:124190.
[408] Su X, Jia S, Cao L, Yu D. High performance polylactic acid/thermoplastic polyurethane blends with in-situ fibrillated morphology. J Appl Polym Sci 2021;138:51014.
[409] Li Z, Ye X, Meng C, Zhou H, Guo W, Chen S, Zhang J, Yan C, Dufresne A. Effects of epoxy resin crosslinking networks on stereocomplexation of poly(L-lactic acid)/poly(D-lactic acid) racemic blends. Polym Int 2021;70:656–66.
[410] Cui W, Wei X, Luo J, Xu B, Zhou H, Wang X. CO_2-assisted fabrication of PLA foams with exceptional compressive property and heat resistance via introducing well-dispersed stereocomplex crystallites. J CO_2 Util 2022;64:102184.
[411] Zhang ZC, Sang ZH, Huang YF, Ru JF, Zhong GJ, Ji X, Wang R, Li ZM. Enhanced heat deflection resistance via shear flow-induced stereocomplex crystallization of polylactide systems. ACS Sustain Chem Eng 2017;5:1692–703.
[412] Song Y, Zhang X, Yin Y, Zhang C, De Vos S, Wang R, Joziasse CAP, Liu G, Wang D. Crystallization of equimolar poly(L-lactide)/poly(D-lactide) blend below the melting point of α crystals under shear. Eur Polym J 2016;75:93–103.
[413] Song YN, Zhao QX, Yang SG, Ru JF, Lin JM, Xu JZ, Lei J, Li ZM. Flow-induced crystallization of polylactide stereocomplex under pressure. J Appl Polym Sci 2018;135:46378.
[414] Song Y, Zhang X, Yin Y, De Vos S, Wang R, Joziasse CAP, Liu G, Wang D. Enhancement of stereocomplex formation in poly(L-lactide)/poly(D-lactide) mixture by shear. Polymer 2015;72:185–92.
[415] Tuccitto AV, Anstey A, Sansone ND, Park CB, Lee PC. Controlling stereocomplex crystal morphology in poly(lactide) through chain alignment. Int J Biol Macromol 2022;218:22–32.
[416] Huang W, Shi Y, Wang P, Yang Q, Gobius du Sart G, Zhou Y, Joziasse CAP, Wang R, Chen P. Facile and efficient formation of stereocomplex polylactide fibers drawn at low temperatures. Polymer 2022;246:124743.
[417] Sun M, Lu S, Zhao P, Feng Z, Yu M, Han K. Scalable preparation of complete stereo-complexation polylactic acid fiber and its hydrolysis resistance. Molecules 2022;27:7654.
[418] Kara Y, Molnár K. Decomposition behavior of stereocomplex PLA melt-blown fine fiber mats in water and in compost. J Polym Environ 2023;31:1398–414.
[419] Zhang H, Wang C, Xu Y, Huang X, He X, Zhang C, Lu J. Pressure–controlled crystallization of stereocomplex crystals in enantiomeric polylactides with remarkably enhanced hydrolytic degradation. CrystEngComm 2018;20:7337–47.
[420] Tsuji H, Yamamoto S. Enhanced stereocomplex crystallization of biodegradable enantiomeric poly(lactic acid)s by repeated casting. Macromol Mater Eng 2011;296:583–9.
[421] Torres L, McMahan C, Ramadan L, Holtman KM, Tonoli GHD, Flynn A, Orts WJ. Effect of multi-branched PDLA additives on the mechanical and thermomechanical properties of blends with PLLA. J Appl Polym Sci 2016;132:42858.
[422] Bao J, Guo G, Lu W, Zhang X, Mao H, Dong X, Chen S, Chen W. Thermally induced physical gelation and phase transition of stereocomplexable poly(lactic acid)/poly(ethylene glycol) copolymers: Effects of hydrophilic homopolymers. Polymer 2020;208:122965.
[423] Ma B, Zhang H, Wang K, Xu H, He Y, Wang X. Influence of scPLA microsphere on the crystallization behavior of PLLA/PDLA composites. Compos Commun 2020;21:100380.
[424] Chang Y, Chen Z, Yang Y. Toughening of poly(L-lactide) with branched multiblock poly(ε-caprolactone)/poly(D-lactide) copolymers. J Donghua Univ 2018;35:365–74 (English Edition).
[425] Laske S, Ziegler W, Kainer M, Wuerfel J, Holzer C. Enhancing the temperature stability of PLA by compounding strategies. Polym Eng Sci 2015;55:2849–58.
[426] Cheng L, Hu C, Li J, Huang S, Jiang S. Stereocomplex-affected crystallization behaviour of PDLA in PDLA/PLDLA blends. CrystEngComm 2019;21:329–38.
[427] Fan T, Qin J, Lin S, Ye W, Li J, Zhang Q, Gong L, Liu D, Fan Z. Enhancement of the crystallization and biocompatibility of poly(TMC-b-(LLA-ran-GA)) by poly(lactide) stereocomplex. CrystEngComm 2019;21:6269–80.
[428] Ji N, Hu G, Li J, Ren J. Influence of poly(lactide) stereocomplexes as nucleating agents on the crystallization behavior of poly(lactide)s. RSC Adv 2019;9:6221–7.
[429] Luo Y, Ju Y, Bai H, Liu Z, Zhang Q, Fu Q. Tailor-made dispersion and distribution of stereocomplex crystallites in poly(L-lactide)/elastomer blends toward largely enhanced crystallization rate and impact toughness. J Phys Chem B 2017;121:6271–9.
[430] Shi YD, Cheng YH, Chen YF, Zhang K, Zeng JB, Wang M. Morphology, rheological and crystallization behavior in thermoplastic polyurethane toughed poly(L-lactide) with stereocomplex crystallites. Polym Test 2017;62:1–12.
[431] Shi X, Jing Z, Zhang G. Influence of PLA stereocomplex crystals and thermal treatment temperature on the rheology and crystallization behavior of asymmetric poly(L-lactide)/poly(D-lactide) blends. J Polym Res 2018;25:71.
[432] Yan C, Jiang YP, Hou DF, Yang W, Yang MB. High-efficient crystallization promotion and melt reinforcement effect of diblock PDLA-b-PLLA copolymer on PLLA. Polymer 2020;186:122021.
[433] Yin HY, Wei XF, Bao RY, Dong QX, Liu ZY, Yang W, Xie BH, Yang MB. High-melting-point crystals of poly(L-lactic acid) (PLLA): The most efficient nucleating agent to enhance the crystallization of PLLA. CrystEngComm 2015;17:2310–20.
[434] Yin HY, Wei XF, Bao RY, Dong QX, Liu ZY, Yang W, Xie BH, Yang MB. Enhancing thermomechanical properties and heat distortion resistance of poly(L-lactide) with high crystallinity under high cooling rate. ACS Sustain Chem Eng 2015;3:654–61.

[435] Jia P, Hu J, Zhai W, Duan Y, Zhang J, Han C. Cell morphology and improved heat resistance of microcellular poly(L-lactide) foam via introducing stereocomplex crystallites of PLA. Ind Eng Chem Res 2015;54:2476–88.
[436] Li Y, Han C, Yu Y, Huang D. Morphological, thermal, rheological and mechanical properties of poly(butylene carbonate) reinforced by stereocomplex polylactide. Int J Biol Macromol 2019;137:1169–78.
[437] Zeng Z, Luo Y, Bai H, Zhang Q, Fu Q. Manipulating matrix crystallization and impact toughness of polylactide/elastomer blends via tailoring size and packing density of stereocomplex crystallites formed at the interface. Macromol Mater Eng 2022;307:2100698.
[438] Luoma E, Välimäki M, Rokkonen T, Sääskilahti H, Ollila J, Rekilä J, Immonen K. Oriented and annealed poly(lactic acid) films and their performance in flexible printed and hybrid electronics. J Plast Film Sheeting 2021;37:429–62.
[439] Yao J, Zeng Z, Bai H, Zhang Q, Fu Q. Importance of low-temperature melt-mixing on the construction of stereocomplex crystallites with superior nucleation efficiency in asymmetric poly(L-lactide)/poly(D-lactide) blends. Macromol Mater Eng 2021;306:2100091.
[440] Samsuri M, Iswaldi I, Purnama P. The effect of stereocomplex polylactide particles on the stereocomplexation of high molecular weight polylactide blends. Polymers 2021;13:2018.
[441] Park HS, Hong CK. Relationship between the stereocomplex crystallization behavior and mechanical properties of PLLA/PDLA blends. Polymers 2021;13:1851.
[442] Zhu Q, Chang K, Qi L, Li X, Gao W, Gao Q. Surface modification of poly(L-lactic acid) through stereocomplexation with enantiomeric poly(D-lactic acid) and its copolymer. Polymers 2021;13:1757.
[443] Liu W, Tian Y, Tian X, Wang J, Zhao L. Improvement of poly(propylidene carbonate) mechanical properties by using stereocomplex crystals of polylactide to anchor graphene oxide at the interface of poly(propylidene carbonate)/poly(L-lactide) blends. J Mater Sci 2021;56:8497–510.
[444] Lv T, Li J, Huang S, Wen H, Li H, Chen J, Jiang S. Synergistic effects of chain dynamics and enantiomeric interaction on the crystallization in PDLA/PLLA mixtures. Polymer 2021;222:123648.
[445] Chen X, Li C, Ding Y, Li Y, Li J, Sun L, Wei J, Wei X, Wang H, Zhang K, Pan L, Li Y. Fully bio-based and supertough PLA blends via a novel interlocking strategy combining strong dipolar interactions and stereocomplexation. Macromolecules 2022;55:5864–78.
[446] Li F, Zhou F, Romano D, Rastogi S. Synthesis and characterization of well-defined high-molecular-weight PDLA-b-PLLA and PDLA-b-PLLA-b-PDLA stereo-block copolymers. Macromolecules 2023;56:1995–2008.
[447] Xie Q, Chang X, Qian Q, Pan P, Li CY. Structure and morphology of poly(lactic acid) stereocomplex nanofiber shish kebabs. ACS Macro Lett 2020;9:103–7.
[448] Arias V, Odelius K, Höglund A, Albertsson . Homocomposites of polylactide (PLA) with induced interfacial stereocomplex crystallites. ACS Sustain Chem Eng 2015;3:2220–31.
[449] Bai D, Liu H, Bai H, Zhang Q, Fu Q. Powder metallurgy inspired low-temperature fabrication of high-performance stereocomplexed polylactide products with good optical transparency. Sci Rep 2016;6:20260.
[450] Bai D, Liu H, Bai H, Zhang Q, Fu Q. Low-temperature sintering of stereocomplex-type polylactide nascent powder: Effect of crystallinity. Macromolecules 2017;50:7611–19.
[451] Chen Y, Hua WQ, Zhang ZC, Xu JZ, Bian FG, Zhong GJ, Xu L, Li ZM. An efficient, food contact accelerator for stereocomplexation of high-molecular-weight poly(L-lactide)/poly(D-lactide) blend under nonisothermal crystallization. Polymer 2019;170:54–64.
[452] Cui L, Wang Y, Guo Y, Liu Y, Zhao J, Zhang C, Zhu P. Effects of temperature and external force on the stereocomplex crystallization in poly(lactic acid) blends. Adv Polym Tech 2018;37:962–7.
[453] Li Y, Xin S, Bian Y, Dong Q, Han C, Xu K, Dong L. Stereocomplex crystallite network in poly(D,L-lactide): Formation, structure and the effect on shape memory behaviors and enzymatic hydrolysis of poly(D,L-lactide). RSC Adv 2015;5:24352–62.
[454] Ma P, Shen T, Xu P, Dong W, Lemstra PJ, Chen M. Superior performance of fully biobased poly(lactide) via stereocomplexation-induced phase separation: Structure versus property. ACS Sustain Chem Eng 2015;3:1470–8.
[455] Naga N, Yoshida Y, Noguchi K. Crystallization of poly(L-lactic acid)/poly(D-lactic acid) blend induced by organic solvents. Polym Bull 2019;76:3677–91.
[456] Chen W, Bessif B, Reiter R, Xu J, Reiter G. Controlled switching from the growth of monolamellar polymer crystals to the formation of stacks of uniquely oriented lamellae. Macromolecules 2021;54:8135–42.
[457] Shao J, Xu L, Pu S, Hou H. The crystallization behavior of poly(L-lactide)/poly(D-lactide) blends: effect of stirring time during solution mixing. Polym Bull 2021;78:147–63.
[458] Li R, Zhao X, Coates P, Caton-Rose F, Ye L. Highly reinforced poly(lactic acid) foam fabricated by formation of a heat-resistant oriented stereocomplex crystalline structure. ACS Sustain Chem Eng 2021;9:12674–86.
[459] Chen P, Bai D, Tang H, Liu H, Wang J, Gao G, Li L. Polylactide aerogel with excellent comprehensive performances imparted by stereocomplex crystallization for efficient oil-water separation. Polymer 2022;255:125128.
[460] Yu K, Wu Y, Zhang X, Hou J, Chen J. Microcellular open-cell poly(L-lactic acid)/poly(D-lactic acid) foams for oil-water separation prepared via supercritical CO_2 foaming. J CO_2 Util 2022;65:102219.
[461] Sun XR, Cao ZQ, Bao RY, Liu Z, Xie BH, Yang MB, Yang W. A green and facile melt approach for hierarchically porous polylactide monoliths based on stereocomplex crystallite network. ACS Sustain Chem Eng 2017;5:8334–43.
[462] Ning Z, Liu J, Jiang N, Gan Z. Enhanced crystallization rate and mechanical properties of poly(L-lactic acid) by stereocomplexation with four-armed poly(ϵ-caprolactone)-block-poly(D-lactic acid) diblock copolymer. Polym Int 2017;66:968–76.
[463] Si WJ, Yang L, Zhu J, Li YD, Zeng JB. Highly toughened and heat-resistant poly(L-lactide) materials through interfacial interaction control via chemical structure of biodegradable elastomer. Appl Surf Sci 2019;483:1090–100.
[464] Bao J, Han L, Shan G, Bao Y, Pan P. Preferential stereocomplex crystallization in enantiomeric blends of cellulose acetate-g-poly(lactic acid)s with comblike topology. J Phys Chem B 2015;119:12689–98.
[465] Kobayashi K, Kanmuri S, Hayashi Y, Masutani K, Kimura Y. Preparation of chain-extended poly(hexamethylene carbonate)s and their block copolymerization with poly-L-lactide to synthesize partly biobased thermoplastic elastomers. Macromol Mater Eng 2014;299:1384–94.
[466] Tsuji H, Hayakawa T. Hetero-stereocomplex formation between substituted poly(lactic acid)s with linear and branched side chains, poly(l-2-hydroxybutanoic acid) and poly(D-2-hydroxy-3-methylbutanoic acid). Polymer 2014;55:721–6.
[467] Tsuji H, Ogawa M, Arakawa Y. Stereocomplex crystallization of linear two-armed stereo diblock copolymers: effects of chain directional change, coinitiator moiety, and terminal groups. J Phys Chem B 2017;121:2695–702.
[468] Tsuji H, Yamasaki M, Arakawa Y. Stereocomplex formation between enantiomeric alternating lactic acid-based copolymers as a versatile method for the preparation of high performance biobased biodegradable materials. ACS Appl Polym Mater 2019;1:1476–84.
[469] Luo C, Yang M, Xiao W, Yang J, Wang Y, Chen W, Han X. Relationship between the crystallization behavior of poly(ethylene glycol) and stereocomplex crystallization of poly(L-lactic acid)/poly(D-lactic acid). Polym Int 2018;67:313–21.
[470] Gardella L, Basso A, Prato M, Monticelli O. On stereocomplexed polylactide materials as support for pamam dendrimers: synthesis and properties. RSC Adv 2015;5:46774–84.
[471] Hyun J, Lee CW, Kimura Y. Synthesis of novel hyper-branched polymers from trimethoxysilyl-terminated polylactides and their utilization for modification of poly(L-lactide) materials. Macromol Mater Eng 2015;300:650–60.
[472] Jing Z, Shi X, Zhang G, Li J, Li J, Zhou L, Zhang H. Formation, structure and promoting crystallization capacity of stereocomplex crystallite network in the poly(lactide) blends based on linear PLLA and PDLA with different structures. Polymer 2016;92:210–21.
[473] Tsuji H, Masaki N, Arakawa Y, Iguchi K, Sobue T. Ternary stereocomplex and hetero-stereocomplex crystallizability of substituted and unsubstituted poly(lactic acid)s. Cryst Growth Des 2018;18:521–30.
[474] Tsuji H, Arakawa Y, Matsumura N. Screening of crystalline species and enhanced nucleation of enantiomeric poly(lactide) systems by melt-quenching. Polym Bull 2019;76:1199–216.
[475] Nouri S, Dubois C, Lafleur PG. Homocrystal and stereocomplex formation behavior of polylactides with different branched structures. Polymer 2015;67:227–39.
[476] Han L, Pan P, Shan G, Bao Y. Stereocomplex crystallization of high-molecular-weight poly(L-lactic acid)/poly(D-lactic acid) racemic blends promoted by a selective nucleator. Polymer 2015;63:144–53.
[477] Xie Q, Bao J, Shan G, Bao Y, Pan P. Fractional crystallization kinetics and formation of metastable β-form homocrystals in poly(L-lactic acid)/poly(D-lactic acid) racemic blends induced by precedingly formed stereocomplexes. Macromolecules 2019;52:4655–65.
[478] Dai S, Dai Z, Jiang N, Ning Z, Gan Z. Highly toughened poly(L-lactide) by poly(D-lactide)-containing crosslinked polyurethane shows excellent malleability, flexibility and shape memory property. Polymer 2022;262:125482.
[479] Gu Z, Zhang J, Cao W, Liu X, Wang J, Zhang X, Chen W, Bao J. Extraordinary toughness and heat resistance enhancement of biodegradable PLA/PBS blends through the formation of a small amount of interface-localized stereocomplex crystallites during melt blending. Polymer 2022;262:125454.
[480] Guo M, Zhao Z, Xie Z, Wu W, Wu W, Gao Q. Role of the branched PEG-b-PLLA block chain in stereocomplex crystallization and crystallization kinetics for PDLA/m PEG -b-PLLA-g-glucose blends with different architectures. Langmuir 2022;38:15866–79.
[481] He Y, Jia SH, Fang C, Tan LC, Qin S, Yin XC, Park CB, Qu JP. Constructing synergistically strengthening-toughening 3D network bundle structures by stereocomplex crystals for manufacturing high-performance thermoplastic polyurethane nanofibers reinforced poly(lactic acid) composites. Compos Sci Technol 2023;232:109847.
[482] Pérez-Camargo RA, Liu GM, Wang DJ, Müller AJ. Experimental and data fitting guidelines for the determination of polymer crystallization kinetics. Chin J Polym Sci 2022;40:658–91.
[483] Lorenzo AT, Arnal ML, Albuerne J, Müller AJ. DSC isothermal polymer crystallization kinetics measurements and the use of the avrami equation to fit the data: Guidelines to avoid common problems. Polym Test 2007;26:222–31.